RIDE DYNAMIC RESPONSE OF COMMERCIAL VEHICLES SUBJECTED TO WHEEL UNBALANCE AND NON-UNIFORMITY EFFECTS

Aniket Deodhar

A Thesis

in

The Department

of

Mechanical & Industrial Engineering

Presented in Partial Fulfillment of the Requirements
for the Degree of Master of Applied Science at
Concordia University
Montreal, Quebec, Canada

April 2005

Your file Votre référence
ISBN: 0-494-04416-0
Our file Notre référence
ISBN: 0-494-04416-0

ABSTRACT

RIDE DYNAMIC RESPONSE OF COMMERCIAL VEHICLES SUBJECTED TO WHEEL UNBALANCE AND NON-UNIFORMITY EFFECTS

Aniket Deodhar

Self-exciting sources of vibration wheel unbalance and wheel non-uniformities are known to contribute to ride vibration environment of road vehicles and also to potential road damage in addition to excitations arising from terrain undulations. The present study investigates vehicle vibrations induced by non-uniformities and unbalance of the tire-wheel assembly in conjunction with terrain irregularities. A four degrees-of-freedom pitch plane model of a truck is developed to analyze ride and tire load variations under measured random road excitations. The nonlinear vehicle model comprising the adaptive foot-print tire model is analyzed under excitations arising from a range of mass unbalance and wheel non-uniformity, and phase differences in the defects of the front and rear wheels. A comprehensive parametric sensitivity analysis is carried out to study the vehicle response subjected to all the excitations. The response characteristics are evaluated in terms of measures relevant to ride quality and road damage potential, namely the overall unweighted and frequency-weighted vertical and pitch rms accelerations of the sprung mass and dynamic load coefficient (DLC), respectively. The results show that wheel unbalance and non-uniformities could yield considerable bounce and pitch vibration of the vehicle, specifically on smooth roads. Furthermore, the wheel unbalance and wheel non-uniformity contribute to the dynamic tire forces transmitted to the pavements. The results show that the vertical ride quality is significantly deteriorated by

the considered sources of self-excitation. The relative contributions due to self-excitation sources of vibration are small when vehicle interactions with rough roads are considered.

ACKNOWLEDGMENTS

Life in graduate school is defined, largely, by the thesis supervisors and the colleagues one has. Considering that I have spent a good part of my life in graduate school, I am very fortunate to have been in the company of the best people I could ever wish for. First and foremost, I would like to express my sincere gratitude to my supervisors, Dr. Subhash Rakheja and Dr. Rama Bhat. Throughout my research, they provided me intellectual and financial support. Above and beyond this, they afforded me their valuable time, endless patience, tolerance and steady encouragement.

I would like to thank Dr. Bhat for guiding my initial doddering steps in Concordia, and for helping me discover a sense of joy in mathematics. Your guidance and principles are much appreciated.

Dr. Rakheja has opened my eyes to a world of knowledge, asking crucial questions at critical times, and helping me find direction. I have knocked his office door many a time, for matters both urgent and seemingly important, and I have never been turned away. His help and counsel have been invaluable.

Thanks to all my colleagues, faculty and staff of CONCAVE research center for their assistance and valuable inputs in my work.

I wish to sincerely thank my dear parents and brother, Subodh, for their support, love and many sacrifices. Their confidence in me helped me face the slings and arrows of the M. A. Sc. program with decisive certainty.

TABLE OF CONTENTS

CHAPTER 3

RESPONSE EVALUATION OF THE VEHICLE MODEL AND PERFORMANCE MEASURES

CHAPTER 4

ANALYSIS OF WHEEL UNBALANCE AND NON-UNIFORMITY

LIST OF FIGURES

LIST OF TABLES

NOMENCLATURE

SYMBOL	DESCRIPTION
α_{wi}	Half of the wheel terrain contact patch angle (rad) ($i = f, r$)
β_i	Contact patch angle of the wheel ($i = f, r$)
$(C_{rw})_i$	Equivalent viscous damping coefficient for the wheel (N-s/m) ($i = f, r$)
C_{si}	Damping coefficient for the suspension (N-s/m) ($i = f, r$)
δ_i	Radial deflection of the wheel (m) ($i = f, r$)
δ_{Si}	Static deflection of the suspension (m) ($i = F, R$)
δ_{ui}	Static deflection of the wheel (m) ($i = f, r$)
e_i	Distance of C.G. of the unbalanced mass from the wheel center ($i = f, r$)
F_{Di}	Damping force due to suspension (N)
F_{Si}	Total suspension force ($i = F, R$)
$(F_{st})_i$	Static load at the wheel (N) ($i = f, r$)
$(F_{wn})_i$	Net normal footprint force at the wheel (N) ($i = f, r$)
$(F_{wz})_i$	Net vertical footprint force (N) ($i = f, r$)
g	Acceleration due to gravity (9.81 m/s^2)
γ_i	Vertical inclination of the net footprint force with respect to fixed Z-axis (rad) ($i = f, r$)
I_s	Pitch mass moment of inertia of a sprung mass of vehicle about its centroid (kg-m^2)
$(K_{rw})_i$	Continuous radial spring constant (N/m/rad) ($i = f, r$)

K_{si}	Spring constant for the suspension (N/m) ($i = f, r$)
ℓ_i	Distance between C.G. of the sprung mass of vehicle and axle (m) ($i = f, r$)
L	Wheel base of the vehicle (m)
m_i	Mass unbalance in the tire-wheel assembly (kg) ($i = f, r$)
M_s	Sprung mass of the vehicle (kg)
M_{ui}	Unsprung mass of the vehicle (kg) ($i = f, r$)
$(N_I)_i$	Number of terrain profile points within instantaneous wheel–terrain contact patch ($i = f, r$)
$(N_S)_i$	Number of terrain profile points within the horizontal diametrical range or shadow of wheel center ($i = f, r$)
ϕ_i	Angle of unbalanced mass in the tire-wheel assembly from the wheel center (rad) ($i = f, r$)
R_w	Free radius of the tire (m)
Δr_i	Magnitude of radial run-out or wheel non-uniformity (m) ($i = f, r$)
θ	Angular displacement of the sprung mass with respect to its C.G. (rad)
θ_i	Angular displacement of the wheel (rad) ($i = f, r$)
V_x	Forward speed of the vehicle (m/s)
ω	Angular frequency of the wheel (rad/s)
X_{wi}, Z_{wi}	Cartesian coordinates of the wheel center (m)
$\ddot{Z}_s$	Sprung mass acceleration (m/s^2)
$\ddot{Z}_{ui}$	Unsprung mass acceleration (m/s^2) ($i = f, r$)
Z_{oi}	Road excitation at the wheel (m) ($i = f, r$)

CHAPTER 1

INTRODUCTION AND REVIEW OF RELEVANT LITERATURE

1.1 INTRODUCTION

Cargo trucks encounter ride vibrations in a wide frequency range, which are induced by a variety of sources such as road roughness, structural flexibility and drive-train. Wheel unbalance and tire non-uniformity also contribute to the overall ride vibration environment of the vehicle. While the ride dynamic responses of road and off-road vehicles induced by road roughness and drive-train have been extensively investigated, the effects of wheel unbalance and tire non-uniformity have gained only minimal attention. This study is focused on the vibrations induced by the wheel non-uniformities and unbalance of the tire-wheel assembly in conjunction with the terrain irregularities. Tire-wheel non uniformities in truck wheels such as geometric imperfections and mass concentrations can lead to measurable dynamic tire force variations, which studies have been associated with ride discomfort and road damage. Dynamic force variations due to unbalance and non uniformities occur in the vicinity of the wheel rotation frequency and higher harmonics [1]. The operating speed of the vehicle thus plays a major role in the ride dynamics and road damaging effects of wheel unbalance and non-uniformity.

In order to study the dynamic behavior of the vehicles, a vast number of ride models have been developed which invariably neglect the effects of wheel unbalance and non-uniformity. The model selected for the purpose of vibration analysis is largely dependent on the objective of the analysis. A common first step usually involves developing an

analytical model of vehicle-terrain dynamical system comprising physical relations for the basic components. Over the years, a number of analytical models of varying complexities have been developed to represent each of the subsystems of the vehicle-terrain system. The normal selection process consists of choosing the appropriate model through the trade-off between the analytical complexity and simulation realism [2].

The roll motions of the road vehicles with low center of gravity height are known to be considerably smaller in magnitude. Moreover, the wheelbase of majority of ground vehicles (the longitudinal distance between centers of the front and rear axles) is significantly larger than the track width (lateral distance between the wheels). The vehicular roll motions can thus be considered negligible compared to magnitude of vertical and pitch motions to realize a simplified pitch plane model [3]. These models can be used to study the ride dynamics and tire force responses subjected to road and self-excited vibration sources, such as wheel unbalance and nonuniformities. The dynamic interactions between the road and tire can be modeled using a variety of tire models reported in published studies [2].

The unbalanced forces and moments due to wheel unbalance and nonuniformities as mentioned above can cause ride vibration in the frequency range to which human occupant is more sensitive. *Static* and *dynamic balancing* procedures are applied to achieve force and moment balance of the wheels. Vehicle and tire manufacturers, however, generally specify the amount of weight that can be added to a certain size and type of tire and wheel assembly. Nevertheless, vehicle manufacturers can still find assemblies that have unacceptable imbalances, especially under the dynamic balance screening. Since the use of dynamic balance screening is becoming more widespread,

there is a need to study the contributions of tire and wheel to the assembly so that reasonable component specifications can be defined [4].

This dissertation research is therefore directed towards analyzing the effects of wheel nonuniformities and unbalance on ride and road damage potential at various speed and road conditions.

1.2 REVIEW OF RELEVANT LITERATURE

Reported studies on tire modeling, vehicle modeling, effects and modeling of nonuniformities and unbalance in tire/wheel assembly and ride comfort assessment criteria are thoroughly reviewed to enhance the focus of study and to identify appropriate analytical methods. The highlights of the reported studies are grouped under different relevant topics and briefly described in the following sections.

1.2.1 AN OVERVIEW AND COMPARISON OF TIRE MODELS

Ride dynamic analysis of the vehicle traversing over varying road conditions and also subjected to the self excited vibration generally demands for accurate modeling of the vehicle-terrain dynamical system. The selection (and justification) of the tire model is a difficult task since a wide range of model formulations exist. The complexity of the tire-road interactions compound the problem since models that are more sophisticated than necessary lead to high penalty in terms of setup time and computing cost [2].

The most extensively used tire model in vehicle simulations is the point contact tire model which represents a wheel by an equivalent vertical spring/damper unit having a single ground contact point directly beneath the wheel center [2]. The main advantage of

the point contact model is that it is very simple to set-up for simulation purposes. The net foot-print force resulting from the vertical motion of wheel relative to the terrain is assumed to act normal to the local terrain surface. Thus, a horizontal component of net foot-print force is generated whenever the local terrain profile is inclined to the horizontal, and is related to the vertical component through the tangent of the local profile angle. Several variations of this model have been reported in the literature. These include: (a) A single linear spring [5]; (b) A linear spring whose stiffness depends on lateral force [6]; (c) A linear spring and viscous damper [7, 8, 9, 10]; (d) A linear spring with wheel hop capability [7]; (e) A damped linear spring and damper with wheel hop capability [5, 9]; (f) A linear spring with an elastic stop and wheel hop capability [11]; and (g) A linear spring and damper with elastic stop [9]. All these models have been primarily restricted to consideration of the vertical tire force component, and, with one exception which analyses for the fore-and-aft force [7]. Ride dynamic responses obtained from the linear and nonlinear tire motions for various vehicles and terrain models have been documented in many studies [5, 8, 9, 10]. The validity of the point contact model has not been demonstrated through a systematic study of tire forces derived from the experimental data or from a more sophisticated analytical model.

Several other tire models have been described in the literature in which the terrain contact occurs through finite footprint area rather than at a single point.

Kozin and Bogdanoff [12, 13] described a fixed footprint tire model for application in a linearized vehicle simulation, to determine the effects of wheelbase and other parameters on vehicle vibration levels. In this work, only vertical tire forces are considered and tire is represented by a number of linear parallel springs distributed

uniformly over a footprint of constant length and constrained to remain in ground contact (i.e., no wheel hop). A similar tire model is also described by Schuring [7].

A more sophisticated tire model has been developed by Lessem [14], and is included in the Army Mobility Code (AMC) [15]. In this model the tire is divided into several radial segments, and each segment is assumed to deflect independent of the adjacent segments as it enters the contact zone. By assuming each segment with an equivalent stiffness, the force in each deformed segment can be found from the localized deflection. The total tire force is then computed from the sum of those caused by individual segments. The study also obtained vertical and fore-and-aft force due to the tire as it moved slowly over a cleat. The comparisons of the predicted forces and deflection with the measured data showed reasonably good agreements. Davis [16] applied the same methodology by considering radial stiffness of various independently deflecting segments of a tire. The total force derived from the radial deflections of individual segments is employed to represent the terrain under the tire by an equivalent ground plane.

In all the models described above, the inflation pressure and carcass force components are not computed independently, but combined and characterized by a single equivalent stiffness obtained from the plane footprint test data. This combination implies that the carcass forces and pressure forces vary in the same manner with tire deflection. In a real tire, especially under nonplanar footprint conditions, the load sharing characteristics of the carcass and pressure forces will be substantially different. More complex analyses of the tire force components based upon different empirical formulations, have also been developed [17, 18, 19]. The model developed by Clark [17] analyzes the tire carcass as a thin damped elastic shell under internal pressure, centrifugal

loading and arbitrary footprint deformation. Unfortunately, this type of model is unsuited for dynamic analyses of vehicles which contain many wheels because general equations are complex, and amenable to solution only for some simple cases such as plane footprint loading.

Captain *et al.* [2] presented a comparison of different lumped parameter models of a pneumatic tire and demonstrated the influence of analytical tire model on the ride predictions of a wheeled vehicle subjected to undeformable terrain undulations. Four basic tire models suitable for ride dynamic simulation were adopted and formulated, namely, point contact, rigid tread band, fixed foot-print and adaptive foot-print. "Rigid tread band model" is a modified point contact model, where the point follower is replaced by a roller follower having the wheel or tread band radius. Consequently, the terrain contact is not constrained to lie vertically beneath the wheel center, but is free to move fore and aft of the wheel center depending on the local terrain profile. The motion transmitted to the wheel center is thus different from the terrain profile due to the geometrical filtering effects of the rolling wheel. A rigid tread band model can thus be referred to as an equivalent point contact model operating over a modified filtered profile. However, for gradually varying terrain profile, the filtering becomes insignificant, and the rigid tread band and point contact models are similar and yield equivalent results. "Fixed foot-print model" represents the wheel-terrain interaction through a foot print of fixed size. This model is represented as a parallel combination of various vertical springs and damping elements distributed uniformly over the fixed contact length, and has the ability to envelope the terrain irregularities through the local deformations within the foot-print. Thus, the fixed foot-print model also filters the terrain irregularities like the

rigid tread band model, where the filtering is dictated by the fixed foot-print length rather than the wheel radius. An "Adaptive foot-print model" of a tire is also considered, which comprises parallel combinations of discrete spring and damping elements, which are radially distributed over the lower circumference of the wheel. Like the fixed foot-print model, this model has the ability to envelope terrain irregularities through local deflections. The model thus permits for analysis of the net foot-print force arising from the nonplanar foot-print, which comprises both the vertical and horizontal components. The horizontal and vertical components are not related to the terrain slope alone, as in the case of point contact and rigid tread band models. The footprint size and the orientation relative to the wheel center changes, depending upon the radial portion of wheel in contact with the terrain profile and elevation of the localized terrain profile. The four tire models were compared through a ride simulations of a 5 ton, 6x6 cargo truck, which is a three axle military truck having an independent suspension in the front and bogie suspension in the rear. The truck was modeled as a six-degrees-of freedom dynamical system comprising pitch and bounce motions associated with vehicle sprung body, bounce motion of front wheel and axle assembly, and bounce (for wheel pair) and pitch motions for rear bogie assembly configuration. The study concluded that the point contact and rigid tread band models consistently over-estimate the transmitted vertical tire forces, particularly in the frequency range 1-100 Hz, while the fixed foot-print model under estimates the tire forces. Moreover, a nonlinear point contact model yields more frequent wheel-hop. Adaptive foot-print tire model showed a relatively closer agreement with the field-measured tire force spectra.

In 1986, Creighton [21] reported a revised vehicle ride prediction module for military vehicles, referred to as VEHDYN II. It is improved version of the AMC-74 Vehicle Ride Dynamic Module (VEHDYN) [22]. VEHDYN II predicts the gross motions of a tracked or wheeled vehicle traversing over an arbitrary non-deformable terrain at a constant forward speed, and computes the average absorbed power (ride performance criterion) and peak vertical acceleration at the driver's location or any other specified location in the vehicle (shock performance criterion). Although the basic vehicle-terrain simulation model is the same as in the previous version, VEHDYN, the analytical models for sub-systems, such as suspension spring and damping characteristics, and dynamic wheel-track-terrain interactions were modified. In particular, the dynamic wheel-track-terrain interface was modeled using the concept of a continuous ring of radial springs instead of discrete radially segmented group of springs.

Dhir and Sankar [20] investigated the ride quality of high mobility wheeled/tracked off-road vehicles implementing the continuous radial spring tire model proposed by Creighton [21]. They further proposed an effective algorithm for fast and accurate computation of the wheel-terrain contact patch. The new method was based on a simple *circle-line intersection*, and was found to be more accurate and 5 to 6 times faster than the previous approach of dividing the wheel into a sufficient number of segments, and establishing the end points of tire contact patch by checking the elevation of each segmented point with respect to the terrain profile elevation at the respective horizontal location. A multi-purpose ride dynamic simulation model (RIDSIM) was developed and proposed as an effective and precise tool to study and improve the ride comfort and safety, and thus the performance of wheeled /tracked off-road vehicles.

More recently, Wang [23] carried out dynamic analysis and ride quality assessment of a tracked snowplowing vehicle using the continuous radial spring tire model and the algorithm for computation of wheel-terrain contact patch proposed by Dhir and Sankar [20]. A twelve-degrees-of–freedom ride dynamic model of vehicle was developed and analyzed through systematic considerations of the track dynamics, track-terrain interaction, road wheel suspension, snowplowing forces, road wheel-track interactions, secondary suspension and biodynamic behavior of the driver.

1.2.2 WHEEL NONUNIFORMITIES AND UNBALANCE

The reduced roughness of modern highways imposes stricter and more specific requirements on characteristics of a vehicle as a whole, and on its components. Hence, special attention is given to tire and rim as elements which contact the road and transmit all forces from vehicle to the road and from road to the vehicle [24]. It is reported that the two most obvious types of tire/wheel irregularities which excite cab shake are, unbalance and radial run-out [25].

WHEEL NONUNIFORMITIES

As is well known, a tire is very heterogeneous system. The radial, tangential and lateral stiffness variations along the wheel perimeter or variation in geometric form of tires, however affect its characteristics [26, 28, 29, 30, 31]. Kenny [29] has listed following sources of wheel assembly vibration in his investigation: (i) vehicle stud or center hub run outs, (ii) rim stud hole or hub hole eccentricities, (iii) rim flange run outs, (iv) variation in tire run outs, and (v) variations in tire stiffness.

These variations mostly arise from the misalignments or manufacturing tolerances, and cause vibratory excitations that are transmitted to rims and then to the body and the

whole vehicle. These worsen the parameters of vibratory comfort and interior vehicle noise. Excessive radial force variation of a tire-wheel assembly is the cause of a phenomenon in today's automobiles called "smooth road shake" [32]. Tire and wheel non-uniformities have been reported to be a cause of at least three kinds of vehicle disturbances, viz, smooth road shake, roughness, and thump [32]. Table 1.1 summarizes speed range, frequency range, and description of each disturbance. It is reported that the lateral force variation and lateral wheel run out are not related to smooth road shake [32]. Tire non-uniformity draws special attention because it is reported that the tire non-uniformity gets reflected in vibrations of seat cushion and steering wheel [27]. Measurements of vibration producing characteristics of the disc wheels are done by properly mounting a wheel on a freely rotating spindle; common dial indicators are positioned to measure the variations in the tire bead seat and inner vertical wall of the rim flange. The typical production values for radial and lateral run outs for truck tires range

Table 1.1: Disturbances caused by tire nonuniformities

Disturbance	**Speed Range, [km/h]**	**Description**	**Frequency Range, [Hz]**
High Speed Smooth Road Shake	80-130	Feels like unbalanced wheels; vibration feel; no audible noise.	11-17
Roughness	50-112	Low frequency rumble noise; floor pan and steering wheel vibration; sometimes feels like unbalanced prop shaft; worse on smooth blacktop roads.	30-130
Thump	32-112	Feels like a boot in tire; audible noise; floor vibration; worse on smooth blacktop roads.	30-60

from 0.10 mm to 2.38 mm [25].

Very recently, Rakheja *et al.* [33] carried out an extensive investigation to measure and analyze ride vibration environment of the Montreal metro cars. The study was basically focused on assessment of nature of whole body vibration transmitted to the operators, and the role of various operating factors. The results of the analysis revealed vibration of the car body, specifically at speeds above 60 km/h, whereas the effects of maintenance and tires were observed to be relatively small. Above 60 km/h the magnitude of vibration was observed to be predominant around 6 Hz, which is known to be detrimental to human body comfort. It has been reported that the human body is the most sensitive to vertical vibration in the frequency range of 4-8 Hz [69]. The maximum allowable tolerance of the Metro car tires for non-uniformity is approx. 2 mm (0.08 in) but the typical tires in operation revealed non-uniformities in the range 0.625 mm to 3.25 mm (0.025 in to 0.13 in). The results showed significant vibration along the vertical and roll directions, while the magnitudes of vibration along the longitudinal, lateral, pitch and yaw axes were observed to be very low.

A few models of varying complexity have been proposed to incorporate the tire-wheel non-uniformity. Stutts [34] has proposed a simple model of the effect of concentrated radial stiffness non-uniformity in a passenger car tire. The model treats the tread band of the tire as a rigid ring supported on a viscoelastic foundation. The distributed radial stiffness is lumped into equivalent horizontal (fore-and-aft) and vertical stiffness. The concentrated radial stiffness non-uniformity is modeled by treating the tread band as fixed, and the stiffness non-uniformity as rotating around it at the nominal angular velocity of the wheel. Due to loading, the center of mass of the tread band ring

model is displaced upward with respect to the wheel spindle and, therefore, the rotating stiffness non-uniformity is alternatively compressed and stretched through one complete rotation. This stretching and compressing of the stiffness non-uniformity results in force transmission to the wheel spindle at twice the nominal angular velocity in frequency, and therefore would excite a given resonance at one-half the nominal angular wheel velocity that a mass unbalance would. The forcing produced by non-uniformity is parametric in nature, thus creating the possibility of parametric resonance.

Bohler [35] investigated the generation of load spectra for the tractor chassis using multi body system package, SIMPACK, to account for the tire non circularity. The tire model based on Pacejka Similary Method [121], was used in the source code in conjunction with empirical relations. Demic [24] defined the limits of admissible peak-to-peak radial and lateral force variation, and peak-to-peak first harmonic radial and lateral force variations associated with non uniformity using vehicle vibratory model. The tire non-uniformity parameters were defined in terms of vertical seat cushion and the steering wheel rim vibrations using an optimization program. It has been reported that the tire non-uniformity yields stronger influence on the ride dynamics of a vehicle at lower speeds because of the fact that the shock absorbers absorb more high frequency vibrations than the lower frequency vibrations [36, 37].

Manufacturers have been attempting to reduce the sensitivity of vehicles to shake input forces from tire-wheel assemblies by changing suspensions, body-frame structure stiffness, tuning of engines on their rubber mounts, and so forth. However, in spite of all these efforts, tires as they are produced today have been reported to cause shaking. It is possible to make major inroads on this problem without a major improvement in tires,

wheels, or vehicles, by indexing tires on the wheels such that their run outs oppose each other, resulting in good tire-wheel assemblies. Since production tires and wheels have the same order of magnitude of first harmonic run out, it would be theoretically possible to angularly locate the tire on the wheel to reduce the run out of the assembly. This technique is referred to as "matching" the tire to the wheel and is done by indexing the tire on the wheel in such a way as to make their first harmonics subtract each other. In practice the *matching* procedure is done on a tire uniformity machine. Force variation measurements of the production tire-wheel assembly that is desired to be improved will yield the information necessary for the best angular position of the tire on the wheel [32].

WHEEL UNBALANCE

A few studies have suggested that the wheel unbalance is one of the major causes of vehicle ride discomfort. The International Standard Organization (ISO) defines unbalance as: the condition which exists in a rotor by which vibratory motion or force is imparted to its bearing as a result of centrifugal forces [38]. It relates to uneven distribution of mass about a rotor's rotating centerline [39]. The key phrase being "rotating centerline" as opposed to "geometric centerline". The rotating centerline being defined as the axis about which the rotor would rotate if not constrained by its bearings. (Also called the Principal Inertia Axis or PIA). The geometric centerline being the physical centerline of the rotor. When the two centerlines coincide, the rotor is said to be in a static balance. When they are apart, the rotor will be unbalanced which can be classified into two types; a) Static Unbalance: In which PIA is displaced parallel to the geometric centerline; and b) Dynamic Unbalance: In which the PIA and the geometric centerline do not coincide or touch.

The wheel unbalance may arise from many contributing factors including material defects such as variations in density, porosity, voids, and blowholes; fabrication defects such as defective castings, eccentric machining, and poor assembly and distortion problems such as rotational stresses, aerodynamics, and temperature changes. Many of these occur during manufacturing, others during the operational life of the machine (tire-wheel assembly) [39]. Apart from the "wheel wobble", which is one of the major factors responsible for ride discomfort, the other effects of wheel unbalance can be listed as; reduction of wheel bearing life, uneven tire wear, and transmission of high dynamic loads to the pavement leading to their rapid fatigue and premature failure.

In 1956, Srinivasan [40] carried out experimental analysis of an unbalanced wheel on *Chevrolet* sedan car and concluded that: (i) Unbalance excites two modes of vibration, bounce and wobble, simultaneously; (ii) Both wobble and bounce resonate at the same frequency; (iii) The amplitude of vibration increases as the amount of unbalance increases for the same speed; and (iv) As the amount of unbalance is increased, the vibrations begin to appear at decreasing speeds.

Cebon [1] reported that the wheel unbalance induced vibrations can sometime lead to measurable dynamic tire force variation at wheel rotation frequency (6-8 Hz) and higher harmonics. The wheel forces caused by mass unbalance are usually only significant for smooth roads, when they can be of comparable magnitudes to the forces due to road roughness excitation. Only few studies have been reported on the characterization and the effects of wheel unbalance. Long [25] has reported that the typical values of wheel unbalance mass for brake drum and hub assembly are in the range of 0.014-0.13 kg-m. In this study, the ride vibration data was measured with an on-board

accelerometer package in 6 directions. The data was transformed into quantitative "ride discomfort" numbers using an empirical model developed by NASA. The results suggested that all sources of run-out and mass imbalance contribute to ride discomfort evenly.

1.2.3 ANALYTICAL VEHICLE MODELS

The study of pavement vehicle interaction and ride quality of heavy vehicles involves the development of a representative dynamic model that closely describes the vehicle behavior. Many vehicle models ranging from linear quarter vehicle models with two degrees-of-freedom (DOF) to complex three-dimensional models with as many as 19 DOF have been reported in the literature. While the majority of the models consider the sprung and unsprung masses as rigid bodies, few models have incorporated the flexibility of the trailer structure to study the contributions due to frame bending modes [41, 42, 43]. Simple one and two DOF linear vehicle models have been used by several investigators to study the dynamic interaction of the heavy vehicle with the pavement [44, 45, 46]. Such models permit the analysis of different suspension concepts under uncoupled vertical motions in a highly convenient manner. These models, however, cannot be used to analyze the total dynamic interactions of heavy vehicles with the roads, which comprise various vibration modes associated with vertical, roll, and pitch motions of axles and sprung masses, nonlinearities due to friction, and influence of coupled suspension systems.

Many analytical and experimental studies on pavement damage and dynamic wheel loads have been reported in the literature. The primary objective of these studies is the analysis of influence of various design and operating parameters of vehicle on the

dynamic wheel loads and thus the pavement damage potential. Since the simple one-dimensional vehicle models cannot be used to predict the complex dynamics associated with heavy vehicles, a number of comprehensive two and three-dimensional vehicle models have been developed to study the tire forces and ride quality of the vehicle. Analytical models with limited number of DOF, but realistic enough to provide reasonable estimate of the tire force characteristics and ride quality are desirable for design and optimization studies [47, 48]. The majority of the studies, related to dynamic pavement vehicle interactions and ride quality, have concluded that the contributions of the roll-plane dynamics of highway vehicles are relatively insignificant [49]. Many research studies have demonstrated that a four DOF in-plane model of a single unit can be effectively used to determine vehicle behavior pertaining to dynamic tire loads and ride quality [50, 51].

Bending vibrations of the frame, that are known to exhibit bending modes in the 6 to 9 Hz frequency range, have been included in some of the reported models of heavy vehicles in order to study the contributions due to frame bending [52]. The motion imposed on the axles by frame bending is relatively small when compared to the motion induced by the resonances of the sprung and unsprung masses. Thus, the majority of the studies have concluded that the contributions of the frame bending modes to the overall dynamic behavior are insignificant [43, 52, 53]. These studies have established that the development of an analytical vehicle model for the analysis of dynamic tire forces and ride quality primarily involves the characterization of the suspension and tires. Vehicle suspension systems often exhibit non linearities associated with Coulomb friction of leaf springs and progressive hardening nature of the air springs, and variable force-velocity

properties of the dampers due to bleed and blow-off hydraulic flows. Majority of the analytical investigations, however, have been based on the assumption of linear suspension damping, while the influence of nonlinear and asymmetric suspension damping, on the dynamic behavior of the vehicle has been addressed only in a few studies [54].

Muluka [117] established an analogy between the dynamic wheel loads and ride quality performance characteristics of heavy vehicles through analysis of an in-plane vehicle model for a two axle truck, assuming negligible contributions due to roll dynamics. It was concluded that vehicle model describing the vehicle-road interactions associated with vertical and pitch modes of vibration can yield significant insight into road-and driver-friendliness performance characteristics.

More recently, Siddiqui [55] carried out assessment of ride quality and dynamic wheel load of a modern urban bus using a six degrees-of-freedom pitch plane model under measured urban road excitations. The validity of the model was demonstrated by comparing the response characteristics with available measured data. This investigation also established influence of variations in design and operating variables on the ride performance through a comprehensive parametric study.

1.2.4 ASSESSMENT METHODS FOR RIDE AND TIRE LOADS

Ride quality is concerned with driver's sensation of the terrain-induced vibration environment of a vehicle, and is generally difficult to assess. Numerous studies have been conducted to establish the ride assessment criteria for preservation of driver comfort, health, safety, and performance. Two different methods are frequently used to evaluate the whole body vibration: subjective and objective. Subjective methods are often based

upon subjective responses of vehicle ride comfort on an absolute scale and used to assess relative ride ranking of a group of vehicles, operator tolerance in relation to productivity, vibration interference with normal operator control tasks, health aspects to vocational exposure, competitive significance and cost/benefit ratio of potential ride improvement [56]. Subjective methods, however, often lead to misleading information due to a multitude of inconsistencies dependent upon age, preference, and moods of the subjects at the time of experiment. Alternatively, objective methods provide an assessment methodology based on direct measure of physical quantities such as velocity, acceleration, absorbed power, and jerk over the frequency range of interest. Over the years, numerous objective ride comfort criteria have been proposed, however, a generally acceptable criterion is yet to be established. Some of the proposed criteria are summarized below.

Goldman [59] analyzed the vibration data acquired from several sources, and deduced three comfort levels in the vertical mode in terms of acceleration and frequency contents. The comfort levels were referred to as *perceptible, unpleasant,* and *intolerable.* The vibration data used by Goldman were obtained from a variety of experiments where the subjective and physical environments varied considerably. Janeway [60] recommended exposure limits for vertical vibration of passenger cars in terms of maximum jerk in the frequency range of 0-6 Hz, and maximum acceleration for middle frequency range of 6-20 Hz. The safe limits of vibration exposure were proposed based on the survey of subjective tolerance data, which represented an attempt to set a level at which no discomfort is experienced by the most sensitive passenger.

A comparison of the Dieckman, Janeway and Goldman ride criteria revealed that the human is most sensitive to vertical vibration below 20 Hz [57]. Since the above ride assessment criteria have been established based on sinusoidal vibrations at a constant frequency, their application to assess the vehicle's random ride vibrations is questionable. Von Eldick Thieme [61] and Butkunas [62] have outlined methods for applying existing ride comfort criteria (including those mentioned above) to random vibration environment of vehicles.

Lee and Pradko [64, 65] proposed a scalar quantity called absorbed power to measure the average rate of energy dissipated by complex damped elastic properties of the human anatomy. The proposed measure was developed based on a purely mechanical approach (ride simulator tests) while excluding subjective evaluation. The average absorbed power is determined from the intensity and frequency content of the input vibration as:

$$P = \sum_{i=1}^{n} K_i a_i^{\,2} \tag{1.1}$$

where P is average absorbed power, a_i is rms acceleration at a frequency 'i' in m/s^2, K_i is absorbed power constant of the body at frequency 'i', and n is the number of discrete frequencies. The total absorbed power is computed from the scalar sum of absorbed powers associated with each of three translational axes. The absorbed power criterion has been extensively used to assess military vehicle ride due to its simplicity. It provides a single number rating of the ride environment, which is a complete function of the vibratory modes, intensities, frequency contents, body orientation, posture, etc. The absorbed power criterion is also supported by the Janeway recommended safe limits [60], particularly in the low frequency range, i.e., the 2.7 W power curve coincides very

closely with the Janeway limit up to about 5 Hz. Average absorbed power in the range of 6-10 W, is considered acceptable for off-road vehicles, and has been extensively used to assess military vehicle ride.

The ride performance of a vehicle is assessed in terms of magnitude and frequency contents of vibration transmitted to the driver's location. Human driver is known to be the most fatigue sensitive to vertical and horizontal vibrations in the 4-8 Hz and 1-2 Hz frequency range, respectively. The human sensitivity to rotational vibration is mostly in the 0.5-1.5 Hz frequency range [69]. The International Standard (ISO-2631/1, 1997) has outlined a procedure to assess the human exposure to whole-body ride vibrations in terms of overall frequency-weighted rms acceleration at the driver/passenger –seat interface. The standard defines frequency-weighting W_k for vertical vibration in the 0.5-80 Hz frequency range, and W_e for pitch vibration in the 0.1-80 Hz frequency range. The frequency weighted accelerations are computed as per the band-limiting and weighting filters, defined in ISO-2631.

FAILURE OF THE PAVEMENT

The modern road surfaces (or pavements) can be classified as *flexible, composite or rigid.* A *flexible* pavement consists of one or more layers of asphalt supported by a granular subgrade. *Composite* pavements consist of a flexible surface layer supported by a stiff Portland cement concrete (PCC) base; and *rigid* road surfaces consist of a layer of PCC on a granular foundation. Rigid pavements can further be classified according to their arrangement of steel reinforcement and joints [1]. The pavements are also classified by the volume of traffic by *high*, *intermediate* and *low type*. *High* type pavements are used for heavily trafficked principal roads and truck routes. They usually have a strong

surface layer of asphalt or Portland cement concrete, of thickness 150 mm (6 inches) or more, built on one or more layers of compacted granular material. *Intermediate* and *low* type pavements are used for moderate traffic local routes and unsealed rural roads. The primary response of a pavement is the stress, or displacement (or time derivatives thereof) at a particular point in the pavement when it is loaded by a vehicle.

Road damage refers to degradation of the structural integrity or surface profile of a road when it is trafficked by vehicles. Since roads are designed for a finite service life and are expected to deteriorate with time, it may alternatively be called wear. The most important types of road damage due to heavy vehicles are *fatigue cracking* and permanent *deformation* (or rutting)-formation of longitudinal ruts [1].

The vertical force applied to the road surface by each tire of a heavy vehicle can be separated into two components: the static load, due to weight, and a fluctuating component known as the dynamic tire force or dynamic wheel (axle) load. Both the static and dynamic components could cause road damage.

The static load depends on the geometry and mass distribution of the vehicle and the static load sharing characteristics of the suspension system. Uneven load sharing can result in unnecessarily high average tire forces with consequently high stresses and strains in the road surface and additional damage [1]. The vehicle induced road damage has been investigated using the static tire loads as a first approximation, while neglecting the dynamics of the vehicle. In 1958-60, the AASHO (American Association of State Highway Officials) performed a very large, full-scale road test in Ottawa and Illinois [70, 71]. The most important result of AASHO road test was the 'fourth power law' which had a profound influence on pavement design and operating practice throughout the

world ever since. A regression analysis on the results of the test indicated that the decrease in 'pavement serviceability' caused by a heavy vehicle axle could be related to the fourth power of its static load [72]. A 'fourth power law' was thus proposed, which has been extensively used to express the loads due to different vehicles into a number of *Equivalent Standard Axle Loads* (ESAL s), by applying the fourth power law to each axle [72, 73]. The number of ESAL s, N, attributed to static load P, is given by

$$N= (P/P_0)^n, \text{ with } n = 4. \qquad (1.2)$$

where the standard axle load P_0 is generally taken to be 80 KN, and P is the axle load of the vehicle.

This equation provided enormous simplification for pavement design, and a simple tool for evaluating the road damaging potential of vehicles. It is used universally throughout the world, for assigning road user charges for heavy goods vehicles and it will continue to be used for the foreseeable future. The validity of the 'fourth power law' is, however, questionable [75], particularly for current axle loads and axle group configurations; tire sizes and pressures; road construction; and traffic volumes: all of which are significantly different from the conditions of the AASHO road test [71, 76]. More recent research has indicated that the damage exponent n in above equation may take a wide range of values ranging from 2 to 6 [75] and 1.3 to 4.1 [77]. For composite and rigid pavements values are thought to be as high as 8 to 12 [80] and 11 to 33 [78, 79].

Gillespie *et al.* [81] performed an extensive theoretical study of vehicle-road interactions and concluded that the gross vehicle weight is the dominating factor in rutting damage, whereas the individual static axle loads are responsible for the fatigue damage. Most tandem and tri-axle truck suspension systems are designed to equalize the

static loads carried by the individual axles in a group. In practice, the effectiveness of load equalization on moving vehicles varies significantly among different suspension design [1]. Uneven static load sharing increases fatigue damage, since the power-law damage relationships accentuate the effects of more heavily loaded axles [1]. Sweatman [82] introduced the 'Load Sharing Coefficient' (LSC), defined as the ratio of mean measured wheel load to nominal static load to study the influence of load sharing on the road damage. The nominal static load was defined as the mean load acting on a single wheel in the group. The LSC is theoretically 1.0 for perfect load sharing. For a tri-axle group with leaf spring suspension, the lightest axle revealed loads, which were typically 60-70% of the most heavily loaded axle. The study reported that air suspensions, with load variation being in the vicinity of 10%, offer enhanced load equalization. Although tandem-axle suspensions generally equalize better than the tri-axle suspension groups, the walking-beam tandem suspension was observed to yield poor load sharing properties [83], which was attributed to inappropriate installation practice and incorrect torque rod location. The study further concluded that ± 5% variations in the LSC yield only insignificant fatigue damage, while the fatigue damage increases by 40-50 % when LSC approaches 1.2, depending on the axle spacing, and the type and strength of the pavement [81].

Dynamic interactions between the tire and road surface cause considerable fluctuations in the tire loads. Such fluctuations about the static load are referred to as the dynamic wheel loads (DWL) or dynamic tire forces. They normally occur at frequencies below 20 Hz. For continuous flexible or rigid pavements, the dynamic tire forces generated by the vehicles generally occur in a broad frequency band, and could follow a

Gaussian distribution [84, 85]. Dynamic tire forces generate additional dynamic stresses and strains in pavements which are thought to accelerate road surface deterioration, although the damage mechanisms are not well understood. A number of analytical and experimental studies have been carried out to assess the dynamic tire forces, their road damage potential, and to derive reliable pavement damage assessment tools. These studies have established that the magnitude of the dynamic tire loads is directly influenced by the vehicular vibration modes associated with the vertical and pitch motions of the sprung and unsprung masses [86], vehicle and axle configurations, inertial and geometric properties of the vehicle, speed, road roughness, and restoring and dissipative properties of suspension and tire [87, 88, 89]. The DWL's generated by heavy vehicles predominate in two distinct frequency ranges:

- 1.5-4 Hz, corresponding to bounce, pitch and roll mode resonant frequencies of the sprung masses, and
- 8-15 Hz, corresponding to bounce and roll mode frequencies of the unsprung masses, and 'load-sharing' pitch modes of the suspensions.

The above frequency bands associated with sprung and unsprung mass resonances correspond to roughness irregularities with wave lengths ranging from 6.9 m to 18.5m and from 1.9 m to 3.5 m, respectively, at a speed of 100 km/h. Various experimental and theoretical studies have shown that the lower frequency sprung mass modes usually dominate the dynamic tire forces on highways, except for vehicles equipped with axle group suspension with poorly damped bogie pitch modes [89]. The natural frequencies of heavy vehicles equipped with nonlinear suspension may depend upon the amplitude of vibration and thus the roughness of the road surface. The leaf-spring suspensions with

considerable interleaf friction result in lower natural frequencies under high levels of excitations. Low level excitations arising from smooth roads can result in lockup of suspension with high interleaf friction. The vehicle thus exhibits lightly damped resonant oscillations in the 3-4 Hz frequency range due to compliance of the tires. The walking beam suspensions, due to their poor pitch mode damping, and air suspensions, due to their reduced spring rate in rebound, yield high dynamic loads in the higher frequency range (8-15 Hz) associated with the resonance of the unsprung masses [86].

The dynamic wheel loads of vehicles employing multiple-axle suspensions are strongly influenced by the suspension design, and load sharing mechanism. Tandem air-spring suspensions behave largely like two independent air suspensions due to slow reaction time of the pneumatic load equalization system [90]. Although walking-beam tandem suspension yield superior load equalization during bump encounters at high speeds, their performance is deteriorated by high interleaf friction. While the walking beam suspension provides good at static load equalization, it is prone to 'tandem-hop' vibration at high speeds, resulting in relatively high dynamic loads [90]. The influence of axle spacing on the pavement wear depends on the degree to which the response under one axle is affected by the response induced by a nearby axle. Rigid pavements distribute loads over distances that are of the same order as the common axle spacing. The axle spacing is thus a factor in determining rigid pavement fatigue. The influence of axle spacing on the potential damage of flexible pavements, however, is insignificant since the stresses are more localized in the wear course of a flexible pavement. It has been established that axle spacing has only insignificant influence on the rutting [91].

The response characteristics of the road materials and structures are sensitive to vehicle speed, and thus to the roughness profile of the road interacting with the tires. Recent studies have shown that spatial repeatable dynamic loads result in rapid wear of spatially the most severely loaded locations of pavements [71, 82]. Higher speeds reduce the time duration of the application of the wheel load on a given pavement location. The decrease in exposure time can reduce fatigue and rutting of the viscoelastic material in flexible pavements [81]. As the speed increases, the peak strain under a constant moving load diminishes in amplitude and occurs behind the point of application of the load [92, 93]. The dominant frequencies of dynamic tire forces, however, may vary significantly with vehicle speed due to the phenomenon known as 'wheel-base filtering' [94, 95, 96, 97]. Although the excitations caused by the road surface roughness comprise various frequency components, the geometric effects can result in relative attenuation or amplification of certain frequency components [95]. These geometric effects depend on the spacing between axles and the vehicle speed.

The vibration of heavy trucks, transmitted through the tires to the pavement, is a major cause of pavement damage. In recent years, cross-ply tires have largely been replaced by radial-ply tires, and average inflation pressures have increased from 550 kPa to 690-760 kPa [98]. Furthermore, wide-base single tires with enhanced load capacities are replacing the dual tires, particularly for the tri-axle group suspensions. The engineering community has expressed serious concern that such changes in tires and inflation pressure may cause increased pavement damage, particularly the rutting [99]. The wide-base single tires have the potential to do more damage to the pavement due to a relatively smaller contact area. On the basis of asphalt strain measurements, Huhtala

[100] reported that wide-base single tires are likely to cause 3.5 to 7 times more damage than the dual tires. Bonaquist [101] reported that wide single tires generate pavement strains approximately twice as large as those of the dual tires under identical loads. They also generate twice the rutting damage, and four times the fatigue damage. Furthermore, wide single tires are likely to cause up to 10 times more damage than dual tires on relatively thin asphalt pavements that fail by fatigue cracking. For thicker pavements, where permanent deformation is the main mode of failure, wide single tires are likely to cause 1.5 to 2 times more damage than dual tires. For rigid pavements, wide single tires are likely to cause a relatively small increase in fatigue damage [81].

An increase in tire inflation pressure tends to increase the road damage considerably. The tire-road contact conditions, such as the contact area and the pressure distribution over the contact patch, affect the stresses and strains in the surface of the pavement, whereas the corresponding response of the lower layers depends mainly on the overall load [98, 102, 103]. From the strain measurements performed on asphalt pavement, it was reported that a 40% increase in tire pressure can increase fatigue damage by 26% [75].

The magnitudes of the dynamic tire forces strongly depend on the road surface roughness and speed of the vehicle as well as on the suspension and tire properties, vehicle configuration, geometry and mass distribution of the vehicle. The road-damaging effects of dynamic tire forces have been primarily estimated using two methods. The first approach is based upon the assumption that the loading at each point along the road is essentially random and the localized zones incur statistically similar forces leading to uniformly distributed damage along the road. The studies based upon this assumption

have estimated that the dynamic loads increase the road damage approximately by 20-30% [104, 105]. The second approach assesses the road damage through spatial repeatability of the tire forces on the basis that the peak forces applied by the heavy vehicle fleet are concentrated at specific locations along the road [106]. The heavily loaded locations along the road may thus be expected to incur up to four times more damage than that due to static loads [90].

A parameter often used to characterize the magnitude of dynamic tire forces is the dynamic load coefficient (DLC), which is defined as [89]:

$$\text{DLC} = \frac{RMS\ dynamic\ tire\ force}{Static\ tire\ force} \tag{1.3}$$

Here the RMS (Root Mean Square) tire force is estimated from the standard deviation of the random tire force. Under normal operating conditions, heavy vehicles typically yield DLC ranging from 0.05 to 0.3. Many studies have reported that the DLC increases with the increasing road roughness, speed, tire inflation pressure, and suspension stiffness [45], while the influence of roll mass moment of inertia of sprung and unsprung masses, roll center height, auxiliary roll stiffness, lateral suspension spread, track width, and cornering and longitudinal stiffness of tires on the DLC is found to be relatively insignificant [108].

From the truck manufacture's view point, suspensions and tires are identified as the most important elements in the design process, when pavement life is to be taken into account [109]. Many experimental studies have established that the properties of heavy vehicle suspensions strongly affect the magnitude of the dynamic loads transmitted to the road surfaces [110]. A reliable methodology to assess the pavement failure, however, does not yet exist due to the complex dynamics associated with the wheel-road

interactions and the pavement structure. Although considerable efforts have been made to derive effective assessment tools, the agreement between theory and experiment is often unsatisfactory [111]. Concerns on the validity of the fourth power law, variations in the vehicle configurations, and climatic effects are some of the complicating factors that can result in underestimating pavement fatigue by a factor of 100 [111, 112]. The damage caused by dynamic wheel loads is thus considered to be an area of high uncertainty [45]. It has thus been proposed that, the various vehicle configurations should be classified based on the magnitudes of tire forces, represented by the dynamic load coefficients in order to assess their road damage potentials.

1.3 SCOPE OF THE PRESENT RESEARCH WORK

From the review of literature, it is concluded that the ride dynamic environment and dynamic wheel loads of the heavy commercial vehicles could be strongly influenced by the self-excitation sources of vibration, such as the wheel unbalance and tire non-uniformity. Furthermore, the characterization and effect of the sources discussed above have been explored in a very few studies. In view of the ride comfort and road damaging potentials, it is vital to quantify the influence of varying magnitude and phase of wheel unbalance and radial run-out. It is also very essential to establish the influence of various operating factors, such as speed and road roughness, on the ride responses due to wheel unbalance and nonuniformities.

Owing to relatively small effects on the roll responses of the vehicle, a pitch plane model of the vehicle may be considered appropriate for fundamental investigation into wheel unbalance and non-uniformity.

The overall objective of this thesis is to study the effects of wheel unbalance and non-uniformity on the ride vibrations and dynamic tire force responses of a highway vehicle. The specific objectives of this thesis are:

1. To develop a comprehensive pitch plane model of a commercial vehicle to study its vibration and tire force responses to road roughness, wheel unbalance and tire non-uniformity.

2. To characterize the wheel-terrain interactions, using an adaptive foot-print tire model.

3. To characterize rotating wheel unbalance and wheel non-uniformity and to incorporate them into the vehicle model.

4. To analyze the effects of rotating wheel unbalance and wheel non-uniformity on ride performance and dynamic tire forces using three different road roughness conditions and speeds.

5. To carry out comprehensive parametric sensitivity analysis to illustrate the influence of vehicle speed and road roughness conditions in conjunction with wheel unbalance and non-uniformity on ride and tire load performance measures.

1.4 ORGANIZATION OF THE THESIS

In Chapter 2, a review of limitations of the most widely used point contact tire model is taken in the context of wheel non-uniformity and wheel unbalance. A pitch plane model is developed employing adaptive foot-print tire model. The equations of motion for the vehicle models are derived using Newton's second law of motion. Modeling of wheel unbalance and tire non-uniformity and their inclusion in the vehicle model is explained.

In Chapter 3, response evaluation of the vehicle model is presented. Vehicle as well as suspension and tire parameters are obtained from the available data. Road profile characterization is done by computing their roughness indices. Validation of the vehicle

models is done by comparing the simulation results with those from similar previous study.

In Chapter 4, a detailed analysis of wheel unbalance and tire non-uniformity is presented. A parametric sensitivity analysis is carried out to study the influence of individual as well as the combined effects of wheel unbalance and non-uniformity with varying vehicle speed and road conditions.

The highlights and the major conclusions drawn from the study with recommendations for the future work are finally presented in Chapter 5.

CHAPTER 2

DEVELOPMENT OF THE RIDE DYNAMIC MODEL

2.1 INTRODUCTION

The excitations arising from the terrain have been considered as the major external sources of vibration for ride dynamic analysis of road and off-road vehicles. The other types of sources inducing vibrations in the vehicle are self-exciting sources, which are mostly neglected in the analyses. Wheel unbalance and non-uniformities fall under the latter type and could cause considerable vibration, specifically when the vehicle operates on a smooth road [1]. Moreover, the effect of such excitation on heavy vehicle ride has been generally believed to be small due to the large weights and dimensions of such vehicles. A few studies, however, have shown that such wheel irregularities could cause appreciable vibrations in the frequency bands to which the human rider is more sensitive [1, 3]. The analyses of contributions of such factors require a mathematical model of a commercial vehicle to characterize the dynamics associated with self-exciting sources of vibration and wheel-terrain interactions. The wheel enveloping characteristics are particularly important in view of characterizing tire nonuniformities. Although vehicle suspensions exhibit strongly nonlinear force-deflection and asymmetric force-velocity characteristics, majority of the studies consider only linear suspension properties. Other studies have established insignificant contributions due to roll dynamics of the vehicle [3]. A pitch plane model of the vehicle with linear suspension properties may thus be adequate for the study of fundamental contribution due to wheel unbalance and non-

uniformity. During the modeling stage, it is usually desirable to develop a simple and credible model such that the dynamics of the vehicle is fully described. Simplicity of the model is determined by the number of its degrees-of-freedom, whereas the credibility of the vehicle model is demonstrated by its capability to simulate the vehicle behavior realistically within the desired accuracy.

In this chapter, characterization of wheel-terrain interaction, wheel unbalance, and wheel non-uniformity is described. An in-plane vehicle model is developed to study the vertical and pitch ride responses due to terrain roughness, wheel unbalance, and non-uniformity. The systematic development of the ride model is presented along with the underlying assumptions.

2.2 DEVELOPMENT OF ADAPTIVE FOOT-PRINT TIRE MODEL

2.2.1 THE POINT CONTACT TIRE MODEL, AN OVERVIEW

The point contact model is the simplest tire model for estimating the static and dynamic interaction between the tire and the road. It is represented by a parallel spring-dashpot combination (Figure 2.1) that transmits the support force from the terrain to the vehicle and contacts the ground through a point follower. Terrain contact occurs at a single point vertically beneath the wheel center. Dynamic support forces occur due to deflection of the spring and dashpot caused by the motion of the wheel relative to the terrain. The tire mass is concentrated at the wheel center, and the terrain follower is free to leave the ground to simulate the wheel hop motion.

A comprehensive study performed by Captain *et al.* [2] describes the comparison of all four different tire models including the point contact, rigid tread band, fixed foot-print, and an adaptive foot-print model, as described in section 1.2.1. The study concluded a

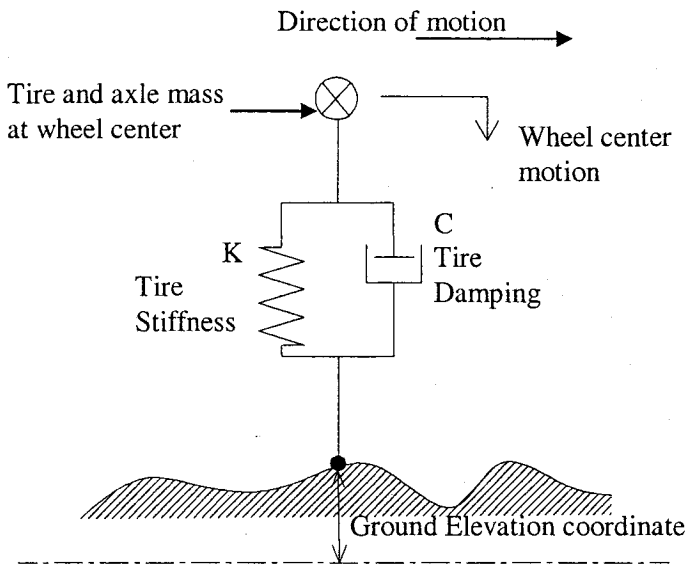

Figure 2.1: Schematic diagram of point contact tire model

point contact tire model yields vertical force predictions significantly greater than the adaptive foot-print tire model; three and one half times higher for vertical force, and eleven times higher for the fore-and aft force. Moreover, a point contact model does not permit the consideration of the mass unbalance and the radial run-out of the wheel, which would require the characterization of the periphery as an elliptical object. Furthermore, a point contact model does not permit for the consideration of the terrain enveloping property adequately.

2.2.2 ADAPTIVE FOOT-PRINT TIRE MODEL

Alternatively, an adaptive foot-print tire model can be considered to account for the radial run-out and wheel unbalance. The dynamic wheel-terrain interactions can be

realized in terms of the net foot-print force arising from the resultant motion of the wheel and sprung mass, and the terrain profile. Details regarding the modeling aspects on net foot-print force are presented in the following sub-sections.

THE NET FOOT-PRINT FORCE

The road wheel-terrain interaction is modeled based on the concept of continuous radial spring representation [21, 113], and is expanded to include damping effects. Following assumptions are made in the formulation:

- The wheel sinkage is considered negligible due to assumption of non-yielding ground.
- Shear stresses in the foot-print are negligible since braking/acceleration and turning operations are not included in the simulation model.
- The mass due to wheel assembly is assumed to be concentrated at the wheel center in the absence of mass unbalance.

As illustrated in Figure 2.2, the road wheel interaction is represented by a radially distributed continuous spring taking into account an equivalent stiffness and a damping element. An equivalent damper is incorporated to account for the dissipative characteristics of the tire.

The expression for the net foot-print force is obtained by considering a differential element of the wheel-terrain contact patch shown in Figure 2.3 and magnified sectional view along section line A-A of the wheel-terrain contact patch in Figure 2.4, which represents a radial force, dF_w applied at an angle α with respect to normal axis (n), and the corresponding radial deflection, δ, due to tire's interactions with the non-deformable terrain. The radial force is, then, expressed as:

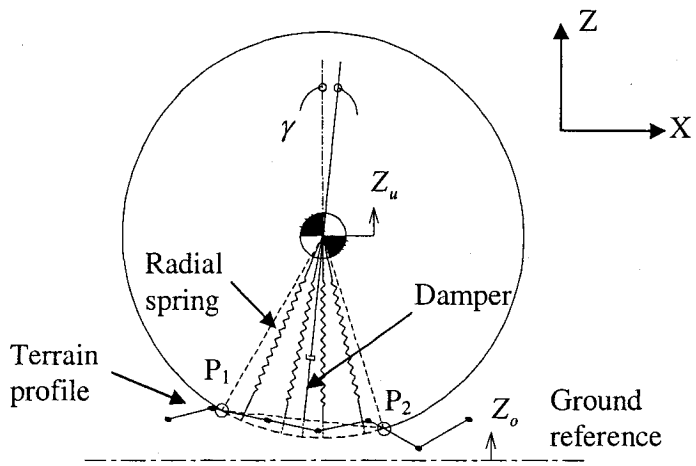

Figure 2.2: An adaptive foot-print radial tire model

$$dF_w = (K_{rw}\, d\alpha)\delta \tag{2.1}$$

where K_{rw} is the radial spring constant (N/m/rad), and $(K_{rw}\, d\alpha)$ represents an equivalent spring constant for the differential element ($d\alpha$). In Figures 2.3 and 2.4, 'n' and 't' define the normal and transverse axis of the wheel, and points P_1 and P_2 at the wheel circumference define the extreme contact locations of the tire with the terrain surface. R_w is the undeflected wheel radius. Assuming an idealized wheel deflection characterized by a straight line joining the first and last wheel-terrain contact points on the lower wheel circumference (P_1P_2), the radial deflection, δ, can, then, be conveniently expressed as:

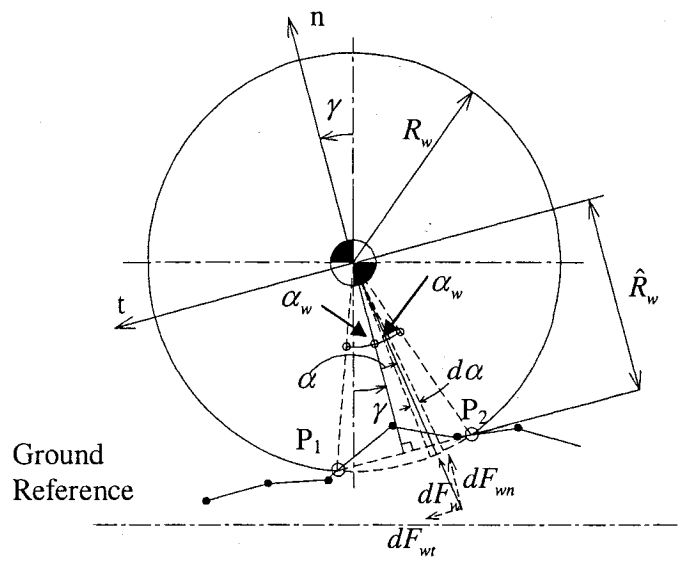

Figure 2.3: Determination of the elemental foot-print force

$$\delta = R_w - \frac{\hat{R}_w}{\cos\alpha} \tag{2.2}$$

where $\hat{R}_w$ is the deflected road wheel radius, defined by the co-ordinates P_1 and P_2 and assumption of the straight line intersection with the undeformed wheel circumference. The normal and tangential components of the elemental radial foot-print force are given as:

$$dF_{wn} = dF_w \cos\alpha \tag{2.3}$$

$$dF_{wt} = dF_w \sin\alpha \tag{2.4}$$

where dF_{wn} and dF_{wt} are the normal and tangential components of the elemental foot-print

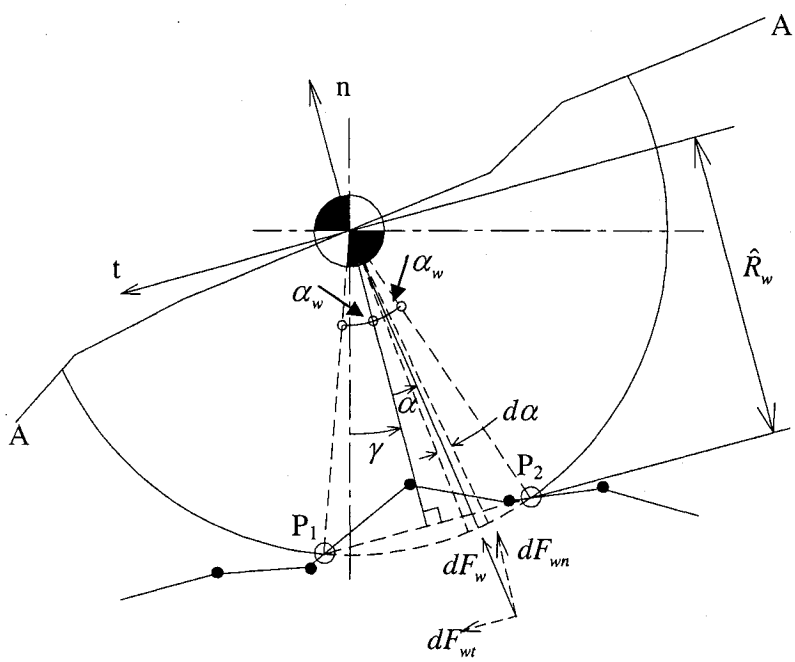

Figure 2.4: Magnified sectional view of the wheel-terrain contact patch for determination of the elemental foot-print force

force, dF_w.

Substituting equations (2.1) and (2.2) into equation (2.3), the elemental normal radial foot-print force can be expressed as:

$$dF_{wn} = (K_{rw}\, d\alpha)\left[R_w - \frac{\hat{R}_w}{\cos\alpha}\right]\cos\alpha \tag{2.5}$$

Upon integrating equation (2.5) in the limits of the entire wheel-terrain contact patch $(-\alpha_w, \alpha_w)$, the net normal foot-print force is obtained as:

$$F_{wn} = 2\,K_{rw}\,R_w[\sin\alpha_w - \alpha_w\cos\alpha_w] \tag{2.6}$$

where α_w is the one-half of the wheel-terrain contact patch angle, given as:

$$\alpha_w = \cos^{-1}\left[\frac{\hat{R}_w}{R_w}\right] \tag{2.7}$$

The radial spring constant, K_{rw}, is established by measuring the static deflection of the wheel center, δ_u, on a flat surface under a vertical static load, P, as shown in Figure 2.5. Using equation (2.6) the static force, P, can be expressed as:

$$P = 2K_{rw}R_w[\sin\alpha_{ws} - \alpha_{ws}\cos\alpha_{ws}] \tag{2.8}$$

where α_{ws} is the arc angle of the tire periphery enveloping the flat surface under the static load, P, given by:

$$\alpha_{ws} = \cos^{-1}\left[\frac{R_w - \delta_u}{R_w}\right] \tag{2.9}$$

Using equation (2.8), the radial spring constant, K_{rw}, can be expressed as:

$$K_{rw} = \frac{P}{2R_w[\sin\alpha_{ws} - \alpha_{ws}\cos\alpha_{ws}]} \tag{2.10}$$

The damping force can be conveniently incorporated in the net normal force, F_{wn}, by computing the terrain-imposed vertical velocity input at the mid-point of the wheel-terrain contact patch, given as:

$$\dot{Z}_o = V_x \tan\gamma \tag{2.11}$$

where V_x is the forward velocity of the vehicle, 'γ' is the vertical inclination of the net foot-print force at the mid-point of the tire-terrain contact patch with respect to Z-axis, as shown in Figure 2.4. This inclination is also equal to the horizontal inclination of the straight line joining two end points P_1 and P_2 of the tire-terrain contact patch. The term ($\tan\gamma$) thus accounts for the slope of terrain profile at the mid-point of contact patch, and

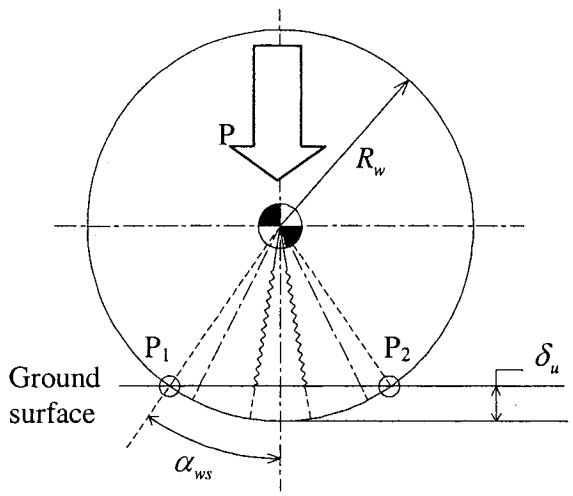

Figure 2.5: Road wheel deformation under a static load

$\dot{Z}_o$ is the terrain imposed vertical velocity input at the mid-point of the tire-terrain contact patch.

Assuming linear viscous damping due to the tire, damping force is expressed as:

$$F_{dw} = C_{rw}\,\dot{r}_w \tag{2.12}$$

where C_{rw} is the viscous damping coefficient and $\dot{r}_w$ is the normal relative velocity given as:

$$\dot{r}_w = (\dot{Z}_u - \dot{Z}_o)\cos\gamma = \dot{Z}_u \cos\gamma - V_x \sin\gamma \tag{2.13}$$

where $\dot{Z}_u$ is the vertical velocity of the wheel center.

The net normal force, F_{wn}, developed at the wheel-ground interface can thus be rewritten as:

$$F_{wn} = 2K_{rw}R_w[\sin\alpha_w - \alpha_w\cos\alpha_w] + F_{dw} \tag{2.14}$$

The net tangential component F_{wt}, is, however, equal to zero due to assumed equilateral construction of contact patch triangle (as shown in Figure 2.3) under both static and dynamic conditions.

WHEEL-TERRAIN CONTACT PATCH

The wheel-terrain contact patch has to be established in order to calculate the net foot-print force using equation (2.14). The contact patch angle, β, and the horizontal inclination of the line, P_1P_2, or the vertical inclination of the net foot-print force, γ, are computed in an adaptive manner from the local co-ordinates of the road profile. The contact patch angle as shown in Figure 2.6 is obtained as: $\beta = \beta_2 - \beta_1$, where, β_1 and β_2 define the angular positions of the extreme contact points P_1 and P_2, respectively, and given by:

$$\beta_1 = \tan^{-1}((Z_1 - Z_w)/(X_1 - X_w)) \text{ and } \beta_2 = \tan^{-1}((Z_2 - Z_w)/(X_2 - X_w)) \tag{2.15}$$

where, (X_w, Z_w) are the instantaneous coordinates of the road wheel center, while (X_1, Z_1) and (X_2, Z_2) represent the coordinates of the first and last wheel-terrain contact points (P_1 and P_2), respectively. The angle γ describes the inclination of the net foot-print force with respect to fixed Z-axis, and is computed as:

$$\gamma = \beta_1 + \alpha_w - 1.5\pi \tag{2.16}$$

where, $\alpha_w = \beta/2$

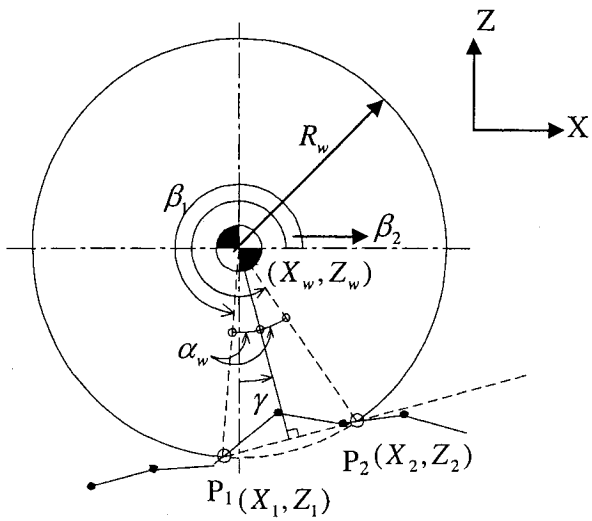

Figure 2.6: Wheel-terrain contact patch

It is apparent that determination of the wheel-terrain contact points, P_1 and P_2, along the lower circumference of the road wheel, is essential in order to compute the orientation and magnitude of the net foot-print force, as it is evident from equations (2.6), (2.7), (2.14), and (2.16). The computational procedure [20] to establish first and last points (P_1, P_2) of the wheel-terrain contact patch, involves the following steps:

(a) Terrain profile points, N_S, which lie within the *shadow* of a given wheel are established as: X_{Sn}, Z_{Sn}, $n = 1,2,3,...,N_S$, where the *shadow* is defined by the horizontal range between $X_w - R_w$ and $X_w + R_w$, as shown in Figure 2.7.

(b) The terrain profile points which lie inside the wheel are, then, identified using the following criteria based upon the distance formula in geometry for determination of distance between two points,

$$\left\{Z_w - \sqrt{R_w{}^2 - (X_{Sn} - X_w)^2}\right\} - Z_{Sn} < 0; n = 1, 2, 3, ..., N_S \qquad (2.17)$$

and are indicated by N_I, where $N_I < N_S$.

(c) Once the points inside the wheel, N_I, are determined, the first and last profile points which lie inside the wheel are identified in order to establish the L.H.S. (Left Hand Side) and R.H.S. (Right Hand Side) profile segments intersecting the wheel and to compute the corresponding appropriate intersection points (P_1, P_2).

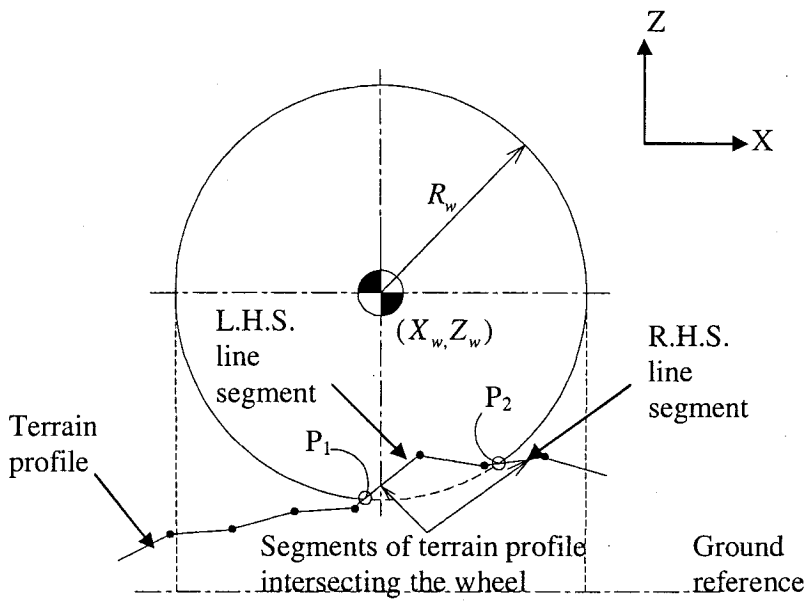

Figure 2.7: Determination of wheel-terrain contact patch based on circle-line intersection

The approach to compute the wheel-terrain contact patch is based on circle-line intersection [20]. Basis of this computational procedure can be described by considering a circle intersected by a line, as illustrated in Figure 2.8, where circle and line represent a wheel of specified radius (R_w) and center co-ordinates (X_C, Z_C), and two linear segments of the terrain profile intersecting the circle, L.H.S. segment with specified end points ($X_{L1}, Z_{L1}; X_{L2}, Z_{L2}$) and R.H.S. segment with specified end points ($X_{R1}, Z_{R1}; X_{R2}, Z_{R2}$).

The coordinates of the center (X_C, Z_C) change with time and can be derived from the following equation:

$$X_C = V_x t \tag{2.18}$$

$$Z_C = R_w - \{(Z_u(t) - \delta_u - Z_o(t)\} \tag{2.19}$$

where V_x is the forward velocity of the vehicle in m/s, t is time in s, and δ_u in m is the vertical static deflection of the wheel along fixed Z-axis.

The equation of the circle can be written as:

$$Z_c = Z_C \pm \sqrt{R_w^{\,2} - (X_c - X_C)^2} \tag{2.20}$$

where X_c and Z_c are the coordinates of any point on the periphery of the circle.

This equation yields two values of Z_c, which correspond to elevations of arbitrary points located on upper-half and lower-half of the circle circumference at the longitudinal location, X_c. Since, the wheel-terrain contact occurs along the lower-half circumference only, the circle equation can be rewritten as:

$$Z_c = Z_C - \sqrt{R_w^{\,2} - (X_c - X_C)^2} \tag{2.21}$$

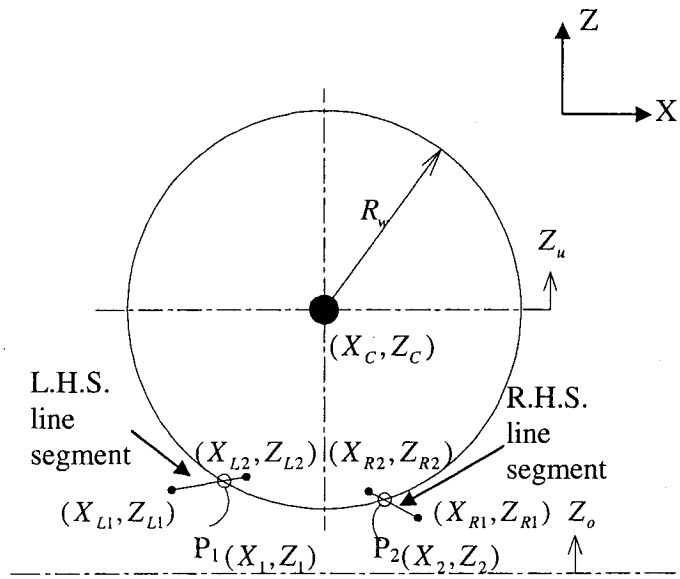

Figure 2.8: Circle-line representation

The equation describing the L.H.S. line is given as:

$$Z_1 = Z_{L1} + m(X_1 - X_{L1}) \tag{2.22}$$

where, $m = \dfrac{Z_{L2} - Z_{L1}}{X_{L2} - X_{L1}}$ is the slope of the L.H.S. line and (X_1, Z_1) is any arbitrary point along that line.

At the circle-line intersection points, the following condition is satisfied,

$$X_c = X_1 \text{ and } Z_c = Z_1 \tag{2.23}$$

Let, $X_c = X_1 = X$ and $Z_c = Z_1 = Z$.

Therefore, following quadratic equation is derived from equations (2.21) and (2.22) in conjunction with the above mentioned condition.

$$aX^2 + bX + c = 0 \tag{2.24}$$

where, $a = 1 + m^2$; $b = 2(Am - X_C)$; $c = A^2 - R^2 + X_C^2$

and $A = Z_{L1} - Z_C - m X_{L1}$

The solution of the equation (2.24) yields two values of the X coordinate, considering the elevation of the terrain profile and dimensions of the circle, the higher value can not be accepted and thus the lower value of X corresponds to X_1, the X-coordinate of intersecting point of the circle and L.H.S. line segment. Subsequently, elevation of intersection point Z_1 can be obtained by substituting horizontal co-ordinate X_1 into either equation (2.21) or (2.22) in conjunction with equation (2.23). Thus (X_1, Z_1) locate the point P_1, as shown in Figures 2.6 and 2.8. Using the similar procedure described above, the intersection point of the circle and the R.H.S. line segment, P_2 (X_2, Z_2) is determined.

2.3 DEVELOPMENT OF PITCH PLANE MODEL OF THE VEHICLE

An in-plane model of a two axle truck is represented as shown in Figure 2.9. This model is formulated to study its interactions with the road in terms of vertical tire loads transmitted to the road, and vertical acceleration transmitted to the driver station, assuming negligible contributions due to roll dynamics of the vehicle. The vehicle body, chassis and cargo are characterized by a rigid sprung mass M_s with two-degrees-of-freedom (DOF): vertical and pitch. The front and composite rear wheel and axle assemblies are represented by rigid masses, referred to as unsprung masses, with only vertical DOF. Each unsprung mass is coupled to the sprung mass through the respective

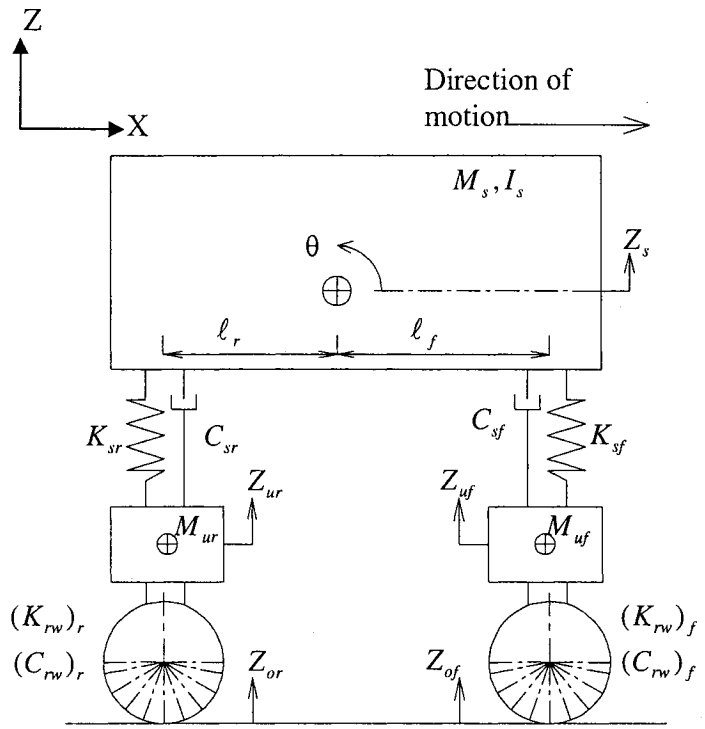

Figure 2.9: In-plane model representation of a straight truck

suspension components, modeled as parallel combinations of energy restoring and dissipative elements. The front and rear axle tires are modeled using adaptive foot-print tire model, as described in section 2.2. The contributions of the frame bending modes to the vibration behavior of the vehicle are considered to be insignificant due to relatively small deflections of the frame, and location of the suspensions near the nodes. The equations of motion of four-DOF in-plane vehicle model are derived using Newton's second law of motion and are expressed as:

$$M_s\ddot{Z}_s + F_{SF}(Z_s, Z_{uf}, \theta, t) + F_{SR}(Z_s, Z_{ur}, \theta, t) + (M_s g) = 0,$$

$$I_s\ddot{\theta} + \ell_f F_{SF}(Z_s, Z_{uf}, \theta, t) - \ell_r F_{SR}(Z_s, Z_{ur}, \theta, t) = 0,$$

$$M_{uf}\ddot{Z}_{uf} - F_{SF}(Z_s, Z_{uf}, \theta, t) + (F_{wz})_f + \left[\frac{M_s g \ell_r}{L}\right] + (M_{uf} g) = 0,$$

$$M_{ur}\ddot{Z}_{ur} - F_{SR}(Z_s, Z_{ur}, \theta, t) + (F_{wz})_r + \left[\frac{M_s g \ell_f}{L}\right] + (M_{ur} g) = 0. \qquad (2.25)$$

where M_s, M_{uf} and M_{ur} are the masses due to sprung weight of the vehicle, and front and rear axles, respectively. I_s is the pitch mass moment of inertia of the sprung weight about its centroid. Z_s and θ denote the vertical and angular displacements, respectively, of the sprung weight, and Z_{uf} and Z_{ur} denote the vertical displacements of the front and rear unsprung weights respectively. ℓ_f and ℓ_r denote the horizontal distances between center of gravity of the sprung mass and the front and rear axles, respectively.

F_{SF} and F_{SR} are suspension forces developed by the front and rear suspension, respectively. The suspension forces depend upon the type of suspension employed in the vehicle. Heavy vehicles employ leaf spring or air suspension together with a hydraulic damper. Assuming linear stiffness and damping properties of the suspension components, the forces can be expressed as:

$$F_{SF}(Z_s, Z_{uf}, \theta, t) = K_{sf}(Z_s - Z_{uf} + \ell_f\theta - \delta_{SF}) + F_{DF},$$

$$F_{SR}(Z_s, Z_{ur}, \theta, t) = K_{sr}(Z_s - Z_{ur} - \ell_r\theta - \delta_{SR}) + F_{DR}. \qquad (2.26)$$

where K_{sf} and K_{sr} are the linear or equivalent spring rates due to front and rear suspension springs, and δ_{Si} is the static deflection of the suspension $i(i = F, R)$, expressed as:

$$\delta_{SF} = \frac{M_s g}{K_{sf}}\left(\frac{\ell_r}{L}\right),$$

$$\delta_{SR} = \frac{M_s g}{K_{sr}}\left(\frac{\ell_f}{L}\right). \tag{2.27}$$

F_{DF} and F_{DR} are the respective damping forces given by:

$$F_{DF} = C_{sf}(\dot{Z}_s - \dot{Z}_{uf} + \ell_f \dot{\theta});$$

$$F_{DR} = C_{sr}(\dot{Z}_s - \dot{Z}_{ur} - \ell_r \dot{\theta}). \tag{2.28}$$

The tires are modeled using adaptive foot-print tire model, which renders a contact patch at the interface of the tire and the road. $(F_{wz})_f$ and $(F_{wz})_r$ are the net vertical forces developed by the front and composite rear axle tires, expressed as:

$$(F_{wz})_f = (F_{wn})_f(\cos\gamma_f); \qquad \text{for } (F_{wn})_f > 0$$

$$(F_{wz})_r = (F_{wn})_r(\cos\gamma_r); \qquad \text{for } (F_{wn})_r > 0$$

where the net foot-print forces, $(F_{wn})_f$ and $(F_{wn})_r$ are obtained from equation (2.14), and γ_f and γ_r are the vertical inclinations of the net foot-print forces arising from the front and rear tires, which are obtained from equation (2.16). $(F_{st})_f$ and $(F_{st})_r$ are the total static loads on the front and rear wheels respectively.

2.4 MODELING OF WHEEL UNBALANCE

Wheel unbalance is caused by the uneven distribution of mass about the wheel center. The wheel unbalance may be caused by many factors, such as, manufacturing defects/constraints, fabrication problems, operational effects, brake system design, etc. Cebon [1] reported that the wheel unbalance induced vibrations can sometime lead to

measurable dynamic tire force variation at wheel rotation frequency (6-8 Hz) and higher harmonics.

An experimental analysis of an unbalanced wheel on *Chevrolet* sedan car was carried out by Srinivasan [40]. The following conclusions were reported; (i) Unbalance excites two modes of vibration, bounce and wobble, simultaneously; (ii) Both wobble and bounce resonate at the same frequency; (iii) The amplitude of vibration increases as the amount of unbalance increases for the same speed; and (iv) As the amount of unbalance is increased, the vibrations begin to appear at decreasing speeds. Only few studies have been reported on the characterization and the effects of wheel unbalance.

Kenny [29] analyzed six sources of wheel assembly vibration including uneven tire weight distributions. A three phase approach was applied to quantify each source: (i) an objective ride test was conducted, (ii) a subjective ride evaluation was used to correlate the objective data into specific levels of discomfort defined by NASA [120], and (iii) a vibration analysis was conducted to confirm the results. The centrifugal force due to rotating tire imbalance was quantified as the product of the magnitude of mass unbalance, the centroidal radius of the tire, and square of the angular velocity of the tire.

Ahmed [3] reported a linear quarter car vehicle model considering the effect of the self exciting source of vibration, the wheel unbalance. The force due to unbalance was modeled as harmonic force which gets included in the equation of motion of the unsprung mass of the vehicle. In this study, the frequency response functions have been derived for the ratios of sprung mass displacement to the mass unbalance force as well as unsprung mass displacement to the mass unbalance force.

Although the unbalance may exist in any plane of the wheel, the analyses in this dissertation is limited to wheel unbalance in the longitudinal (X-Z) plane. Figure 2.10 shows unbalanced mass m_i located at an eccentricity e_i and making angle ϕ_i with the wheel center. The total unsprung mass of the wheel and axle assembly is represented by M_{ui}. Considering the undeflected position of the center of gravity of unsprung mass, the displacement of the unbalanced mass m_i can be expressed as:

$$Z_{mi} = Z_{ui} + e_i \sin \phi_i - \delta_{ui} \tag{2.29}$$

where Z_{mi} is the vertical deflection of the rotating unbalanced mass. For a given angular speed ω, the acceleration of m_i can be obtained as:

$$\ddot{Z}_{mi} = \ddot{Z}_{ui} - e_i \omega^2 \sin \omega t \tag{2.30}$$

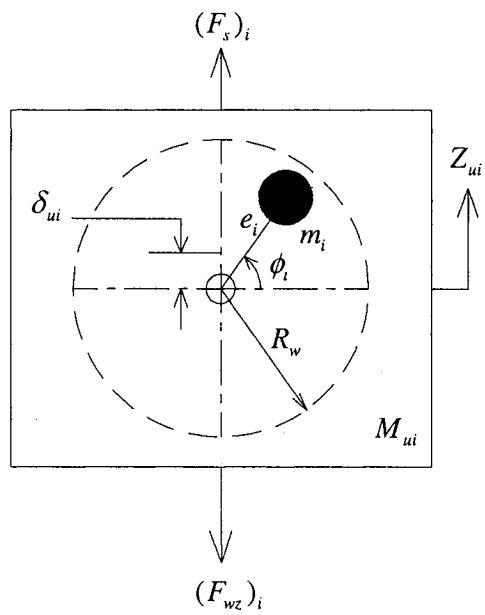

Figure 2.10: Representation of wheel unbalance ($i = f, r$)

where the angular velocity of the wheel in rad/s and can be expressed as a function of the forward speed V_x, such that : $\omega = \frac{V_x}{R_w}$

EQUATIONS OF MOTION

The equations of motion derived in section 2.3 can be modified to include the effect of wheel unbalance. The equations of motion describing the vertical and pitch motions of the sprung mass remain unchanged, while the equations of motion for the unsprung masses are derived to include the excitation forces caused by the rotating unbalance.

$$M_{uf}\ddot{Z}_{uf} - F_{SF}(Z_s, Z_{uf}, \theta, t) + (F_{wz})_f + \left[\frac{M_s\, g\, \ell_r}{L}\right] + (M_{uf}\, g) = m_f e_f \omega^2 \sin(\omega t - \phi_f),$$

$$M_{ur}\ddot{Z}_{ur} - F_{SR}(Z_s, Z_{ur}, \theta, t) + (F_{wz})_r + \left[\frac{M_s\, g\, \ell_f}{L}\right] + (M_{ur}\, g) = m_r e_r \omega^2 \sin(\omega t - \phi_r). \quad (2.31)$$

where m_i is the mass due to rotating unbalance of the wheel $i (i = f, r)$, and e_i is the corresponding eccentricity. The angles ϕ_f and ϕ_r are introduced to account for the phase difference between the front and rear wheels mass unbalance, as shown in Figure 2.11.

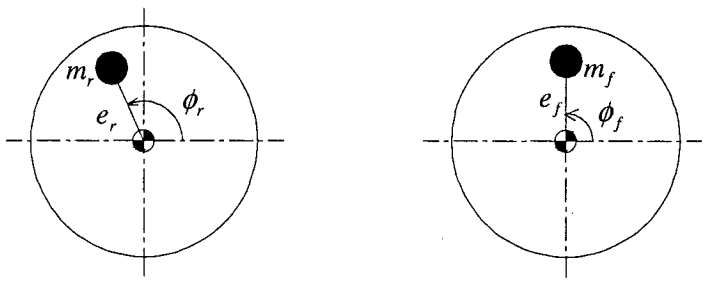

Figure 2.11: Representation of phase angles of the mass unbalance at front and rear wheels

2.5 MODELING OF WHEEL NON-UNIFORMITY

Wheel non-uniformity can be defined as radial, tangential or lateral geometric variation of the tire or the rim. Among these three factors, it has been reported that the radial variation (or radial run-out) is the most significant source of vibration in the vehicle [32]. The radial run-out of a tire could cause increased vehicle vibration and large variation in the dynamic tire force.

A few models of varying complexity have been proposed to incorporate the tire-wheel non-uniformity. Stutts [34] has proposed a simple model of the effect of concentrated radial stiffness non-uniformity in a passenger car tire. The model treats the

tread band of the tire as a rigid ring supported on a viscoelastic foundation. The distributed radial stiffness is lumped into equivalent horizontal (fore-and-aft) and vertical stiffness. The concentrated radial stiffness non-uniformity is modeled by treating the tread band as fixed, and the stiffness non-uniformity as rotating around it at the nominal angular velocity of the wheel. Due to loading, the center of mass of the tread band ring model is displaced upward with respect to the wheel spindle and, therefore, the rotating stiffness non-uniformity is alternatively increased and decreased through one complete rotation. This stretching and compressing of the non-uniformity results in force transmission to the wheel spindle at twice the nominal angular velocity in frequency.

Bohler [35] investigated the generation of load spectra for the tractor chassis using multi body system package, SIMPACK, to account for the tire non circularity. The tire model based on Pacejka model [121], was used in the source code in conjunction with empirical relations.

Demic [24] defined the limits of admissible peak-to-peak radial and lateral force variation, and peak-to-peak first harmonic radial and lateral force variations associated with non uniformity using vehicle vibratory model. The tire non-uniformity parameters were defined from the aspect of vertical seat cushion and the steering wheel rim vibrations using an optimization program. It has been reported that the tire non-uniformity yields stronger influence on the ride dynamics of a vehicle at lower speeds because of the fact that the shock absorbers absorb more high frequency vibrations than the lower frequency vibrations [36, 37].

Kenny [29] analyzed six sources of wheel assembly vibration including, vehicle stud run-out, hub hole eccentricities, rim flange run-outs, variations in tire run-outs, variations

in tire stiffness, and uneven tire weight distributions. It has been reported that each run-out induces both spring and imbalance forces to occur because the tire is forced out of round. The total force due to each type of run-out was quantified as summation of radial force (product of the tire's spring constant and the magnitude of the particular eccentricity) and the imbalance centrifugal force due to the particular run-out (product of mass of the tire-rim assembly, the magnitude of run-out, and square of the angular velocity of the tire).

Ni [4] proposed a mathematical model to account for radial and lateral run outs of the tire-wheel assembly. It has been reported that a tire mounted on the eccentric wheel is forced to be eccentric from the center and produces a new static imbalance, the wheel radial run-out first harmonic effect on the tire. The equation for radial run-out effect on the tire was formulated in terms of mass of the tire, peak to peak first harmonic of wheel radial run-out, and wheel flange radius.

In order to characterize the radial run-out of the wheel, the wheel can be assumed to have an elliptical shape having semi-major axis a and semi-minor axis b, and radius r' along with circle with radius r as shown in Figure 2.12. The co-ordinates of any point on the periphery of an ellipse can be expressed in the polar form as:

$$\begin{aligned} x &= r'\cos\theta' \\ z &= r'\sin\theta' \end{aligned} \tag{2.32}$$

where r' is the radius of the ellipse from the center and θ' is the angular displacement of the radius.

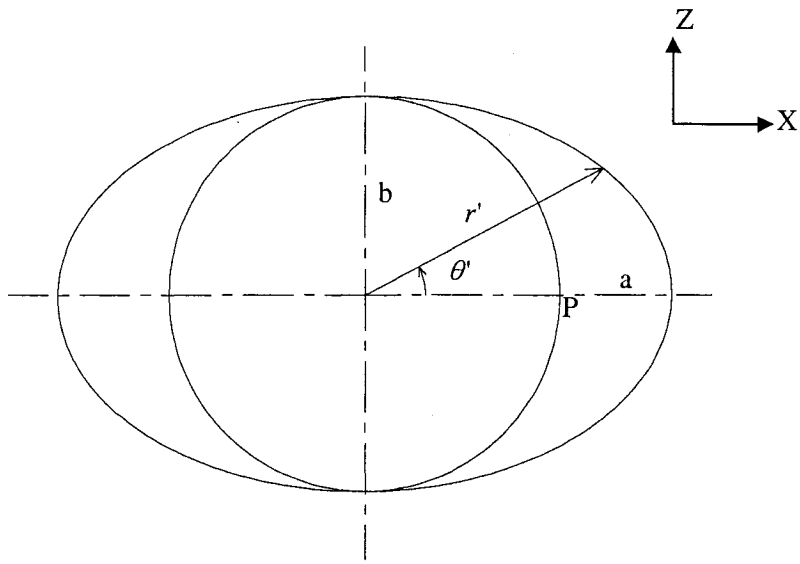

Figure 2.12: Representation of wheel non-uniformity

The equation of an ellipse can be expressed in terms of the polar co-ordinates r' and θ', such that:

$$r' = \sqrt{\frac{a^2 b^2}{b^2 \cos^2 \theta' + a^2 \sin^2 \theta'}} \tag{2.33}$$

$$r = b \tag{2.34}$$

Considering that a uniform wheel forms a circle of radius r (r = b), the radial difference between the elliptical and a circular form can be derived as a function of θ', such that:

$$(\Delta r) = r' - r = \sqrt{\frac{a^2 b^2}{b^2 \cos^2 \theta' + a^2 \sin^2 \theta'}} - b \tag{2.35}$$

where Δr defines the radial run-out of a wheel in terms of radial deviation of the wheel periphery from that of a uniform circular wheel.

The expression for the maximum value of Δr at a specific value of θ' can be derived as follows:

Using equation (2.35),

$$(\Delta r) = r' - r = b\left[\frac{1}{\sqrt{\frac{b^2}{a^2}\cos^2\theta' + \sin^2\theta'}} - 1\right] \tag{2.36}$$

For (Δr) to have the maximum value, we must have,

$$(\Delta r)_{\max} = \frac{\partial \Delta r}{\partial \theta'} = 0.$$

Therefore, using equation (2.36), we have,

$$\frac{\partial \Delta r}{\partial \theta'} = \frac{\frac{1}{2}(\frac{b^2}{a^2} + 1)\sin 2\theta'}{[\frac{b^2}{a^2}\cos^2\theta' + \sin^2\theta']^{3/2}} = 0. \tag{2.37}$$

The equation (2.37) gives,

$\frac{1}{2}(\frac{b^2}{a^2} + 1)\sin 2\theta' = 0$, and this equation has two possible solutions,

$(\frac{b^2}{a^2} + 1) = 0$ or $\sin 2\theta' = 0$. It can be noted that the first solution is not feasible and hence accepting the second solution, $\sin 2\theta' = 0$, we get, $2\theta' = 0, \pi, 2\pi, 3\pi, \ldots$

Therefore, $\theta' = 0, \frac{\pi}{2}, \pi, \frac{3\pi}{2}, \ldots.$

Substituting the first possible value of θ' in equation (2.35), we get,

$$(\Delta r)_{\max} = a - b \tag{2.38}$$

The locus traced by this radial difference (Δr) with respect to θ' about point 'P' (end point on the circle along X-axis), as shown in Figure 2.12, for one revolution can be plotted as shown in Figure 2.13. The values of parameters used are, a=0.503 m and b=0.5 m for $\theta = (0, 2\pi)$. It can be observed that, according to equation (2.38), the maximum value of Δr is the difference between semi-major and semi-minor axes of an ellipse, 'a' and 'b' respectively.

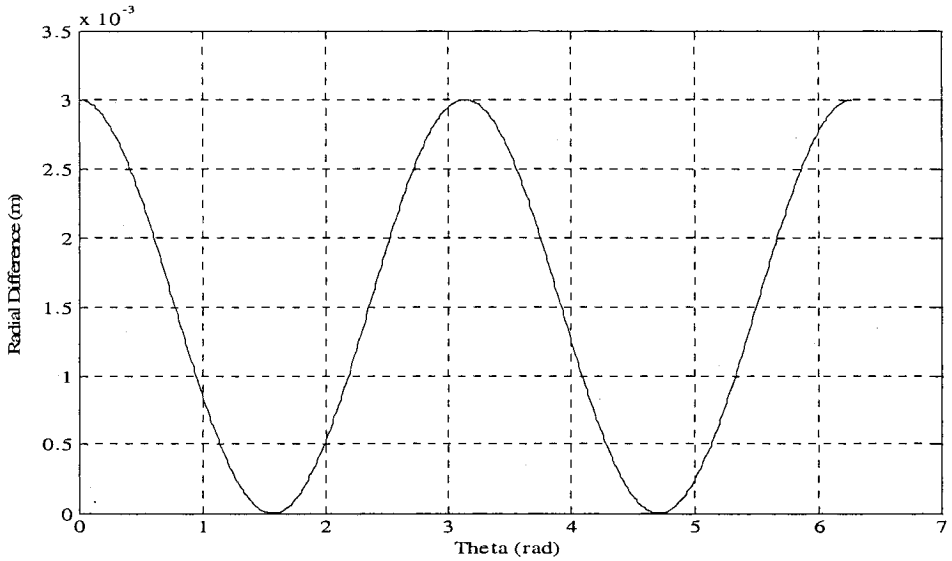

Figure 2.13: The locus of radial difference for one revolution about point 'P'

Now it is observed that this particular motion is imposed at the wheel center. In order to incorporate this motion into the vehicle model, equation (2.19) for computation of vertical co-ordinates of the wheel center can be modified as:

$$(Z_C)'_i = R_w - \{(Z_{ui}(t) - \delta_{ui} - Z_{oi}(t)\} + \Delta r_i(t) \qquad (2.39)$$

where R_w is the free radius of the wheel, Z_{ui} and Z_{oi}, respectively, denote the instantaneous displacement of the unsprung mass i ,$(i = f, r)$ and the instantaneous road input co-ordinate at the corresponding wheel.

Referring to Figure 2.13, it can be observed that $\Delta r\ (t)$ oscillates with a frequency of $2f_1$ Hz, where f_1 is related to the angular speed, $f_1 = \frac{\omega}{2\pi}$.

The wheel non-uniformity is incorporated in the tire model, and the end points of the wheel-terrain contact patch, P_1 and P_2, as shown in Figure 2.6, are determined from the instantaneous coordinates of the wheel center (X_C, Z_C) as explained in equations (2.17) to (2.24). The wheel-terrain contact patch angle ($2\alpha_w$), as derived in section 2.2.2, is determined from the instantaneous coordinates of the wheel center and end points of the contact patch (P_1 and P_2). It can thus be concluded that the variation of contact patch angle is directly dependent upon the variation of coordinates of the wheel center. Owing to period of $\frac{1}{2f_1}$ s of the wheel center, the variation of the contact patch angle also follows the same period. Figure 2.14 shows variation of the wheel terrain contact patch angle for the front and rear wheel in time domain with inclusion of the wheel non-uniformity at both wheels, Δr = 0.002 m at 100 km/h in comparison with balanced and uniform wheel, where the vehicle is subjected to excitations arising from the smooth road. It can be observed that the natural frequency of oscillation (17.7 Hz) is twice the wheel rotation frequency (8.8 Hz). The peak to peak magnitudes of the contact patch angles for the non-uniform wheels show considerable increase as compared to the balanced and uniform wheels.

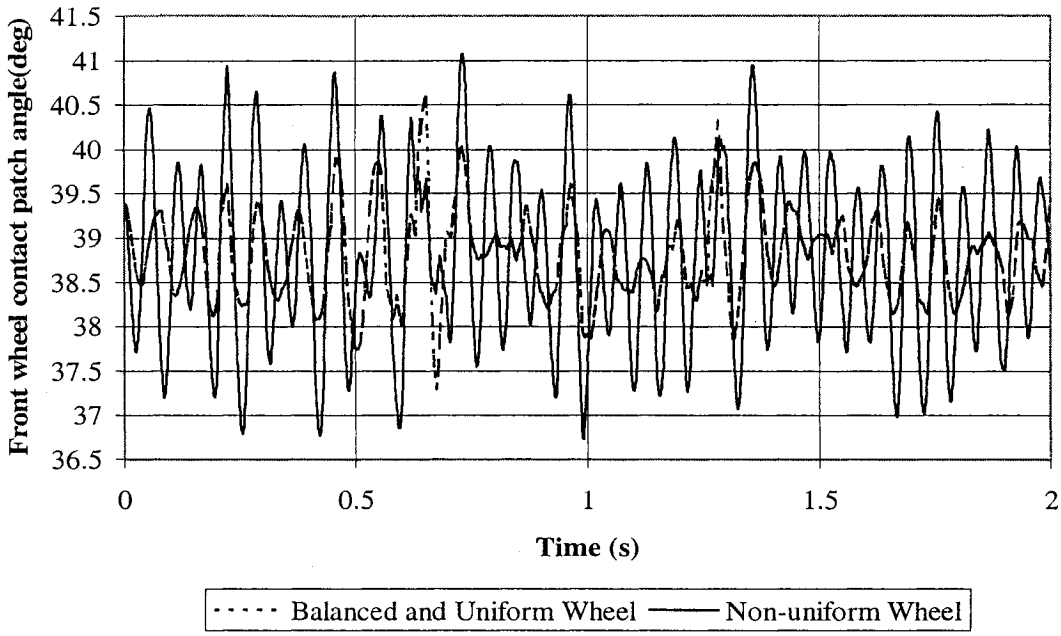

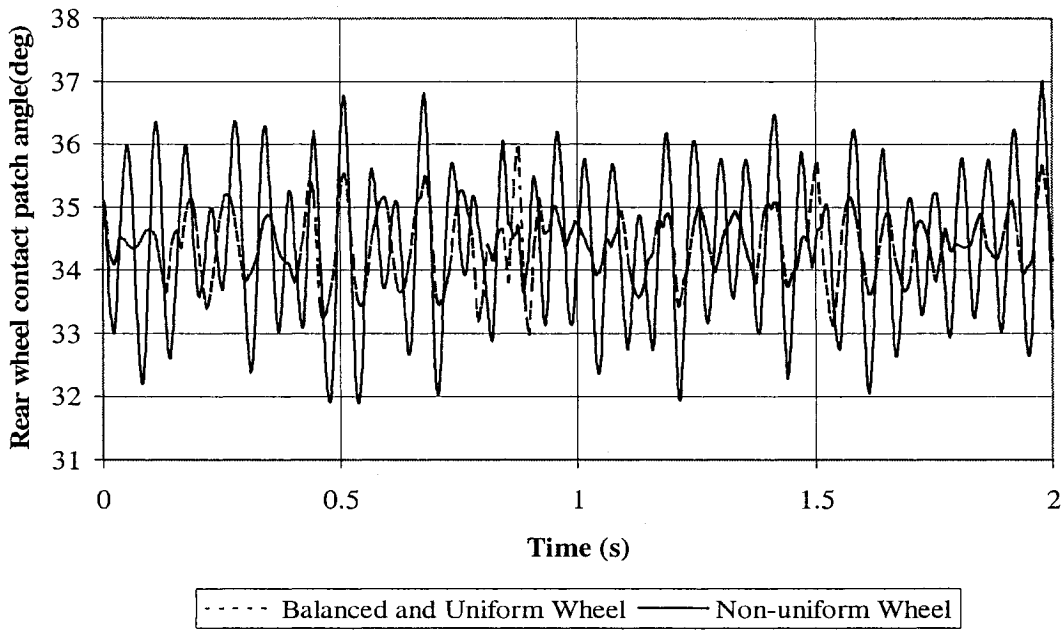

Figure 2.14: Comparison of variation of front and rear wheel contact patch angles for the non-uniform wheels at 100 km/h

The net vertical footprint force F_{wz} is directly proportional to the contact patch angle as explained in equation (2.14). The variations in F'_{wz} for non-uniform wheel follows the same trend as that of contact patch angle with increase in the peak to peak force magnitude. The resulting magnitude of the dynamic vertical foot-print force will thus be higher as compared to that of the balanced and uniform wheel.

2.6 SUMMARY

In this chapter, mathematical model of a two axle truck is developed to study its ride dynamic performance and dynamic tire load variations. The pitch plane model is formulated assuming constant forward speed and non-deformable random terrain profile. The highlight of the vehicle model is the characterization of wheel-terrain interaction using non-linear adaptive foot-print tire model. The next part of this chapter includes characterization of wheel unbalance and wheel non-uniformity (radial run-out), both the sources of excitation are then included in the mathematical model of the vehicle. In the following chapter, road profiles are characterized and vehicle parameters are explained. The performance measures related to ride and tire load are discussed.

CHAPTER 3

RESPONSE EVALUATION OF THE VEHICLE MODEL AND PERFORMANCE MEASURES

3.1 INTRODUCTION

In this chapter attempts are made to validate the pitch plane model of a two axle truck developed in Chapter 2. The validity of the candidate truck pitch-plane model relies upon accurate identification of various inertial and geometric parameters, static and dynamic characteristics of components, and road roughness. The vehicle parameters are taken from the reported data by Road Transport Association of Canada [117]. The road roughness data is taken from the data available at CONCAVE research center [118] for highways near the city of Ottawa. Road roughnesses are characterized based on their elevation data in terms of smooth, medium-rough and rough roads, and are used as input to the four degrees of freedom pitch-plane model for the truck. The displacement time histories are thus analyzed to derive representative road spectra based upon the Power Spectral Density (PSD) of vertical input displacement and acceleration. The data for the typical range of values for the unbalanced mass in wheel assembly is taken from the previous studies [25, 29, 40], while a range of practical values is established on the basis of a survey conducted with local car servicing centers. The data for wheel radial run-out is taken from the reported studies [4, 25, 119] and considering the practical data reported in a recent study by the CONCAVE research center [33].

The validation is carried out in two stages. A free vibration analysis of the pitch plane model is first carried out for undamped conditions. The natural frequencies and the

dominant deflection mode are established. These results are primarily obtained for in depth understanding of the truck dynamics and response in terms of bounce and pitch motions for qualitative validation. Attempts are then made for quantitative validation of the pitch plane model with the previously reported results. Results are compared in terms of PSD of ride accelerations and tire forces. The final part of this chapter contains description of various performance measures that are used in parametric study in view of ride accelerations and dynamic tire loads.

3.2 VEHICLE MODEL PARAMETERS

The model parameters of a two-axle truck are identified from the data reported by Road Transport Association of Canada [117]. The equivalent spring rates of the suspension and tires are also identified from the reported data. The simulation parameters for the vehicle model are thus compiled and summarized in Table 3.1.

Table 3.1: Vehicle model parameters

	Description of the parameter	**Parameter values**
1.	Mass of the vehicle (M_s)	7200.00 kg
2.	Pitch mass moment of inertia (I_s)	100000.00 kg-m^2
3.	Front tire and axle assembly mass (M_{uf})	353.00 kg
4.	Rear tire and axle assembly mass (M_{ur})	653.00 kg
5.	Front axle suspension stiffness (K_{sf})	295.30 KN/m
6.	Rear axle suspension stiffness (K_{sr})	797.30 KN/m
7.	Front axle suspension damping coefficient (C_{sf})	2.90 KN-s/m
8.	Rear axle suspension damping coefficient (C_{sr})	5.90 KN-s/m
9.	Front tire stiffness (K_{tf})	1100.00 KN/m
10.	Rear tire stiffness (K_{tr})	2200.00 KN/m
11.	Front tire damping coefficient (C_{tf})	0.40 KN-s/m
12.	Rear tire damping coefficient (C_{tr})	0.80 KN-s/m
13.	Distance from front axle to CG (ℓ_f)	3.75 m
14.	Distance from rear axle to CG (ℓ_r)	2.44 m
15.	Radius of the wheel (R_w)	0.50 m

3.2.1 WHEEL UNBALANCE AND NON-UNIFORMITY PARAMETERS

It has been reported in many studies that mass concentrations in the tire-wheel assembly can produce imbalance in force and moment in rolling conditions [3, 4, 29, 40]. It may be inherent due to the imperfect balancing of the wheel or it may be induced by the uneven wear of the tires [40]. The unbalanced mass values used in this study are thus representative of the tire-wheel assembly and are selected on the basis of the values reported in the literature [25, 29, 40]. A survey at the local car service station was further conducted to establish a range of practically encountered tire-wheel assembly mass unbalance values to validate and fine-tune the reported values. The angles between wheel centers and unbalanced masses are introduced to account for the phase difference between the front and rear wheels mass unbalance, as discussed in Chapter 2. The phase angles of the front and rear tire-wheel unbalanced masses are used as random numbers in the 0-90° range. Only one radius of unbalanced mass or eccentricity is used considering the free radius of the wheel as 0.5 m. The range of each parameter used for wheel unbalance is shown in Table 3.2.

Table 3.2: Parameters for wheel unbalance

	Parameter	**Range**
1.	Tire-wheel assembly unbalance mass	0.5-1.5 kg
2.	Eccentricity	0.4 m
3.	Phase angle	0-90°

The nonuniformities in the tire-wheel assembly have been reported as one of the major sources of vibration [24, 29, 33, 35]. These nonuniformities include vehicle stud

run-out, hub-hole eccentricities, rim flange run-outs, variations in tire run-outs, and variations in tire stiffness [29]. The values of the wheel non-uniformities used in this study are thus representative of all the sources stated above and are identified considering the reported studies [4, 25, 119] as well as the data collected at CONCAVE research center [33]. The wheel is assumed to have an elliptical shape in order to characterize the non-uniformity. The angle between the major axis of an ellipse and the horizontal fixed X-axis is introduced to account for the phase difference between the front and rear wheel runouts. The range of radial run-out magnitude used is from 1-3 mm and the phase angles of the radial run-out are used as random numbers in the 0-90° range.

3.2.2 CHARACTERIZATION OF ROAD PROFILE

The dynamic characteristics of the road vehicle, and thus the dynamic wheel loads and the ride quality are strongly related to the road profile. The roads are known to exhibit randomly distributed roughness. The road profile data used in this study is taken from the data available at CONCAVE research center [118] for highway 43 and highway 417 near the city of Ottawa. These road profiles are analyzed to derive their *roughness index* values and power spectral density. The *roughness index (RI)* of the road surface is computed as:

$$\mathrm{RI}=\frac{1}{n\Delta x}\sum_{i}^{n}\left|\Delta z_i\right| \tag{3.1}$$

where n is the number of equi-distant measurement points, Δz_i, is the elevation at the i^{th} measurement location, and Δx is the spacing between measurement locations, taken

as 0.3 m. The measured road profiles are characterized by their RI values, and referred to as smooth, medium-rough and rough (Table 3.3).

Table 3.3: RI values of road profiles

	Type	Roughness Index (m/km)
1.	Smooth	1.59
2.	Medium Rough	4.37
3.	Rough	5.94

METHODOLOGY FOR EVALUATION OF SPECTRAL DENSITY OF ROAD ROUGHNESS

The available road profile data in the form of elevation, Δz, at equidistant points (Δx) of 0.3 m is transformed into corresponding time co-ordinates with respect to vehicle speeds of 60 km/h, 80 km/h, and 100 km/h, respectively. The resulting time histories of the road roughness are used to estimate the Power Spectral Density (PSD) of the road profile corresponding to each speed using FFT (Fast Fourier Transform) technique. The total length of the data (L), time period (T) with respect to the vehicle speed, sampling interval (Δt), and the Nyquist frequency for each speed (f_N) are summarized in Table 3.4. The spectral density of acceleration due to road roughness is computed as:

$$S_{\ddot{X}}(\omega) = \omega^4 S_X(\omega) \tag{3.2}$$

where $S_{\ddot{X}}(\omega)$ is the spectral density of the acceleration $\ddot{X}(t)$ due to road roughness and $S_X(\omega)$ is the spectral density of road roughness $X(t)$. Power spectral densities of displacement and acceleration due to road roughness at 60 km/h, 80 km/h, and 100 km/h

for *smooth*, *medium-rough* and *rough* road are presented on log-log scale in Figures 3.1, 3.2 and 3.3, respectively.

Table 3.4: Sample length, time period, sampling interval and Nyquist frequency of the roughness profile of each road as a function of forward speed

Road type	**Vehicle Speed (km/h)**	**L (m)**	**T (s)**	Δt **(s)**	f_N **(Hz)**
Smooth	60	747.6	44.86	0.0179	27.93
	80	747.6	33.64	0.0135	37.04
	100	747.6	26.91	0.0107	46.73
Medium rough	60	747.0	44.81	0.0179	27.93
	80	747.0	33.62	0.0135	37.04
	100	747.0	26.89	0.0107	46.73
Rough	60	447.0	26.81	0.0179	27.93
	80	447.0	20.11	0.0135	37.04
	100	447.0	16.09	0.0107	46.73

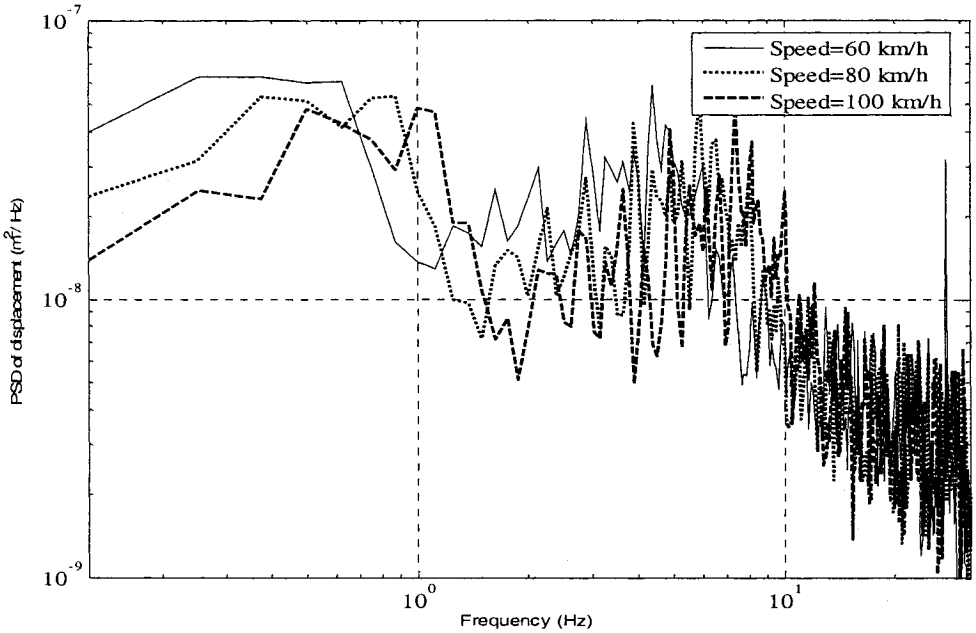

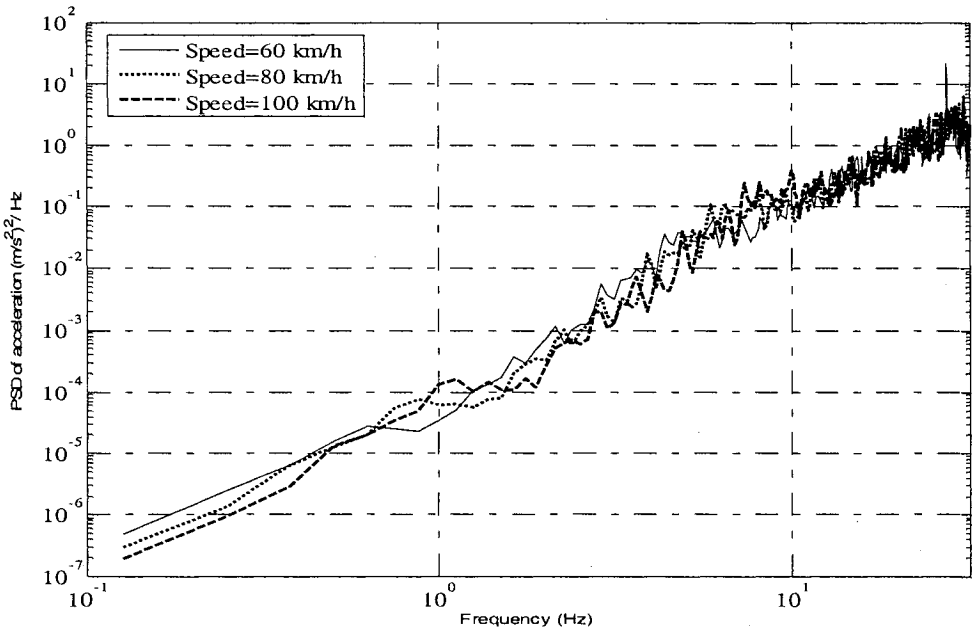

Figure 3.1: Power spectral density of displacement and acceleration due to road roughness at 60 km/h, 80 km/h, and 100 km/h for smooth road

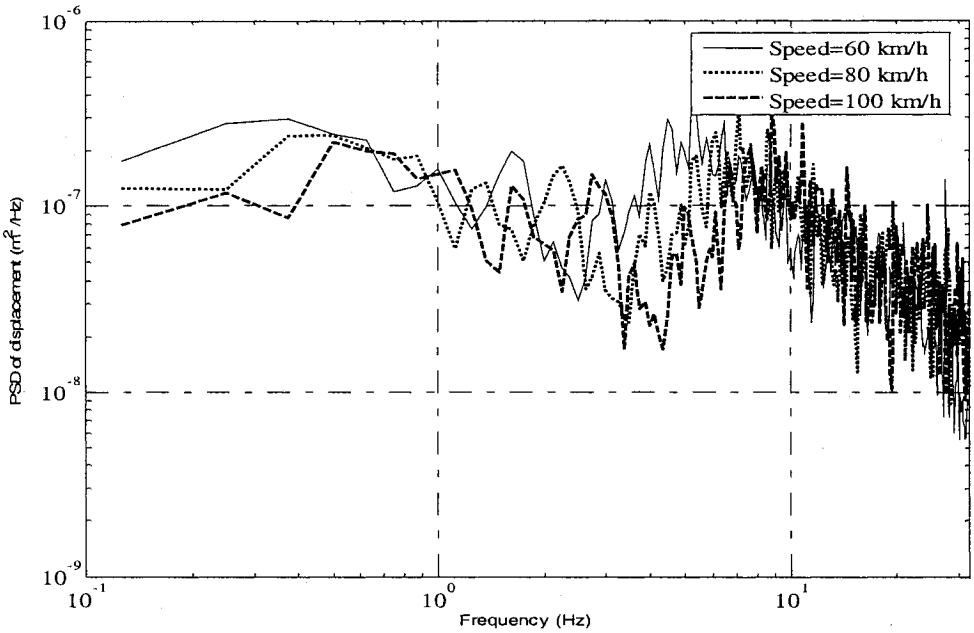

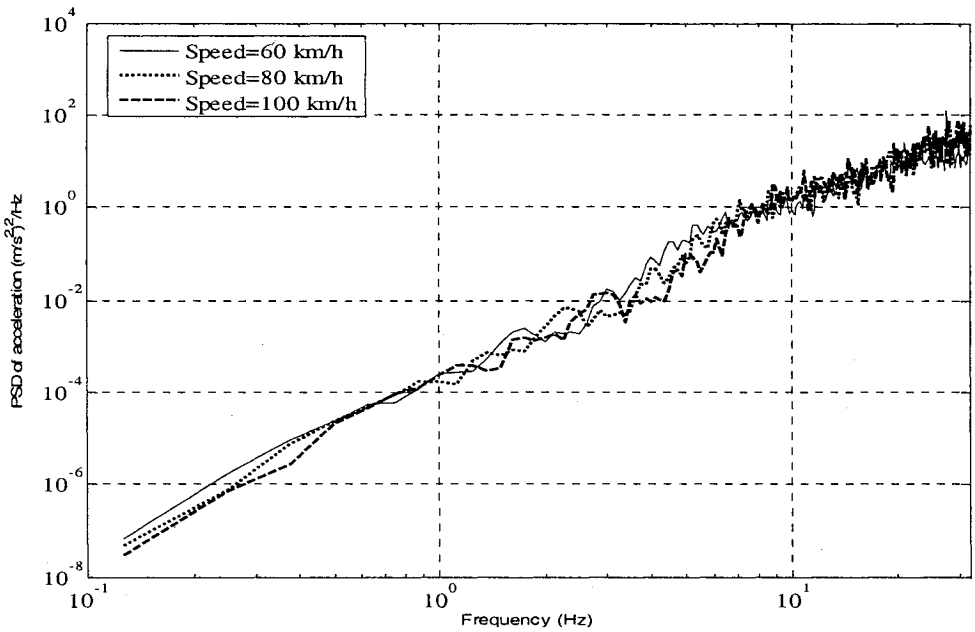

Figure 3.2: Power spectral density of displacement and acceleration due to road roughness at 60 km/h, 80 km/h and 100 km/h for medium-rough road

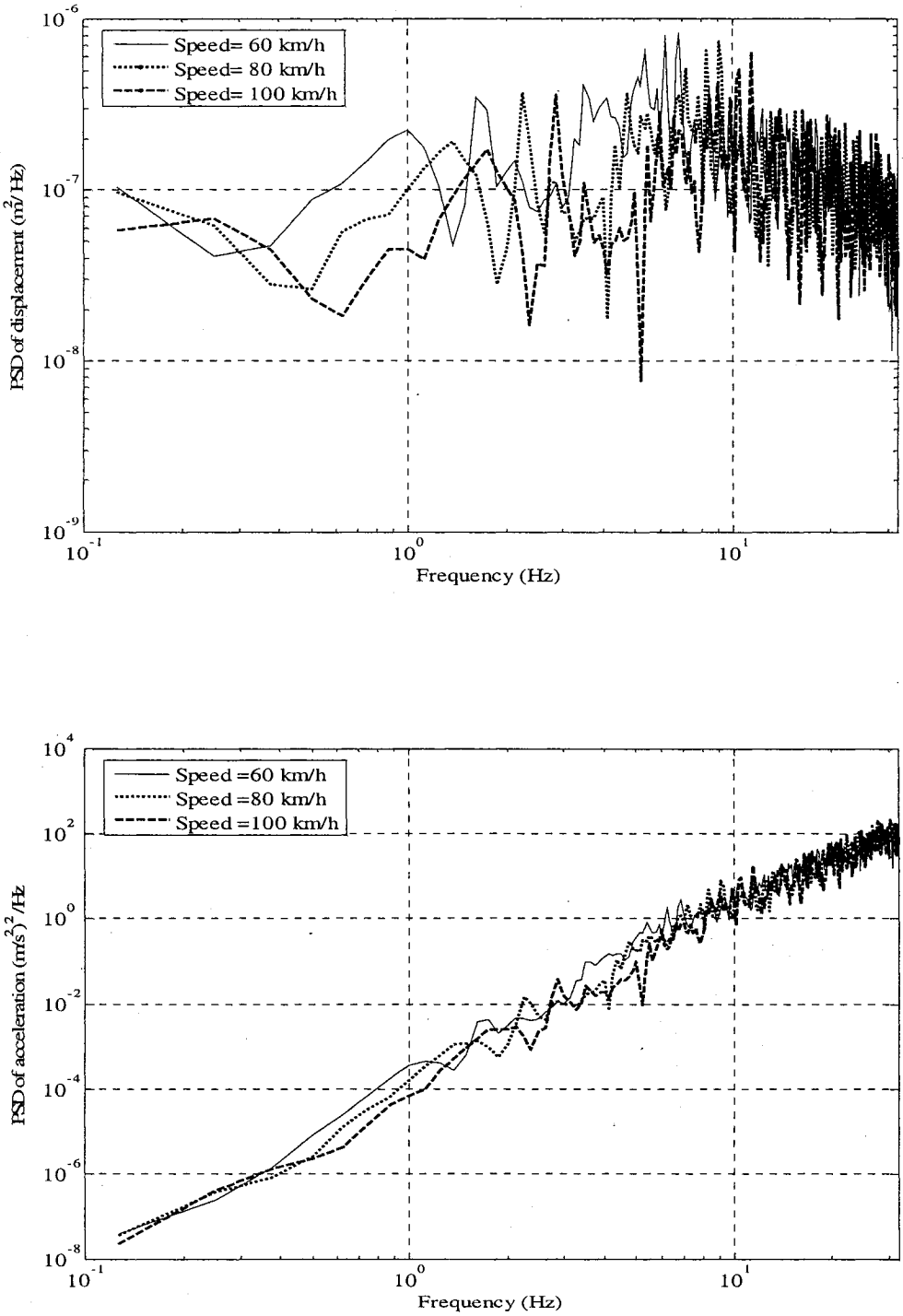

Figure 3.3: Power spectral density of displacement and acceleration due to road roughness at 60 km/h, 80 km/h, and 100 km/h for rough road

3.3 IDENTIFICATION OF NATURAL FREQUENCIES

Since the current designs of truck suspensions offer light damping, the resonant frequencies and dominant deflection modes may be conveniently estimated from the eigenvalue analysis of the undamped vehicle model. Assuming the linear properties of the tire stiffness and axle suspensions, the equations of motion of the vehicle, as derived in Chapter 2, can be expressed in matrix form as:

$$[M]\{\ddot{Z}\}+[K]\{Z\}=0 \tag{3.3}$$

where $[M]$ is the 4x4 mass matrix, $[K]$ is the 4x4 stiffness matrix, and $[Z]$ is the 4x1 response vector. Referring to equation (2.25) these matrices can be expressed as:

$$K=\begin{bmatrix} K_{sf}+K_{sr} & \ell_r K_{sr}-\ell_f K_{sf} & -K_{sf} & -K_{sr} \\ \ell_r K_{sr}-\ell_f K_{sf} & \ell_r{}^2 K_{sr}+\ell_f{}^2 K_{sf} & \ell_f K_{sf} & -\ell_r K_{sr} \\ -K_{sf} & \ell_f K_{sf} & K_{sf}+K_{tf} & 0 \\ -K_{sr} & -\ell_r K_{sr} & 0 & K_{sr}+K_{tr} \end{bmatrix}$$

where K_{tf} *and* K_{tr} are the linearized stiffness constants of the front and rear tire, respectively.

$$M=\begin{bmatrix} M_s & 0 & 0 & 0 \\ 0 & I_s & 0 & 0 \\ 0 & 0 & M_{uf} & 0 \\ 0 & 0 & 0 & M_{ur} \end{bmatrix}$$

The solution is assumed in the form,

$$Z = X\, e^{i\omega t}$$

This solution satisfies the differential equation if

$$[K-\omega^2 M]\{X\}=\{0\} \tag{3.4}$$

This equation is a system of four homogeneous simultaneous equations, and for non-trivial solution we must have:

$$|K - \lambda M| = 0, \text{ where } \lambda = \omega^2.$$

This determinant leads to an eigenvalue problem. The eigenvalues and eigenvectors are then computed using *eig( )* routine in MATLAB®. Table 3.5 shows the eigenvalues and resonant frequencies corresponding to the dominant deflection modes. As the results show, the bounce and pitch natural frequencies of the sprung mass are in between 1-2 Hz range while the bounce natural frequencies of the unsprung masses are around 10 Hz, which is typical for such vehicles. In the next section, attempts are made to carry out quantitative validation for the responses and a comparison of the natural frequencies with those of the reported studies.

Table 3.5: Eigenvalues and resonant frequencies of the vehicle model

Dominant deflection mode	**Eigenvalue (λ)**	**Resonant frequency (Hz)**
Sprung mass (Bounce mode)	139.0	1.87
Sprung mass (Pitch mode)	66.7	1.30
Front unsprung mass (Bounce mode)	3970.0	10.03
Rear unsprung mass (Bounce mode)	4607.8	10.81

3.4 VALIDATION OF THE ANALYTICAL VEHICLE MODEL

The coupled non-linear differential equations of motion for the pitch-plane truck model are solved under the excitations, represented by the time history of the measured road elevations for the smooth, medium-rough, and rough roads. Same input is used for the front and rear axles with appropriate time delay based on the forward speed and the wheel base of the vehicle, such that:

$$Z_{of} = Z_o(t)$$
$$Z_{or} = Z_o(t + \frac{L}{V_x}) \tag{3.5}$$

where Z_{oi} is the road displacement, $(i = f, r)$, L is the wheel base (distance between the front and rear axle) of the vehicle and V_x is the forward speed.

The differential equations of motion derived in Chapter 2, are solved by using the fourth order Runge-Kutta numerical integration routine available in MATLAB®. The total time span of 10 s is used for all simulations. The responses are obtained at center of gravity of the sprung mass and each unsprung mass.

Simulations are initially performed for a vehicle model in the absence of mass unbalance and wheel run-out at forward speeds of 60 km/h, 80 km/h, and 100 km/h. The responses are obtained in terms of time histories of vertical (bounce) and angular (pitch) accelerations of the sprung mass, vertical (bounce) accelerations of the front and rear unsprung masses, and the front and rear dynamic tire forces. The PSD estimates of the bounce and pitch accelerations and tire forces are obtained using FFT (Fast Fourier Transform) technique, and compared with those reported in a published study for a similar vehicle model [117] to examine the validity of the pitch plane model. For this purpose, the PSD of vertical and pitch acceleration responses of the sprung mass of a three-axle truck with and without an axle vibration absorber, reported in [117], are considered, as shown in Figure 3.4. The corresponding PSD of tire force responses are shown in Figure 3.5. The sprung mass accelerations (bounce and pitch) spectra and tire forces (front and rear axle) spectra of the present vehicle model are presented in Figures 3.6 and 3.7, respectively. Figures 3.4 and 3.5 show the PSD of acceleration and tire force responses with and without a dynamic axle vibration absorber, with absorber frequency

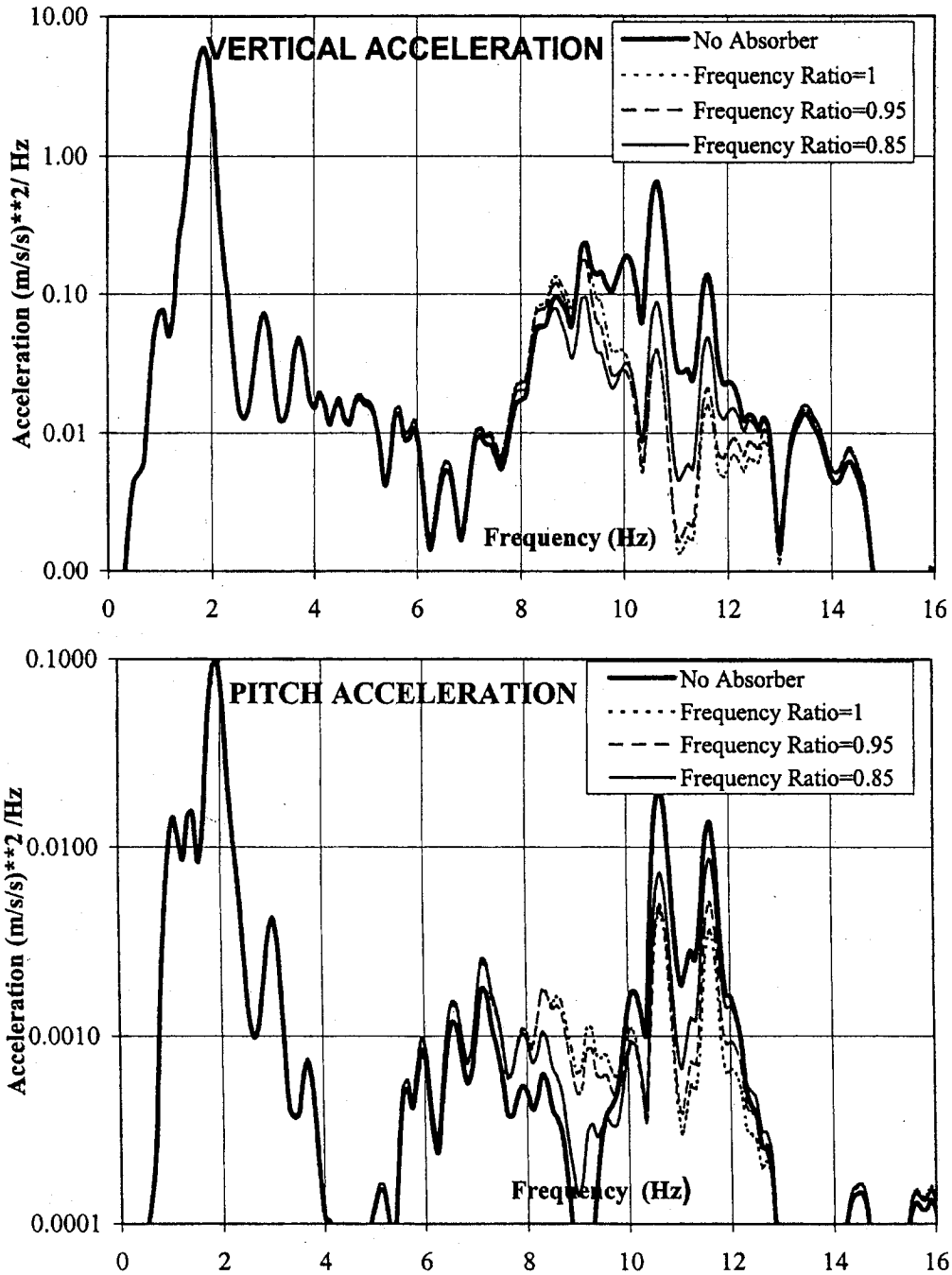

Figure 3.4: PSD of the vertical and pitch acceleration responses of a three-axle truck reported in [117] for different frequency ratios of the axle vibration absorber

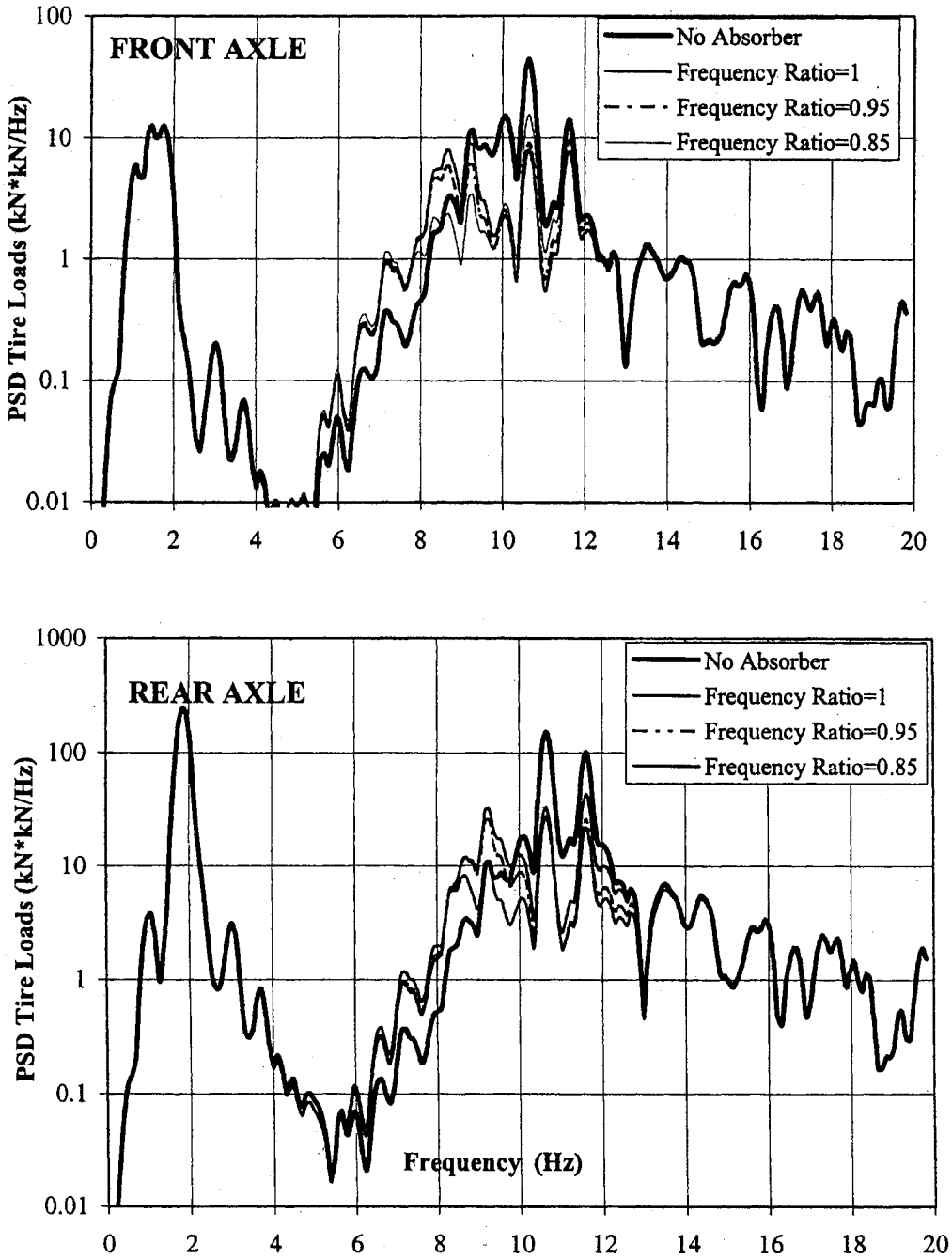

Figure 3.5: PSD of the front and rear tire force responses of a three-axle truck reported in [117] for different frequency ratios of the axle vibration absorber

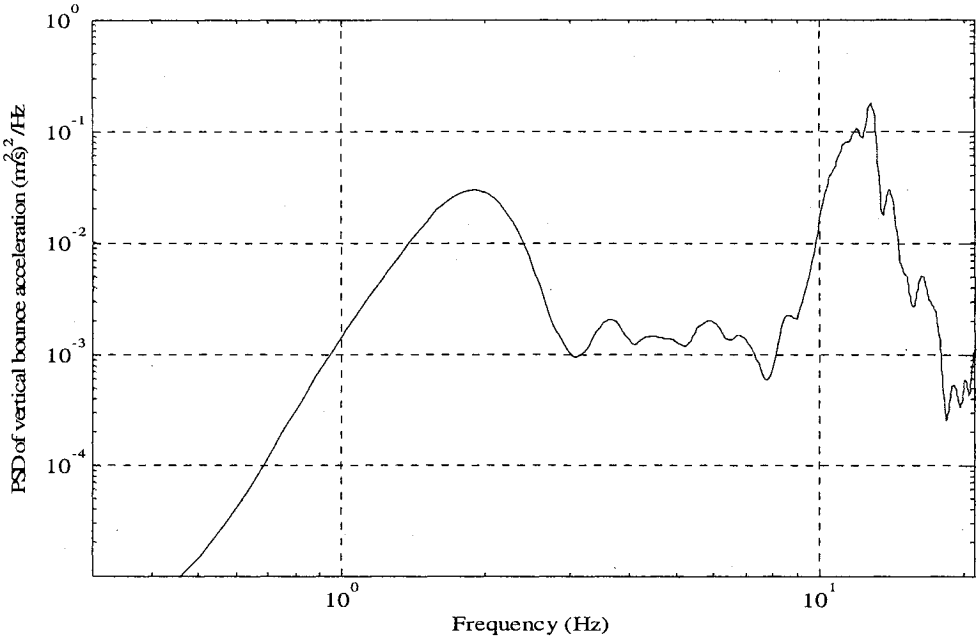

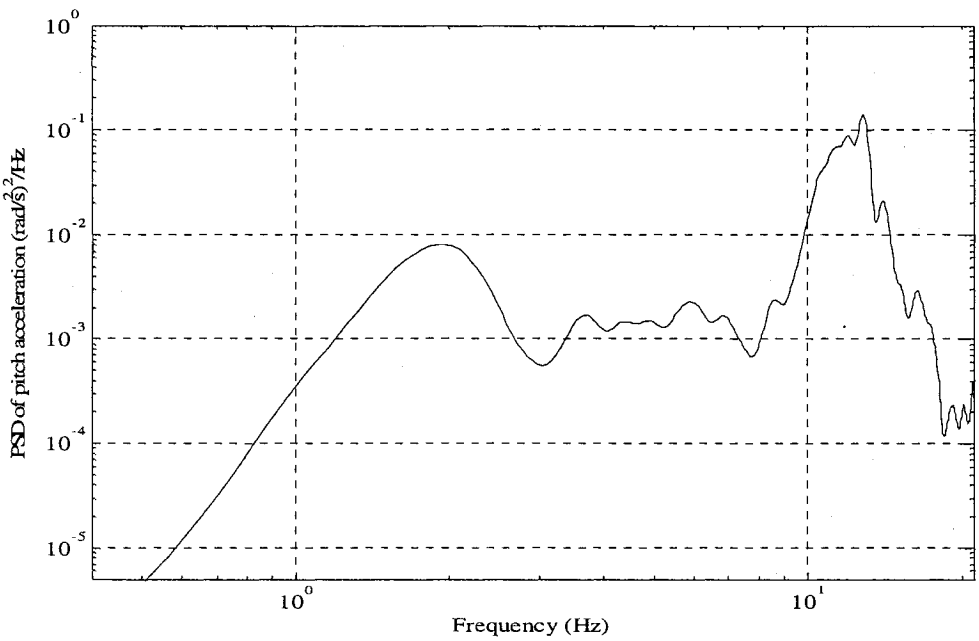

Figure 3.6: PSD of the vertical and pitch acceleration responses of the vehicle model under a rough road excitation at a speed of 120 km/h

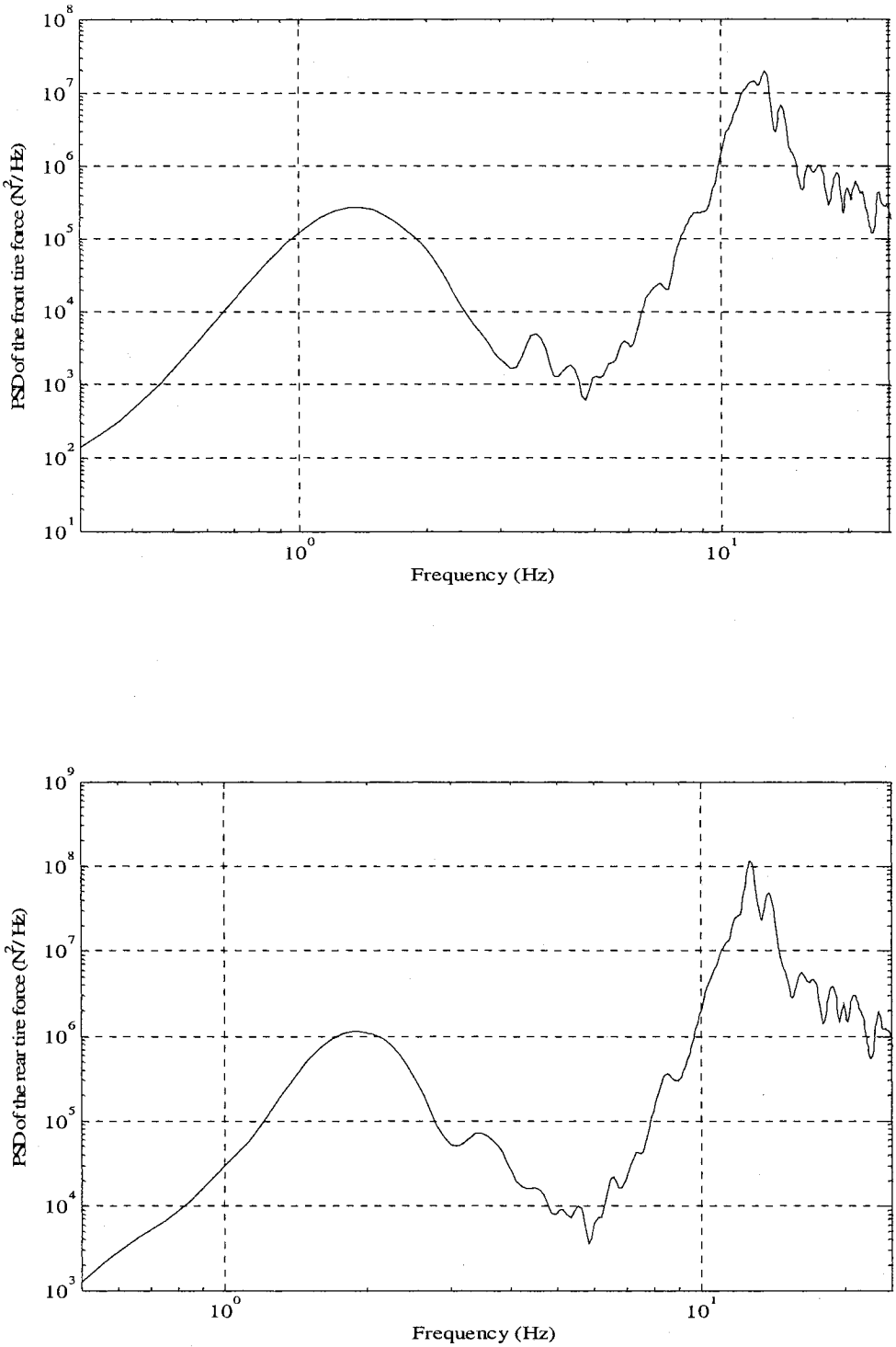

Figure 3.7: PSD of the front and rear tire force responses of the vehicle model under a rough road excitation at a speed of 120 km/h

ratios (ratio of absorber frequency to the unsprung mass natural frequency) 1, 0.95 and 0.85. The results from the present model and those reported have been evaluated for PSD at the vehicle speed of 120 km/h under a rough road excitation. It can be observed that the resonant frequencies of the sprung mass of the present model agree reasonably well with those of the reported model, while the resonant frequencies of the unsprung masses are around 13 Hz, which are higher than those of the reported study. This difference can be attributed to the radial spring tire model used in this study, whereas the reported study uses point contact tire model. Both the acceleration and tire forces spectra show peak values in the vicinity of the sprung mass frequencies, which are lower than those in the reported study. The peak magnitudes in the vicinity of the unsprung mass resonances, however, are comparable. This discrepancy can be attributed to the point-contact tire model used in the reported study, which is known to yield overestimates in the vertical tire forces [2]. The differences in the peak magnitudes could also be attributed in part to the differences in the road profiles used in these studies.

3.4.1 FORCE DUE TO RADIAL RUN-OUT

Kenny [29] suggested that the total force due to wheel run-out can be was quantified as summation of radial force (product of the tire's vertical spring constant and the magnitude of run-out) and the imbalance centrifugal force due to the run-out (product of mass of the tire-rim assembly, the magnitude of run-out, and square of angular velocity of the tire). The total force due to radial run-out of the wheel alone, F_{RO}, is thus expressed as:

$$F_{RO} = (K_t)_i (\Delta r)_i + (M_u)_i (\Delta r)_i (\omega^2) \tag{3.6}$$

where K_t is the equivalent vertical stiffness of the tire in N/m as applied in a point-contact tire model and $(i = f, r)$. This formulation implies that the radial run-out can be considered as eccentricity, and a radial run-out also yields unbalance.

The estimated force, F_{RO}, is compared with the force increment due to radial run-out attained using the adaptive foot-print model. Figure 3.8 illustrates time histories of dynamic tire forces derived for the uniform wheel and for a wheel with $\Delta r = 0.002$ m at a speed of 80 km/h, while subject to smooth road excitations. It should be noted that figure shows tire forces due to rear wheels of the vehicle. The increases in the peak forces caused by radial run-out are computed at selected discrete times, and compared with that derived from equation (3.6). For the selected speeds of 80 km/h and $\Delta r = 0.002$ m, the results attained from the adaptive foot-print model show an increase in the peak force of 8 KN, which compares reasonably well with 7 KN, as estimated from equation (3.6). Similarly for the front tires with $\Delta r = 0.001$ m, the corresponding values were obtained as 2 KN and 1.7 KN, respectively.

3.5 PERFORMANCE MEASURE RELATED TO TIRE LOADS

Vehicle generated road damage is directly related to the magnitude of the tire forces transmitted to the pavement. The tire forces transmitted to the road consist of two components: a static load and the dynamic load. The static load depends on the geometry and mass distribution of the vehicle, and the load sharing characteristics of the suspension system. Dynamic tire forces, on the other hand, are the result of vehicle vibration caused by tire-road interaction. The self-excited sources of vibration would further contribute to the dynamic tire forces. The severity of the dynamic tire forces primarily depend upon

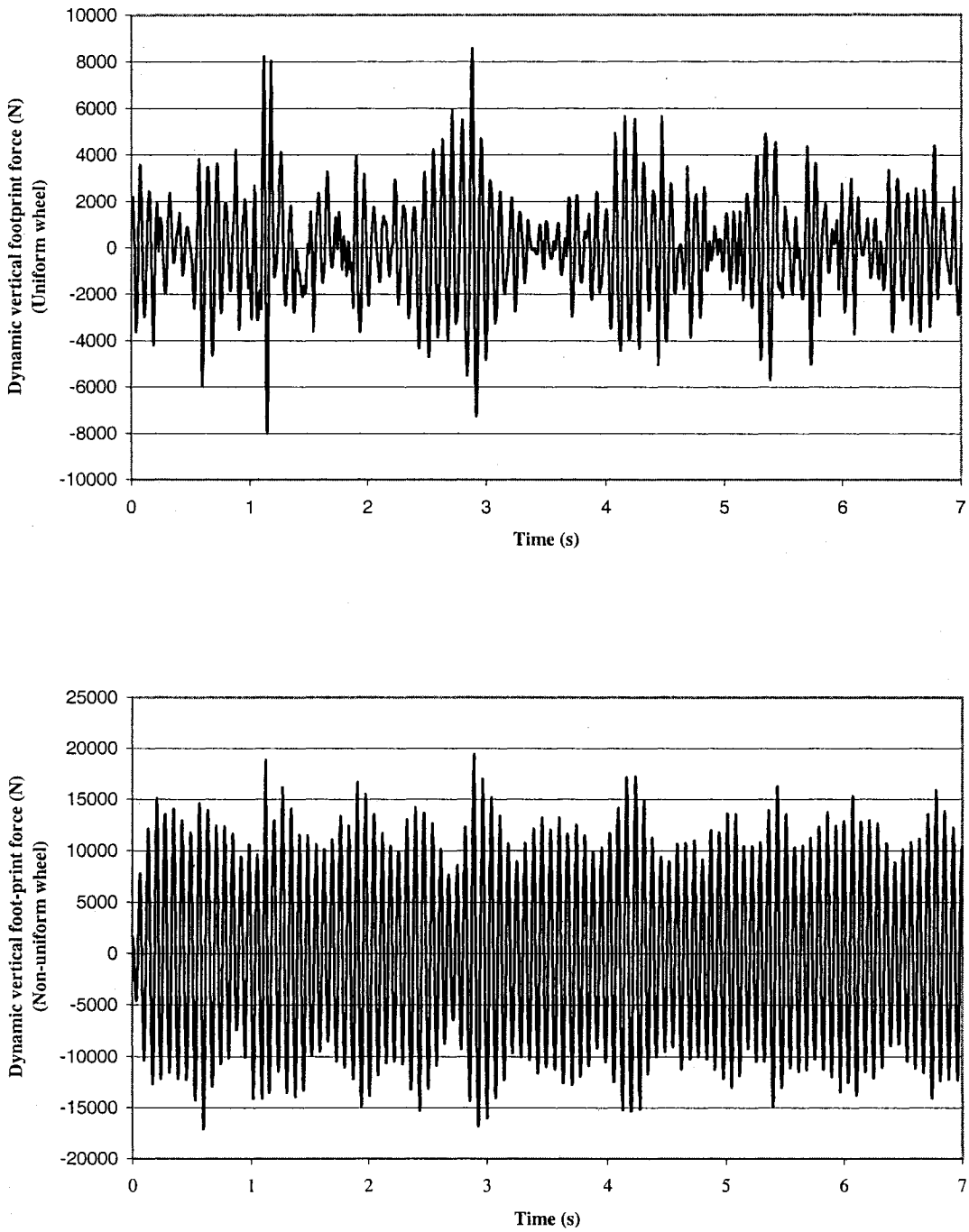

Figure 3.8: Dynamic tire force variation for the uniform wheel and non-uniform wheel ($(\Delta r)_r = 0.002\ m$) at 80 km/h under smooth road excitation

the suspension design and the axle loads.

Dynamic tire forces and their interaction with the pavement is a complex process. The extent of damage caused by these loads to the pavements depends on the road structure and material characteristics, as well as the nature of the applied loads. Although a number of methods have been proposed to estimate the serviceability index or service lives of pavements, serious concerns have been raised on the validity of the methods [115]. In view of the complexity associated with the pavement mechanisms and lack of generally acceptable assessment methods, the performance potentials of suspension systems are assessed in terms of the relative magnitudes of the dynamic tire loads.

Although the dynamic tire forces of heavy vehicles are known to accelerate the pavement fatigue, definite methods to quantify the road damaging potentials have not yet been established. Alternatively a number of performance measures have been proposed to assess the relative agressivity of the heavy vehicles, and to assess the influence of various design and operating factors [46]. Some of these performance measures are, Dynamic Load Coefficient (DLC), Road Stress Factor (RSF), Peak Tire Force, Crest Factor, etc. DLC describes the magnitude of variations in the tire forces. RSF is defined assuming that the road damage is related to fourth power of the instantaneous (dynamic) wheel force at a point on the road [1]. Peak tire force is the maximum force transmitted to the pavement during the entire course of run in a given time history, while the crest factor is defined as the ratio of maximum to the mean tire force. The present study is focused on the contribution of wheel unbalance and non-uniformity in the potential road damage.

After observing the effects of wheel unbalance and non-uniformity on all the performance measures stated above, it was concluded that dynamic load coefficient

(DLC) was the most indicative of the contribution from the wheel unbalance and non-uniformity. So in order to assess influence of various operating factors and wheel unbalance and non-uniformity, DLC is used as a performance measure in this study.

Dynamic Load Coefficient (DLC)

The relative road damaging potentials of heavy vehicles, and the design and operating parameters are frequently expressed in terms of dynamic load coefficient (DLC). The DLC describes the magnitude of variations in the tire forces and is defined as:

$$\text{DLC} = \frac{RMS\ dynamic\ tire\ force}{Mean\ tire\ force} \tag{3.7}$$

While there is considerable civil engineering literature concerned with theoretical and experimental studies of road damage caused by heavy vehicle loads, it is mostly based on the assumption that vehicles apply a constant (static) tire force to the road. Dynamic forces that are caused by the interaction of a heavy vehicle with road surface roughness constitute a significant portion of the total tire forces. Peak tire forces can be as much as twice their static values, and RMS levels are typically 20-30% of the static forces [115]. The road damage assessment thus necessitates appropriate considerations of the dynamic tire forces. Many studies have concluded that the DLC strongly depends on the road surface roughness, vehicle speed, vehicle configuration, geometry and mass distribution, axle loads, properties of the suspension and tires, and the vehicle vibration modes. David Cebon [1] recommended that under normal operating conditions, the DLC of 0.1-0.3 are typical, which are only applicable to straight line driving.

3.6 PERFORMANCE MEASURES RELATED TO RIDE

The two measures used for assessing the vibration ride comfort are absorbed power and RMS acceleration. The absorbed power criterion is based on the hypothesis that ride comfort is related to energy dissipated due to internal damping in the human body [55]. Absorbed power is determined by calculating a weighted integral of the power spectrum of acceleration in all three dimensions. The weighting functions, which are functions of frequency, are the mechanical impedance of the human body at the driver/passenger-seat interface, and are higher for frequencies to which the human body is most sensitive. The rms accelerations due to ride vibration, on the other hand, are computed using a frequency-weighting filter defined in IS0 2631-1 [116] filter.

The ride quality is concerned with driver and passenger comfort related to the road condition and suspension performance. The seat is also a very important element in a ride analysis since the flexibility of the seat isolates the driver from high-frequency vertical vibrations. For simplicity this study uses the center of gravity of the sprung mass location rather than the driver/seat interface for the evaluation of ride performance. The response at center of gravity of the sprung mass of the vehicle is obtained based on vehicle body bounce and pitch motions. The true rms accelerations due to vertical and pitch vibration of the sprung mass cg computed from:

$$\ddot{z}_{rms} = \sqrt{\frac{1}{T}\int_0^T \ddot{z}_s^{\,2}\, dt}\,, \tag{3.8}$$

$$\ddot{\theta}_{rms} = \sqrt{\frac{1}{T}\int_0^T \ddot{\theta}_s^{\,2}\, dt}\,. \tag{3.9}$$

where T is the total simulation time, and $\ddot{z}_{rms}$ and $\ddot{\theta}_{rms}$ are true rms accelerations corresponding to bounce and pitch motions of the sprung mass, respectively.

The ride performance of a vehicle is assessed in terms of magnitude and frequency contents of vibration transmitted to the driver or passenger seat. The frequency, to which a human driver is most fatigue sensitive for the horizontal and vertical vibrations, lies in the range from 1 to 2 Hz and 4 to 8 Hz, respectively. The human sensitivity to rotational vibration is mostly in 0.5 to 1.5 Hz frequency range [116]. The international standard (ISO 2631-1) has outlined a procedure to assess the human exposure to whole-body ride vibrations in terms of overall frequency-weighted rms acceleration at the driver/passenger seat interface [116]. The standard defines frequency-weighting W_k for vertical vibration in the 0.5-80 Hz frequency range, and W_e for the pitch vibration in the 0.1-80 Hz frequency range. In the analysis of the pitch plane model, the ride accelerations are evaluated at the center of gravity of the sprung mass. The frequency-weighted rms accelerations are thus defined as:

$$\ddot{z}_{w,rms} = \sqrt{\frac{1}{T}\int_0^T \ddot{z}_{w,s}{}^2\, dt}\,, \tag{3.10}$$

$$\ddot{\theta}_{w,rms} = \sqrt{\frac{1}{T}\int_0^T \ddot{\theta}_{w,s}{}^2\, dt}\,. \tag{3.11}$$

where $\ddot{z}_{w,rms}$ and $\ddot{\theta}_{w,rms}$ are the frequency-weighted rms accelerations corresponding to bounce and pitch motions of the sprung mass, respectively. $\ddot{z}_{w,s}$ and $\ddot{\theta}_{w,s}$ are the frequency weighted instantaneous bounce and pitch accelerations of the sprung mass, respectively.

The frequency weighting function is defined from the combination of a band limiting transfer function, $H_h(p).H_l(p)$ (i.e. high-pass and low-pass filters), and the weighting transfer function, $H_t(p).H_s(p)$. The total frequency weighting function is obtained by:

$$H(p) = H_h(p).H_l(p).H_t(p).H_s(p) \tag{3.12}$$

where $H_h(p)$ is high pass filter function and expressed as:

$$|H_h(p)| = \left| \frac{1}{1+\sqrt{2}\omega_1 / p + (\omega_1 / p)^2} \right| \tag{3.13}$$

in which, $\omega_1 = 2\pi f_1$, $p = j2\pi f$ and f_1 is the corner frequency (intersection of asymptotes).

$H_l(p)$ is low pass transfer filter function and expressed as:

$$|H_l(p)| = \left| \frac{1}{1+\sqrt{2}p / \omega_2 + (p / \omega_2)^2} \right| \tag{3.14}$$

in which, $\omega_2 = 2\pi f_2$, and f_2 = corner frequency.

$H_t(p)$ is acceleration-velocity transfer function and expressed as:

$$H_t(p) = \left| \frac{1+ p / \omega_3}{1+ p/(Q_4\omega_4) + (p / \omega_4)^2} \right| \tag{3.15}$$

in which, $\omega_3 = 2\pi f_3$, and $\omega_4 = 2\pi f_4$.

$H_s(p)$ is upward step transfer function (steepness approximately 6 dB per octave, proportional to jerk), given by:

$$H_s(p) = \left| \frac{1+ p/(Q_5\omega_5) + (p / \omega_5)^2}{1+ p/(Q_5\omega_6) + (p / \omega_6)^2} \left(\frac{\omega_5}{\omega_6} \right)^2 \right| \tag{3.16}$$

in which, $\omega_5 = 2\pi f_5$, and $\omega_6 = 2\pi f_6$.

The various coefficients used in the transfer functions are listed in the Table 3.6.

Table 3.6: Coefficients of transfer functions of the frequency weightings [69]

Weighting	**Band-limiting**		**Acceleration-velocity transition**			**Upward step**			
	f_1 (Hz)	f_2 (Hz)	f_3 (Hz)	f_4 (Hz)	Q_4	f_5 (Hz)	Q_5	f_6 (Hz)	Q_6
W_k	0.4	100	12.5	12.5	0.63	2.37	0.91	3.35	0.91
W_e	0.4	100	1.0	1.0	0.63	∞	-	∞	-

3.7 SUMMARY

In this chapter, the vehicle parameters and the ranges of magnitudes of wheel unbalance and non-uniformity are described. The available road profiles are characterized into three types on the basis of their roughness indices and their displacement and acceleration spectra are obtained at three different speeds. Further, linearized free vibration analysis is carried out to identify the resonant frequencies and the vehicle analytical model is validated by comparing the results of ride acceleration spectra and the tire force spectra with the results attained from an earlier study. The comparison shows reasonably close match between the two results. Finally a number of performance measures for the road forces and ride quality are outlined. These performance measures are used for the comprehensive parametric study presented in the next chapter.

CHAPTER 4

ANALYSIS OF WHEEL UNBALANCE AND NON-UNIFORMITY

4.1 INTRODUCTION

The tire force and ride acceleration responses of a vehicle are strongly related to various design and operating parameters. The self exciting sources of vibration, arising from wheel unbalance and wheel non-uniformity would fall within the operating parameters. The effects of these parameters are expected to be coupled with other operating factors, such as loads, speed and road roughness. The vehicle model presented in Chapter 2 together with the non linear adaptive radial tire model are analyzed to study the effects of wheel unbalance and non-uniformity, while the variations in other operating parameters, namely the vehicle speed and road roughness are considered. The response characteristics of the vehicle are analyzed using the performance measures described in Chapter 3, including the DLC (Dynamic Load Coefficient), and weighted and unweighted ride accelerations along the vertical and pitch axes. The frequency weighting filters proposed in ISO 2631-1 (1997) [69] are applied to determine the overall weighted rms bounce and pitch accelerations to assess the impact of wheel defects on the ride quality of the vehicle. The effects of magnitudes of self exciting sources on the response measures are also observed through a comprehensive parametric study involving variation in each operating parameter to achieve a better understanding of their contribution individually and collectively to the overall ride quality and road damage. Wheel unbalance and non-uniformity in the front wheel are held constant in order to observe the effect on DLC of the rear wheel and ride accelerations and vice versa. The effect of speed is observed under a *smooth road* condition to ensure minimal contribution

due to road roughness. The effect of variations in the road roughness, however, is investigated at a speed of 80 km/h. The effect of phase angle between the unbalance masses of different wheels and wheel non-uniformities is also observed at a speed of 80 km/h on a *smooth* road.

4.2 EFFECT OF ROTATING WHEEL UNBALANCE

The coupled differential equations of motion for the vehicle model together with the adaptive radial element tire model are solved for different magnitudes of wheel unbalance to study the mass unbalance effects on the performance measures. The analyses are performed in conjunction with variations in the forwards speed, road roughness and phase between the unbalance of the front and rear wheels. It has been reported that effect of wheel unbalance is mainly observed while the vehicle is operated on a smooth road [1]. This is most likely attributed to relatively lower magnitudes of forces arising from the tire's interaction with a smooth road. In the present study, the eccentricity of the unbalanced mass is considered as 0.4 m, while the range considered for the unbalanced mass in the front wheel assembly is 0.5 kg to 2 kg, and 1 kg to 3 kg for rear wheel assembly.

4.2.1 INFLUENCE OF VEHICLE SPEED

The magnitude of the force generated by rotating unbalanced mass in the wheel is directly proportional to the vehicle speed, as discussed in Chapter 2. In this study, the influence of speed on mass unbalance is investigated by analyzing the pitch plane model of the commercial vehicle under the stochastic excitations arising from the *smooth* road, operating at different speeds of 60 km/h, 80 km/h, and 100 km/h. The analyses are

performed for the baseline vehicle with negligible unbalance (me=0) of the front and rear wheels. Figure 4.1 illustrates a comparison of DLC due to front and rear wheel loads under the influence of wheel unbalance. The magnitudes of the wheel unbalance are varied from 0.2 to 0.8 kg-m for the front wheels and from 0.4 to 1.2 kg-m for the rear wheels, which are referred to as $(me)_f$ and $(me)_r$, respectively. The effect of front wheel unbalance are presented in terms of DLC of the front wheel tires, where $(me)_r$ is held as 0.4 kg-m. The DLC of the rear wheel tire is presented for varying value of $(me)_r$, while $(me)_f$ is held constant as 0.2 kg-m. The figure also shows the influence of vehicle speed, ranging from 60 to 100 km/h.

Figures 4.2 and 4.3 illustrate the influence of vehicle speed on the unweighted and frequency weighted vertical and pitch accelerations, respectively, for all the sets of wheel unbalance magnitudes. For the uniform and balanced wheels, the DLC values of both the axles increase with increase in speed, while the overall bounce rms acceleration values (unweighted and weighted) are the maximum at 60 km/h and the minimum at 80 km/h. The overall pitch rms acceleration values (unweighted and weighted) are the maximum at 100 km/h and the minimum at 80 km/h. This can be attributed to the spatial characteristics of the random road profile. The results further show that the weighted vertical acceleration is not affected by the speed, which suggests that the predominant spectral components of vertical vibration occur in frequency bands that are significantly attenuated by the weighting filter ($f < 3$ Hz and $f > 8$ Hz). The weighted pitch acceleration, on the other hand, shows stronger effect of vehicle speed, when compared to that observed for the unweighted acceleration. This is attributed to the predominant spectral components of pitch vibration in the lower frequency range, where the weighting filter emphasizes the contribution.

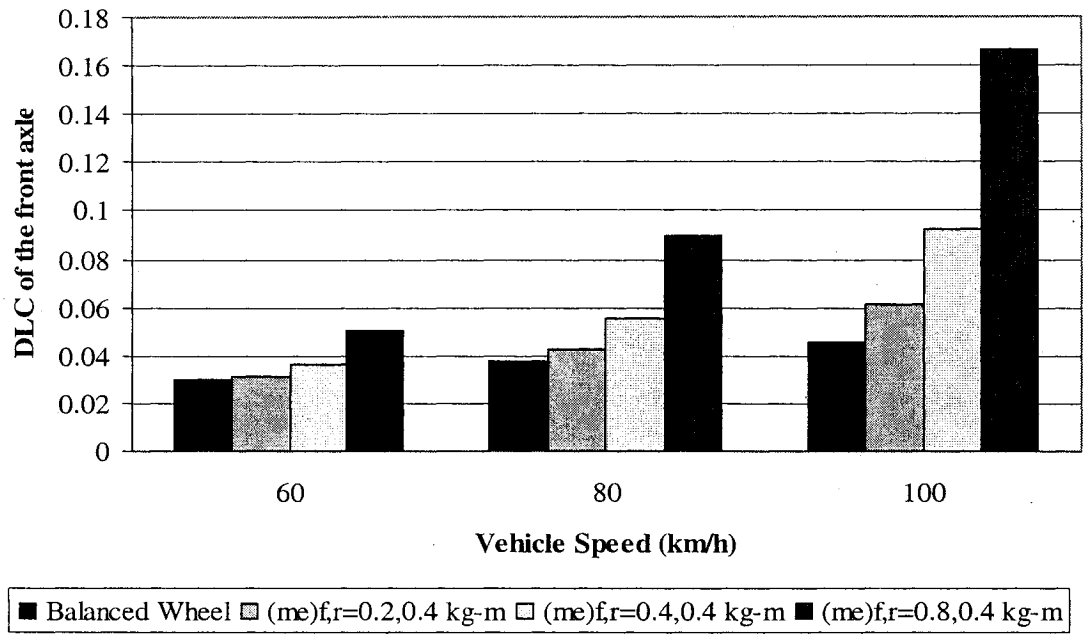

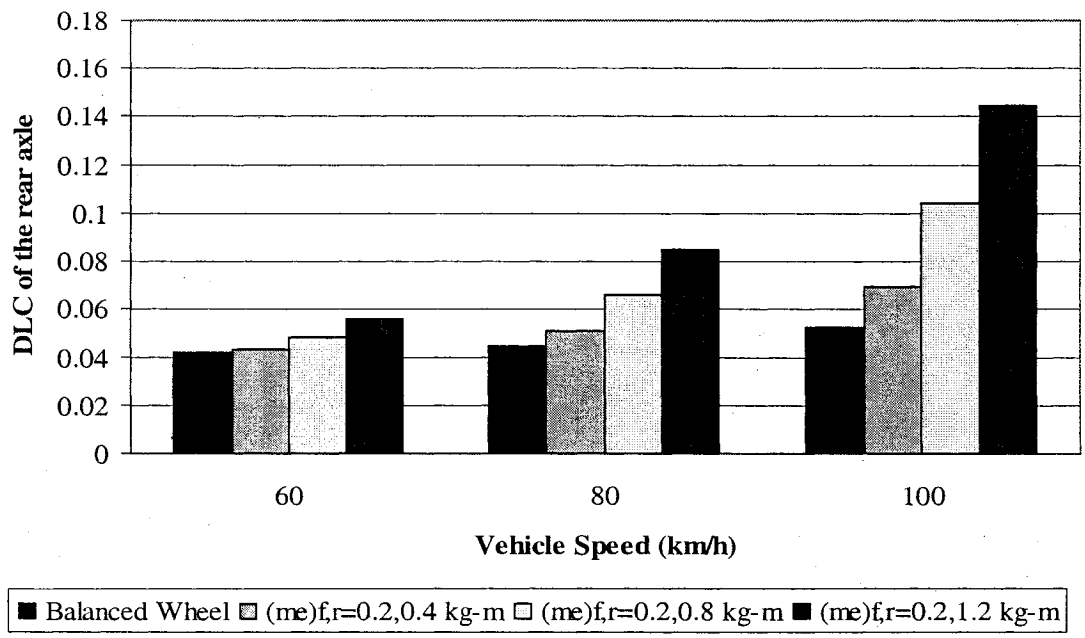

Figure 4.1: Influence of speed on DLC values for the front and rear axles with wheel unbalance (Smooth road)

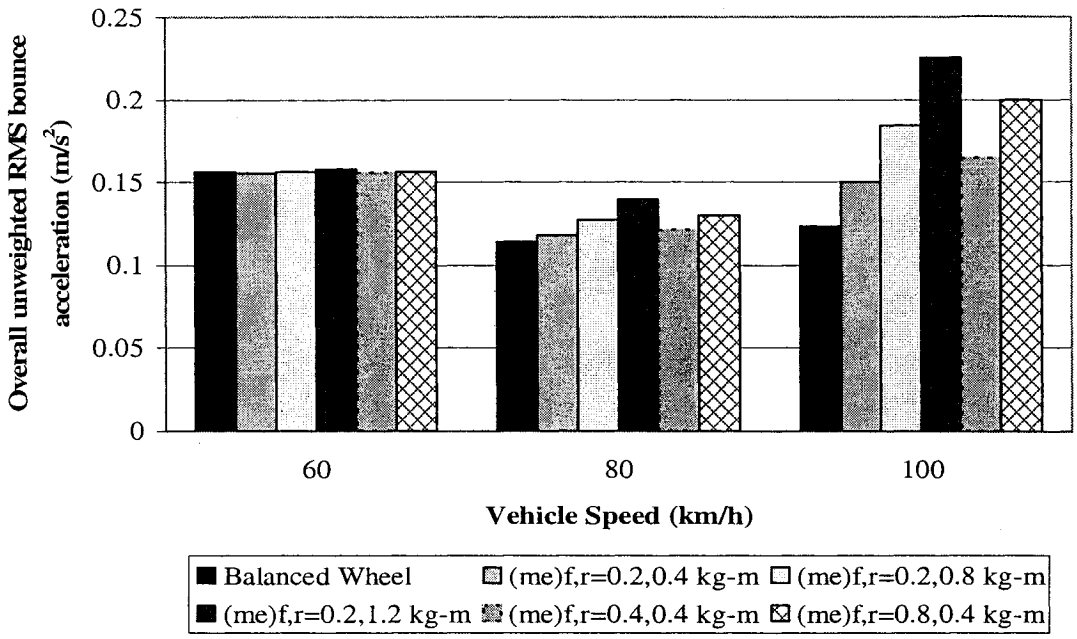

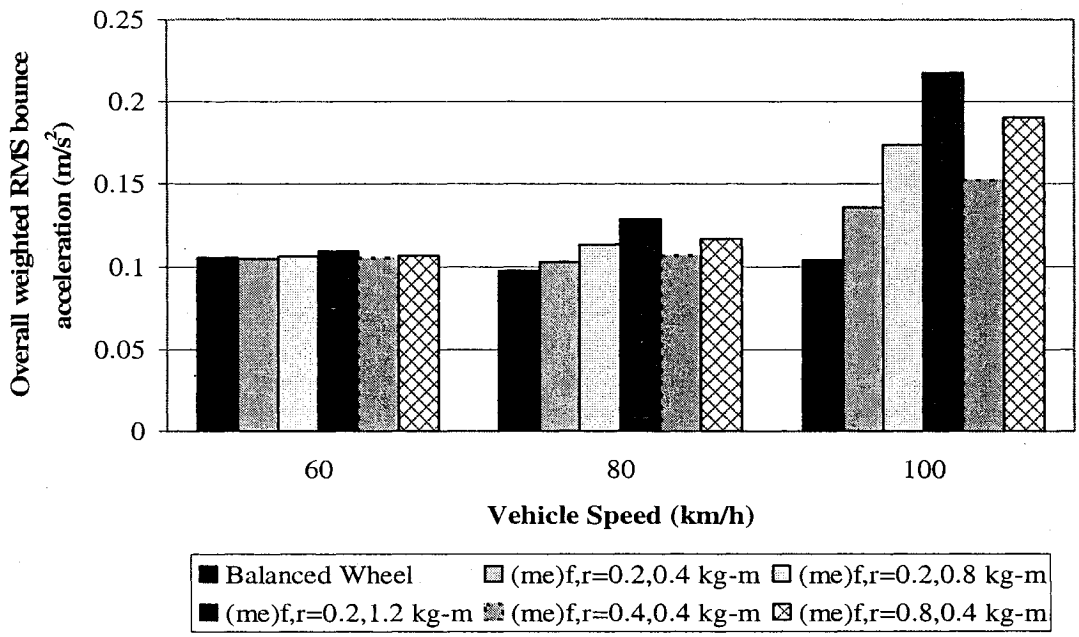

Figure 4.2: Influence of speed on overall unweighted and weighted rms bounce acceleration with wheel unbalance (Smooth road)

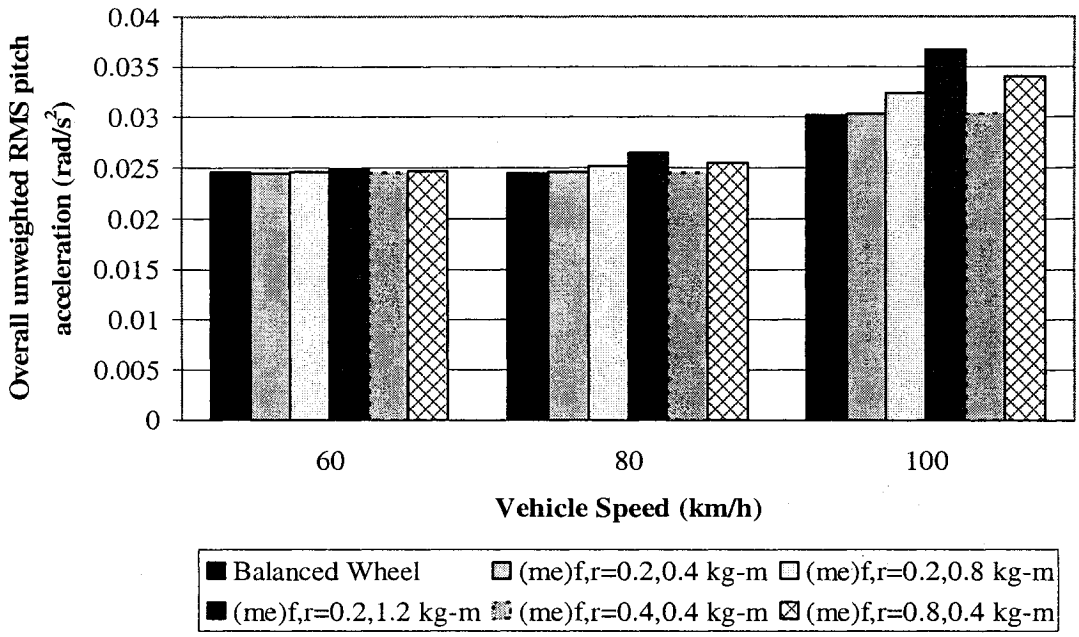

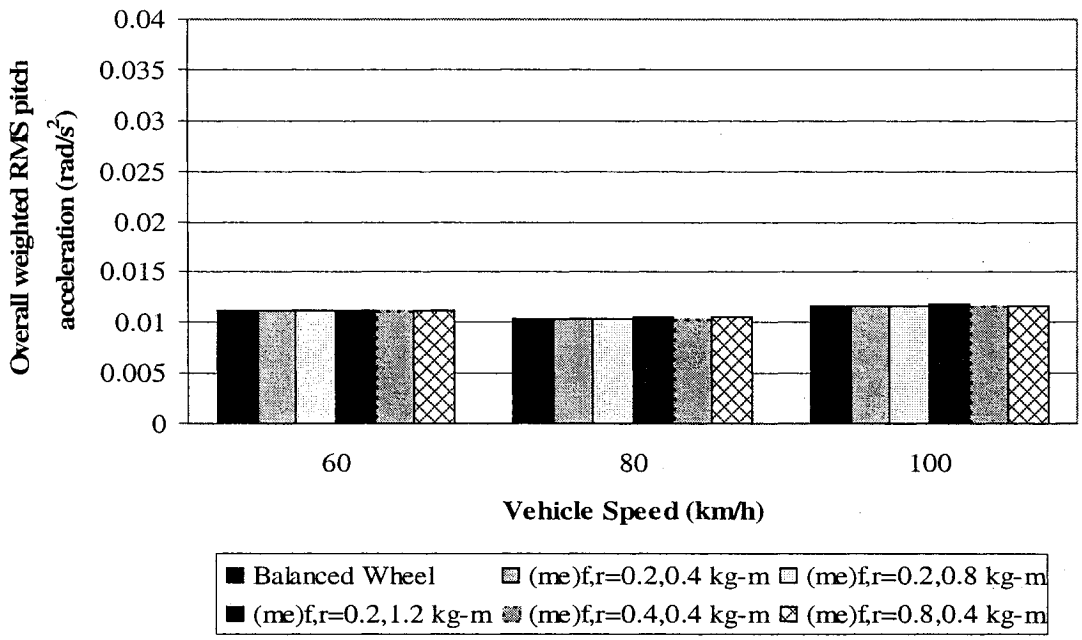

Figure 4.3: Influence of speed on overall unweighted and weighted rms pitch acceleration with wheel unbalance (Smooth road)

The presence of wheel unbalance tends to amplify the DLC due to front as well as rear wheels, significantly, as observed in Figure 4.1. The effect is more pronounced at a higher speed, since the unbalance force is directly related to the angular velocity of the wheel. The maximum increment in the DLC values with increasing magnitude of unbalance is observed at a speed of 100 km/h. The DLC values are 4 and 3 times higher for the front and rear axle tires, respectively, than those observed for the balanced wheels. The results thus suggest that the presence of wheel unbalance could impose significantly larger wheel loads on the pavement, when operating on a smooth road surface, and thereby cause higher potential for the pavement damage.

The weighted and unweighted pitch and vertical rms acceleration responses of the vehicle sprung weight also increase in a similar manner with increasing wheel unbalance at a speed of 100 km/h. The effect of mass unbalance is insignificant at the lower speed of 60 km/h, and the effect is only slight at 80 km/h under extreme unbalance of $(me)_r$ = 1.2 kg-m. The small variations in the unweighted and weighted rms acceleration responses at lower speeds are attributed to two major factors. Firstly, the effective forces due to unbalance are small at lower speeds, and thereby cause relatively small change in the acceleration response. Secondly, the unbalanced wheels cause variations in the acceleration responses only in the vicinity of the wheel's angular speed. Considering the wheel radius of 0.5 m, these correspond to 5.3 Hz, 7.1 Hz and 8.8 Hz, respectively, for operations at 60, 80, and 100 km/h. The frequency-weighting filters recommended in ISO-2631-1 [69] emphasize the pitch vibration below 2 Hz and vertical vibration in the 3 to 10 Hz range. The influence of wheel unbalance on the frequency-weighted pitch acceleration is thus very small, as observed in Figure 4.3. The effects on the weighted

vertical rms acceleration are more pronounced at higher speeds due to relatively higher magnitudes of the unbalance forces, while the contribution due to the frequency-weighting filter is somewhat small.

The spectral components of vertical and pitch acceleration responses are evident from the PSD of bounce and pitch accelerations (weighted and unweighted) presented in Figures 4.4 and 4.5, respectively, for all sets of magnitudes of unbalance at 60 km/h. All the peaks corresponding to wheel unbalance can be observed at wheel rotating frequency of 5.3 Hz. The presence of wheel unbalance tends to emphasize the peak response near 5.3 Hz. The peak magnitudes of vertical and pitch accelerations occur for $(me)_f$ = 0.2 kg-m and $(me)_r$ =1.2 kg-m, while lower levels of mass unbalance, $(me)_{f,r}$ = 0.2, 0.4 and $(me)_{f,r}$ = 0.4, 0.4 kg-m, yield only small increases in the acceleration responses. Comparison of frequency-weighted and unweighted acceleration spectra further show negligible effects of the weighting filter on the vertical and pitch rms accelerations, at the lower speed.

Figures 4.6 to 4.9 illustrate the PSD of vertical and pitch unweighted and weighted acceleration responses of the vehicle at forward speeds of 80 km/h and 100 km/h, respectively, for different levels of wheel unbalances. The results show that the peak magnitudes in the acceleration responses shift towards higher as the forward speed is increased. Both the vertical and pitch acceleration responses in the range of 1-2 Hz, associated with pitch and vertical mode responses of the sprung mass, generally decrease with increasing speed. Moreover, the wheel unbalance does not affect the vibration responses in the lower frequency range. The presence of wheel unbalance causes peaks near 7.1 Hz and 8.8 Hz, respectively, at speeds of 80 and 100 km/h. The magnitudes of peaks in the vertical and pitch acceleration spectra however increase with increasing speed as well the unbalance.

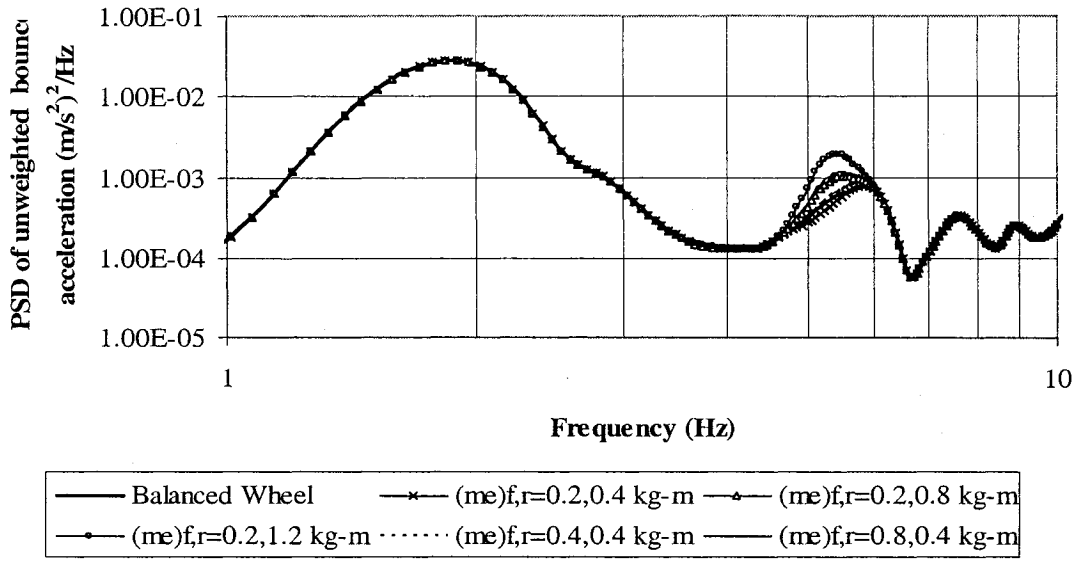

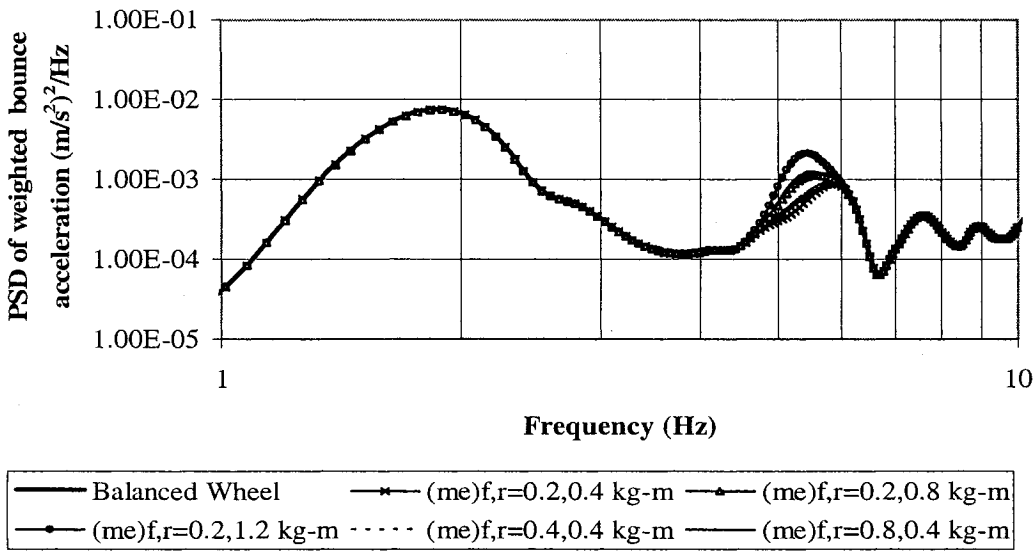

Figure 4.4: Effect of wheel unbalance on PSD of unweighted and weighted bounce acceleration at 60 km/h (Smooth road)

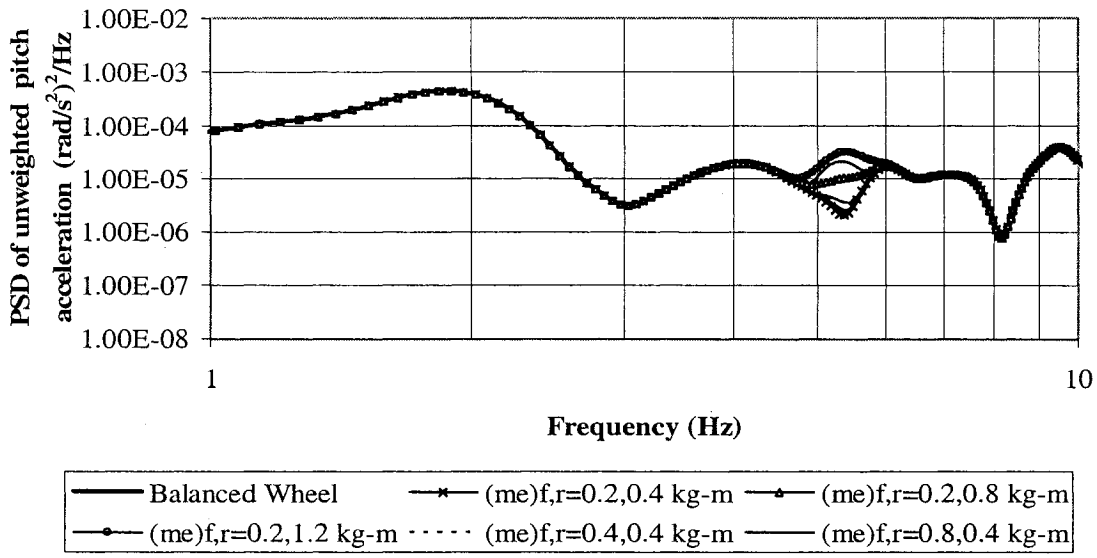

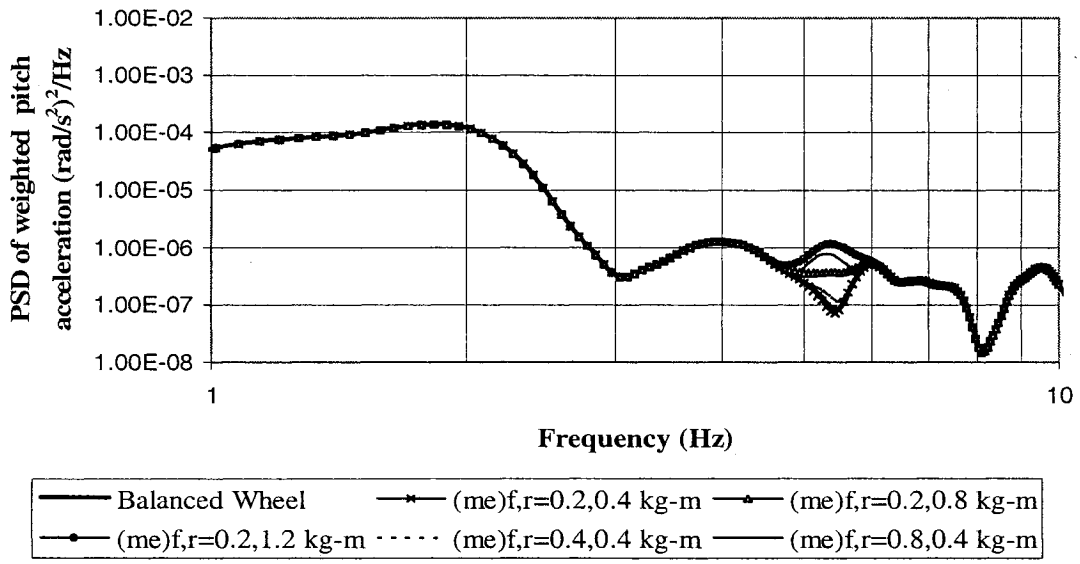

Figure 4.5: Effect of wheel unbalance on PSD of unweighted and weighted pitch acceleration at 60 km/h (Smooth road)

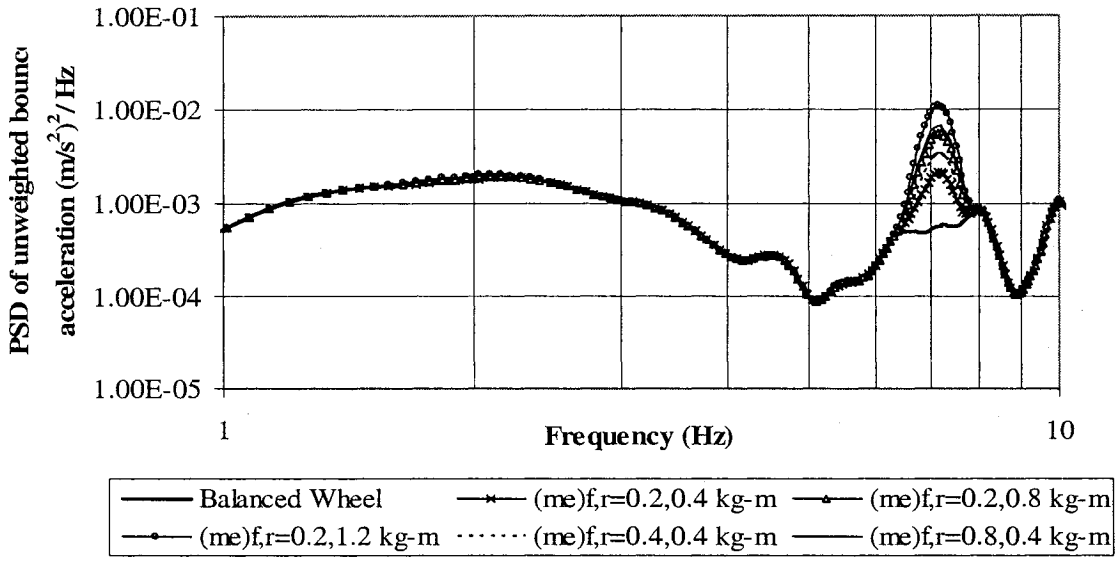

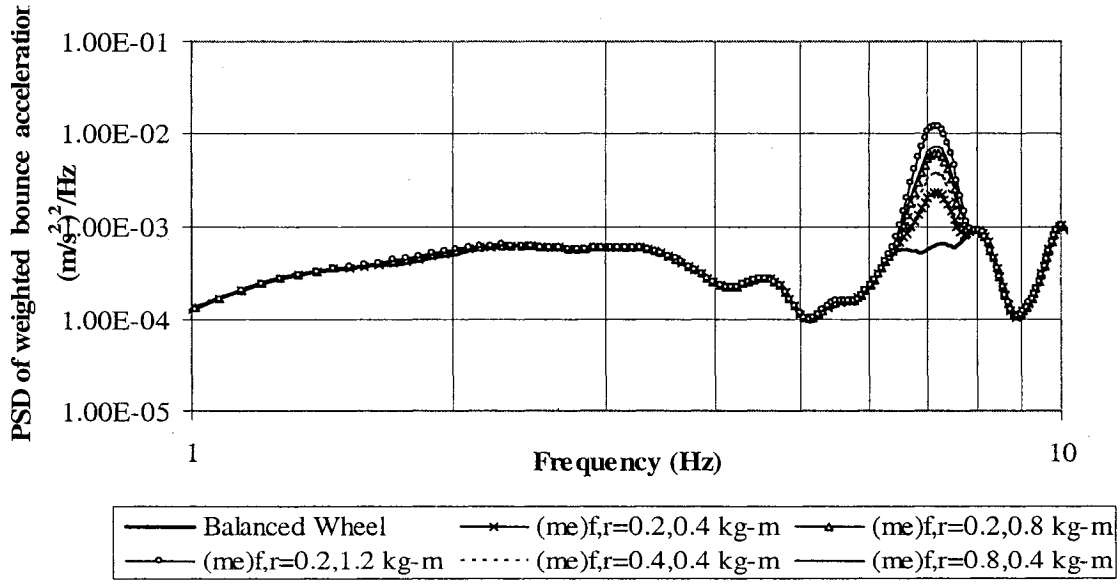

Figure 4.6: Effect of wheel unbalance on PSD of unweighted and weighted bounce acceleration at 80 km/h (Smooth road)

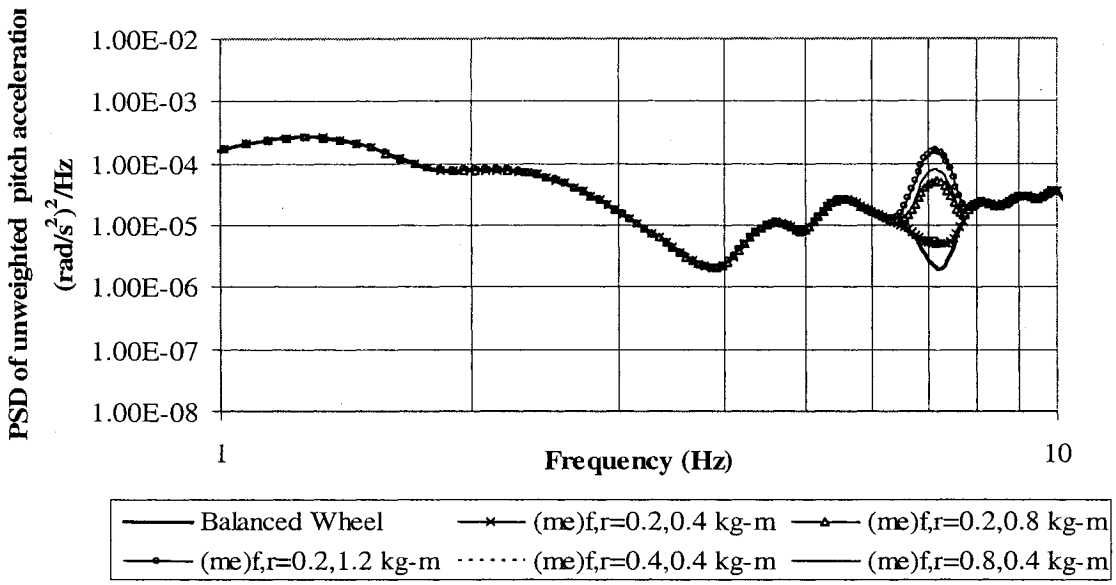

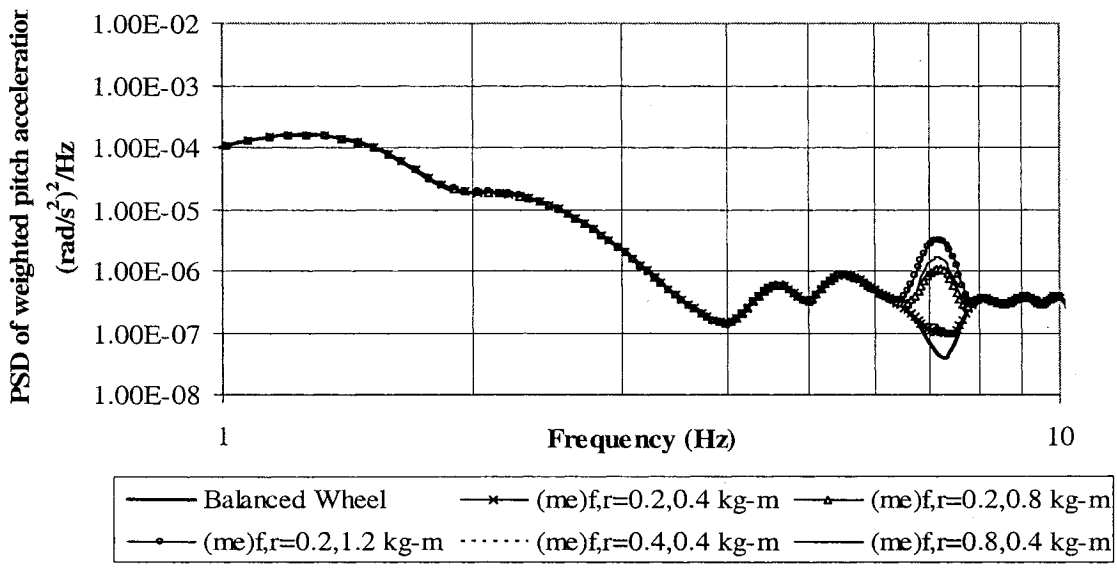

Figure 4.7: Effect of wheel unbalance on PSD of unweighted and weighted pitch acceleration at 80 km/h (Smooth road)

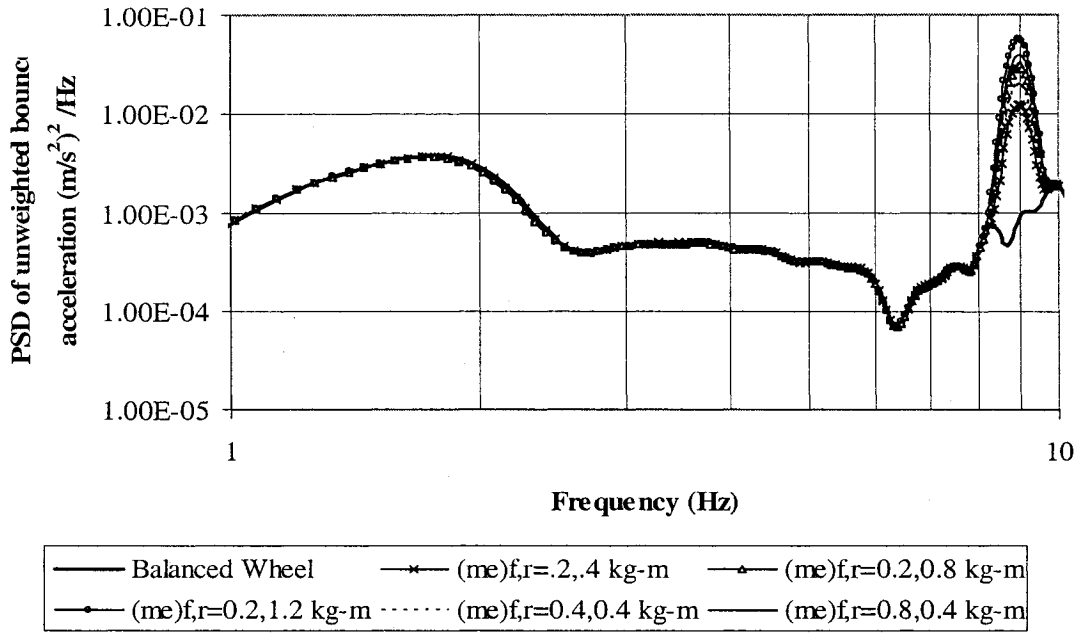

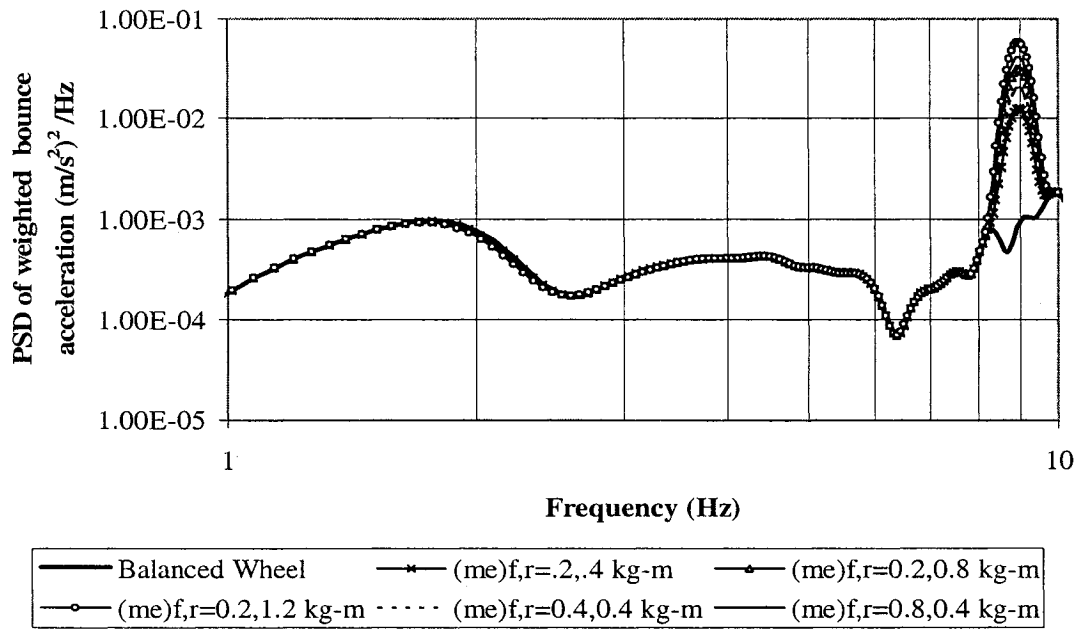

Figure 4.8: Effect of wheel unbalance on PSD of unweighted and weighted bounce acceleration at 100 km/h (Smooth road)

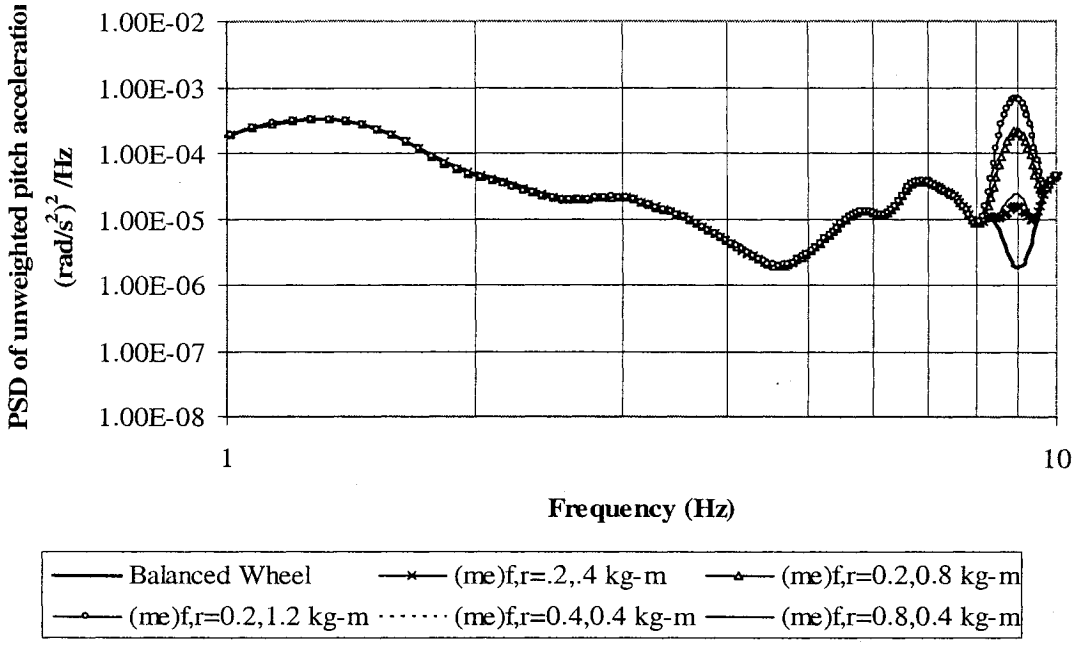

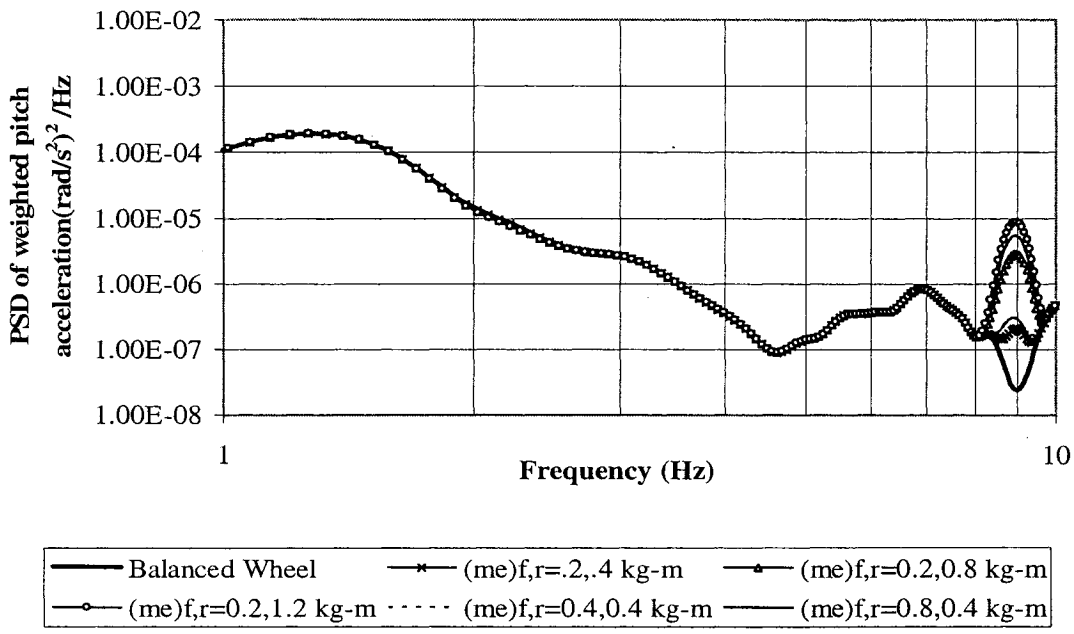

Figure 4.9: Effect of wheel unbalance on PSD of unweighted and weighted pitch acceleration at 100 km/h (Smooth road)

The results further show that the peak magnitudes of frequency weighted vertical acceleration PSD are slightly larger for 60 km/h and 80 km/h speeds, and similar at 100 km/h. These differences are attributed to the magnitude ratio of the W_k-weighting filter.

The magnitudes of the peaks in the frequency-weighted pitch acceleration PSD, on the other hand, are considerably smaller than those observed in the unweighted spectra for all these speeds. This is attributed to the significant attenuations by the W_e-weighting filter near the predominant frequencies. The weighted pitch acceleration responses thus do not show notable effects of the wheel unbalance (Figure 4.3).

Figure 4.10 illustrates the PSD of the front and rear tire forces as function of the magnitudes of wheel unbalance, while the speed is 60 km/h. The PSD for the front tire force shows the maximum peak magnitude corresponding to wheel unbalance at 0.8 and 0.4 kg-m combination, while for the rear axle the maximum magnitude can be observed for 0.2 and 1.2 kg-m combination. The force responses also show peaks of considerable magnitude in the vicinity of 5.3 Hz, which is not present when the wheels are balanced. The peak magnitude tends to increase significantly with increasing mass unbalance, which contributes to relatively higher DLC, as evident in Figure 4.1. The strong influence of operating speed on the peak magnitudes of tire forces and the corresponding frequencies are clearly evident in the responses presented in Figures 4.11 and 4.12, respectively, forward speeds of 80 and 100 km/h. The results further show that higher levels of wheel unbalance cause considerably higher magnitudes of dynamic tire forces, which contribute to higher values of DLC, particularly at higher speed of 100 km/h.

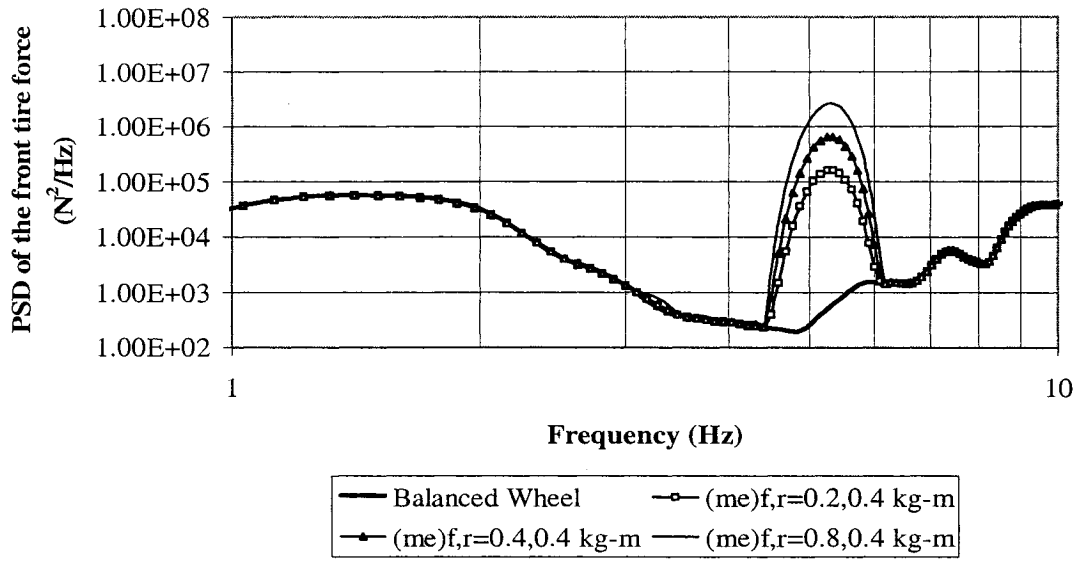

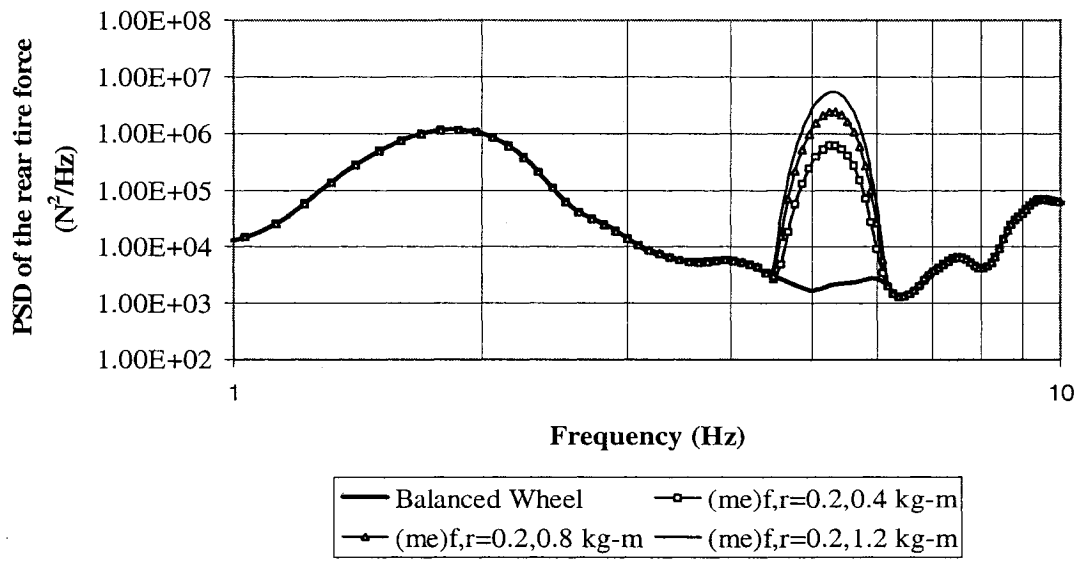

Figure 4.10: Effect of wheel unbalance on PSD of the front and rear tire forces at 60 km/h (Smooth road)

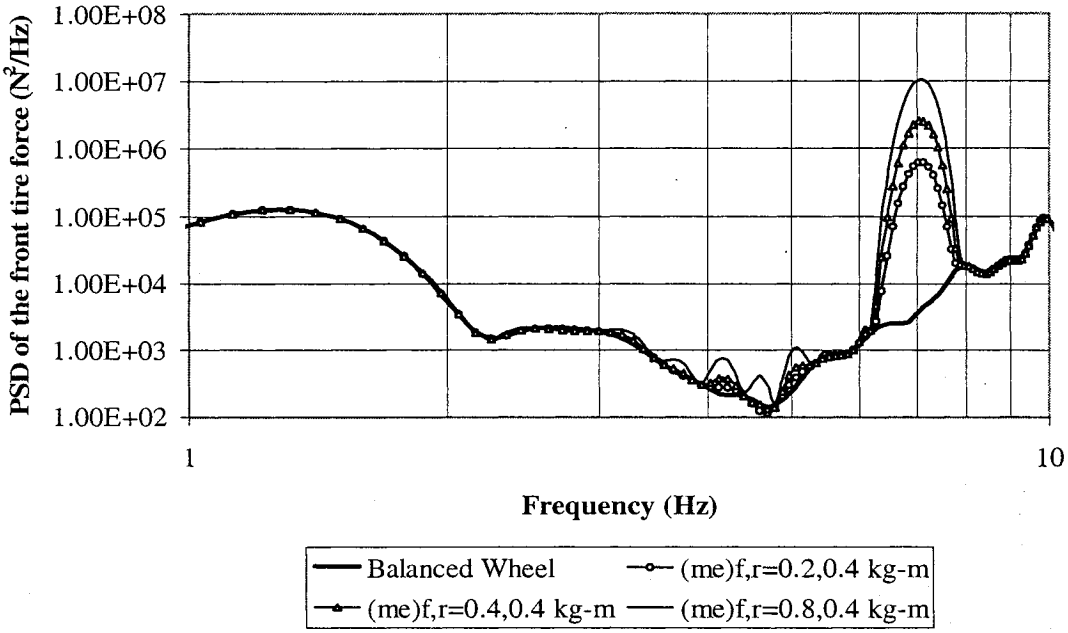

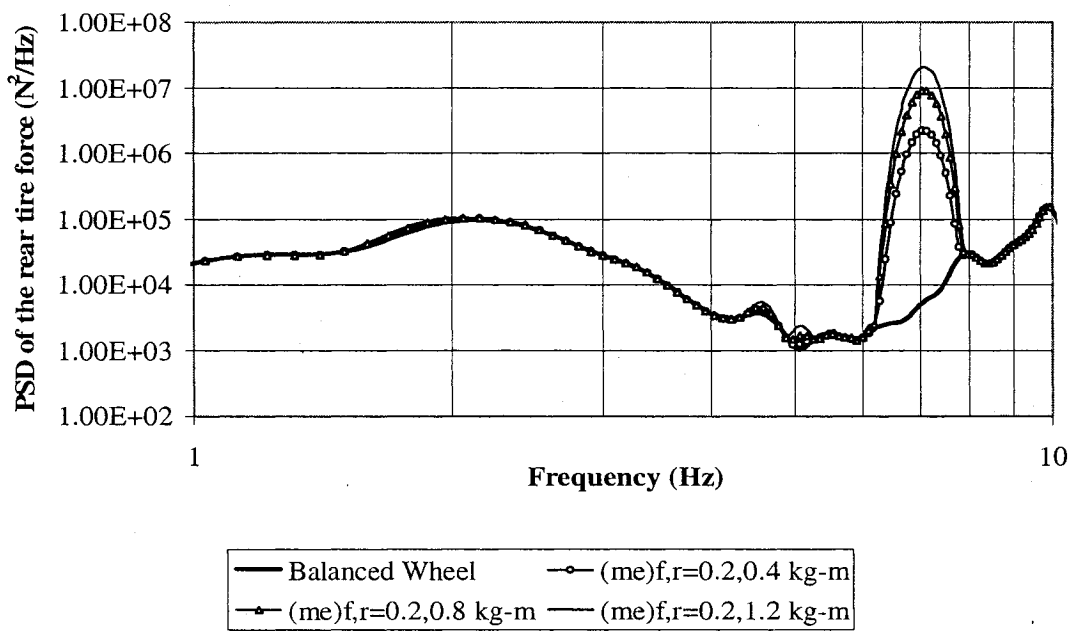

Figure 4.11: Effect of wheel unbalance on PSD of the front and rear tire forces at 80 km/h (Smooth road)

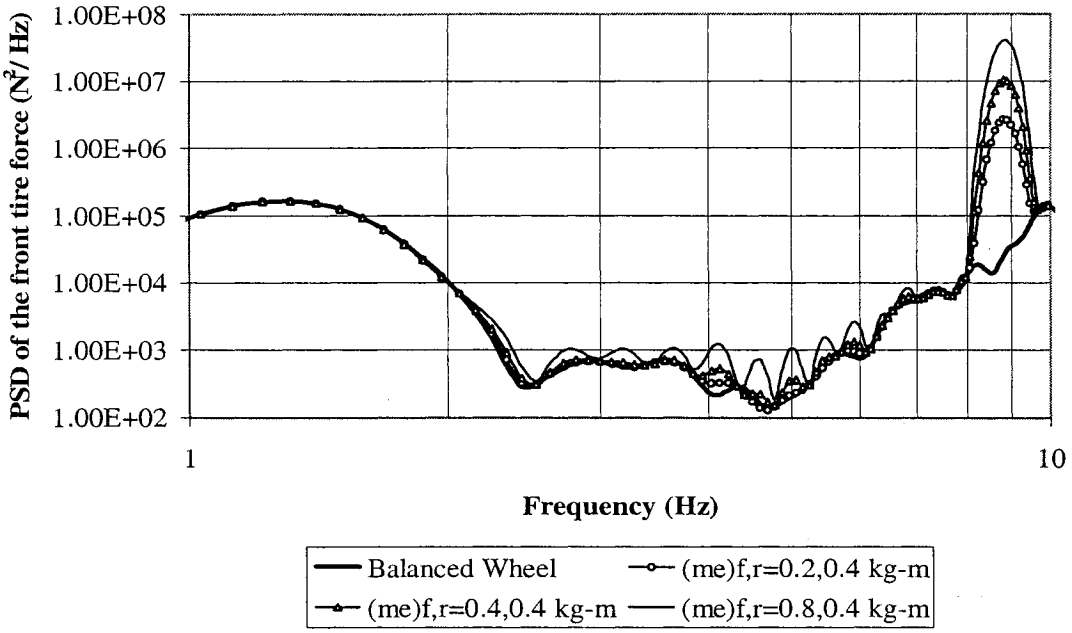

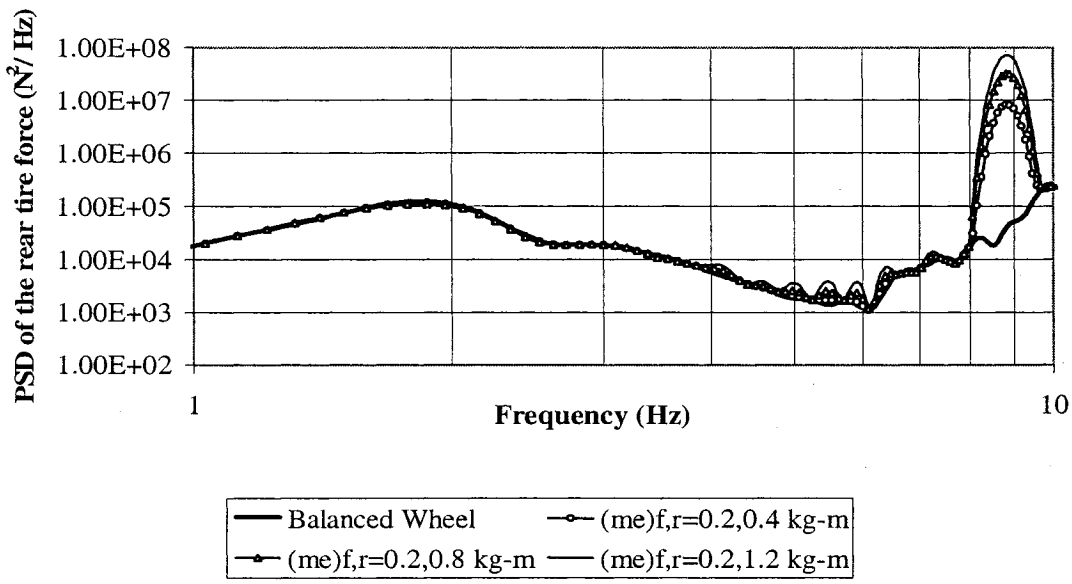

Figure 4.12: Effect of wheel unbalance on PSD of the front and rear tire forces at 100 km/h (Smooth road)

4.2.2 INFLUENCE OF ROAD ROUGHNESS

The results presented in the previous sections show significant effect of the wheel unbalance on both ride and tire load responses at higher speeds when the vehicle operates on a smooth road. Apart from the vehicle speed, the vehicle interactions with the road strongly depend upon the road roughness. Increasing road roughness generally yields higher magnitudes of ride accelerations and tire forces [1, 45]. The relative significance of the forces and accelerations caused by mass unbalance may be small in relation to those caused by the tire interactions with a rough road surface. Many studies have concluded that both the vehicle ride quality and road damage potential are strongly related to the tire-terrain dynamic interactions [1, 117], which are mostly influenced by the magnitude and frequency components of terrain roughness. The relative contribution of the wheel unbalance is thus investigated under excitations arising from the medium-rough and rough roads, as described in Chapter 3. The roughness indices for these roads were computed as 4.37 and 5.94, respectively, while that for the smooth road considered in the previous section was computed as 1.59. The relative contribution of different levels of unbalance of the front and rear wheels are analyzed for a single forward speed of 80 km/h, while the results are presented in terms of dynamic tire loads, and vertical and pitch ride accelerations (weighted and unweighted). Moreover, the analyses are performed for identical combination of unbalances of the front and rear axles.

Figures 4.13 to 4.15 illustrate the influence of three different road roughness types on the performance measures in terms of DLC, due to front and rear axle tire forces, and unweighted and frequency-weighted overall vertical and pitch rms accelerations, respectively.

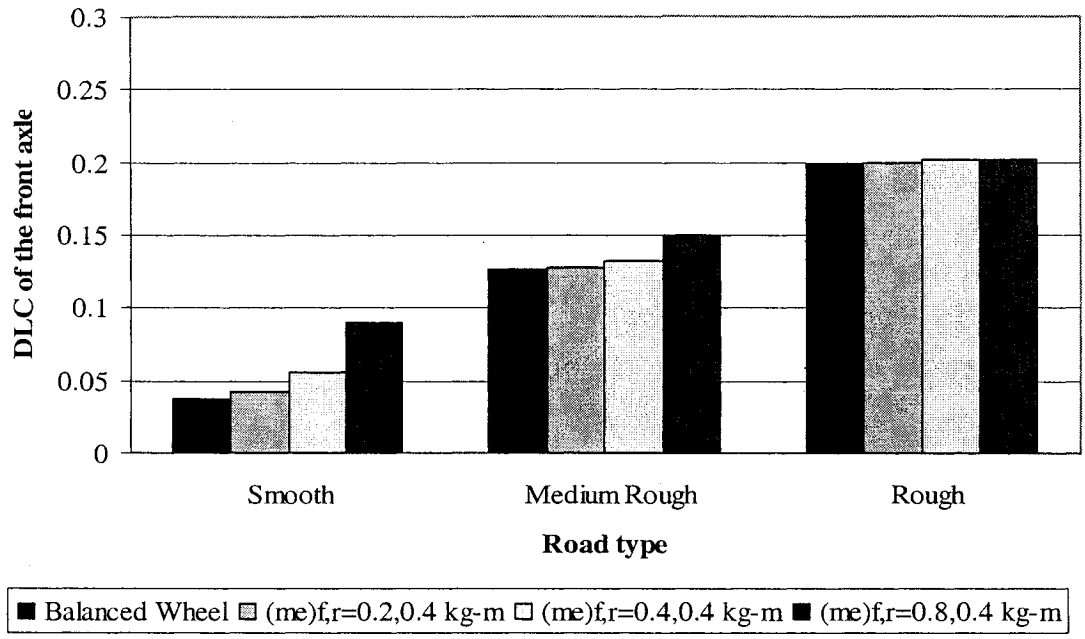

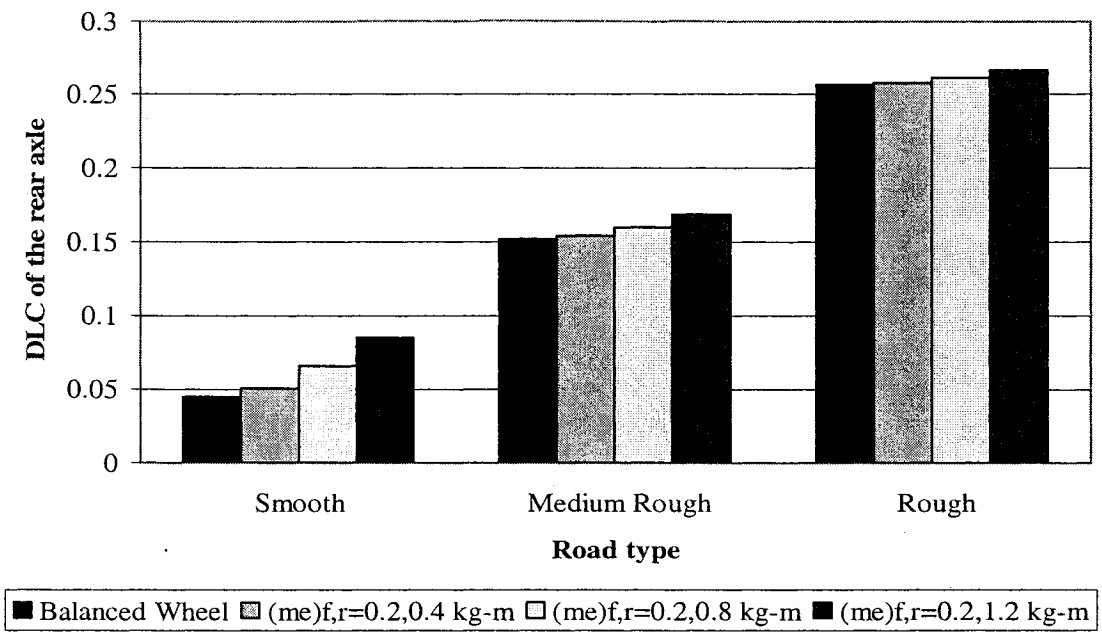

Figure 4.13: Influence of road roughness on DLC values for front and rear axle at 80 km/h with wheel unbalance

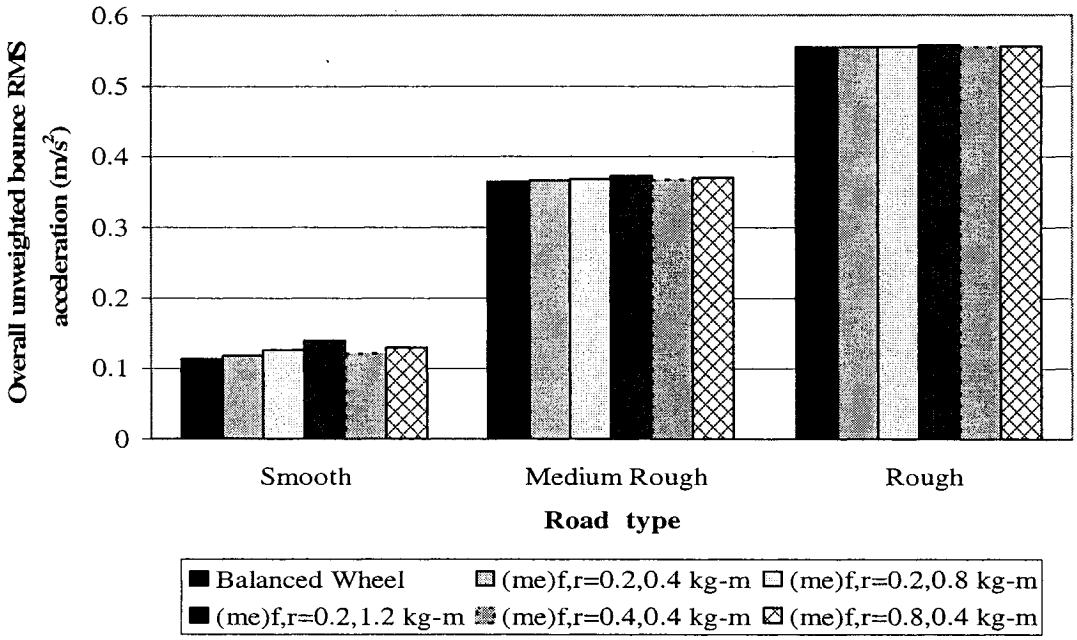

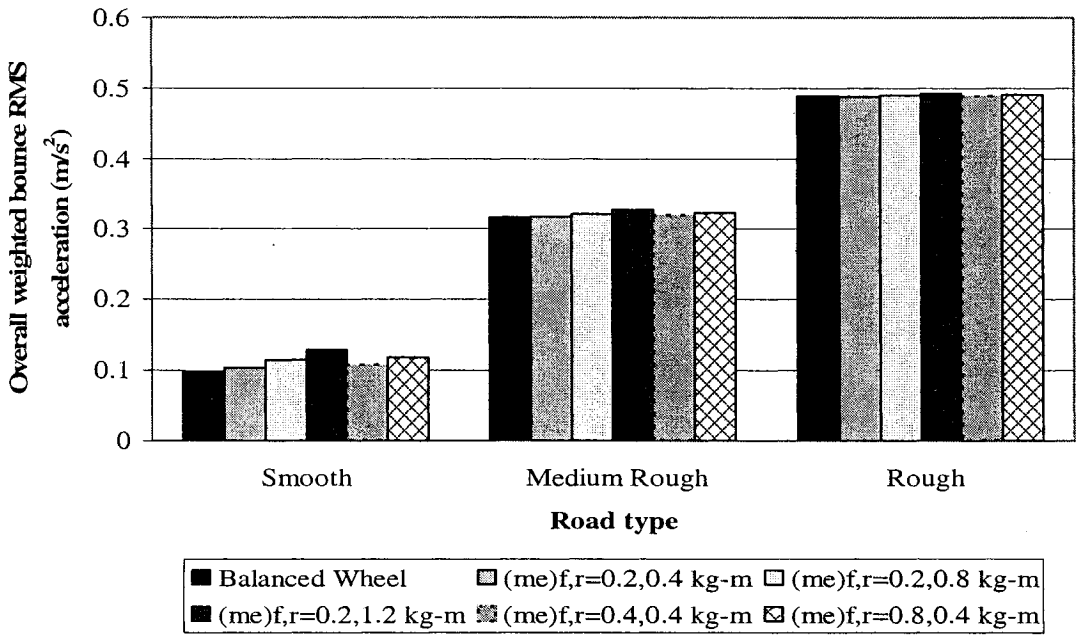

Figure 4.14: Influence of road roughness on overall unweighted and weighted rms bounce acceleration at 80 km/h with wheel unbalance

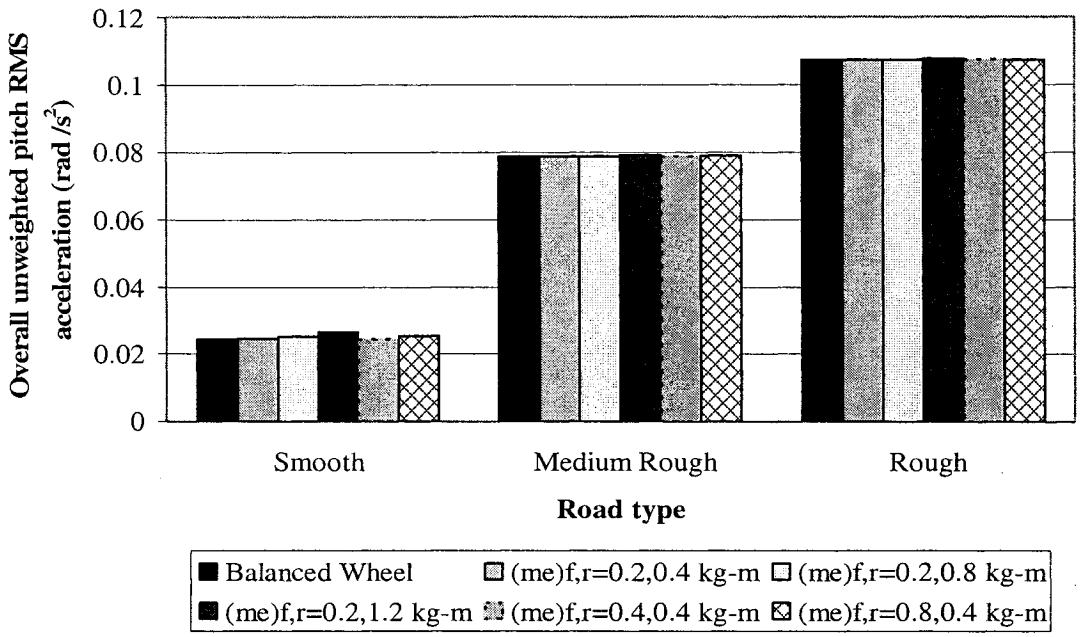

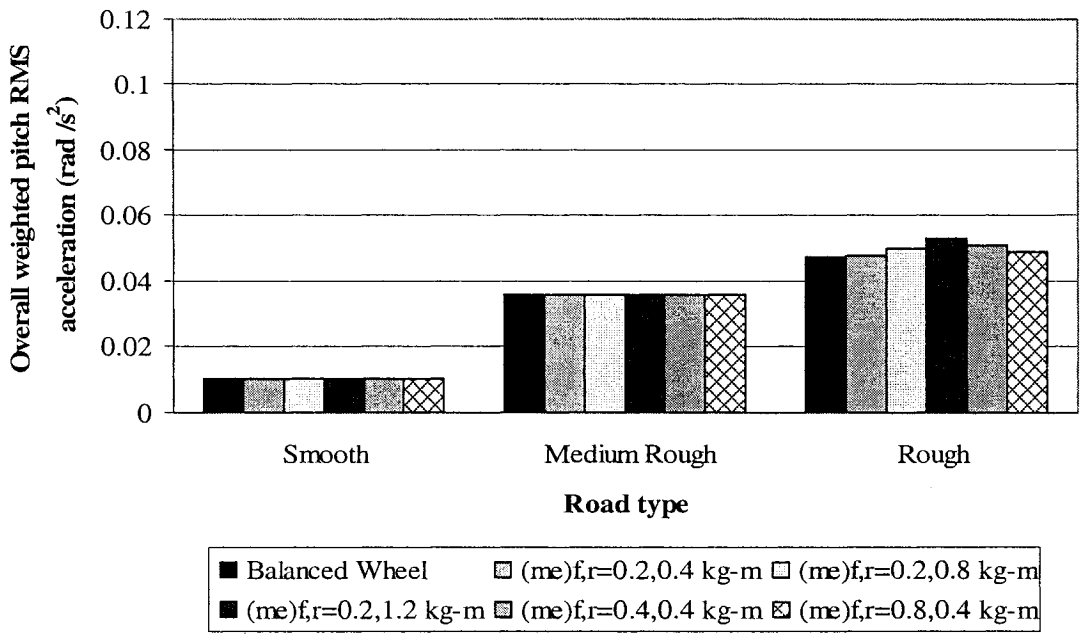

Figure 4.15: Influence of road roughness on overall unweighted and weighted rms pitch acceleration at 80 km/h with wheel unbalance

For the balanced and uniform wheeled vehicle, it is observed that DLC values for both the front and rear axle tires increase considerably with increase in the road roughness. This tendency has also been reported in many published studies on tire loads [1, 55, 117]. The results suggest that the vehicle and the road form a closed loop system, where high road roughness induces higher tire loads, which in turn impose larger dynamic forces on the pavement leading to its further deterioration. An increase in the magnitude of the unbalance of the front or the rear wheels causes considerably larger increase in the DLC of both axle tires, when the vehicle is operating on a smooth road. The relative change in the DLC due to increasing unbalance, however, diminishes under medium-rough and rough road operations, as evident in Figure 4.13. The results, therefore, suggest that the effects of wheel unbalance are more pronounced, when the contribution due to tire-road interactions are relatively small, as in the case of smooth road operation. Similar trends are also evident in the weighted and unweighted overall rms bounce (vertical) and pitch (angular) acceleration responses (Figures 4.14 and 4.15). It can also be noted that the weighted pitch acceleration values are considerably lower than the unweighted values, while the weighted bounce acceleration values are either close to or slightly lower than their respective unweighted values. This can be attributed to the predominant wheel unbalance effect of vertical vibration in the range of 5-10 Hz bands, where the amplitude ratio of the W_k-weighting filter is either close to or only slightly greater than unity. The pitch vibrations in this frequency range are mostly attenuated by the W_e-filter.

From the results presented above, it is apparent that there is considerable increase in all performance measures with increase in unbalance mass for the smooth road. The

percentage increment for all performance measures reduces with increase in road roughness. This can be attributed to the increasing contribution from the road with increase in roughness. The unbalance mass combination of 0.2 and 1.2 kg-m yields the maximum values of all the performance measures for all road types. With varying mass unbalance, the change in weighted bounce and unweighted pitch acceleration values is very small. The weighted pitch values are almost unaffected with increase in the unbalance mass for all the road conditions which can be attributed to the characteristics of a weighting filter.

The diminishing effects of the wheel unbalance with increasing road roughness could be clearly observed from the spectra of the acceleration and tire force responses presented in Figures 4.16 to 4.21. The PSD of front and rear tires forces under vehicle's interactions with the medium-rough and rough roads are presented in Figures 4.16 and 4.17, respectively. The results show that the wheel unbalances yield significant peak responses near 7.1 Hz, irrespective of the road roughness. The magnitudes of the peaks relative to the responses of the baseline vehicle, with balanced and uniform wheels, however, are considerably smaller than those observed for the smooth road in Figure 4.11. Moreover, the relative magnitude tends to be smaller for the rough road. The ratio of the peak response, observed near 7.1 Hz under $(me)_f$ = 0.2 kg-m and $(me)_r$ = 1.2 kg-m, to that obtained for balanced wheels, tends to be approximately 4000 for the smooth road operation. This ratio reduces to approximately 600 to 200 under medium-rough and rough road operations, respectively. These results clearly show that the wheel unbalances

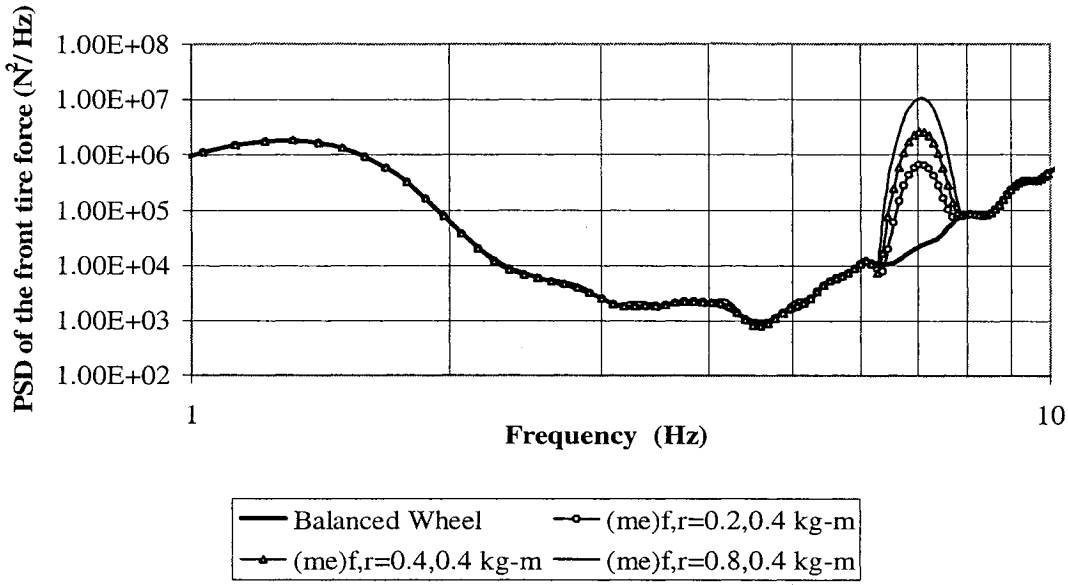

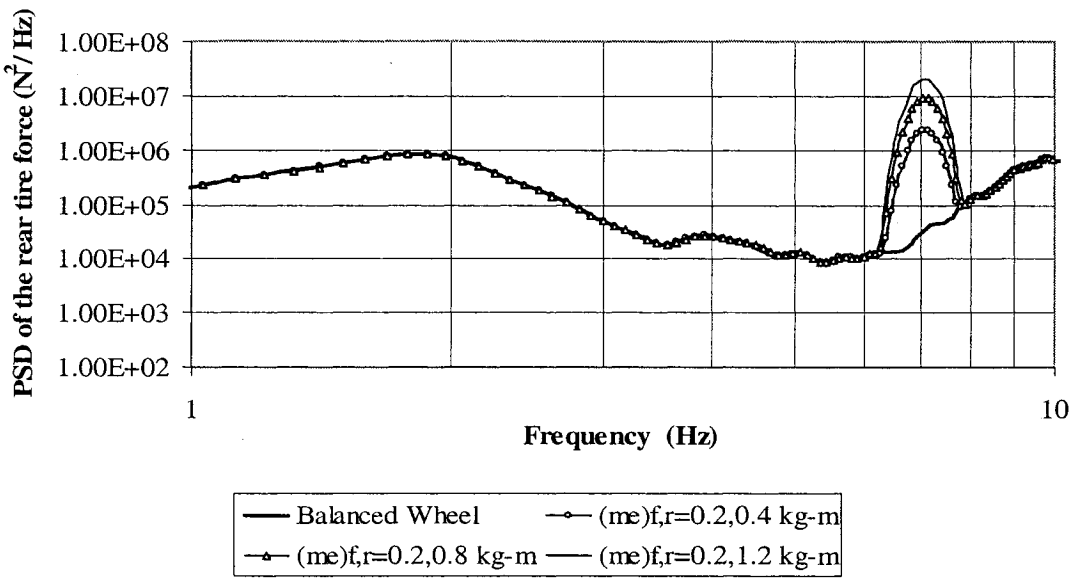

Figure 4.16: Effect of wheel unbalance on PSD of the front and rear tire forces at 80 km/h (Medium-rough road)

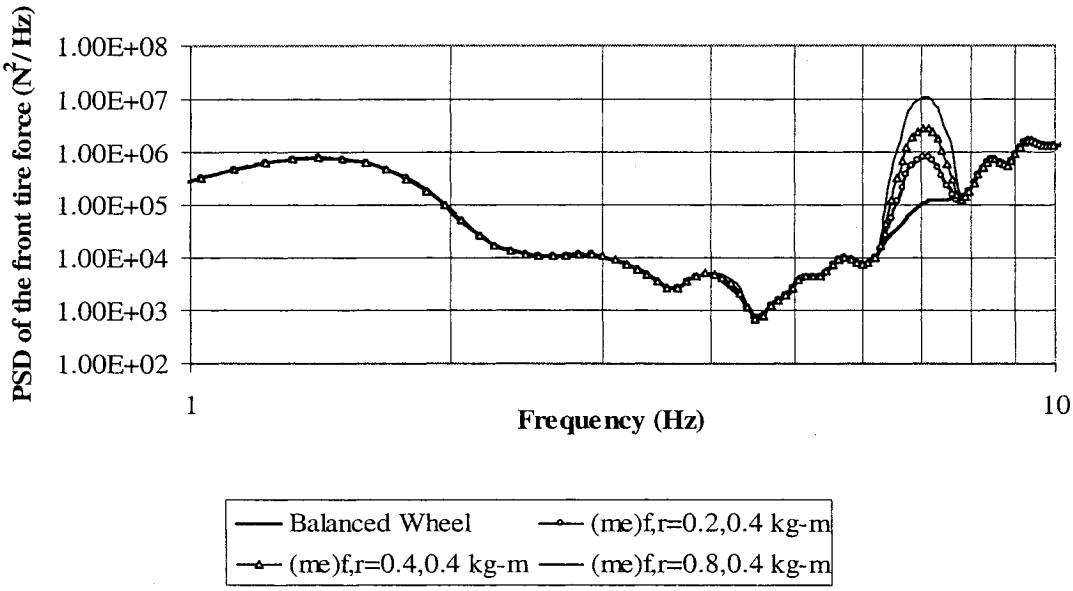

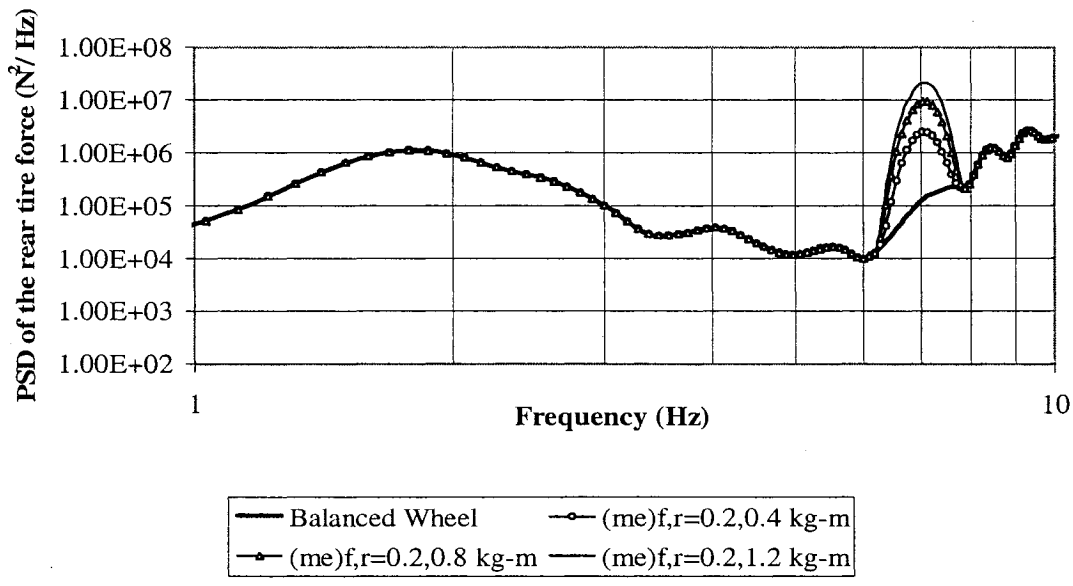

Figure 4.17: Effect of wheel unbalance on PSD of the front and rear tire force at 80 km/h (Rough road)

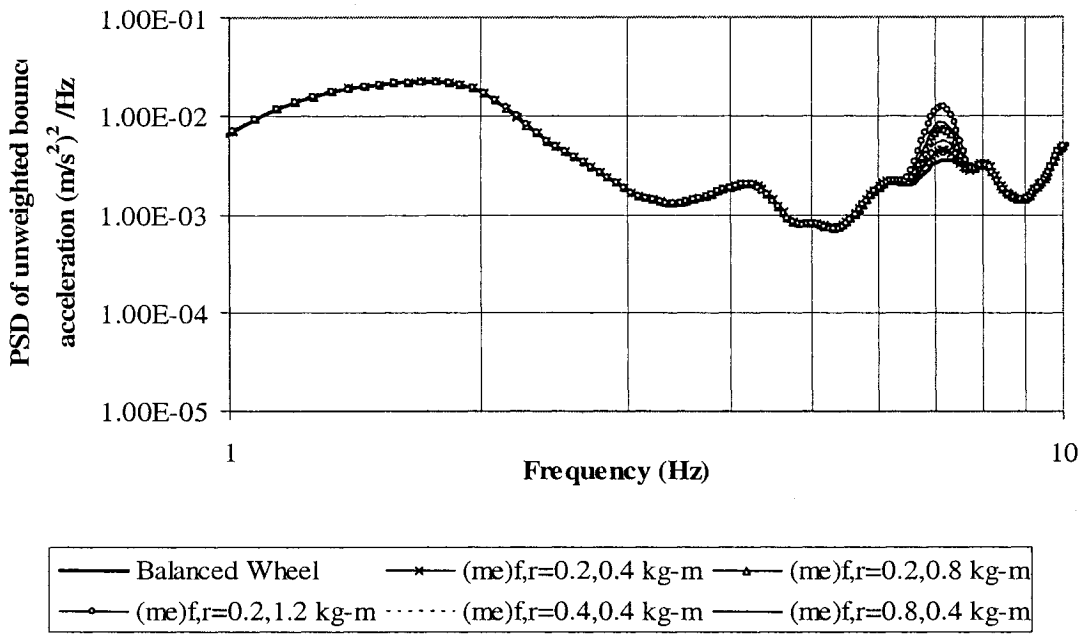

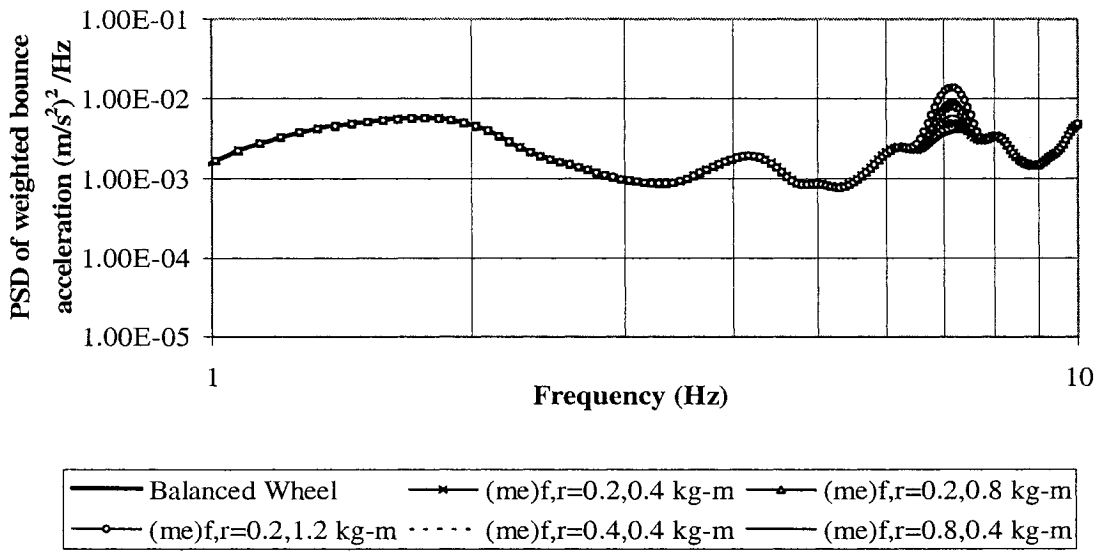

Figure 4.18: Effect of wheel unbalance on PSD of unweighted and weighted bounce acceleration at 80 km/h (Medium-rough road)

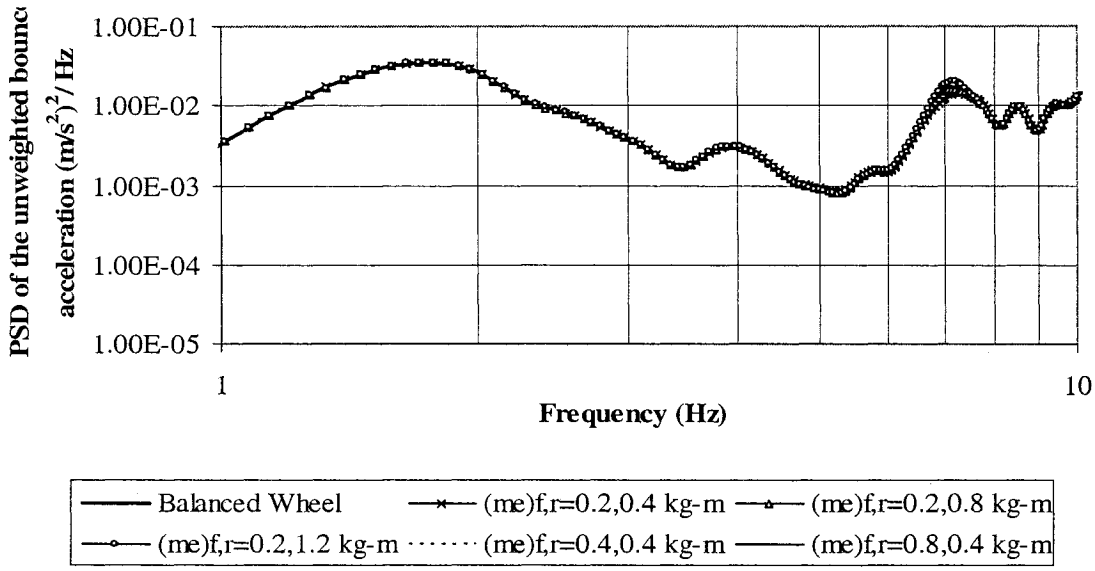

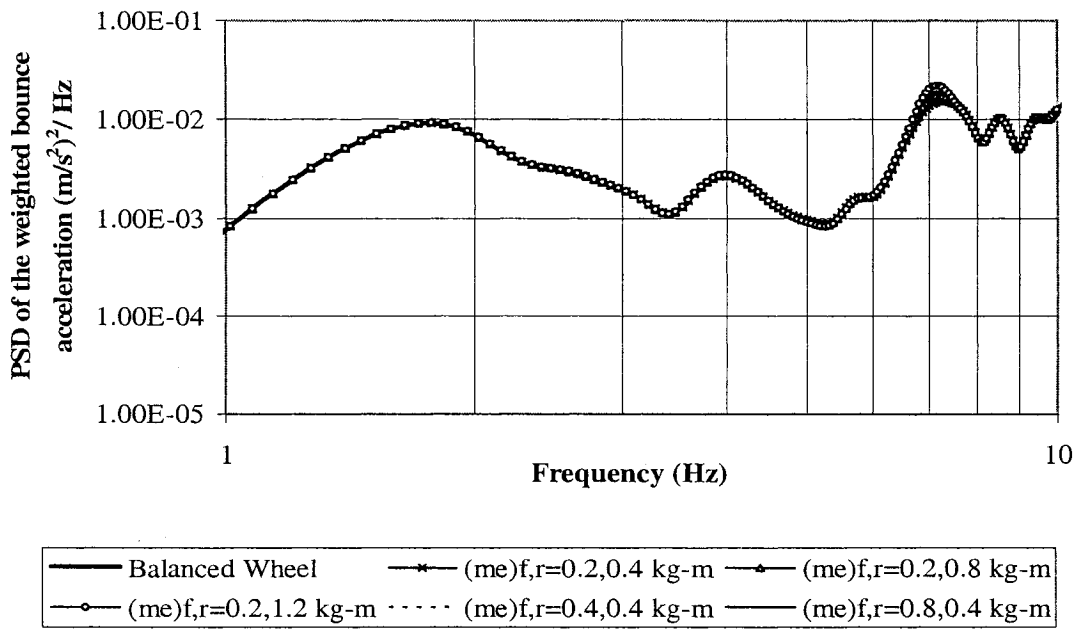

Figure 4.19: Effect of wheel unbalance on PSD of the unweighted and weighted bounce acceleration at 80 km/h (Rough road)

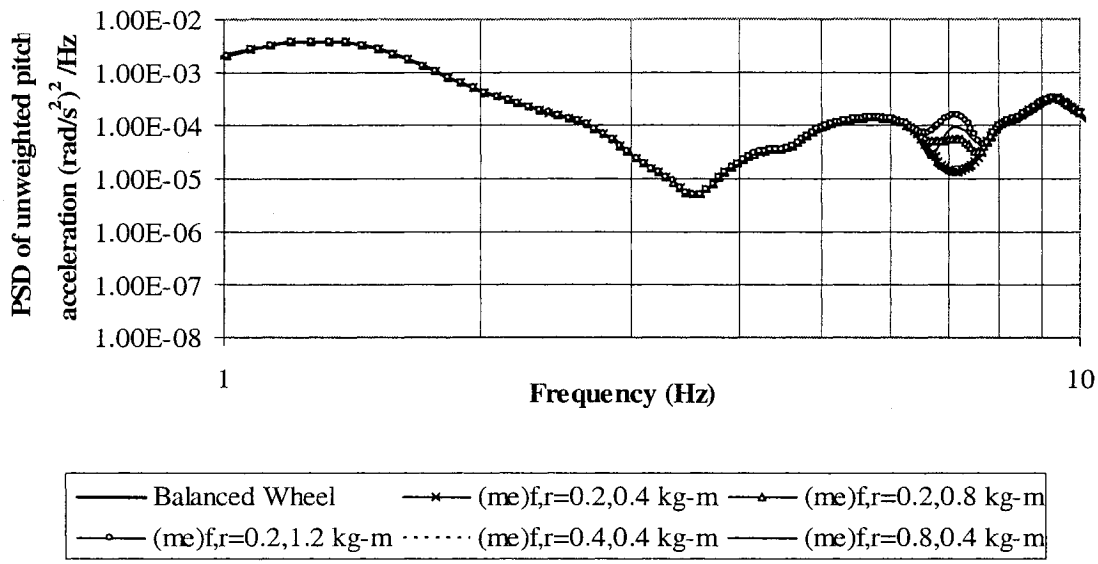

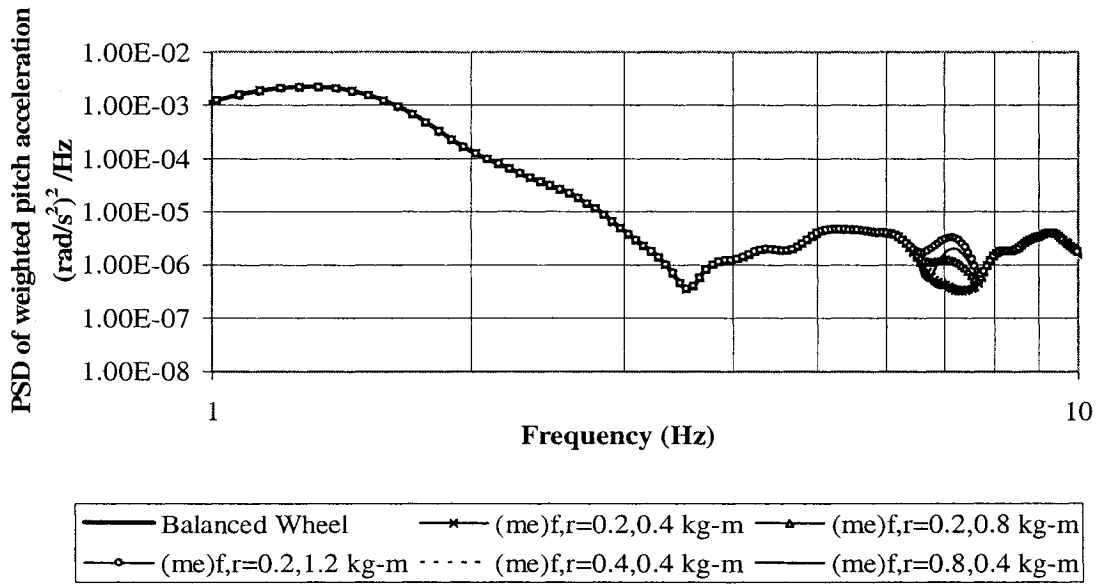

Figure 4.20: Effect of wheel unbalance on PSD of unweighted and weighted pitch acceleration at 80 km/h (Medium-rough road)

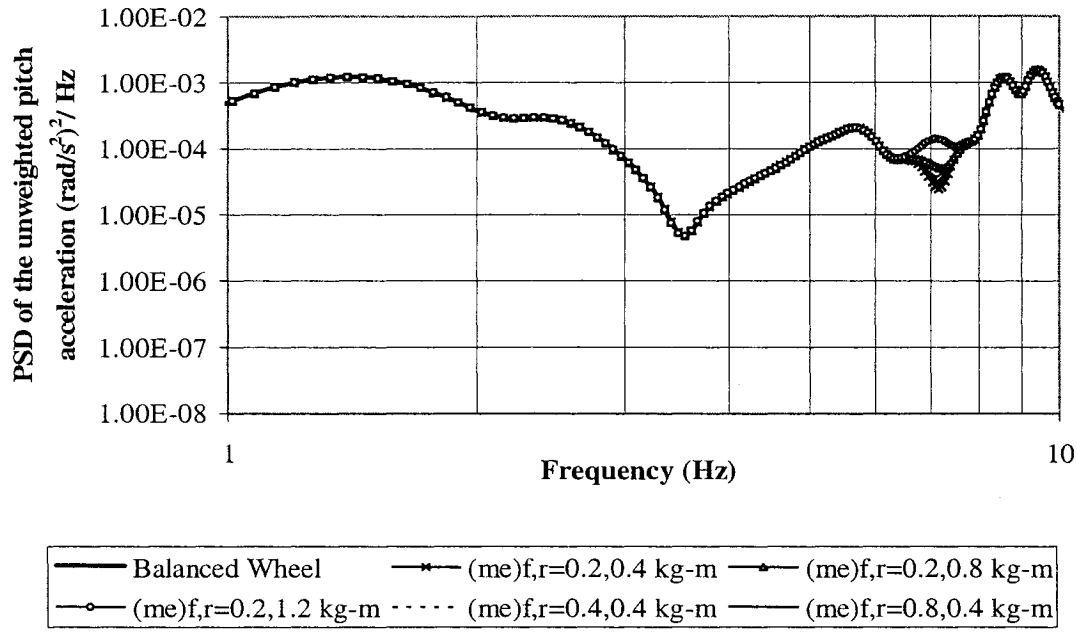

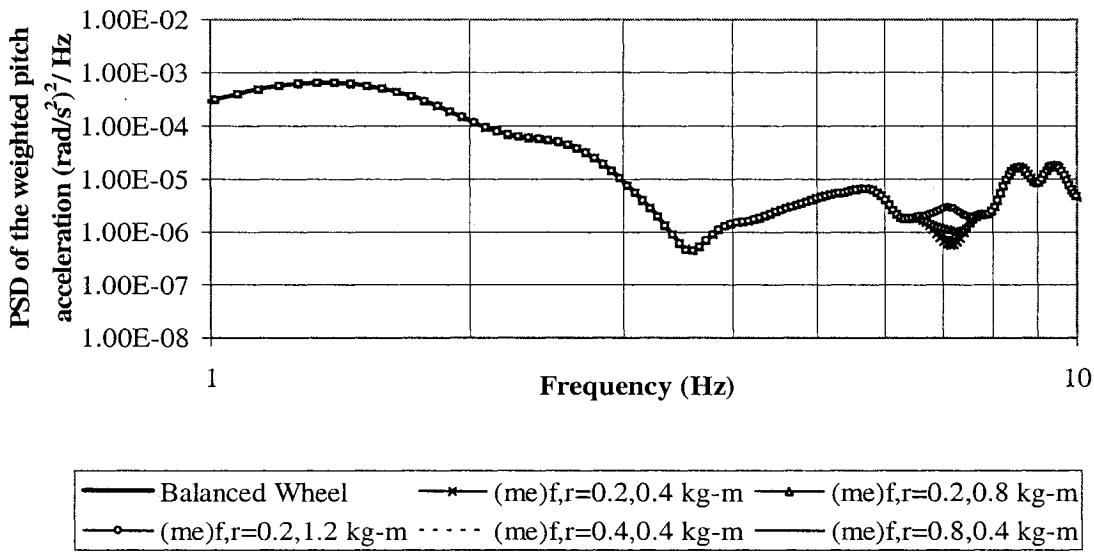

Figure 4.21: Effect of wheel unbalance on PSD of the unweighted and weighted pitch acceleration at 80 km/h (Rough road)

yield most notable effects on the tire forces, when vehicle operations on smooth road are considered.

The vertical and pitch acceleration responses of the vehicle sprung mass tend to increase with increasing road roughness in majority of the frequency range considered, as evident in Figures 4.18 to 4.21. While the wheel unbalance induces larger responses near 7.1 Hz, the relative increase in the acceleration PSD diminishes with increasing road roughness. The insignificant effect of wheel unbalance on the vertical acceleration response is clearly evident under rough road excitation (Figure 4.19). Moreover, the application of frequency-weighting tends to further reduce the effect of wheel unbalance on the pitch acceleration PSD response of the vehicle under rough road excitation which is also evident in Figure 4.21.

4.2.3 INFLUENCE OF PHASE

The centrifugal force generated by rotating unbalanced mass is harmonic in nature. The unbalance masses within the front and rear wheels could be located at two different angles from their respective wheel centers, as illustrated in Figure 2.11. This figure showed the unbalanced masses m_i with eccentricities e_i, located at angles ϕ_i, $i (i = f, r)$. The difference in angular locations of the unbalanced masses leads to phase difference between the two forces, which may yield additional time delays between the forces due to the wheels and thus increased or decreased angular motion (pitch motion) of the sprung mass. In this study, the influence of phase difference is investigated under the smooth road condition with a forward speed of 80 km/h. The results are presented in

terms of overall vertical and pitch rms accelerations (weighted and unweighted). The DLC due to front and rear tire forces are not presented owing to the very small effects of the phase difference. The results are presented for phase differences of $0°, 45°$ and $90°$, while two combinations of mass unbalance considered are, $(me)_{f,r}$ = 0.2, 0.4 kg-m and $(me)_{f,r}$ = 0.8, 0.4 kg-m.

Figures 4.22 and 4.23 illustrate the influence of phase on the unweighted and frequency weighted vertical and pitch rms accelerations, respectively, for both the sets of wheel unbalance magnitudes. It can be observed that the overall unweighted and weighted bounce rms accelerations decrease slightly with increase in the phase difference from $0°$ to $90°$, irrespective of the unbalance magnitudes considered. The weighted bounce rms acceleration values are observed to be close to their unweighted values, which can be attributed to the magnitude ratio of the W_k-weighting filter in the predominant frequency range of 7.1 Hz. The unweighted pitch acceleration values, however, increase with increase in phase angle while the weighted pitch acceleration values remain almost unaffected. This phenomenon can be attributed to the characteristics of W_e-weighting filter. The change in vertical and pitch rms acceleration values with the phase angle is more pronounced for $(me)_{f,r}$ = 0.8, 0.4 kg-m. The phase difference creates a time lag between the peak tire forces developed at the front and rear wheels, which excite the vehicle pitch center located within the wheel base inducing higher pitch motion. The corresponding reduction in the bounce acceleration of the vehicle can be attributed to coupling between the vertical and pitch responses. It should be noted that the bounce center of the vehicle sprung mass lies outside the wheel base.

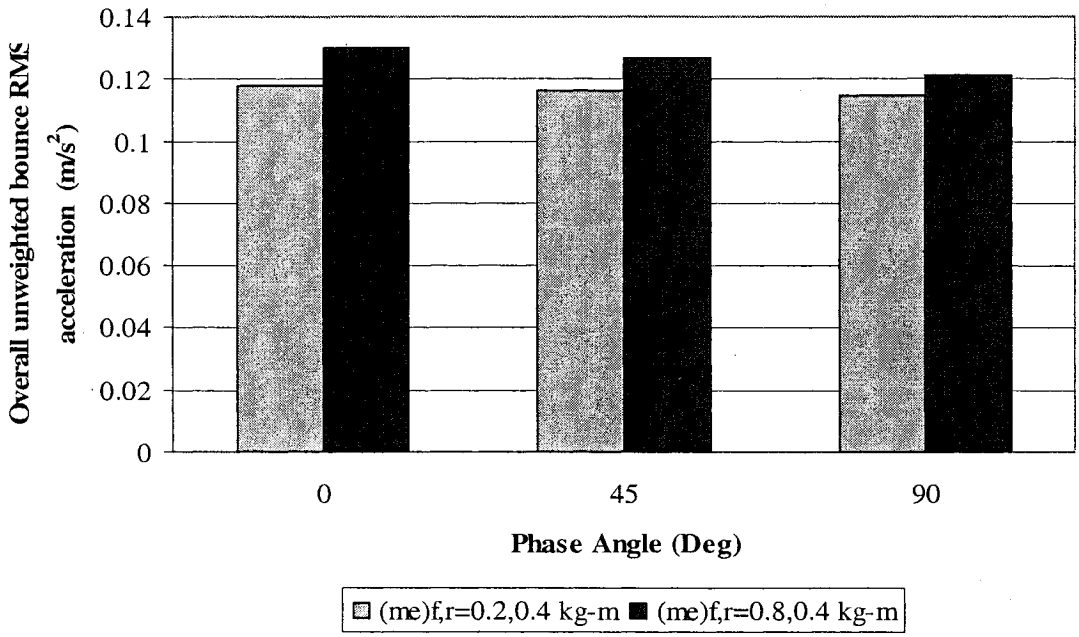

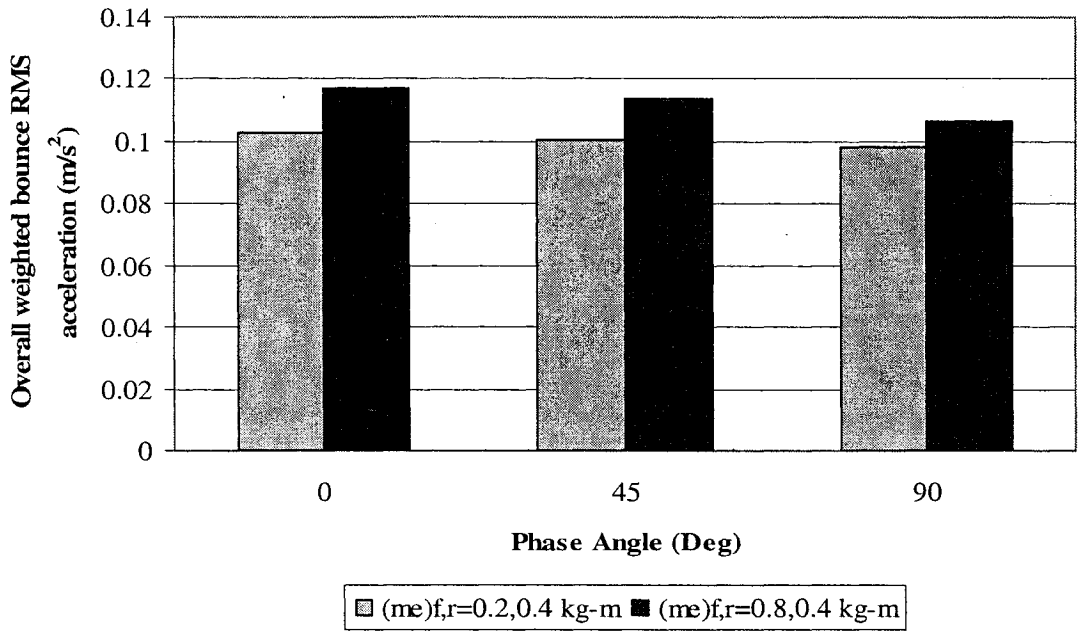

Figure 4.22: Influence of phase angle between the front and rear wheels unbalance on overall unweighted and weighted bounce rms acceleration at 80 km/h (Smooth road)

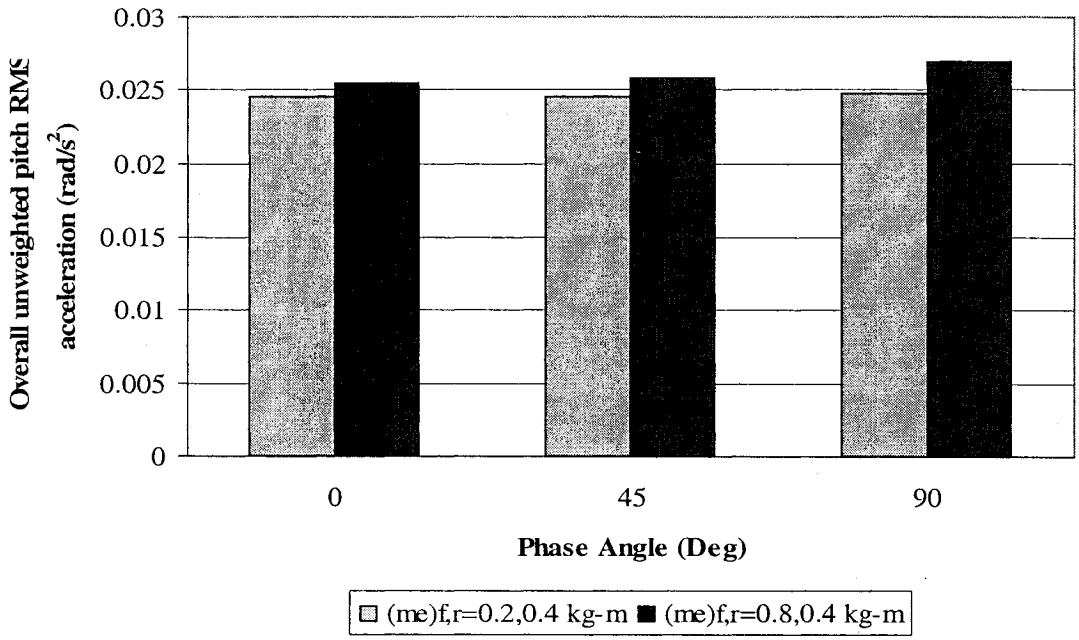

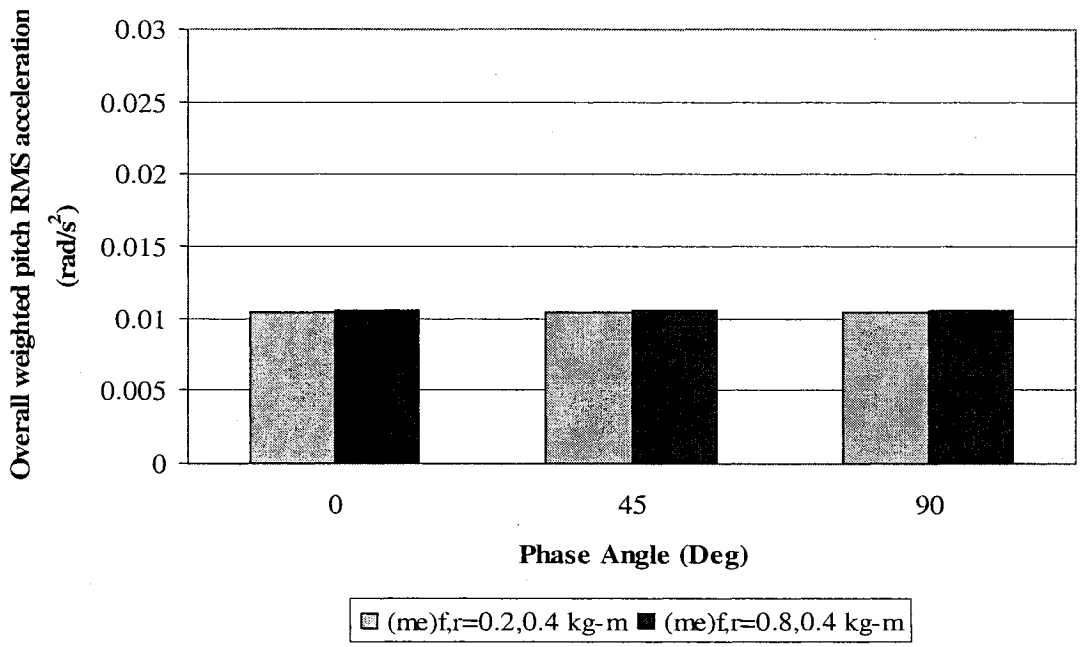

Figure 4.23: Influence of phase angle between the front and rear wheels unbalance on overall unweighted and weighted pitch rms acceleration at 80 km/h (Smooth road)

Figures 4.24 and 4.25 illustrate the PSD of vertical unweighted and weighted acceleration responses for $(me)_{f,r}$ = 0.2, 0.4 kg-m and $(me)_{f,r}$ = 0.8, 0.4 kg-m, respectively. The peaks corresponding to wheel unbalance are observed at wheel rotating frequency of 7.1 Hz. The peak magnitudes of the unweighted and weighted vertical accelerations occur at phase difference of 0° and the peak magnitudes decrease with increase in the phase difference. The increase in the peak magnitudes with increase in phase difference is clearly observed for the unweighted and weighted pitch acceleration PSD responses for both sets of mass unbalance, presented in Figures 4.26 and 4.27. The variation in the relative magnitudes of the peaks is more pronounced for the pitch acceleration than the vertical acceleration responses. The application of W_e-weighting filter considerably attenuates the magnitudes of peak acceleration responses while the relative contribution of each peak is almost unaffected.

4.3 EFFECT OF WHEEL NON-UNIFORMITY

The wheel non-uniformity is modeled as a geometric variation of the wheel from its original circular shape by considering the non uniform wheel with an elliptical shape, as described in Chapter 2. The wheel non-uniformity forms another important source of self-excitation, while its effect on the tire load and ride vibration responses is influenced by other operating factors, namely, the operating speed and road roughness. The phase difference between the geometric shapes of the front and rear axle tires could further affect the ride and tire load performance of vehicle with non-uniform wheels. The effect of non-uniform wheels on the ride accelerations (weighted and unweighted) and tire forces is thus studied under the influence of variations in the vehicle speed, road roughness and the

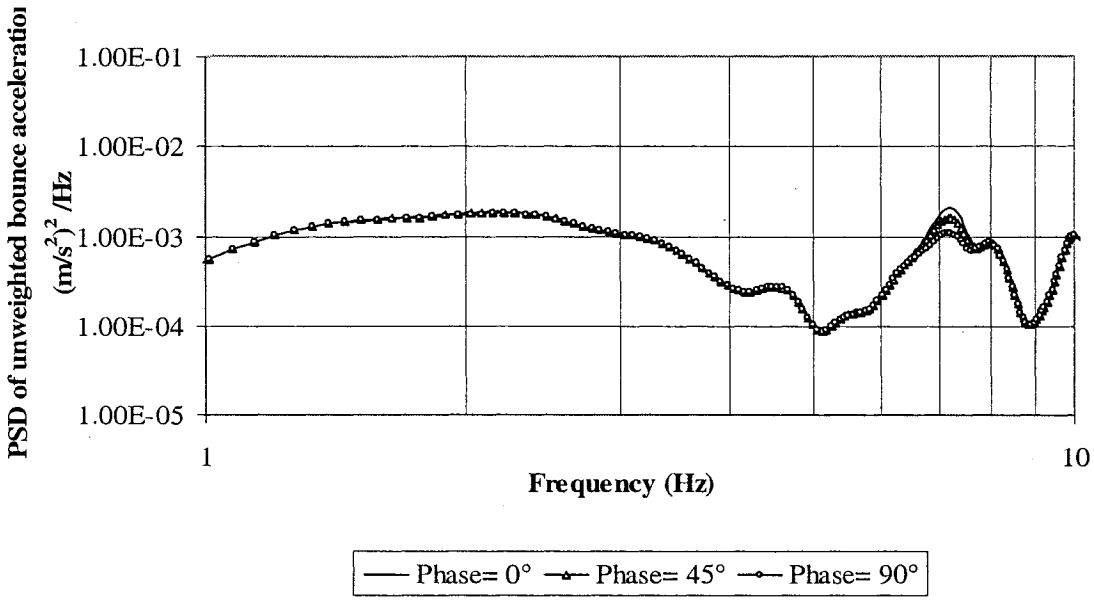

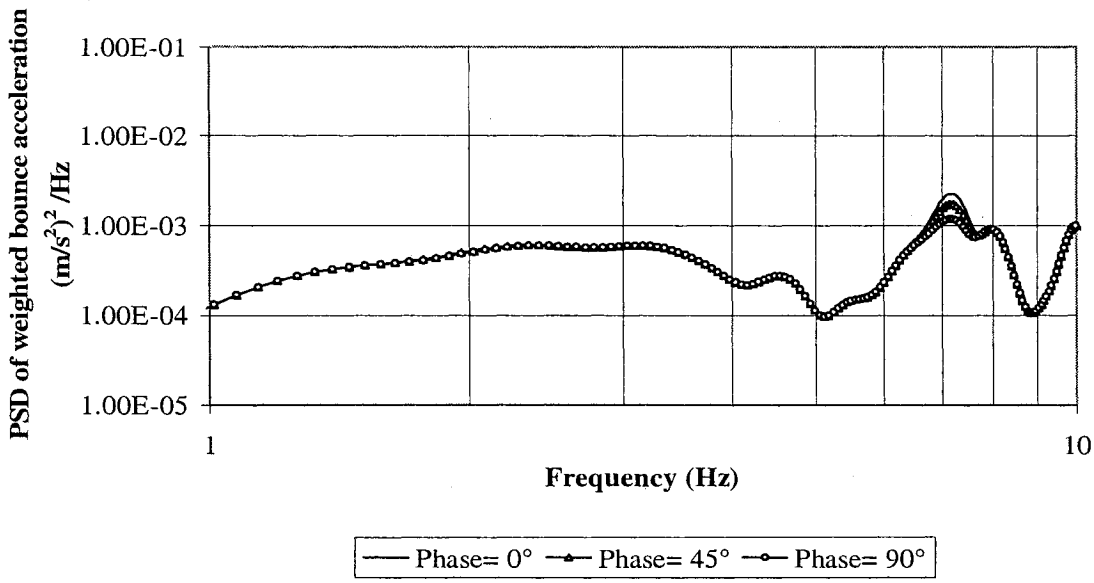

Figure 4.24: Effect of wheel unbalance on PSD of unweighted and weighted bounce acceleration at 80 km/h with smooth road for $(me)_{f,r}$ = 0.2, 0.4 kg-m

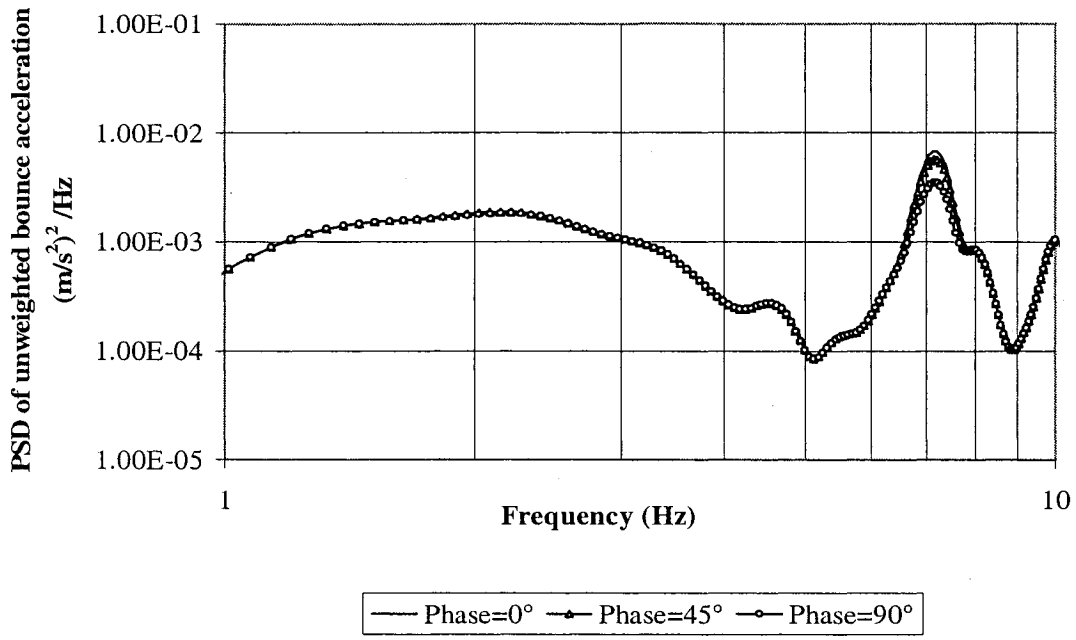

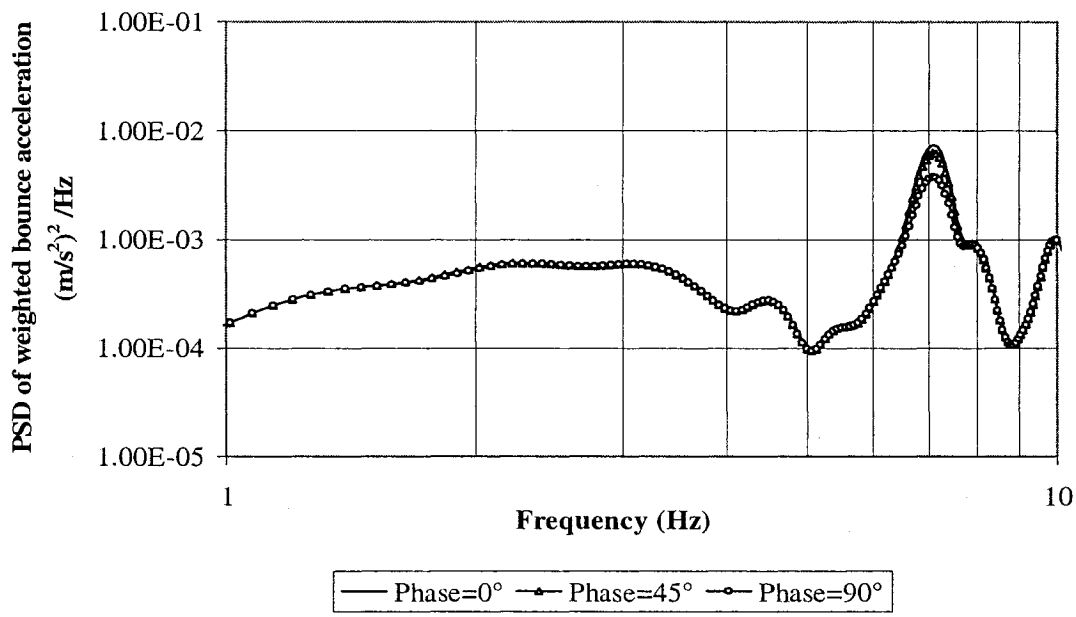

Figure 4.25: Effect of wheel unbalance on PSD of unweighted and weighted bounce acceleration at 80 km/h with smooth road for $(me)_{f,r}$ = 0.8, 0.4 kg-m

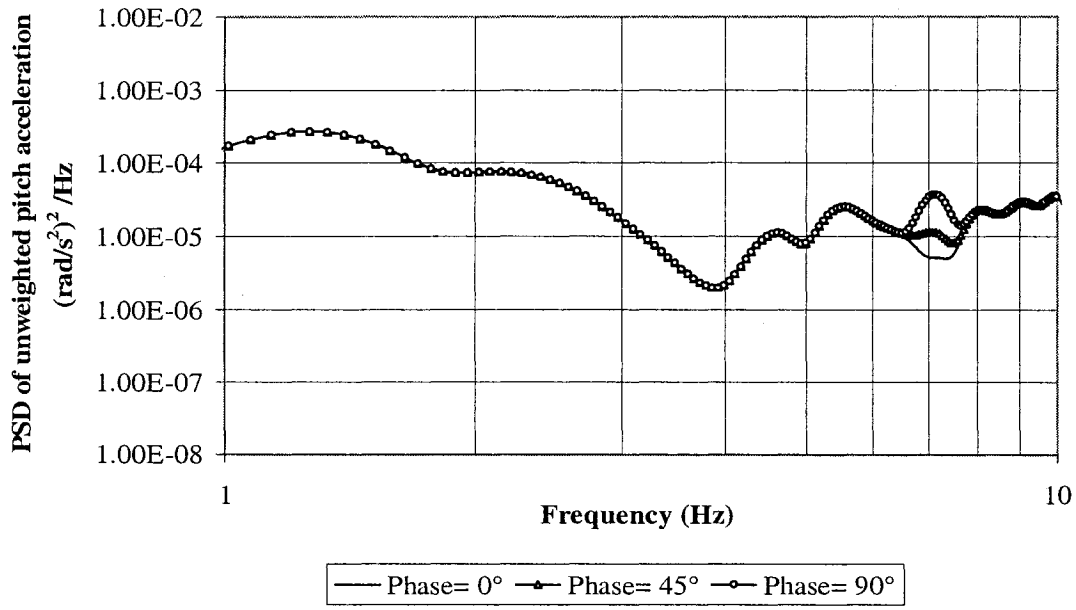

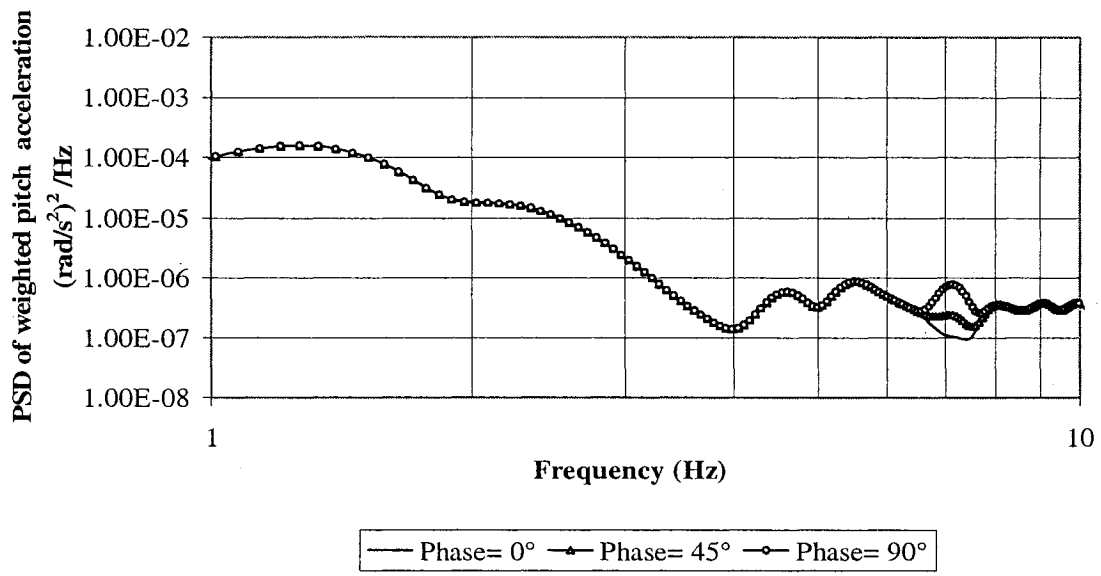

Figure 4.26: Effect of wheel unbalance on PSD of unweighted and weighted pitch acceleration m at 80 km/h with smooth road for $(me)_{f,r}$ = 0.2, 0.4 kg-m

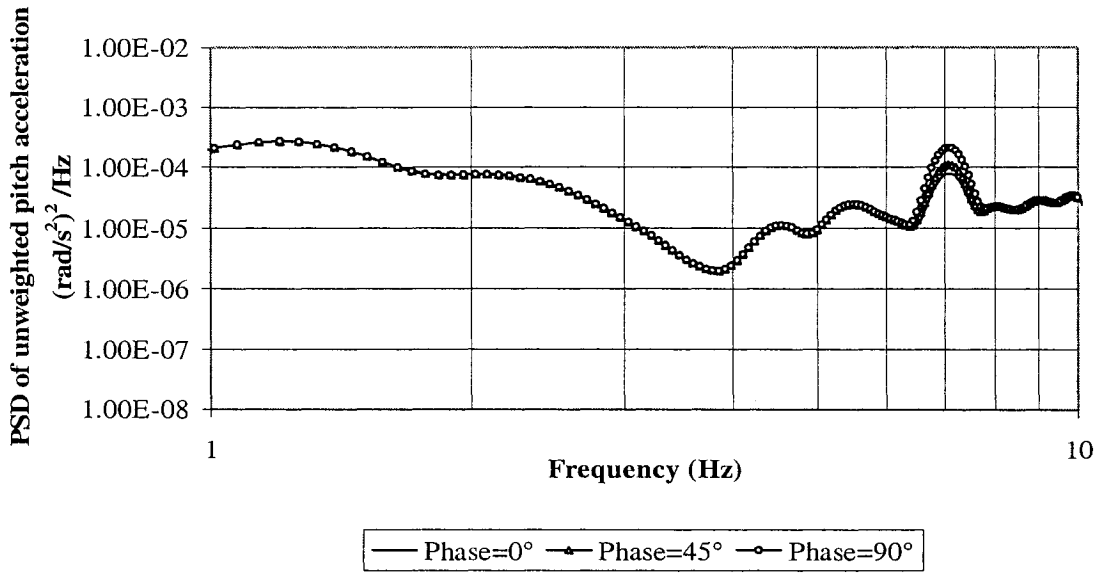

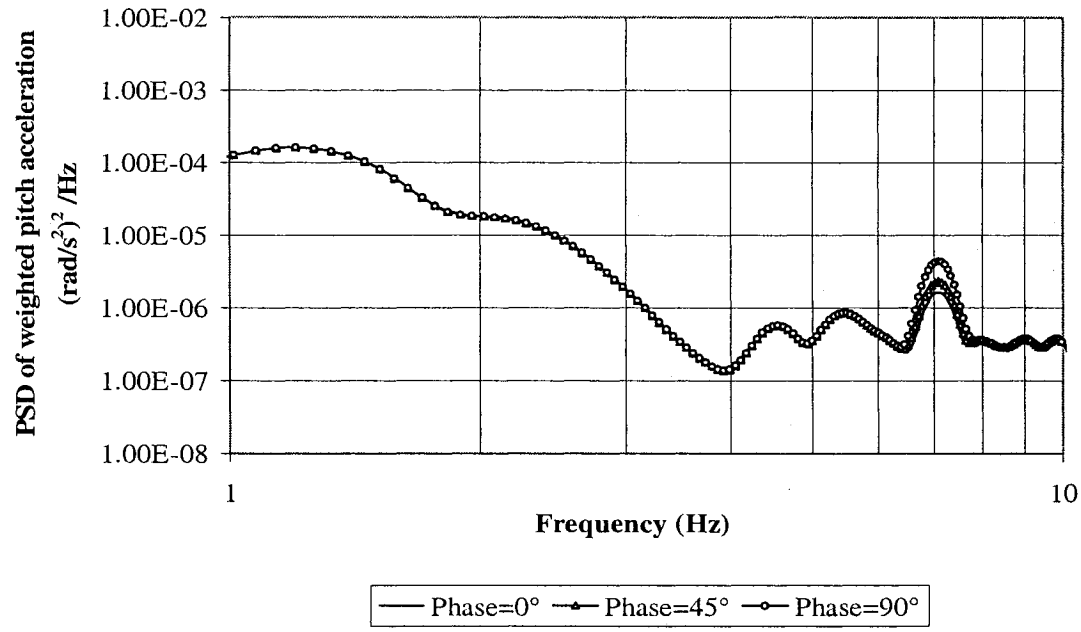

Figure 4.27: Effect of wheel unbalance on PSD of unweighted and weighted pitch acceleration at 80 km/h with smooth road for $(me)_{f,r}$ = 0.8, 0.4 kg-m

phase angle of the non-uniformity. The radial run out (variation from the original radius) magnitudes considered for the analyses range from 0.001 m to 0.003 m. Different combinations of the front and rear wheel runouts, however, considered. These include 0.002 m and 0.001 m, 0.002 m and 0.002 m, 0.002 m and 0.003 m, 0.001 m and 0.002 m, and 0.003 m and 0.002 m, while the effects are investigated in conjunction with variations in the speed, road roughness and phase. In each set the first number corresponds to front wheel run-out and denoted as $(\Delta r)_f$, while the second number corresponds to rear run-out referred to as $(\Delta r)_r$.

4.3.1 INFLUENCE OF VEHICLE SPEED

The ride quality and tire force variation of the vehicle with non-uniform wheels is expected to be strongly affected by the speed. As briefly discussed in Chapter 2, the frequency corresponding to excitation arising from a non-uniform wheel is a function of the vehicle speed. The effects of wheel run-out are thus investigated for three different vehicle speeds of 60 km/h, 80 km/h and 100 km/h, while the results are presented in terms of performance measures relevant to weighted and unweighted overall rms bounce and pitch accelerations and dynamic load coefficients (DLC) due to front and rear wheel forces. In order to clearly show the effect of wheel non-uniformity on the performance measures, the analyses are initially performed for the smooth road.

Figures 4.28 to 4.30 illustrate the influence of vehicle speed on the performance measures for all combinations of radial run-out or non-uniformity considered. Figures show the DLC due to front and rear tire forces, and unweighted and frequency-weighted overall rms values due to vertical and pitch acceleration responses of the sprung mass. The results

reveal that for a uniform and balanced wheel, DLC values of both the axles increase with increase in speed, while the overall bounce rms acceleration values (weighted and unweighted) do not show this trend. The vehicle operations at 60 km/h yield the highest vertical rms acceleration, which could be attributed to the spectral components of the road profile. The pitch rms accelerations, on the other hand peaks at speed of 100 km/h, as discussed in the previous section. The presence of wheel non-uniformity yields considerable increases in the DLC, irrespective of the vehicle speed. While the DLC values of both the axle tires increase nearly linearly with the magnitude of the wheel run-out, the effect is relatively small at the higher speed of 100 km/h. Moreover, the DLC due to front wheel forces increases most significantly at the lower speed of 60 km/h. The effect of speed on the DLC values is related to the predominant excitation frequency due to wheel run-out. The operations at the different selected speeds of 60, 80 and 100 km/h would yield predominant excitation near 10.6, 14.2 and 17.8 Hz, respectively. The vehicle operation at a speed of 100 km/h could thus cause higher tire forces near 17.8 Hz. The lower intensity of the road roughness near this frequency, however, tends to diminish the magnitudes of resulting tire forces leading to relatively smaller DLC values, as evident in Figure 4.28.

Similar tendencies are also observed in the unweighted and frequency-weighted overall rms values due to vertical acceleration of the sprung mass (Figure 4.29). The overall rms vertical acceleration increases with increasing magnitude of wheel run-out, while the effects are far more pronounced at speeds of 60 and 80 km/h. The operation at 100 km/h yields considerably lower values of vertical rms acceleration and relatively small effects of wheel run-out. The application of W_k-weighting filter further diminishes the rms values of vertical accelerations at 80 km/h and 100 km/h due to predominance of

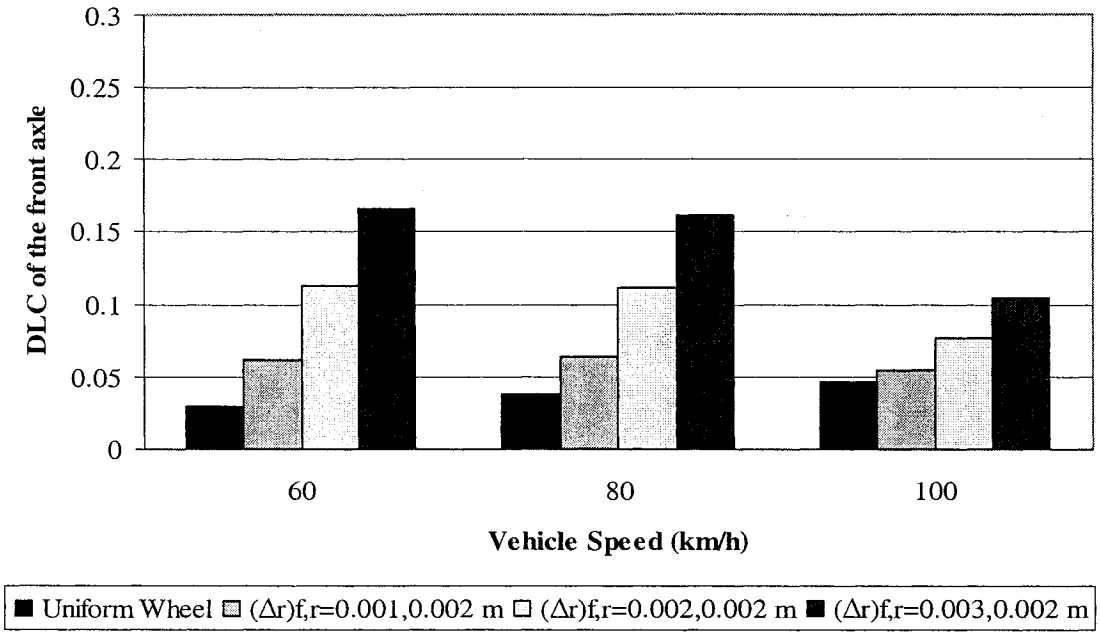

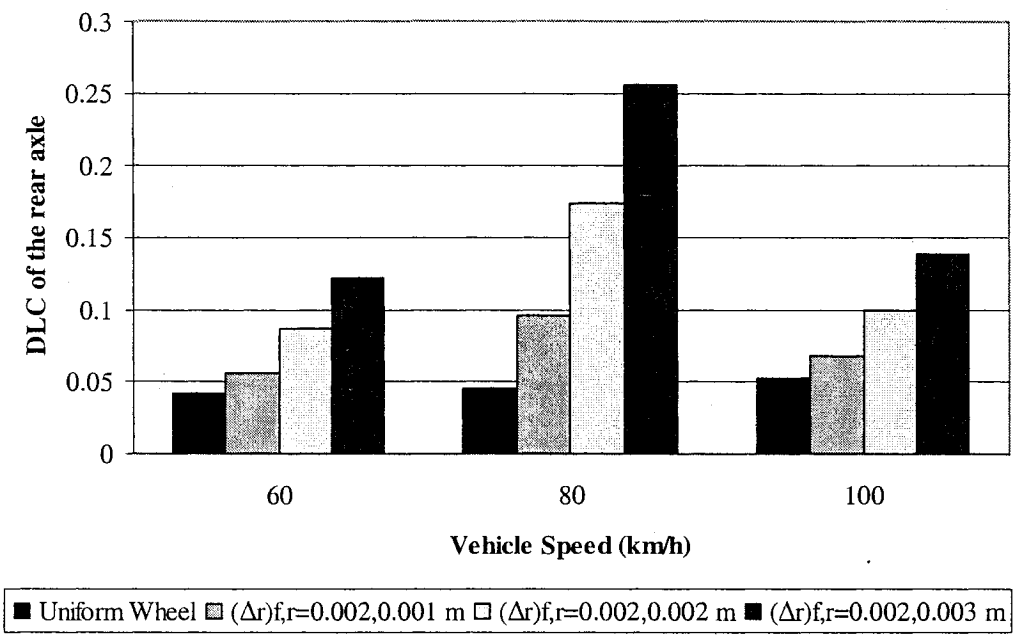

Figure 4.28: Influence of speed on DLC of the front and rear axle with wheel non-uniformity (Smooth road)

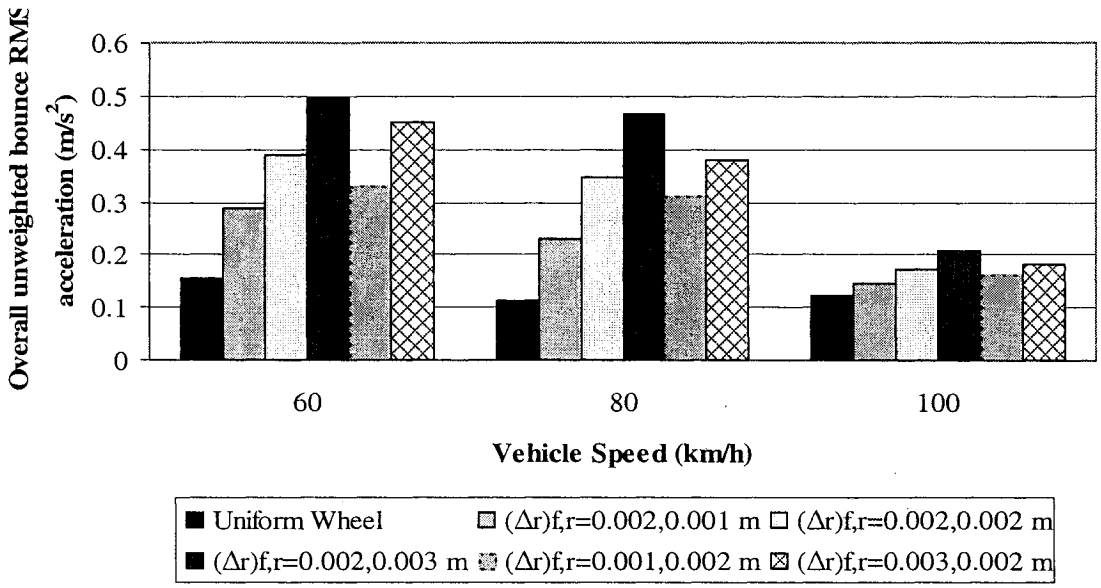

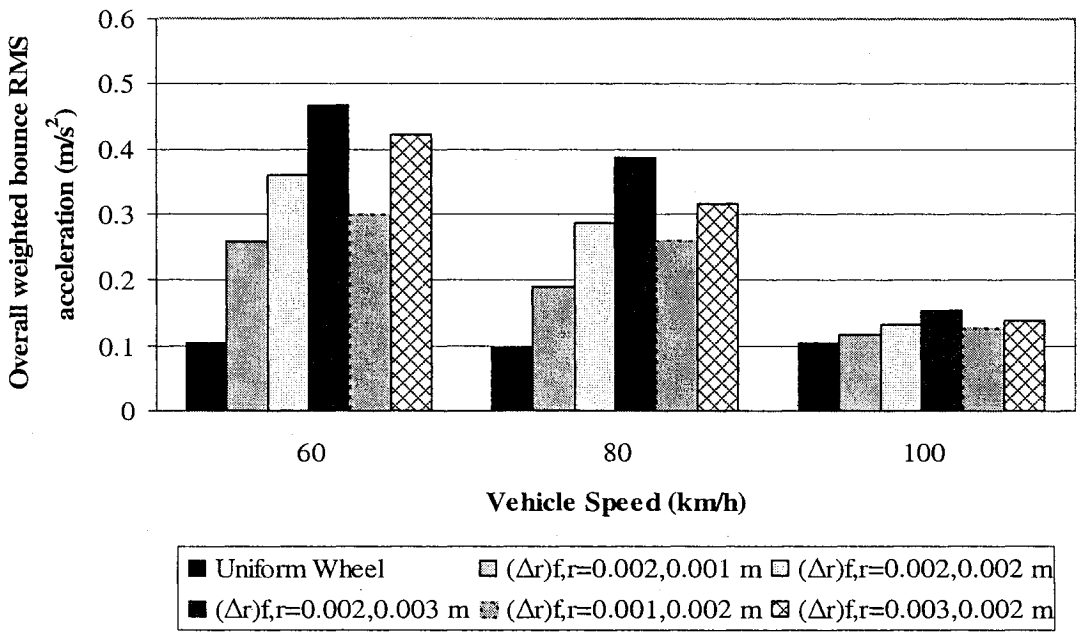

Figure 4.29: Influence of speed on overall unweighted and weighted bounce rms acceleration with wheel non-uniformity (Smooth road)

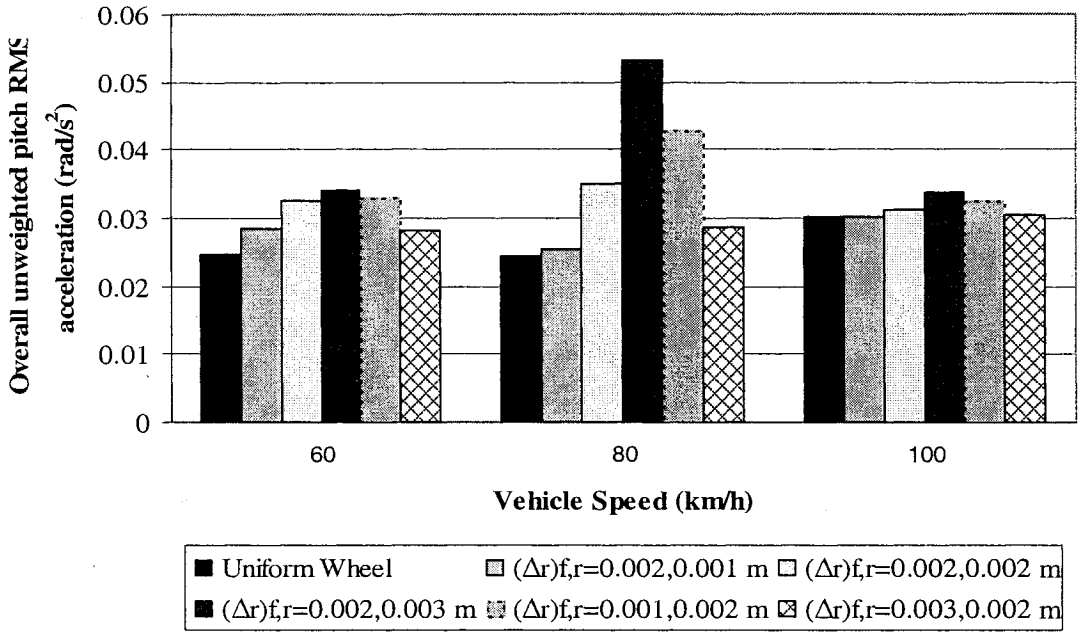

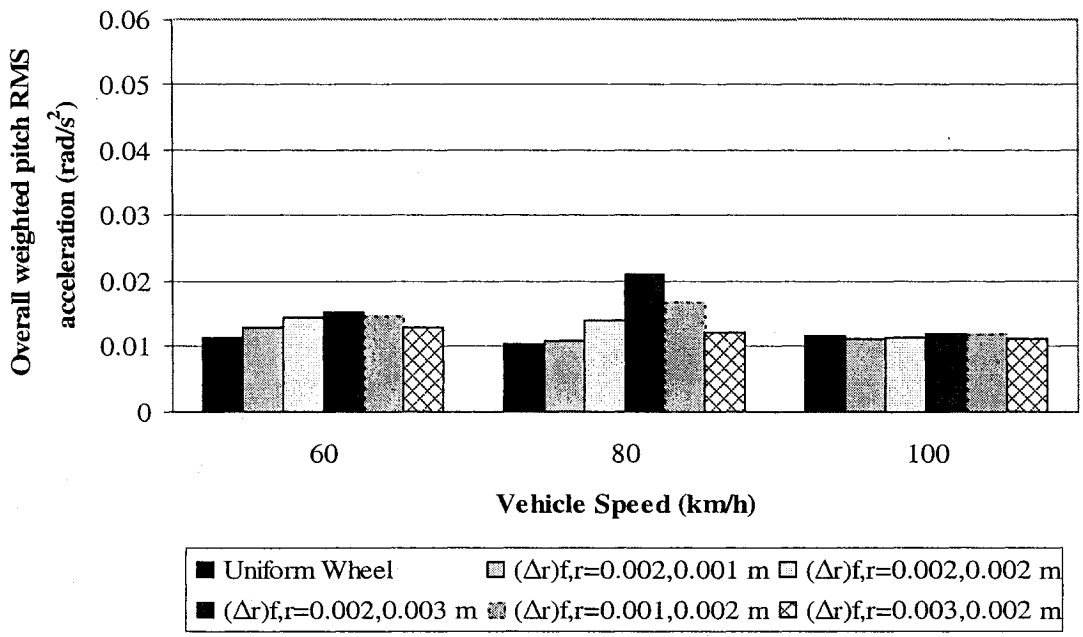

Figure 4.30: Influence of speed on overall unweighted and weighted pitch rms acceleration with wheel non-uniformity (Smooth road)

higher components. The weighted values at 60 km/h, however, tend to be only slightly lower than the unweighted values, since the predominant excitation occur around 10.6 Hz.

The overall rms values of the pitch acceleration show most significant effects of the wheel run-out at a speed of 80 km/h, while the effect at 60 km/h is relatively small (Figure 4.30). Owing to the relatively high frequency of the pitch motion caused by wheel run-out, the application of W_e-weighting filter reduces the rms values of pitch accelerations significantly. The results further show that a higher degree of run-out of the rear wheels yields most significant effects on the pitch and vertical acceleration, and tire forces respectively. This is evident, when the DLC and rms acceleration values attained for $(\Delta r)_f$ = 0.002 m and $(\Delta r)_r$ = 0.003 m, are compared with those obtained for $(\Delta r)_f$ = 0.003 m and $(\Delta r)_r$ = 0.002 m. This effect is most likely caused by higher rear axle load of the vehicle.

The spectral components of vertical and pitch acceleration responses are evident from the PSD of bounce and pitch acceleration responses (unweighted and weighted) presented in Figures 4.31 and 4.32, respectively, for all sets of magnitudes of wheel run-out at 60 km/h. All the peaks corresponding to wheel non-uniformity occur at twice the wheel rotation frequency, 10.6 Hz. The peak magnitudes of vertical and pitch accelerations occur for $(\Delta r)_{f,r}$ = 0.002 and 0.003 m, while the lower magnitudes of wheel runouts, $(\Delta r)_{f,r}$ = 0.002 and 0.002 m, $(\Delta r)_{f,r}$ = 0.003 and 0.002 m, $(\Delta r)_{f,r}$ = 0.002 and 0.001 m, and $(\Delta r)_{f,r}$ = 0.001 and 0.002 m exhibit only small increases in the acceleration responses.

The PSD of vertical and pitch unweighted and weighted acceleration responses of the vehicle, at forward speeds of 80 km/h and 100 km/h are illustrated in Figures 4.33 to 4.36, respectively, for different magnitudes of wheel nonuniformities. The results show that the peak magnitudes in the vertical acceleration responses shift towards a higher frequency as the forward speed is increased, while the peak magnitudes decrease. The magnitudes of pitch acceleration responses however, remain comparable at speeds of 60 and 80 km/h due to wheel run-out near the predominant frequency but decrease slightly at 100 km/h. A small increase in peak magnitudes of bounce acceleration in the vibration frequency range of sprung mass resonance with increasing non-uniformity is also observed at speeds of 80 and 100 km/h. The presence of wheel non-uniformity causes peaks near 14.2 Hz and 17.8 Hz, respectively, at speeds of 80 and 100 km/h. The magnitudes of peaks in the vertical and pitch acceleration spectra however increase with increasing non-uniformity. The results further show that the peak magnitudes of frequency weighted vertical acceleration PSD are almost unaffected at all speeds. This phenomenon can be attributed to the characteristics of the W_k-weighting filter.

The magnitudes of the peaks corresponding to non-uniformity, in the frequency-weighted pitch acceleration PSD, on the other hand, are considerably smaller than those observed in the unweighted spectra for all the speeds. This is attributed to the significant attenuations by the W_e-filter near the predominant frequencies. The weighted pitch acceleration responses thus do not show notable effects of the wheel non-uniformity except a small variation at a speed of 80 km/h (Figure 4.30).

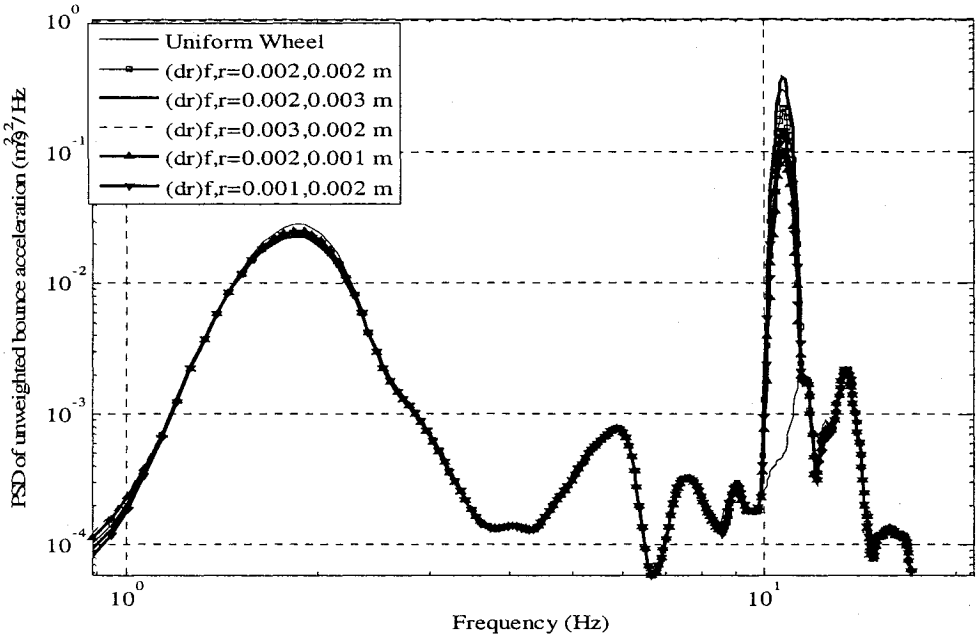

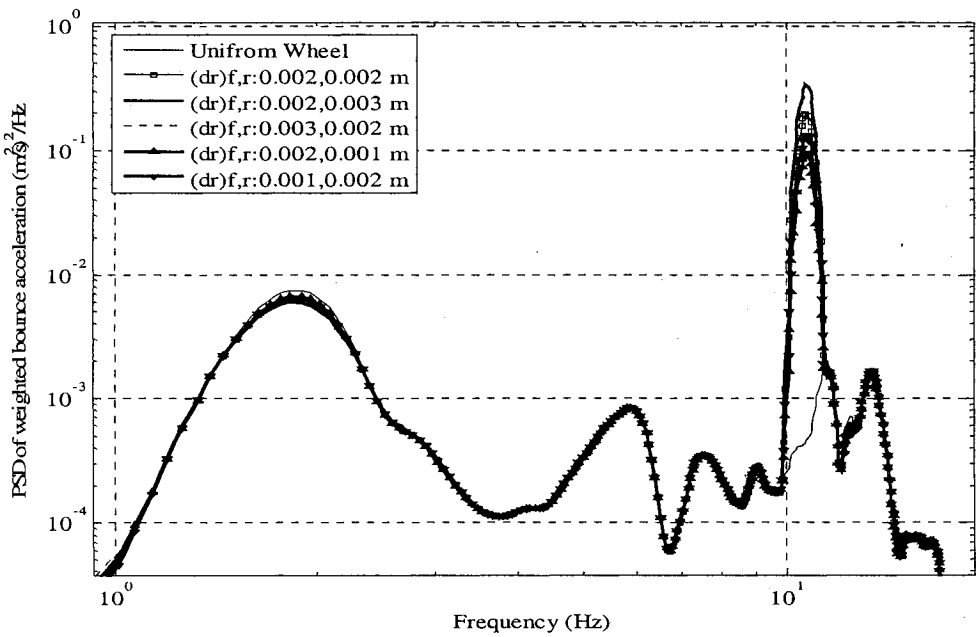

Figure 4.31: Effect of wheel non-uniformity on PSD of unweighted and weighted bounce acceleration at 60 km/h (Smooth road)

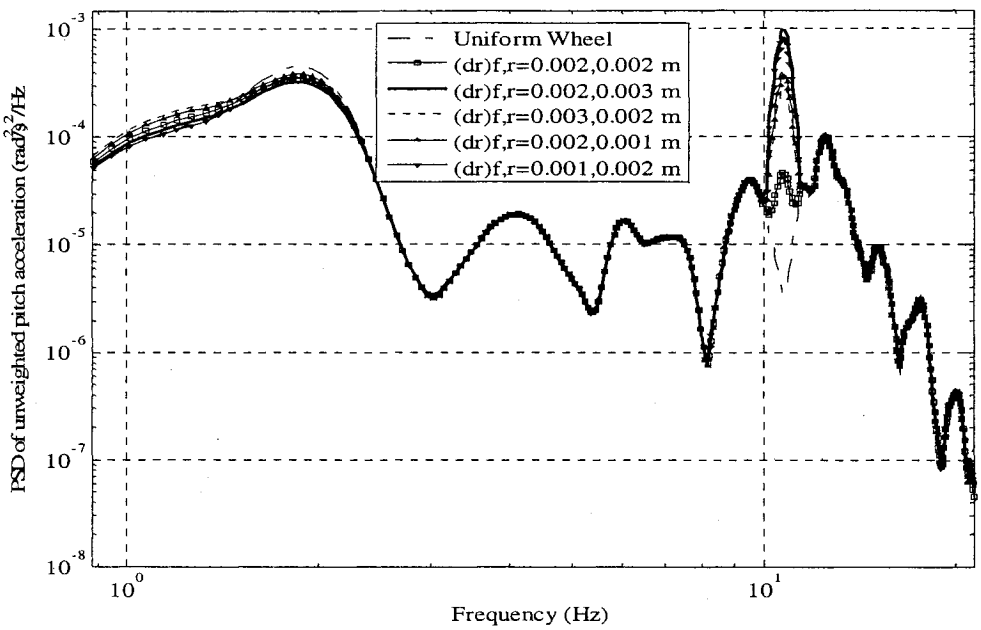

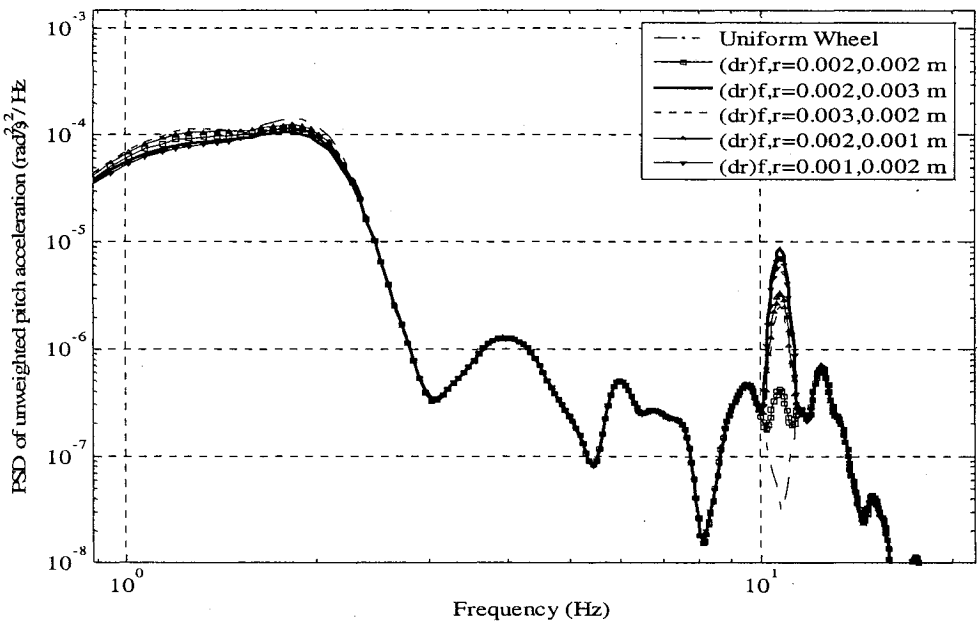

Figure 4.32: Effect of wheel non-uniformity on PSD of unweighted and weighted pitch acceleration at 60 km/h (Smooth road)

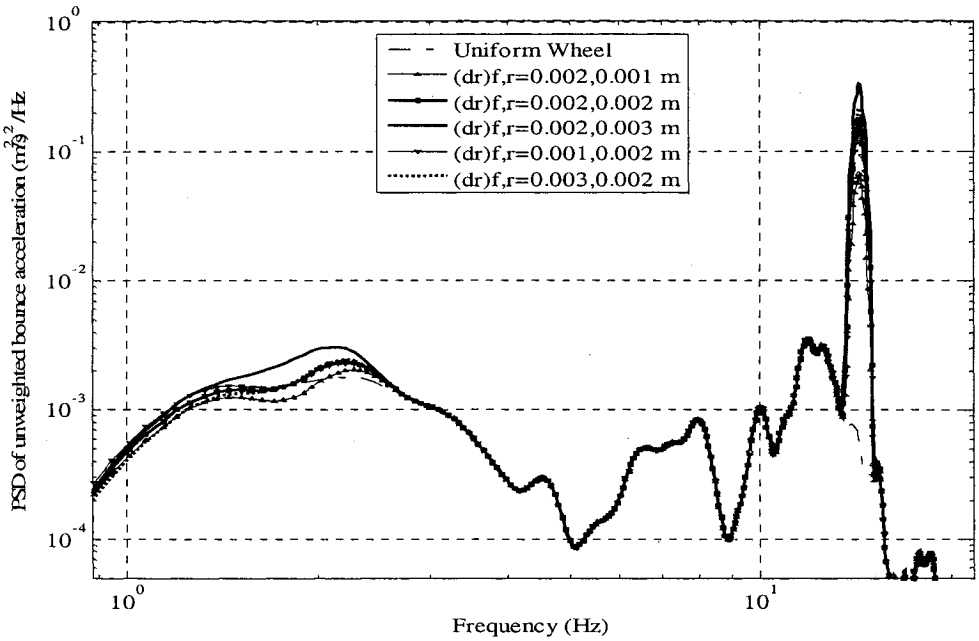

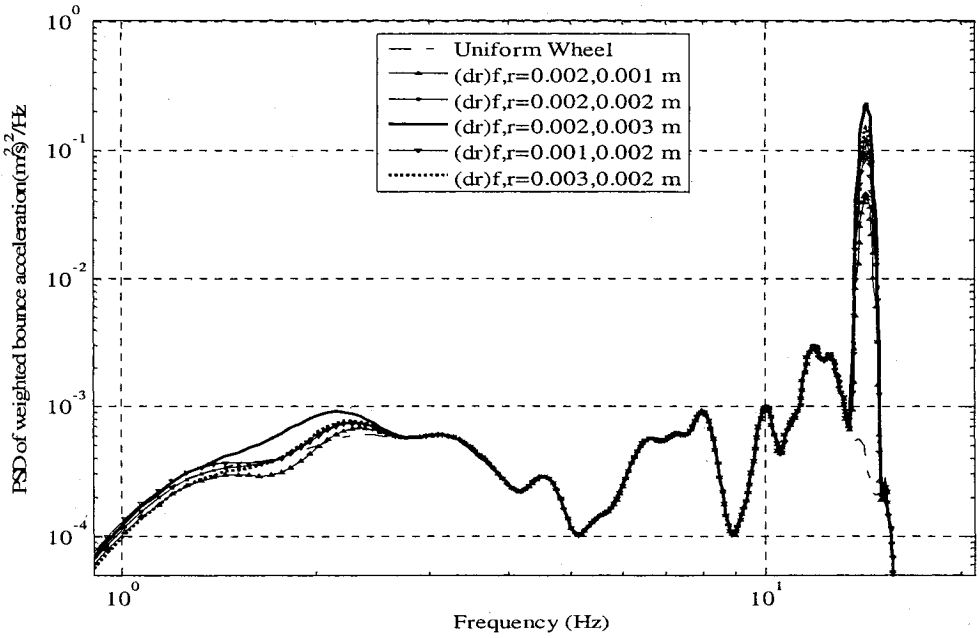

Figure 4.33: Effect of wheel non-uniformity on PSD of unweighted and weighted bounce acceleration at 80 km/h (Smooth road)

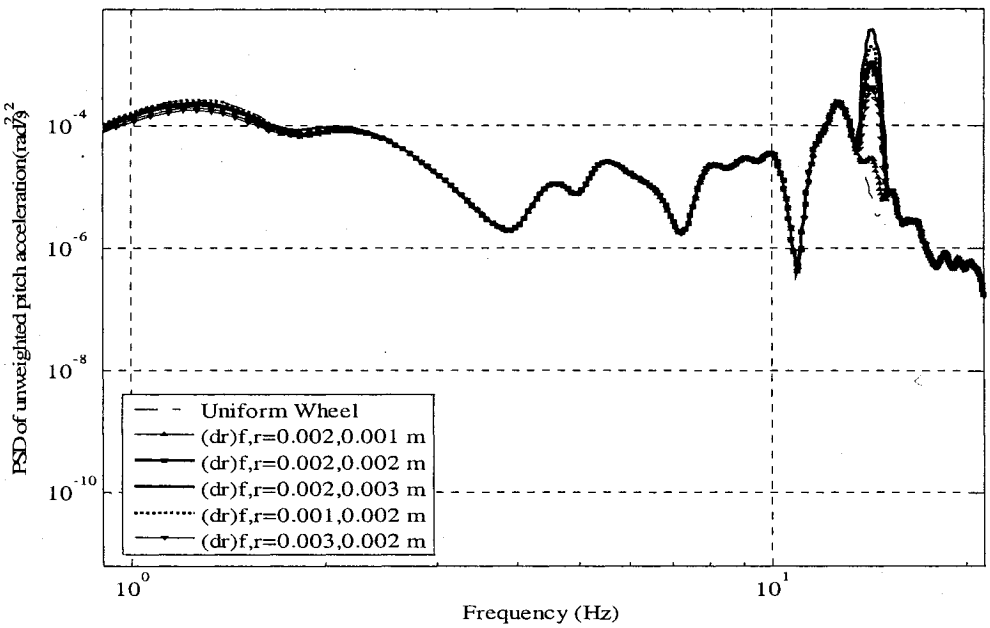

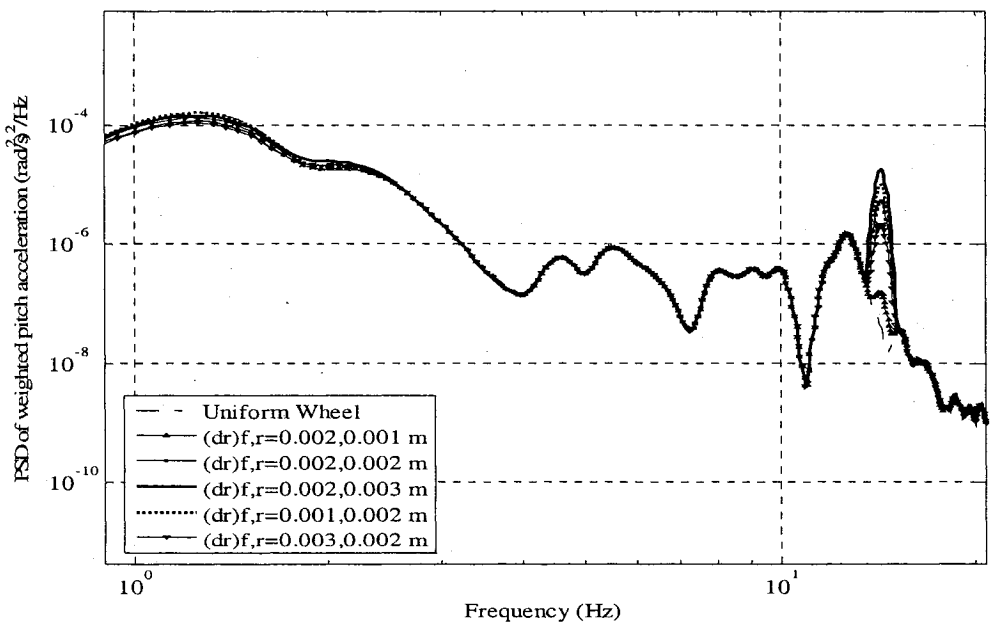

Figure 4.34: Effect of wheel non-uniformity on PSD of unweighted and weighted pitch acceleration at 80 km/h (Smooth road)

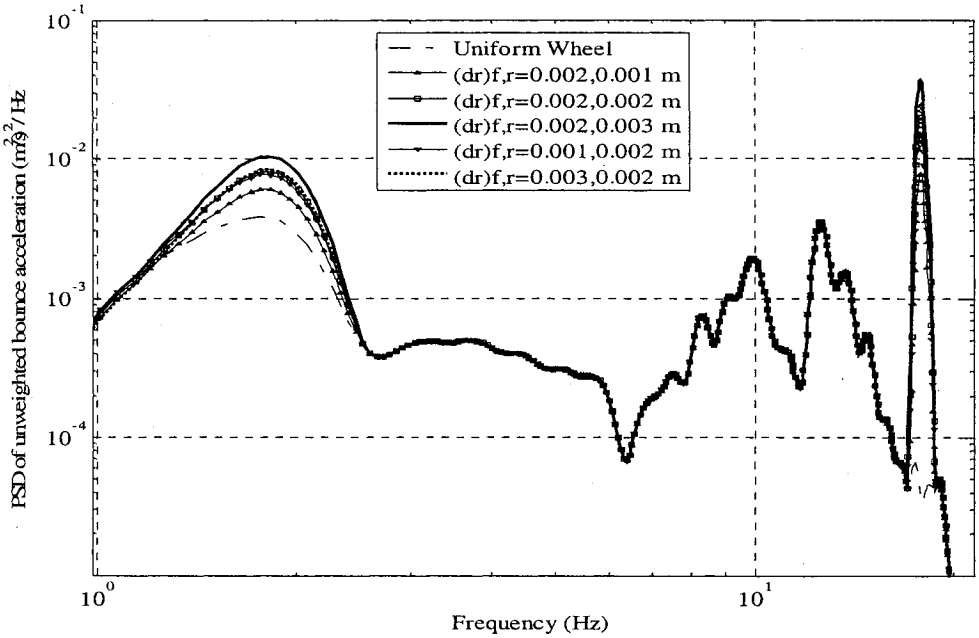

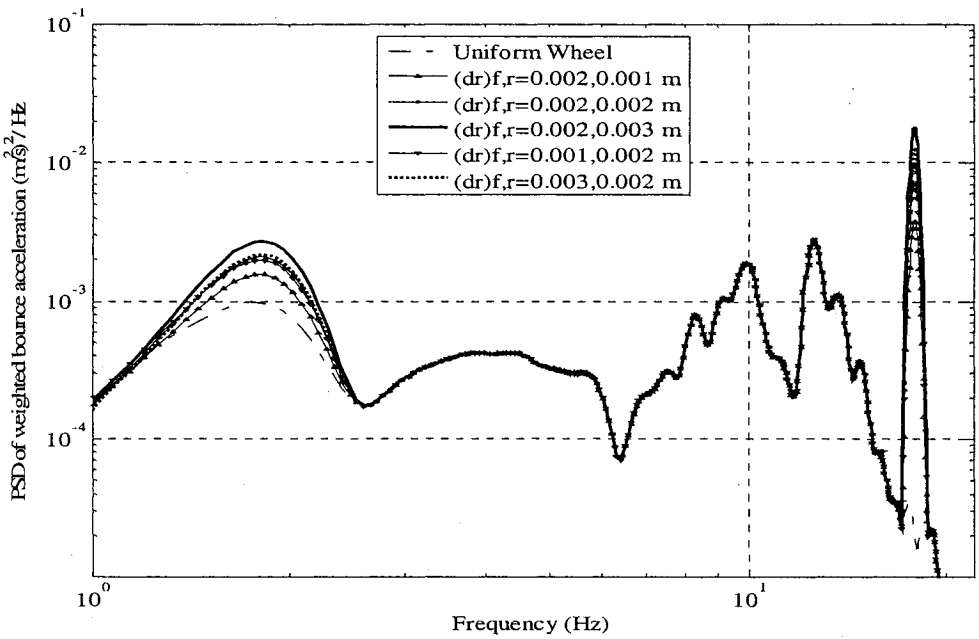

Figure 4.35: Effect of wheel non-uniformity on PSD of the unweighted and weighted bounce acceleration at 100 km/h (Smooth road)

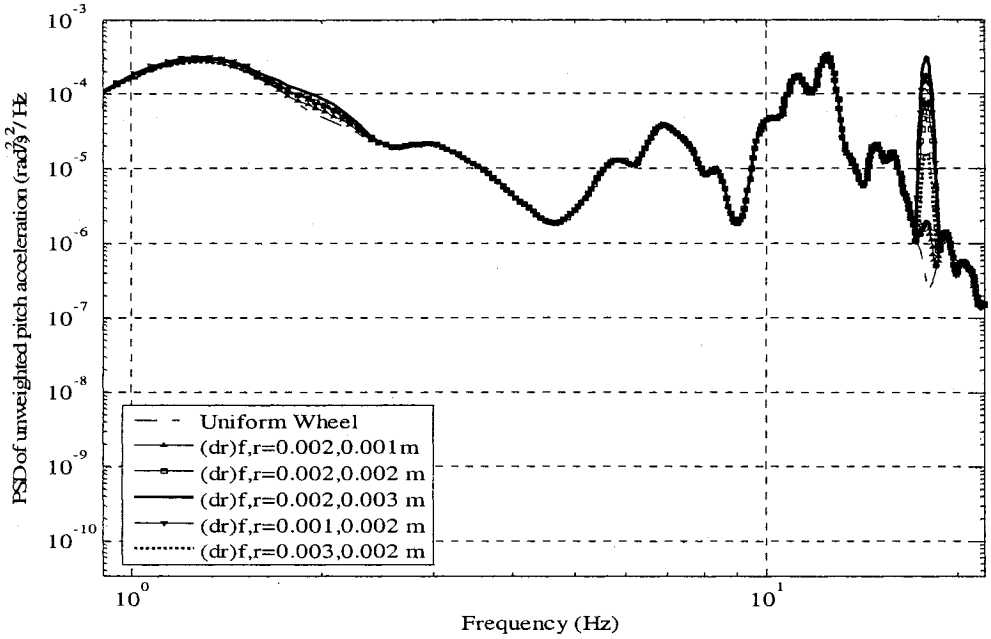

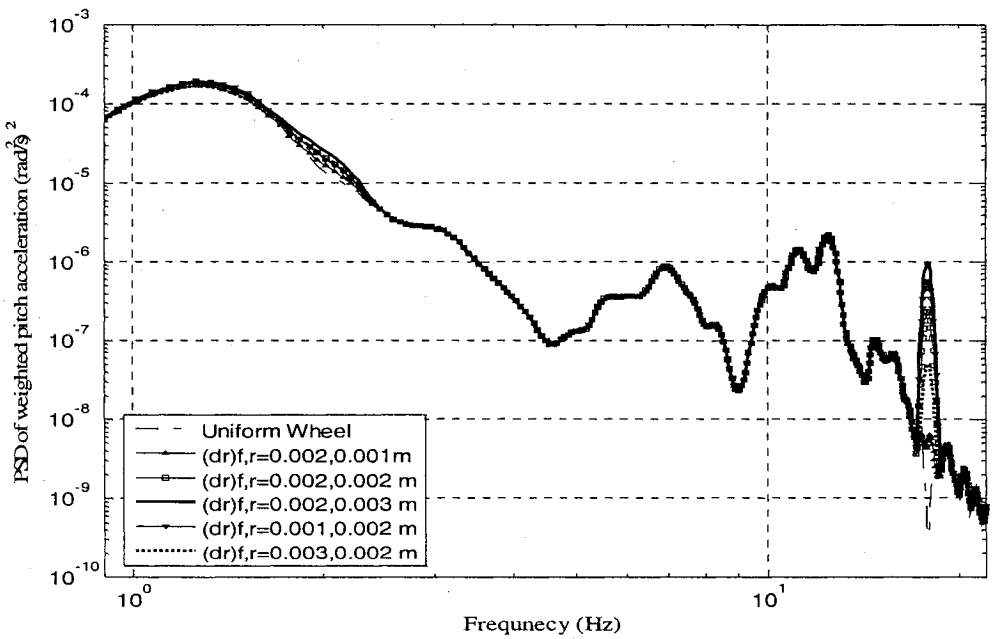

Figure 4.36: Effect of wheel non-uniformity on PSD of the unweighted and weighted pitch acceleration at 100 km/h (Smooth road)

Figure 4.37 illustrates the PSD of the front and rear tire forces as function of the magnitudes of wheel non-uniformity, while the forward speed is 60 km/h. The PSD of the front tire force shows the highest peak magnitude corresponding to wheel non-uniformity combination of 0.003 and 0.002 m, while for the rear axle peak values occur for 0.002 and 0.003 m combination. The force responses peaks occur in the vicinity of 10.6 Hz, which are not present when the wheels are uniform. The peak magnitude tends to increase significantly with increasing non-uniformity, which contributes to relatively higher DLC as evident in Figure 4.28. The strong influence of operating speed on the corresponding predominant frequencies can be observed from the tire force spectra presented in Figures 4.38 and 4.39, respectively, for forward speeds of 80 and 100 km/h. The peak magnitudes of the rear wheel tire forces show a small variation with increasing non-uniformity in the vicinity of sprung mass resonance, at speeds of 80 and 100 km/h. The peak magnitudes at these predominant frequencies are maximum at 60 km/h speed for front wheel and at 80 km/h for the rear wheels, as evident from Figure 4.28. This phenomenon can be attributed to the occurrence of the predominant frequency at particular speed in the vicinity of the front or rear unsprung mass resonance. The results further show that higher levels of wheel non-uniformity cause considerably higher magnitudes of dynamic tire forces, which contribute to higher values of DLC, particularly at speeds of 60 and 80 km/h.

4.3.2 INFLUENCE OF ROAD ROUGHNESS

The results presented in the previous sections show significant effect of the wheel non-uniformity on both ride and tire load responses at lower speeds when the vehicle

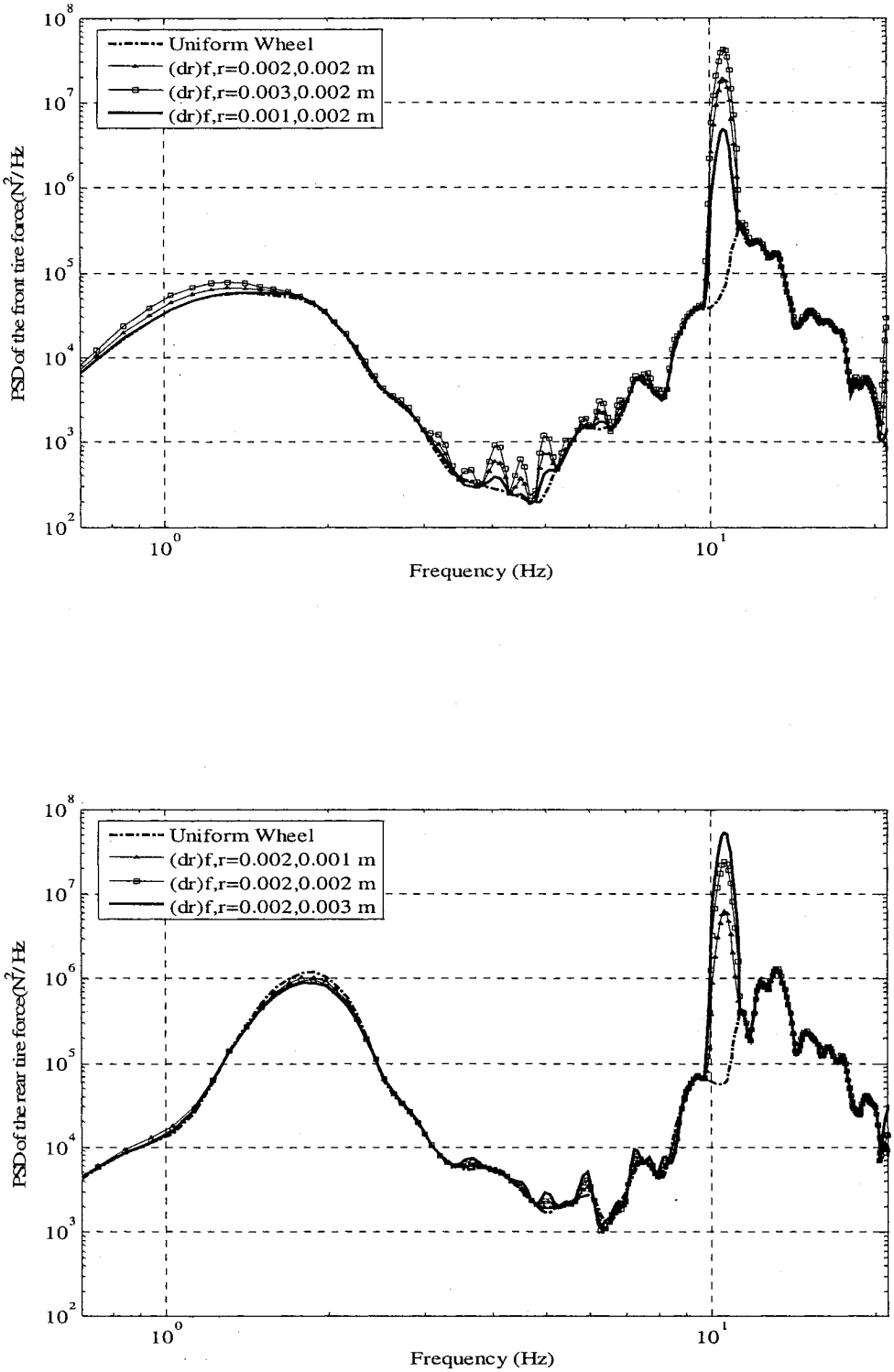

Figure 4.37: Effect of wheel non-uniformity on PSD of the front and rear tire forces at 60 km/h (Smooth road)

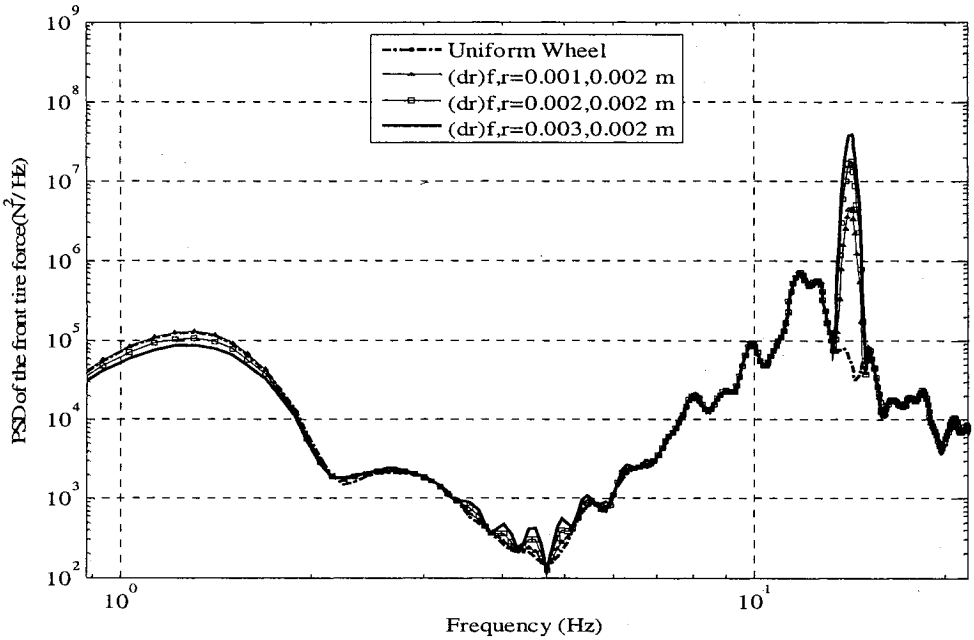

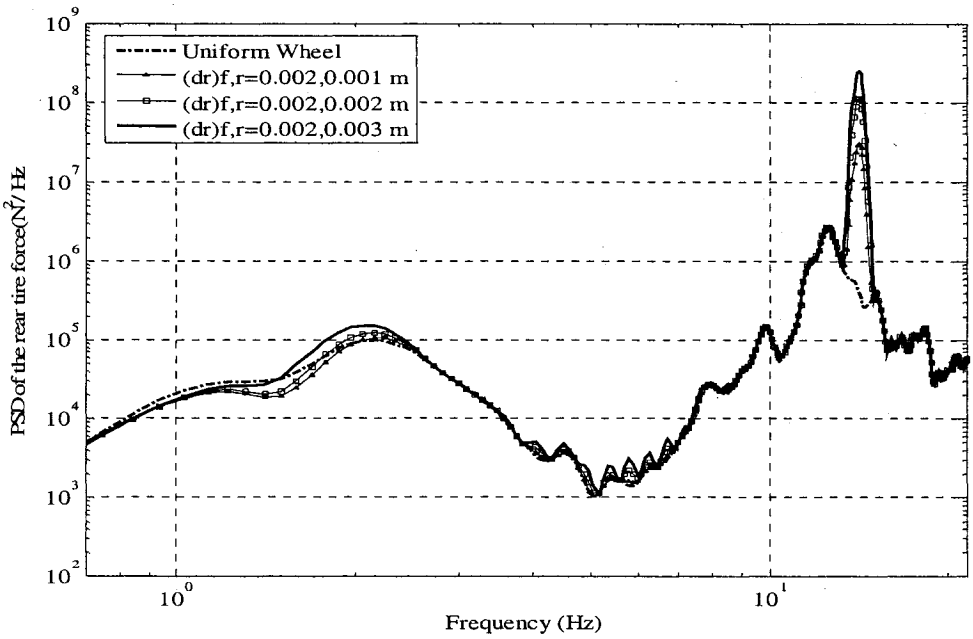

Figure 4.38: Effect of wheel non-uniformity on PSD of the front and rear tire forces at 80 km/h (Smooth road)

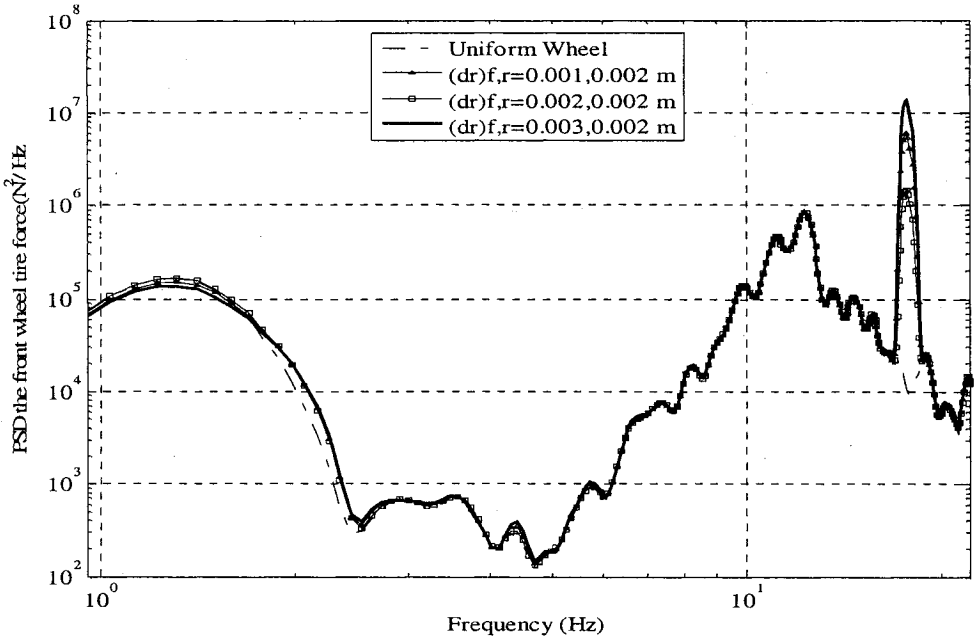

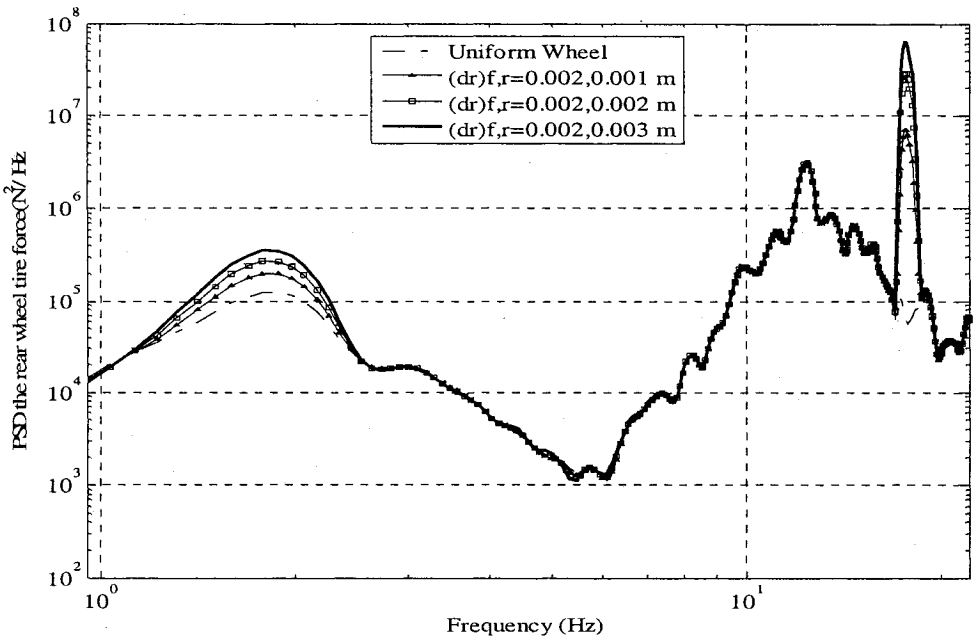

Figure 4.39: Effect of wheel non-uniformity on PSD of the front and rear wheel tire forces at 100 km/h (Smooth road)

operates on a smooth road. Apart from the vehicle speed, vehicle interactions with the road strongly depend upon the road roughness. The relative significance of the forces and accelerations caused by wheel non-uniformity may be small in relation to those caused by the tire interactions with a rough road surface. In this section, the relative contribution of the wheel non-uniformity is investigated under excitations arising from the medium-rough and rough roads, with the roughness indices of 4.37 and 5.94, respectively. The relative contribution of different levels of non-uniformity of the front and rear wheels are analyzed for a single forward speed of 80 km/h, while the results are presented in terms of dynamic tire loads, and vertical and pitch ride accelerations (weighted and unweighted). Moreover, the analyses are performed for identical combination of non-uniformities of the front and rear wheels.

Figures 4.40 to 4.42 illustrate the influence of three different road roughness types on the performance measures in terms of DLC, due to front and rear axle tire forces, and unweighted and frequency-weighted overall vertical and pitch rms accelerations, respectively. It is observed that an increase in the magnitude of the non-uniformity of the front or the rear wheels causes considerably larger increase in the DLC of both axle tires, when the vehicle is operating on a smooth road. The relative change in the DLC due to increasing non-uniformity, however, diminishes under medium-rough and rough road operations, as is evident in Figure 4.40. The results, therefore, suggest that the effects of wheel non-uniformity are more pronounced, when the contribution due to tire-road interactions is relatively small, as in the case of smooth road operation. Similar trends are also evident in the weighted and unweighted overall rms vertical and pitch acceleration responses (Figures 4.41 and 4.42). It can also be noted that the weighted pitch acceleration values are

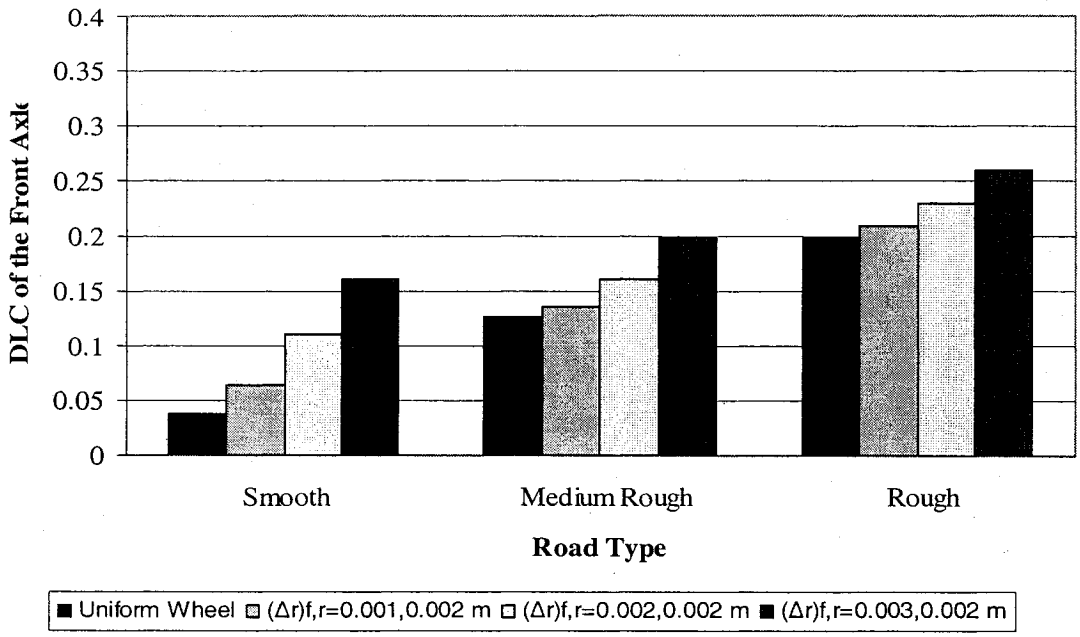

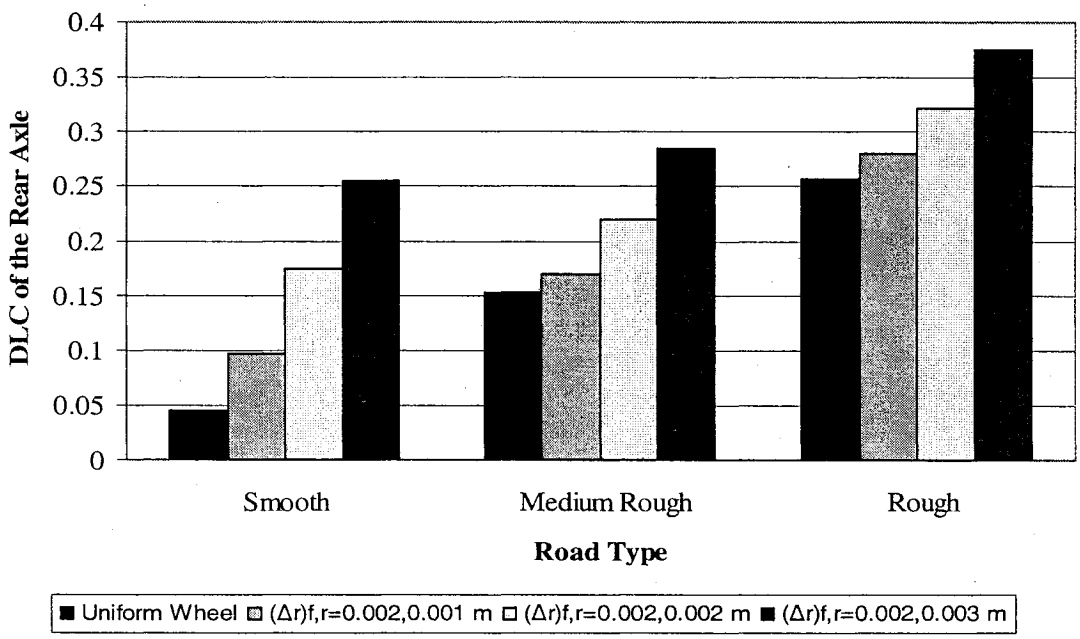

Figure 4.40: Influence of road roughness on DLC values for the front and rear axles at 80 km/h with wheel non-uniformity

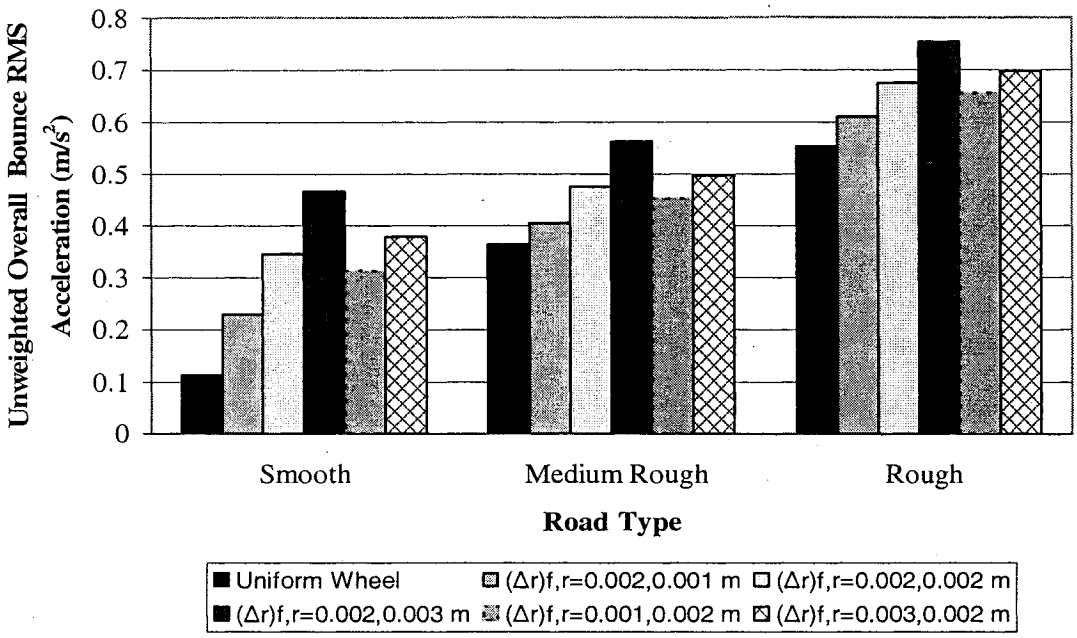

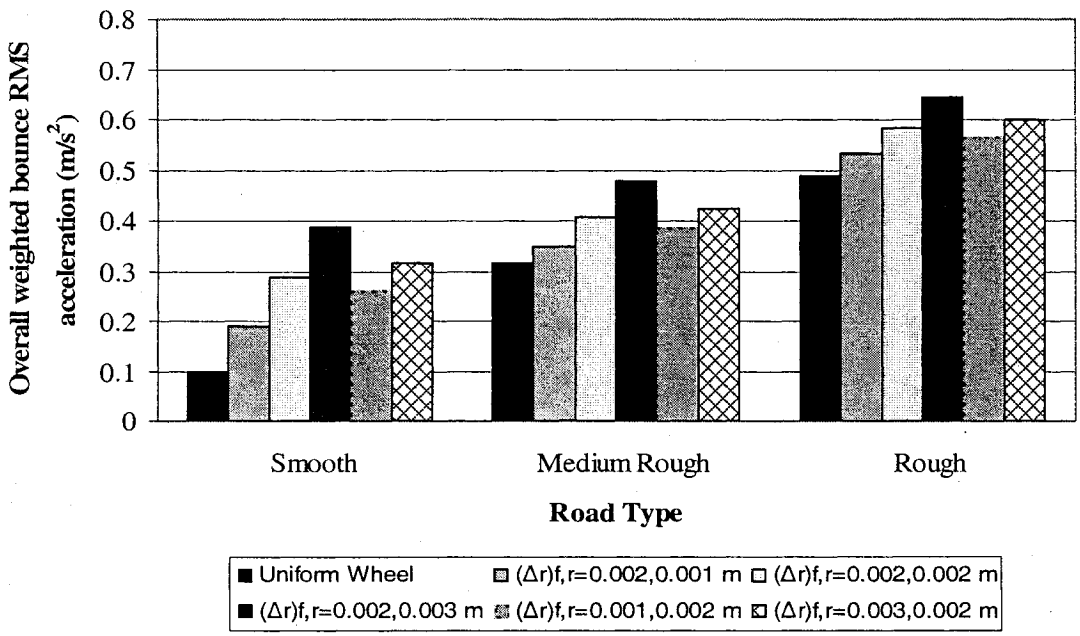

Figure 4.41: Influence of road roughness on overall unweighted and weighted rms bounce acceleration values at 80 km/h with wheel non-uniformity

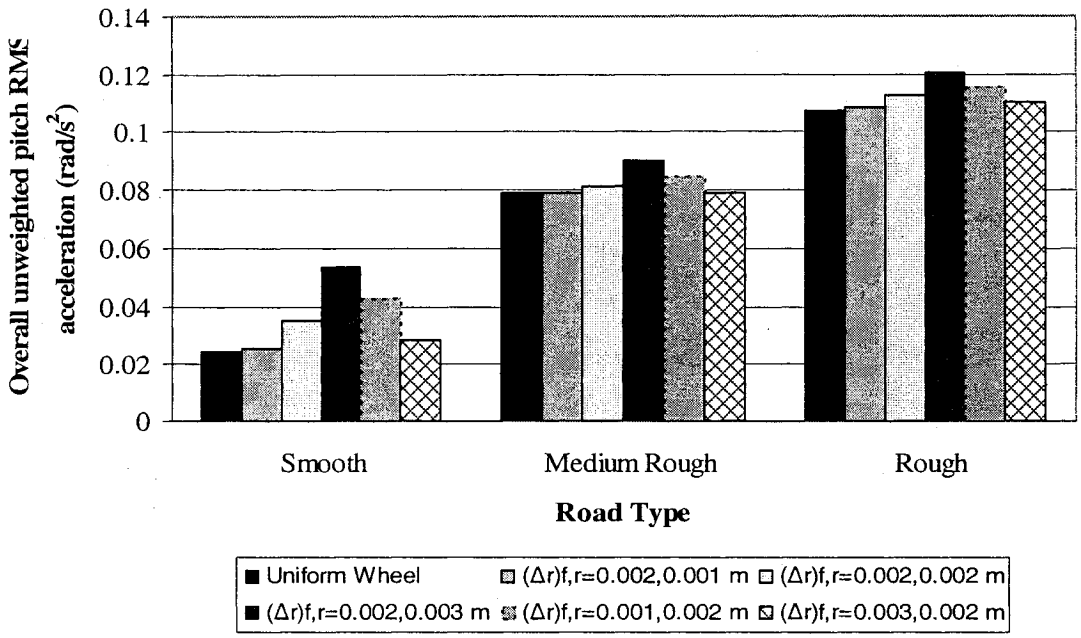

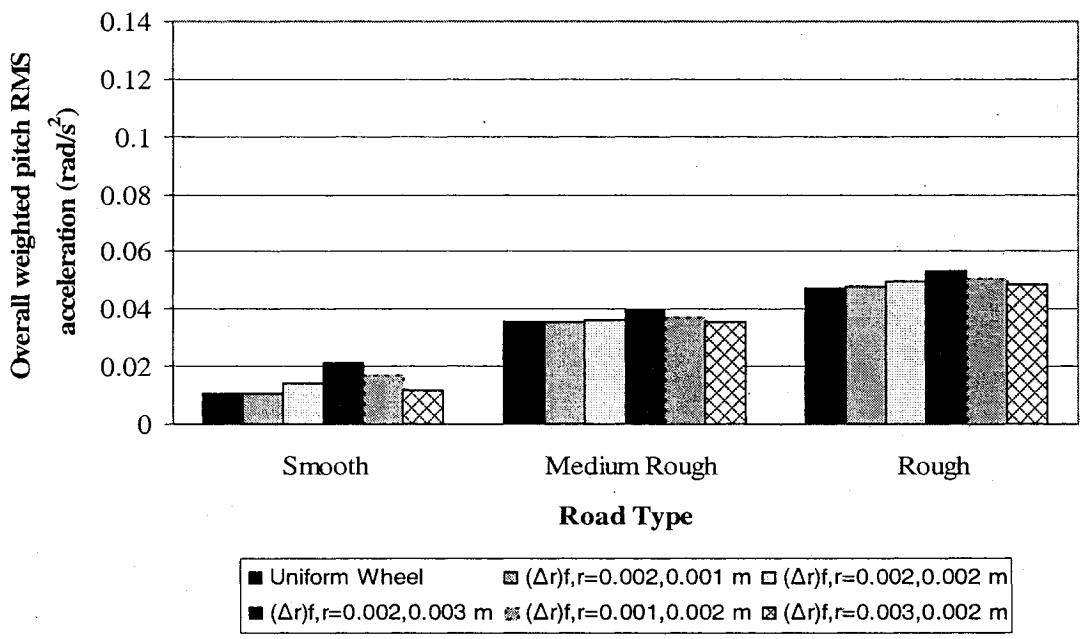

Figure 4.42: Influence of road roughness on overall unweighted and weighted rms pitch acceleration values at 80 km/h with wheel non-uniformity

considerably lower than the unweighted values, especially for the medium-rough and rough road operations, while the weighted bounce acceleration values are either close to or slightly lower than their respective unweighted values. This can be attributed to the predominant wheel non-uniformity effect of vertical vibration in the 10-19 Hz bands, where the amplitude ratio of the W_k-weighting filter is somewhat higher compared to that of the W_e-filter.

From the results presented above, it is apparent that there is considerable increase in all performance measures with increase in non-uniformity for the smooth road. The percentage increment for all performance measures reduces with increase in road roughness. This can be attributed to the increasing contribution from the road with increase in roughness. The non-uniformity combination of $(\Delta r)_{f,r}$ = 0.002 and 0.003 m yields the maximum values of all the performance measures except for the $(\Delta r)_{f,r}$ = 0.003 and 0.002 m combination, which yields maximum values for the DLC of the front axle tire for all road types. With varying non-uniformity, the changes in the weighted bounce and unweighted pitch acceleration values are very small especially for medium-rough and rough road conditions. The weighted pitch values are almost unaffected with increase in the non-uniformity for all the road conditions which can be attributed to the characteristics of a weighting filter.

The diminishing effects of the wheel non-uniformity with increasing road roughness could be clearly observed from the spectra of the tire force, and bounce and pitch acceleration responses presented in Figures 4.43 to 4.48. The PSD of front and rear tire forces under vehicle's interactions with the medium-rough and rough roads are presented in Figures 4.43 and 4.44, respectively. The results show that the wheel non-

uniformities yield significant peak responses near 14.2 Hz, irrespective of the road roughness. The magnitudes of the peaks relative to the responses of the baseline vehicle, with balanced and uniform wheels, however, are considerably smaller than those observed for the smooth road in Figure 4.38. Moreover, the relative magnitude tends to be smaller for the rough road. The ratio of the peak response, observed near 14.2 Hz under $(\Delta r)_{f,r}$ = 0.002, 0.003 m, to that obtained for balanced and uniform wheels, tends to be approximately 500 for the smooth road operation. This ratio reduces to approximately 40 and 20 under medium-rough and rough road operations, respectively. These results clearly show that the wheel nonuniformities yield most notable effects on the tire forces, when vehicle operates on a smooth road.

The vertical and pitch acceleration responses of the vehicle sprung mass tend to increase with increasing road roughness in majority of the frequency range considered, as evident in Figures 4.45 to 4.48. While the wheel nonuniformities induce larger responses near 14.2 Hz, the relative increase in the acceleration PSD diminishes with increasing road roughness. The insignificant effect of wheel non-uniformity on the vertical and pitch acceleration response is clearly evident under rough road excitation from Figures 4.46 and 4.48. Moreover, the application of frequency-weighting tends to further reduce the effect of wheel non-uniformity on the pitch acceleration PSD response of the vehicle under rough road excitation is also evident in Figure 4.48. The peak magnitudes of the bounce acceleration (unweighted and weighted) exhibit a significant variation with increasing non-uniformity in the vicinity of sprung mass resonance, under rough road condition resulting in higher overall bounce rms acceleration values, as evident from the results in Figure 4.41.

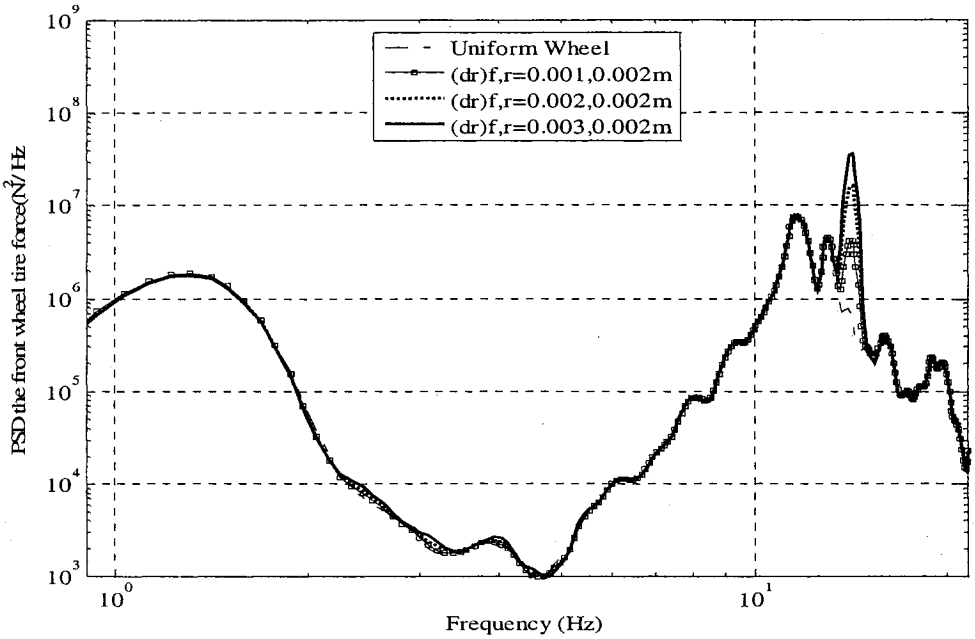

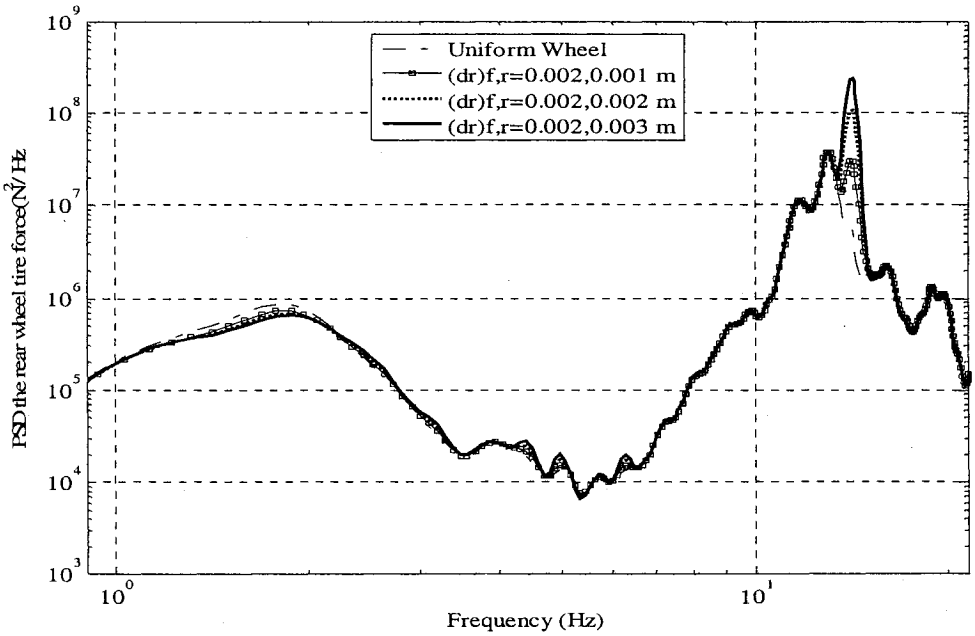

Figure 4.43: Effect of wheel non-uniformity on PSD of the front and rear tire forces at 80 km/h (Medium rough road)

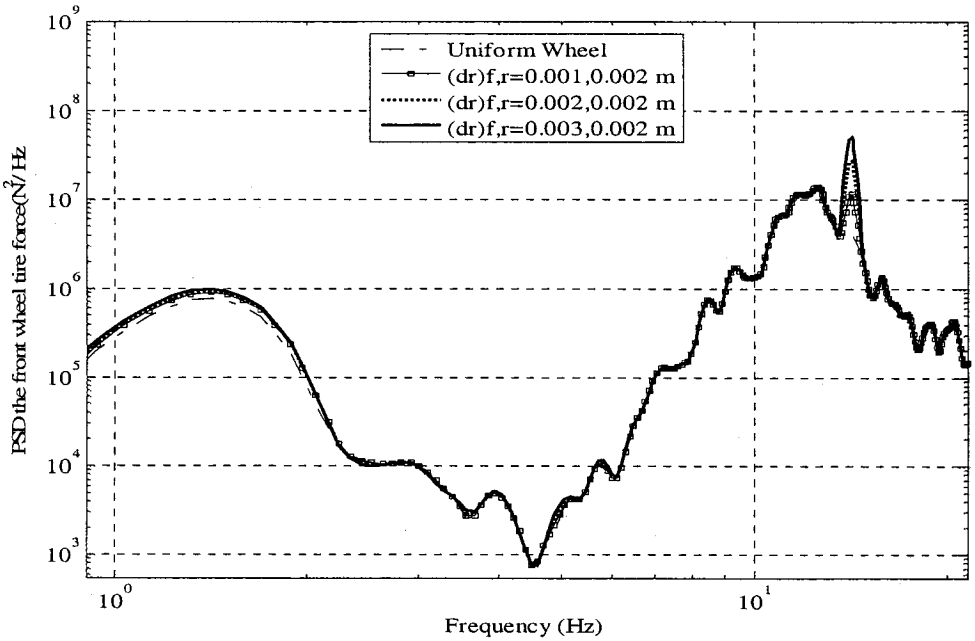

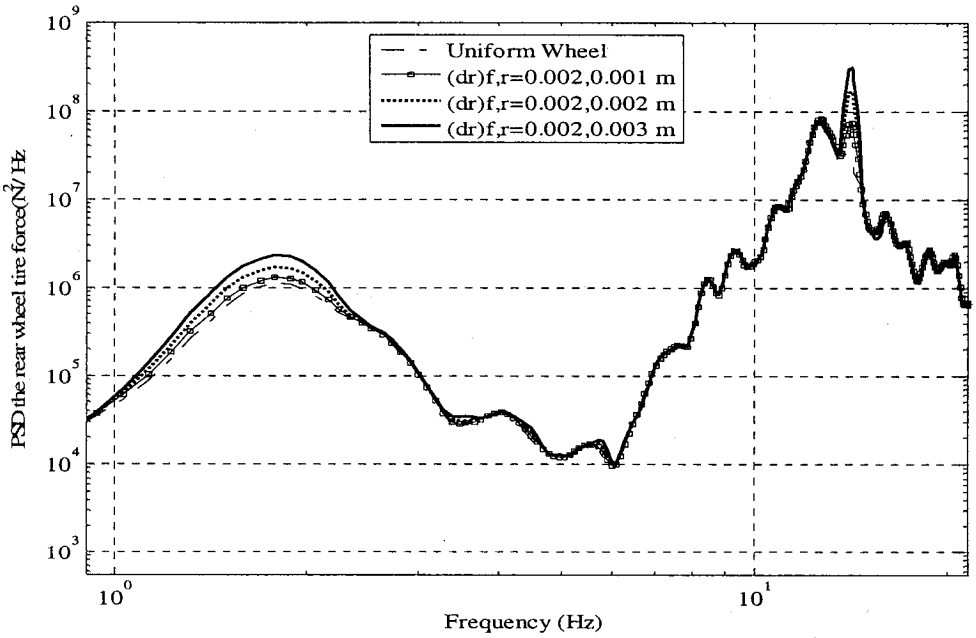

Figure 4.44: Effect of wheel non-uniformity on PSD of the front and rear tire forces at 80 km/h (Rough road)

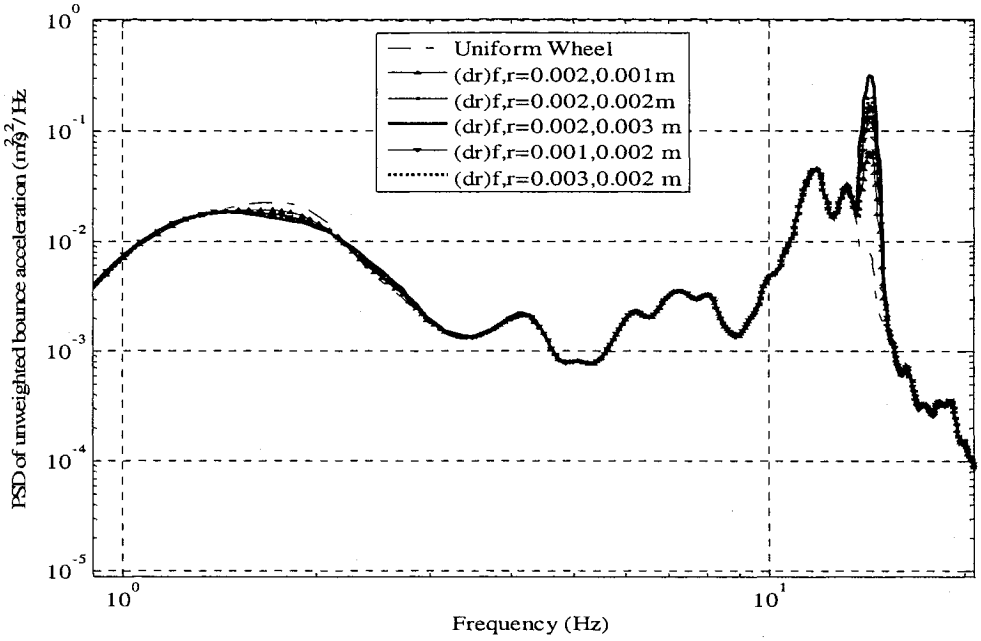

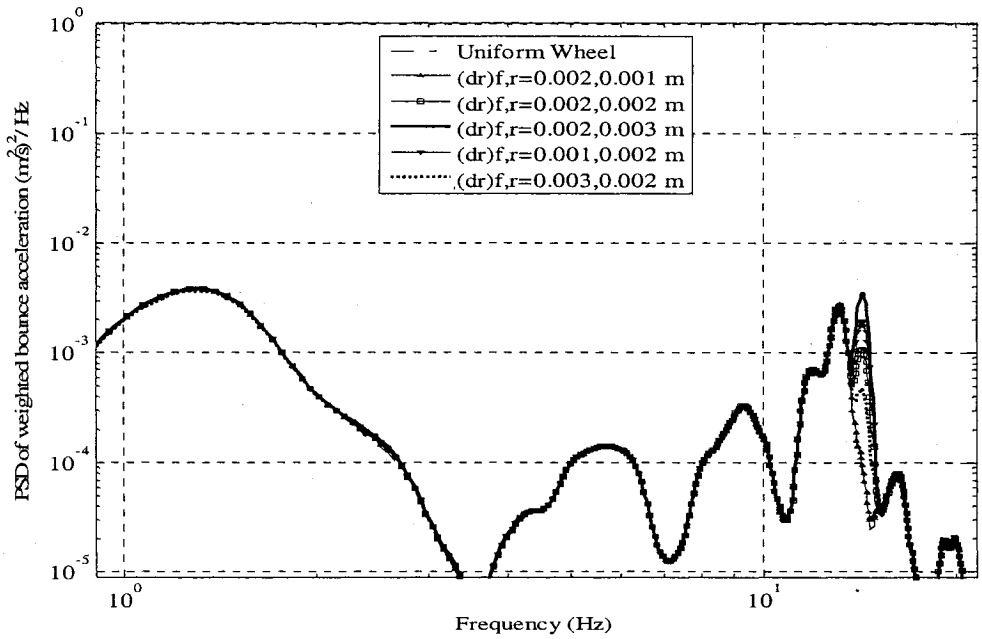

Figure 4.45: Effect of wheel non-uniformity on PSD of the unweighted and weighted bounce acceleration at 80 km/h (Medium-rough road)

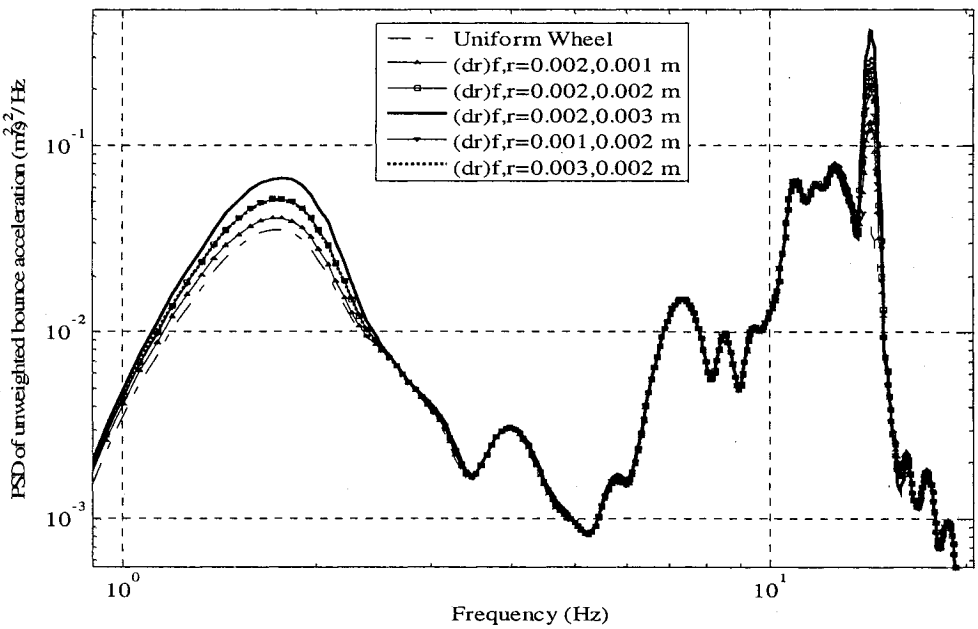

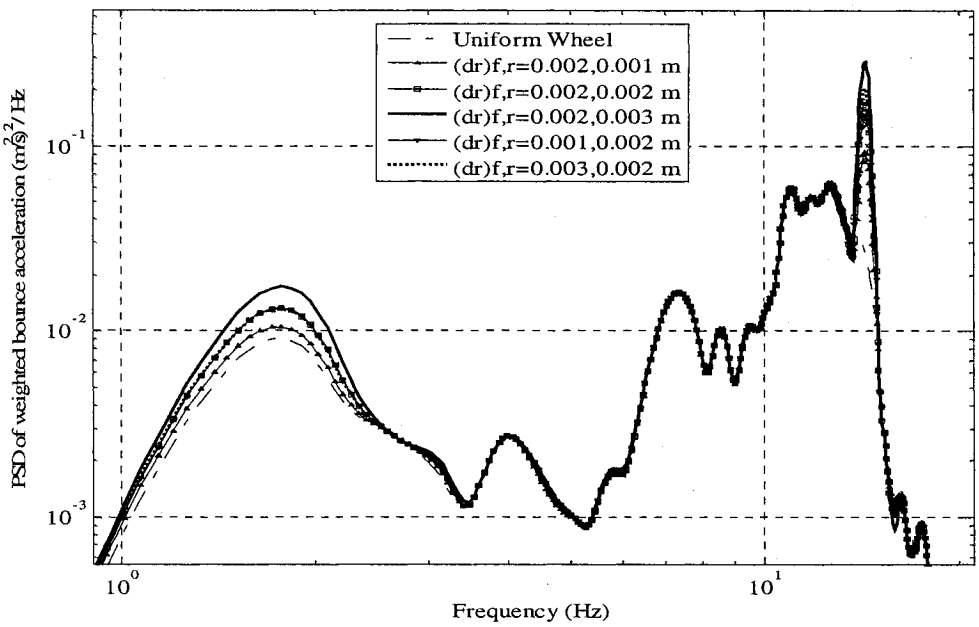

Figure 4.46: Effect of wheel non-uniformity on PSD of the unweighted and weighted bounce acceleration at 80 km/h (Rough road)

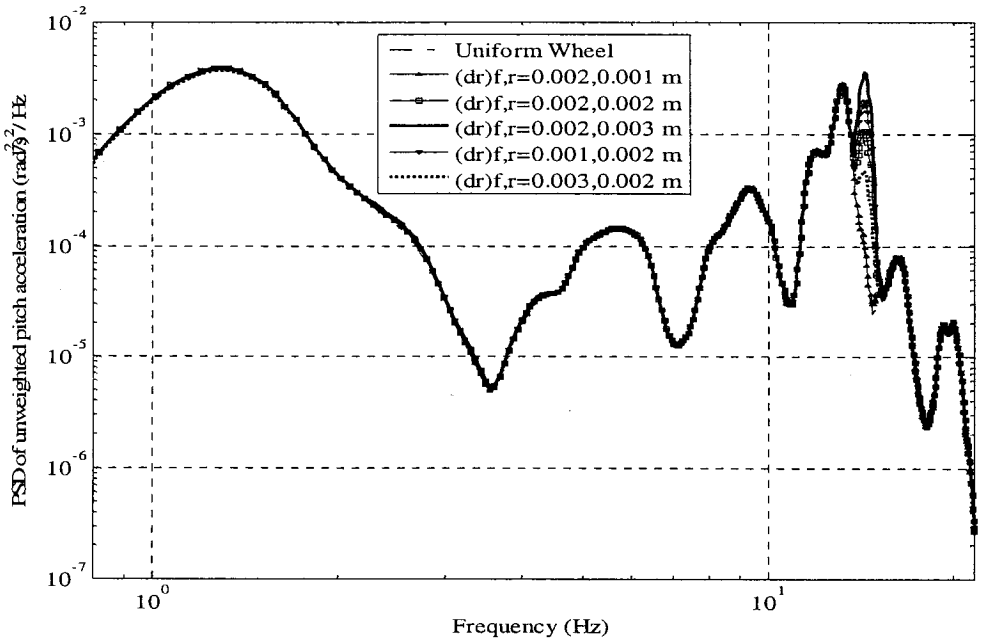

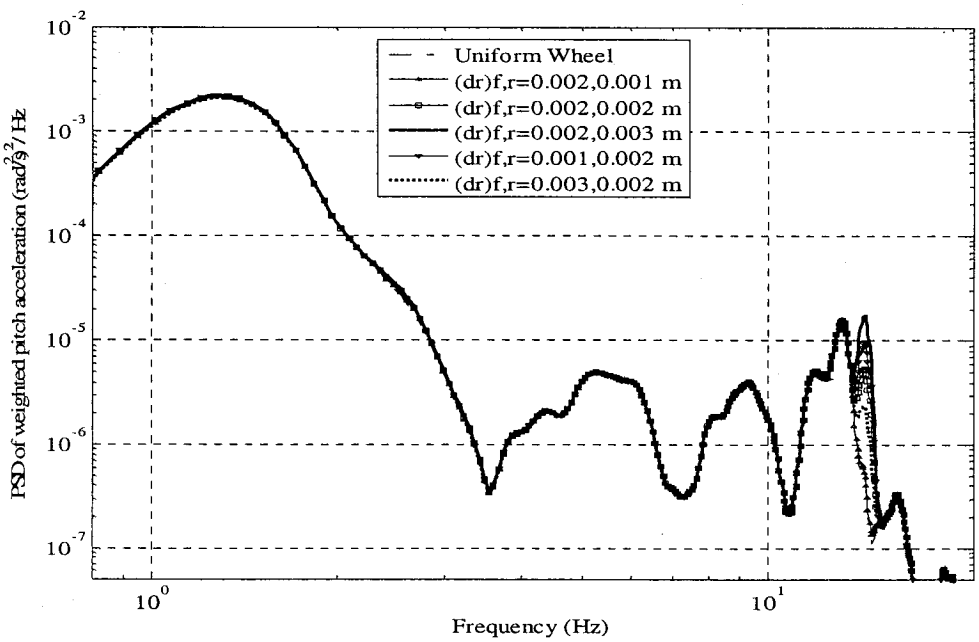

Figure 4.47: Effect of wheel non-uniformity on PSD of the unweighted and weighted pitch acceleration at 80 km/h (Medium-rough road)

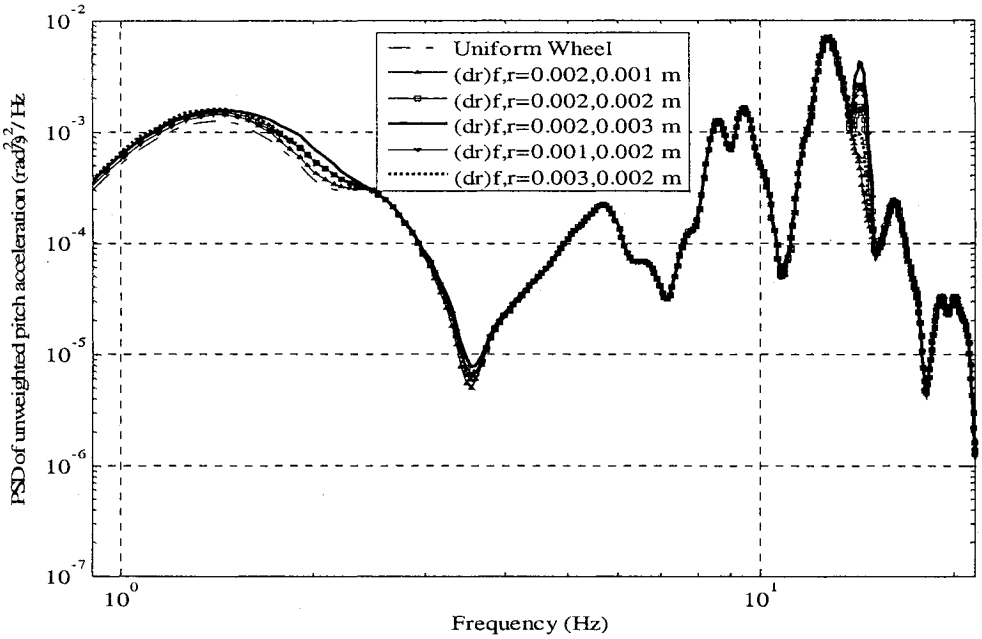

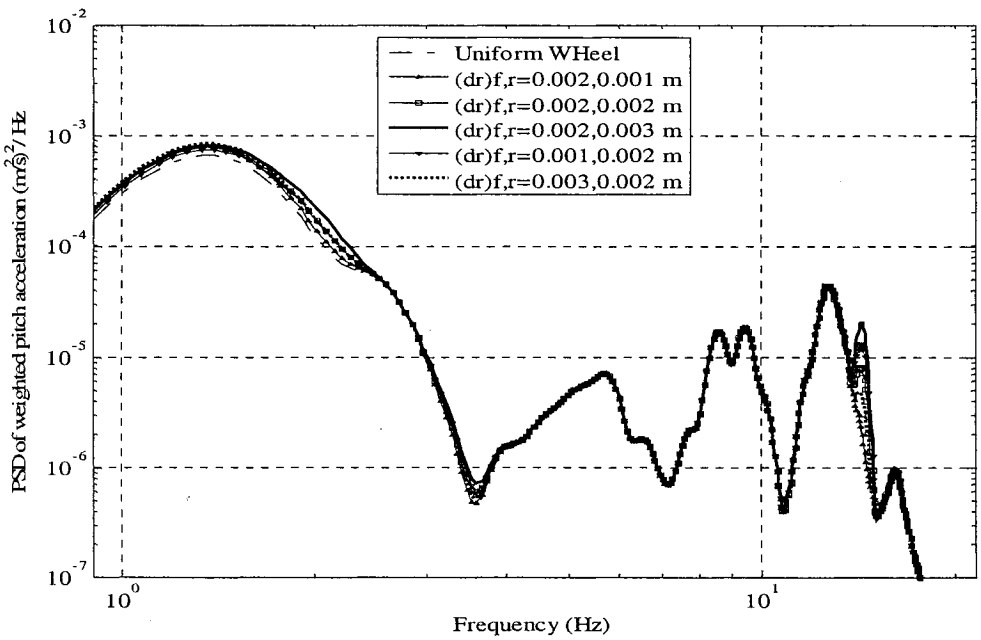

Figure 4.48: Effect of wheel non-uniformity on PSD of unweighted and weighted pitch acceleration at 80 km/h (Rough road)

4.3.3 INFLUENCE OF PHASE

A non-uniform wheel is characterized by assuming an elliptical shape as discussed in Chapter 2 (Figure 2.12), where the major axis of both the wheels are considered to coincide under static condition and remain parallel during rolling. Considering the front and rear non-uniform wheels, the major axes of each elliptical wheel could be located at different angular position from the horizontal plane, as illustrated in Figure 4.49, where ϕ_f and ϕ_r are the angles of the major axes of the front and rear wheels with respect to the fixed X-axis under static condition. The difference in angular locations of the nonuniformities leads to phase difference between the forces generated due to nonuniformities, which could induce the pitch response of the sprung mass. In this study, the influence of phase difference is investigated under excitations arising from the smooth road and a forward speed of 80 km/h. The results are presented in terms of overall vertical and pitch rms accelerations (weighted and unweighted). The DLC due to front and rear tire forces are not presented owing to the very small change for varying phase difference. The results are obtained for phase difference of are $0^\circ, 45^\circ$, and 90° while, two magnitudes of non-uniformity combinations used are, $(\Delta r)_{f,r} = 0.002, 0.003 m$ and $(\Delta r)_{f,r} = 0.003, 0.002 m$.

Figures 4.50 and 4.51 illustrate the influence of phase on the unweighted and frequency weighted vertical and pitch accelerations, respectively, for both the sets of wheel nonuniformities. It can be observed that the overall unweighted and weighted bounce rms acceleration values decrease considerably with increasing phase difference angle from 0° to 90° range. The weighted bounce rms acceleration values are observed to be close to their

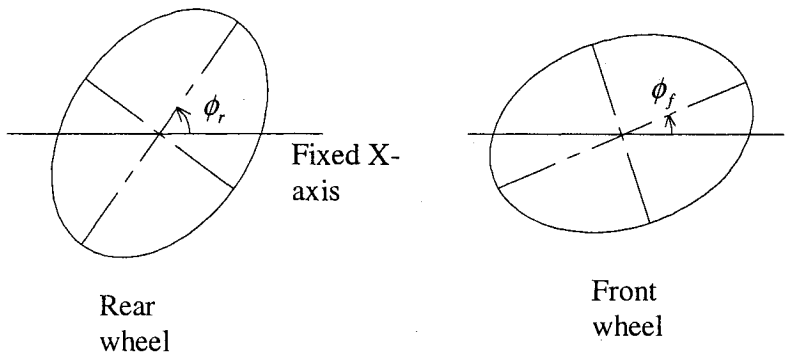

Figure 4.49: Representation of the phase difference between non-uniform wheels

unweighted values, while the unweighted and weighted pitch acceleration values increase considerably with increasing phase angle. The increase in the pitch response is directly attributed to the resulting phase difference in the tire forces at front and rear wheels.

The PSD of vertical unweighted and weighted acceleration responses for both sets of magnitudes of nonuniformities are presented in Figures 4.52 and 4.53. The peaks corresponding to wheel non-uniformity are observed near the frequency of 14.2 Hz. The peak magnitudes of the unweighted and weighted vertical accelerations decrease with increasing phase difference, as it was observed from the overall rms values, while the relative changes in the peak magnitudes are small. The increase in the peak pitch response magnitudes with increase in phase difference is clearly observed in Figures

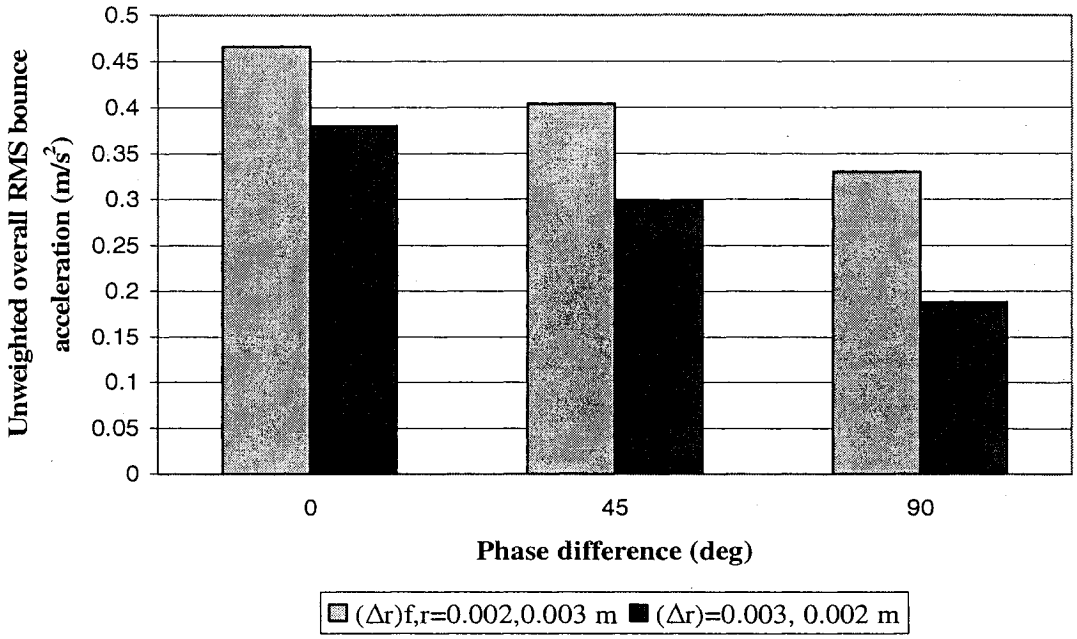

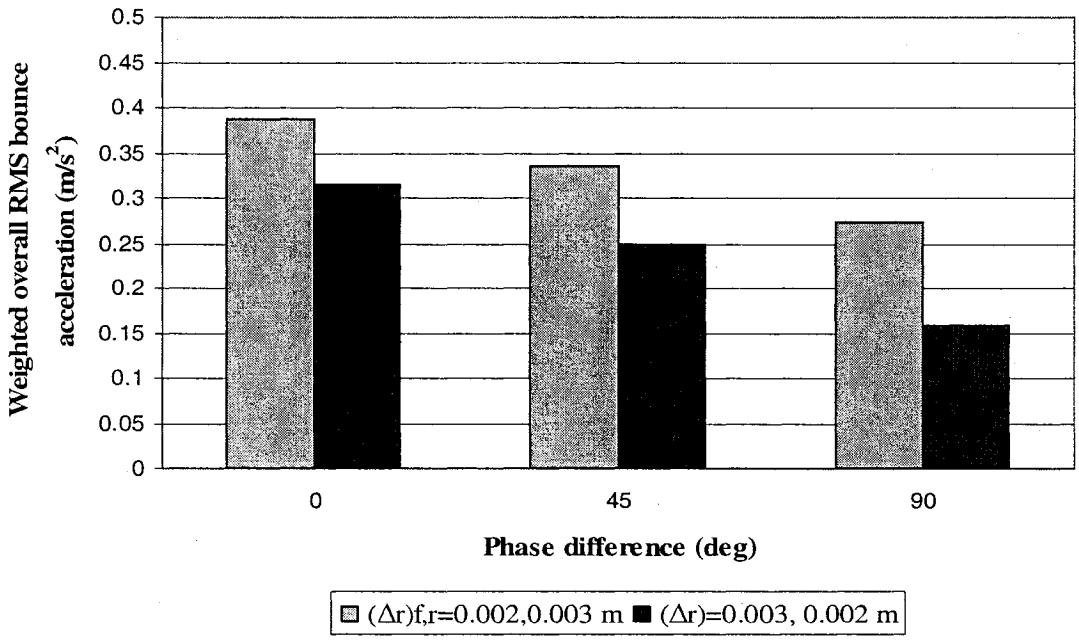

Figure 4.50: Influence of phase angle between the front and rear wheels radial run-out on overall unweighted and weighted rms bounce acceleration at 80 km/h (Smooth road)

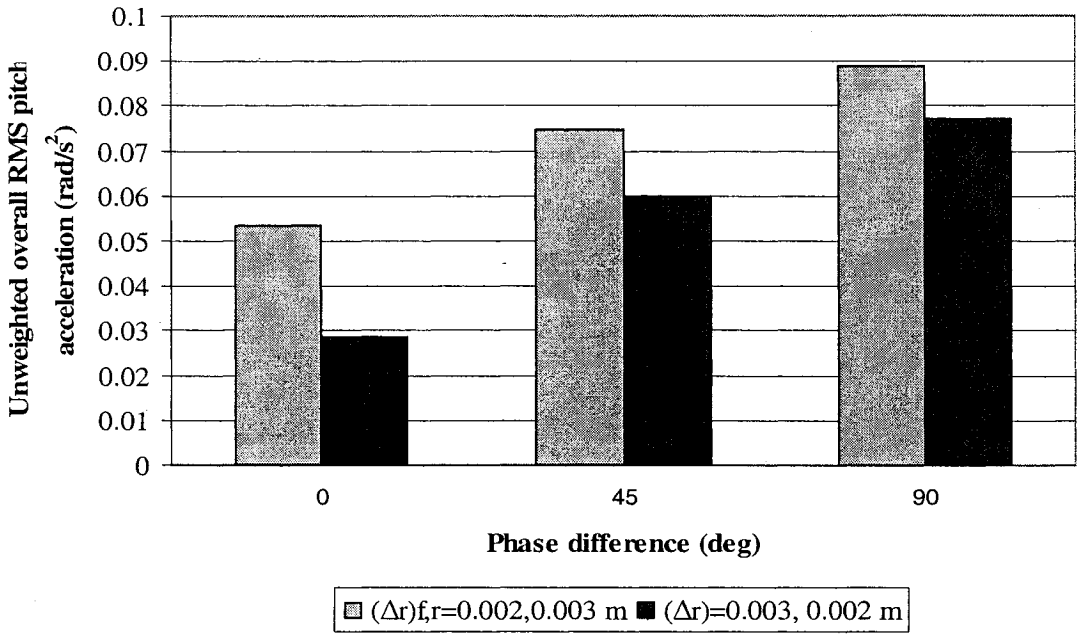

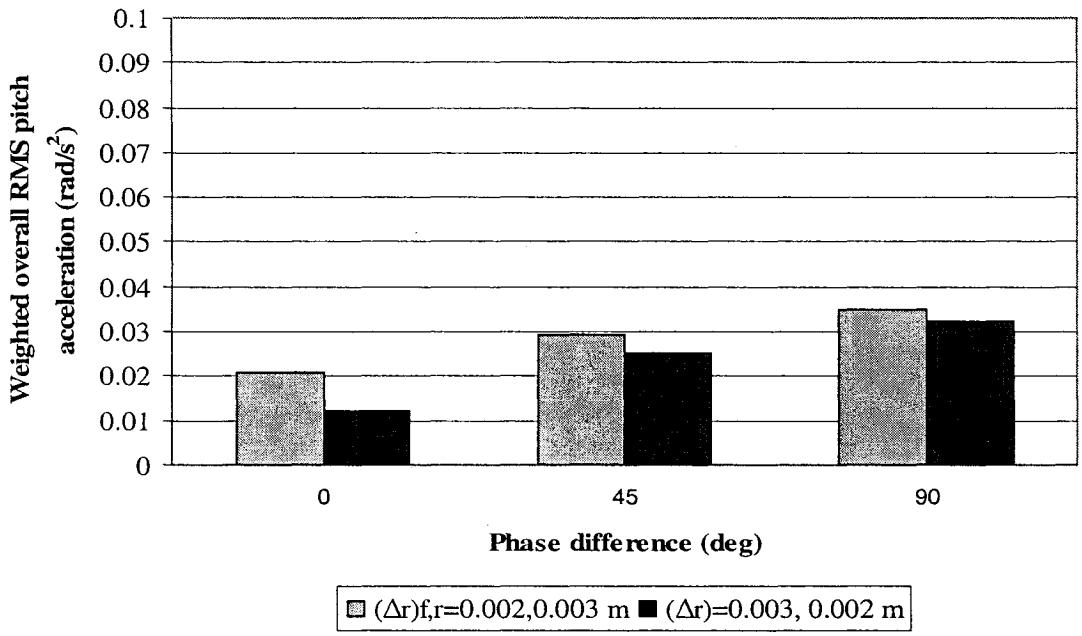

Figure 4.51: Influence of phase angle between the front and rear wheels radial run-out on overall unweighted and weighted rms pitch acceleration at 80 km/h (Smooth road)

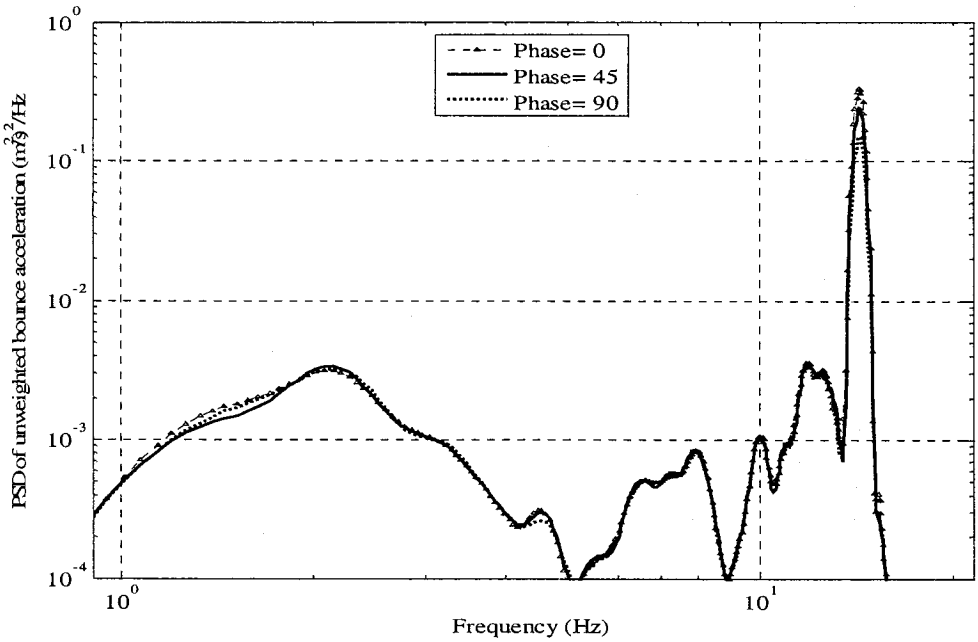

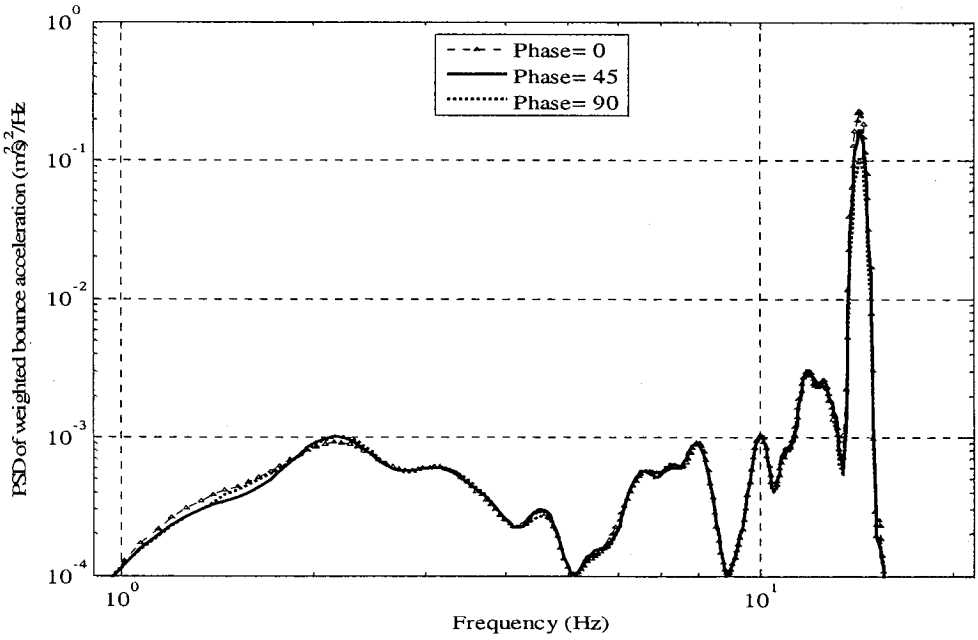

Figure 4.52: Effect of wheel non-uniformity on PSD of unweighted and weighted bounce acceleration for smooth road at 80 km/h with $(\Delta r)_{f,r} = 0.002, 0.003\, m$

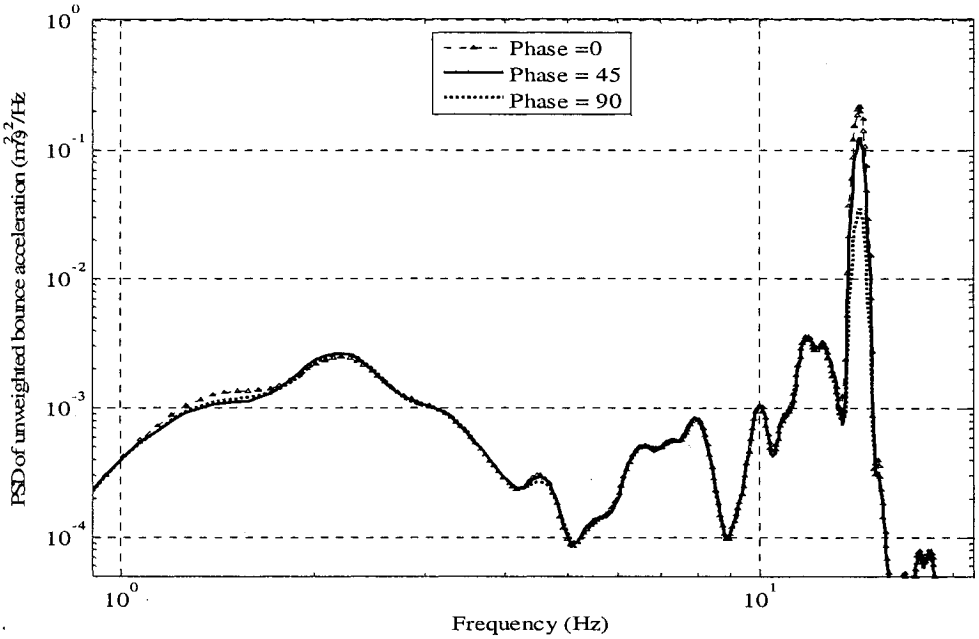

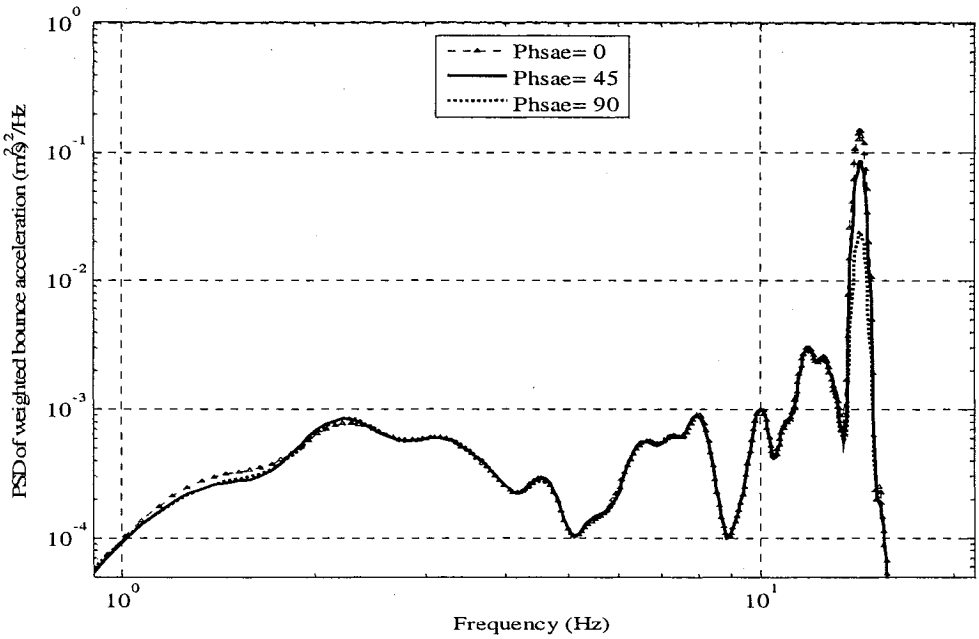

Figure 4.53: Effect of wheel non-uniformity on PSD of unweighted and weighted bounce acceleration for smooth road at 80 km/h with $(\Delta r)_{f,r} = 0.003, 0.002\, m$

4.54 and 4.55 for both sets of nonuniformities. The variations in the relative magnitudes of the peaks are more pronounced in pitch acceleration than the vertical acceleration responses. The application of W_e-weighting filter, however, considerably attenuates the magnitudes of peaks.

4.4 EFFECT OF COUPLED ROTATING WHEEL UNBALANCE AND NON-UNIFORMITY

The results presented in the previous sections consider the presence of either the mass unbalance or a symmetric wheel run-out. The presence of an asymmetric run-out of a wheel, however, would also yield mass unbalance of the wheel. The effects of coupled self-excitation sources arising from both the wheel unbalance and non-uniformity on the performance measures are thus further investigated. The analyses are performed for radial run out magnitudes in the 0.001 m to 0.002 m range, and mass unbalance of the front and rear wheels in the 0.5 to 2.0 kg, and 1.0 to 2.0 kg ranges, respectively. Different combinations of the front and rear wheel runouts with mass unbalance, however, are considered. These include $(me)_{f,r}$ = 0.2, 0.4 kg-m and $(\Delta r)_{f,r}$ = 0.002, 0.001 m; $(me)_{f,r}$ = 0.2, 0.6 kg-m and $(\Delta r)_{f,r}$ = 0.002, 0.0015 m; $(me)_{f,r}$ = 0.2, 0.8 kg-m and $(\Delta r)_{f,r}$ = 0.002, 0.002 m; $(me)_{f,r}$ = 0.8, 0.4 kg-m and $(\Delta r)_{f,r}$ = 0.002, 0.002 m; $(me)_{f,r}$ = 0.4, 0.4 kg-m and $(\Delta r)_{f,r}$ = 0.001, 0.002 m; $(me)_{f,r}$ = 0.6, 0.4 kg-m and $(\Delta r)_{f,r}$ = 0.0015, 0.002 m. The eccentricity of unbalanced mass considered for this analysis is 0.4 m.

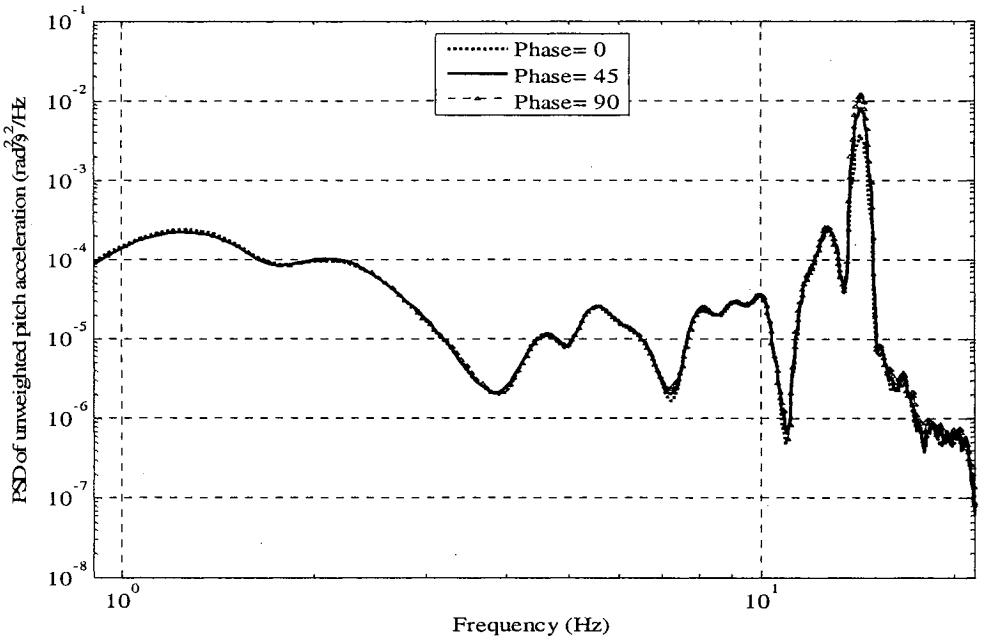

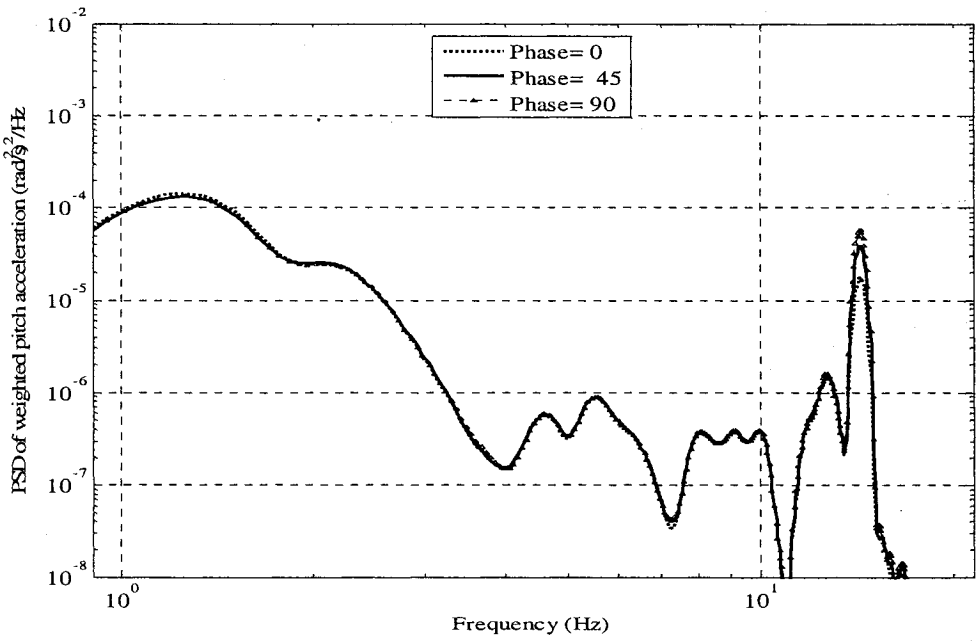

Figure 4.54: Effect of wheel non-uniformity on PSD of unweighted and weighted pitch acceleration for smooth road at 80 km/h with $(\Delta r)_{f,r} = 0.002, 0.003\,m$

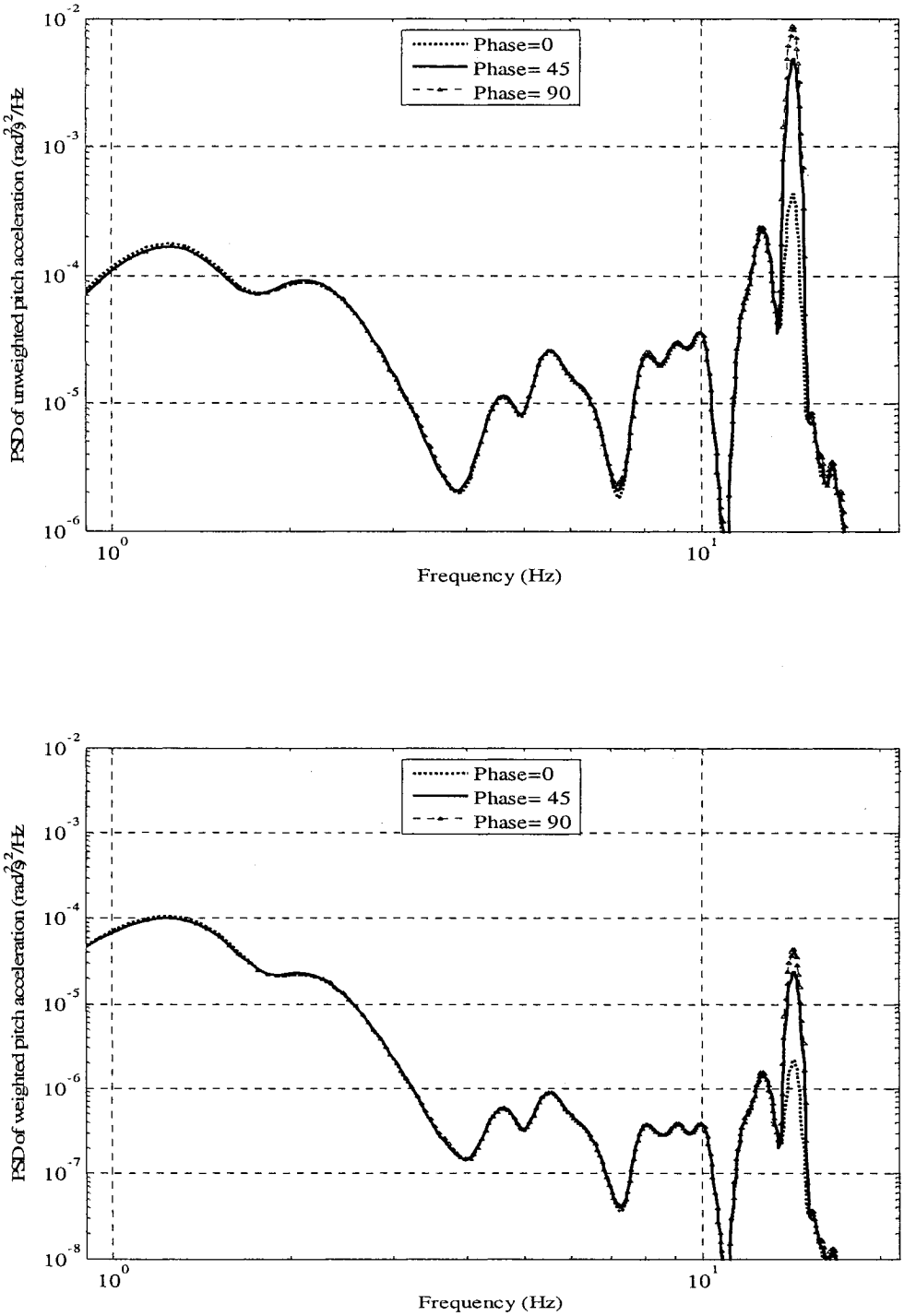

Figure 4.55: Effect of wheel non-uniformity on PSD of unweighted and weighted pitch acceleration for smooth road at 80 km/h with $(\Delta r)_{f,r} = 0.003, 0.002\,m$

4.4.1 INFLUENCE OF SPEED

The ride quality and tire force variation of the vehicle with unbalanced and non-uniform wheels is expected to be strongly affected by the speed. As briefly discussed in Chapter 2, the frequency corresponding to excitations arising from unbalanced and non-uniform wheel is a function of the vehicle speed. The effects of wheel unbalance and non-uniformity (run-out) are thus investigated for three different vehicle speeds of 60 km/h, 80 km/h and 100 km/h, while the results are presented in terms of performance measures relevant to weighted and unweighted overall rms bounce and pitch accelerations and dynamic load coefficients (DLC) due to front and rear wheel forces. In order to clearly show the effect of both sources of self excitation, unbalance and non-uniformity, on the performance measures, the analyses are initially performed for the smooth road.

Figures 4.56 to 4.58 illustrate the influence of vehicle speed on the performance measures for all combinations of mass unbalance and radial run-out considered. Figures show the DLC due to front and rear tire forces, and unweighted and frequency-weighted overall rms values due to vertical and pitch acceleration responses of the sprung mass. The results reveal that presence of wheel unbalance and non-uniformity yield considerable increases in the DLC, irrespective of the vehicle speed. While the DLC values of both the axle tires increase nearly linearly with the magnitude of the wheel unbalance and run-out, the effect is relatively small at the lower speed of 60 km/h. Moreover, the DLC due to front wheel forces increases most significantly at the speed of 100 km/h, while the increase in DLC due to rear wheel forces is more pronounced at 80 km/h. The effect of speed on the DLC values can be related to the predominant excitation frequencies due to wheel unbalance and

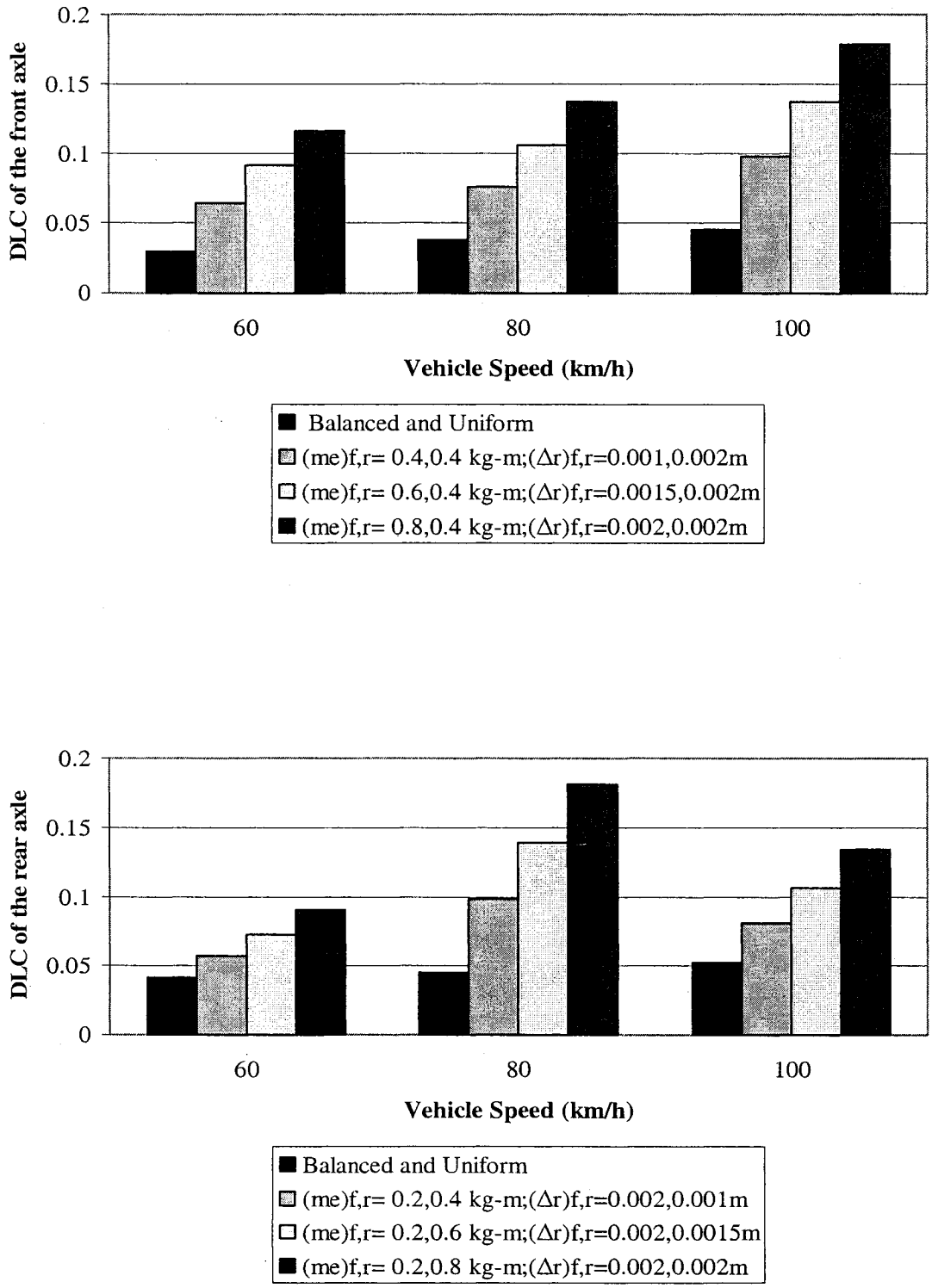

Figure 4.56: Influence of forward speed on the DLC of the front and rear axle tire forces in the presence of wheel unbalance and non-uniformity (Smooth road)

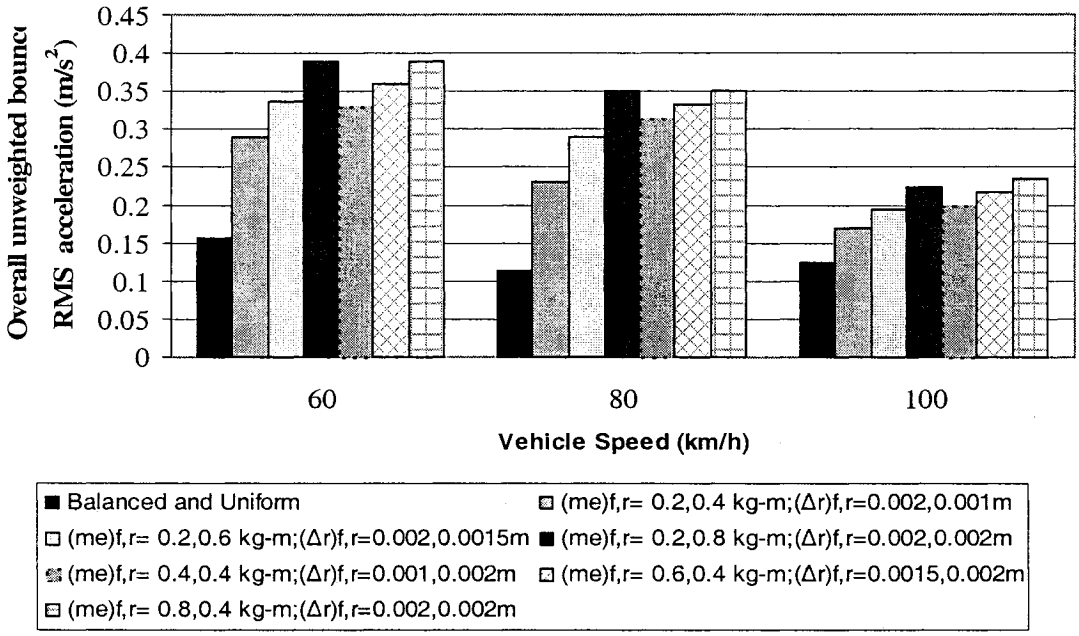

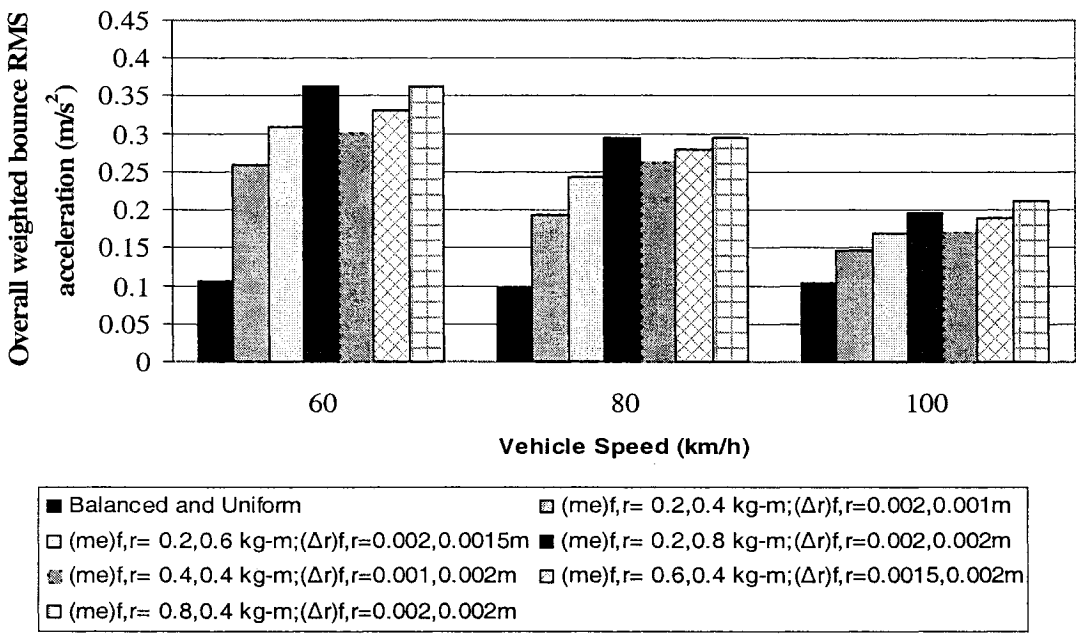

Figure 4.57: Influence of speed on overall unweighted and weighted rms bounce acceleration values with wheel unbalance and non-uniformity (Smooth road)

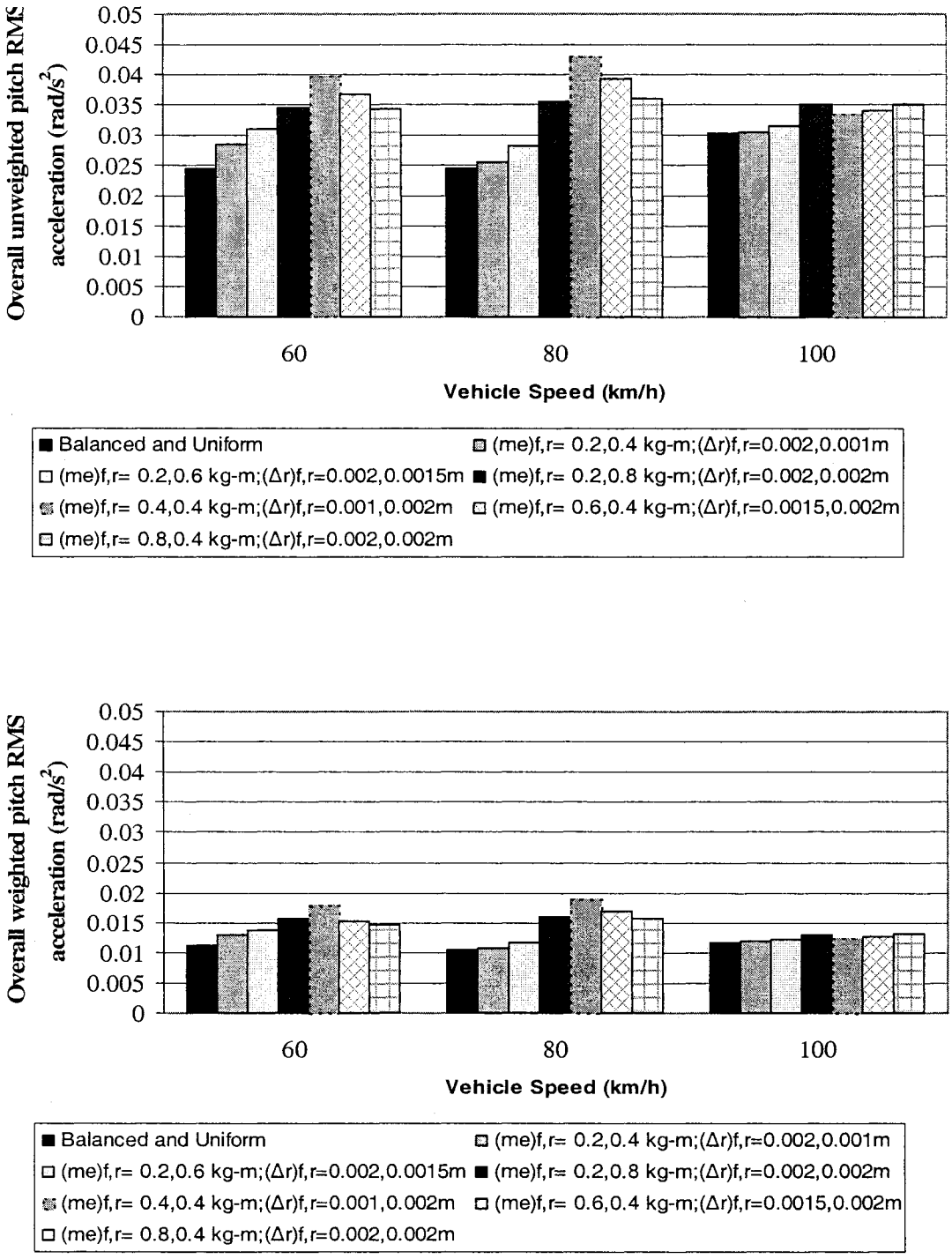

Figure 4.58: Influence of speed on overall unweighted and weighted rms pitch acceleration values with wheel unbalance and non-uniformity (Smooth road)

run-out. The operations at the different selected speeds of 60, 80 and 100 km/h would yield predominant excitation due to wheel unbalance near 5.3, 7.1 and 8.8 Hz, while due to wheel non-uniformity near 10.6, 14.2 and 17.8 Hz, respectively. The vehicle operation at a speed of 100 km/h could thus generate higher front tire forces near 17.8 Hz. The lower intensity of the road roughness near this frequency, however, tends to diminish the magnitudes of resulting tire forces leading to the dominance of force due to wheel unbalance. DLC values due to front axle forces thus show maximum increment at 100 km/h, which is very similar to the response with mass unbalance alone. The resonant frequency of the rear wheel lies very close to the predominant frequency due to wheel non-uniformity at a speed of 80 km/h, which causes relatively higher tire forces.

Figure 4.57 presents the overall rms bounce acceleration (unweighted and weighted), which increases with increasing magnitudes of wheel unbalance and run-out, while the effects are far more pronounced at speeds of 60 and 80 km/h. The operations at 100 km/h yields considerably lower values of vertical rms acceleration and relatively small effects of wheel unbalance and run-out. The application of W_k-weighting filter further diminishes the rms values of vertical accelerations at 100 km/h due to predominance of higher frequency components. The weighted values at 60 and 80 km/h, however, tend to be only slightly lower than the unweighted values, since the predominant excitations corresponding to unbalance and non-uniformity occur in the 5-14 Hz range.

The overall rms values of the pitch acceleration show most significant effect of wheel unbalance and run-out at 80 km/h, while the effect at 100 km/h is relatively small (Figure 4.58). Owing to the relatively high frequency of the pitch motion caused by

wheel unbalance and run-out, the application of W_e-weighting filter reduces the rms values of pitch accelerations significantly. The results further show that a higher degree of wheel unbalance and run-out of the rear wheels yields most significant effects on the pitch and vertical accelerations, and tire forces. This could be attributed to the higher stiffness of the rear wheel suspension and the higher axle load.

The spectral components of vertical and pitch acceleration responses are evident from the PSD of bounce and pitch accelerations (unweighted and weighted) presented in Figures 4.59 and 4.60, respectively, for all sets of magnitudes of wheel unbalance and run-out at 60 km/h. The response show peaks corresponding to wheel balance near the wheel rotation frequency, 5.3 Hz, and corresponding to wheel non-uniformity near 10.6 Hz. The peak magnitude of vertical acceleration occur for $(me)_{f,r}$ = 0.2, 0.8 kg-m and $(\Delta r)_{f,r}$ = 0.002, 0.002 m combination, and that of the pitch acceleration occur for $(me)_{f,r}$ = 0.4, 0.4 and $(\Delta r)_{f,r}$ = 0.001, 0.002 m, lower magnitudes of unbalanced masses and runouts exhibit only small increases in the acceleration responses. The combinations $(me)_{f,r}$ = 0.6, 0.4 kg-m and $(\Delta r)_{f,r}$ = 0.0015, 0.002 m, and $(me)_{f,r}$ = 0.2, 0.4 kg-m and $(\Delta r)_{f,r}$ = 0.002, 0.001 m, however form exception and yield comparably higher peaks for vertical and pitch accelerations.

Figures 4.61 to 4.64 illustrate the PSD of vertical and pitch unweighted and weighted acceleration responses of the vehicle at forward speeds of 80 km/h and 100 km/h, respectively, for different magnitudes of wheel unbalance and nonuniformities. The results show that the peak magnitudes corresponding to wheel non-uniformity frequency in the vertical acceleration responses decrease with increase in speed from 80 to 100 km/h, while the peak pitch acceleration response is higher at 80 km/h, and the lowest at 100 km/h.

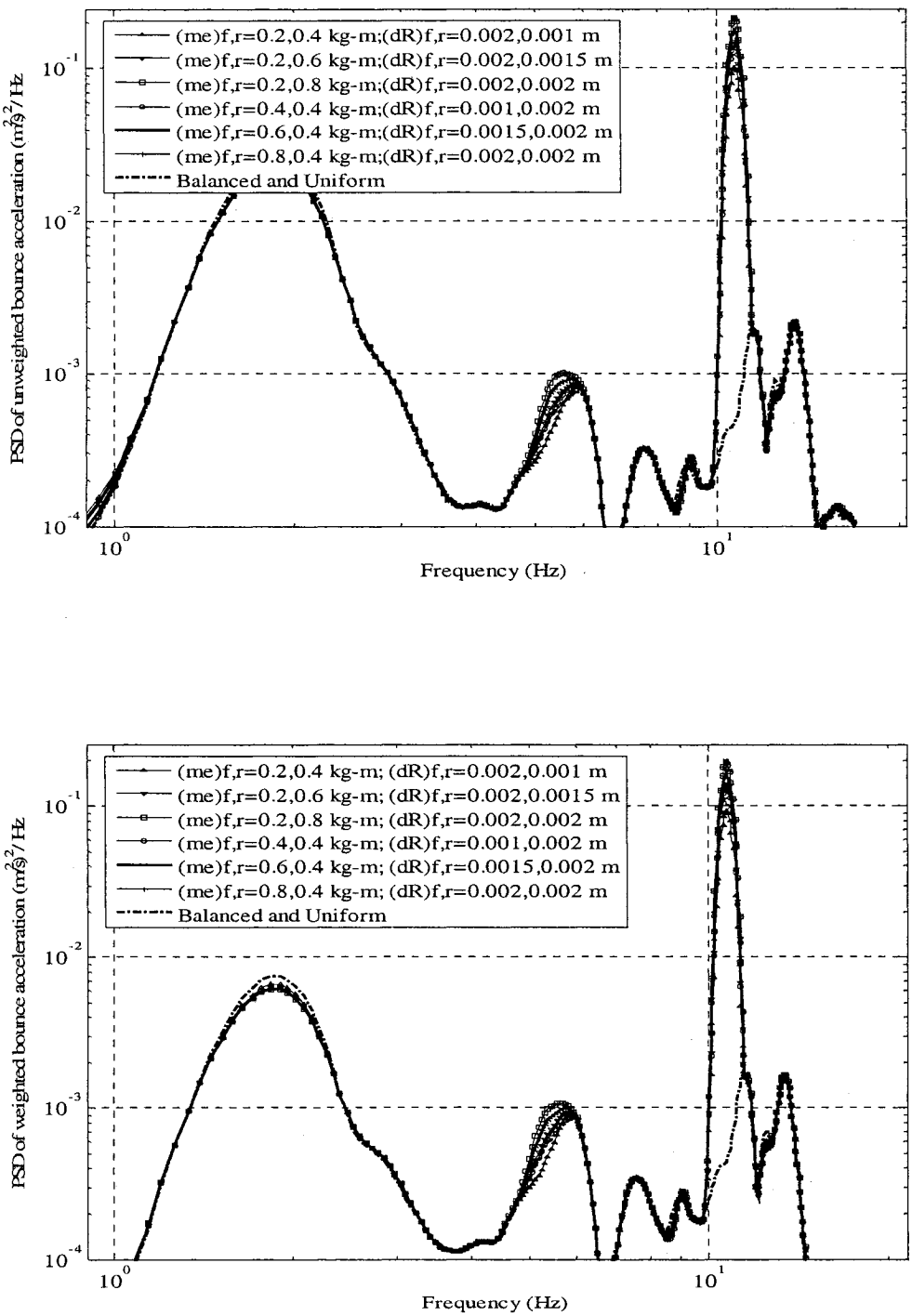

Figure 4.59: Effect of wheel unbalance and non-uniformity on PSD of unweighted bounce acceleration at 60 km/h (Smooth road)

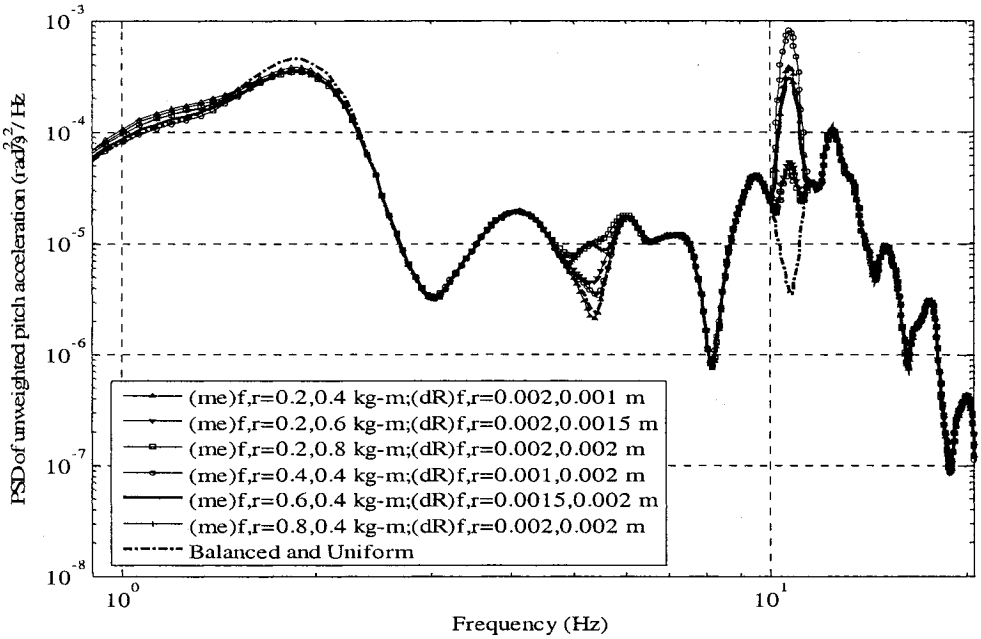

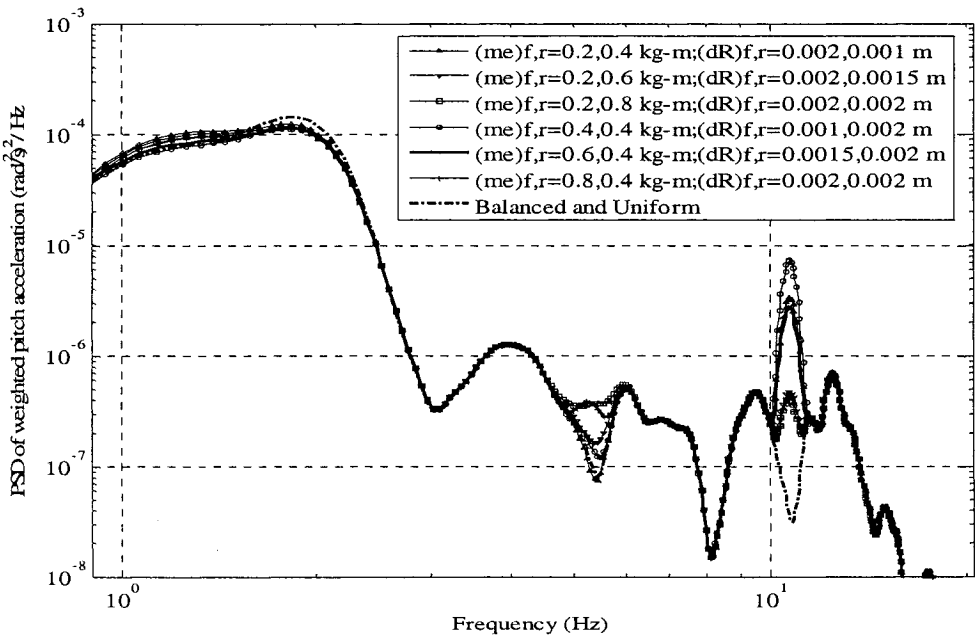

Figure 4.60: Effect of wheel unbalance and non-uniformity on PSD of unweighted and weighted pitch acceleration at 60 km/h (Smooth road)

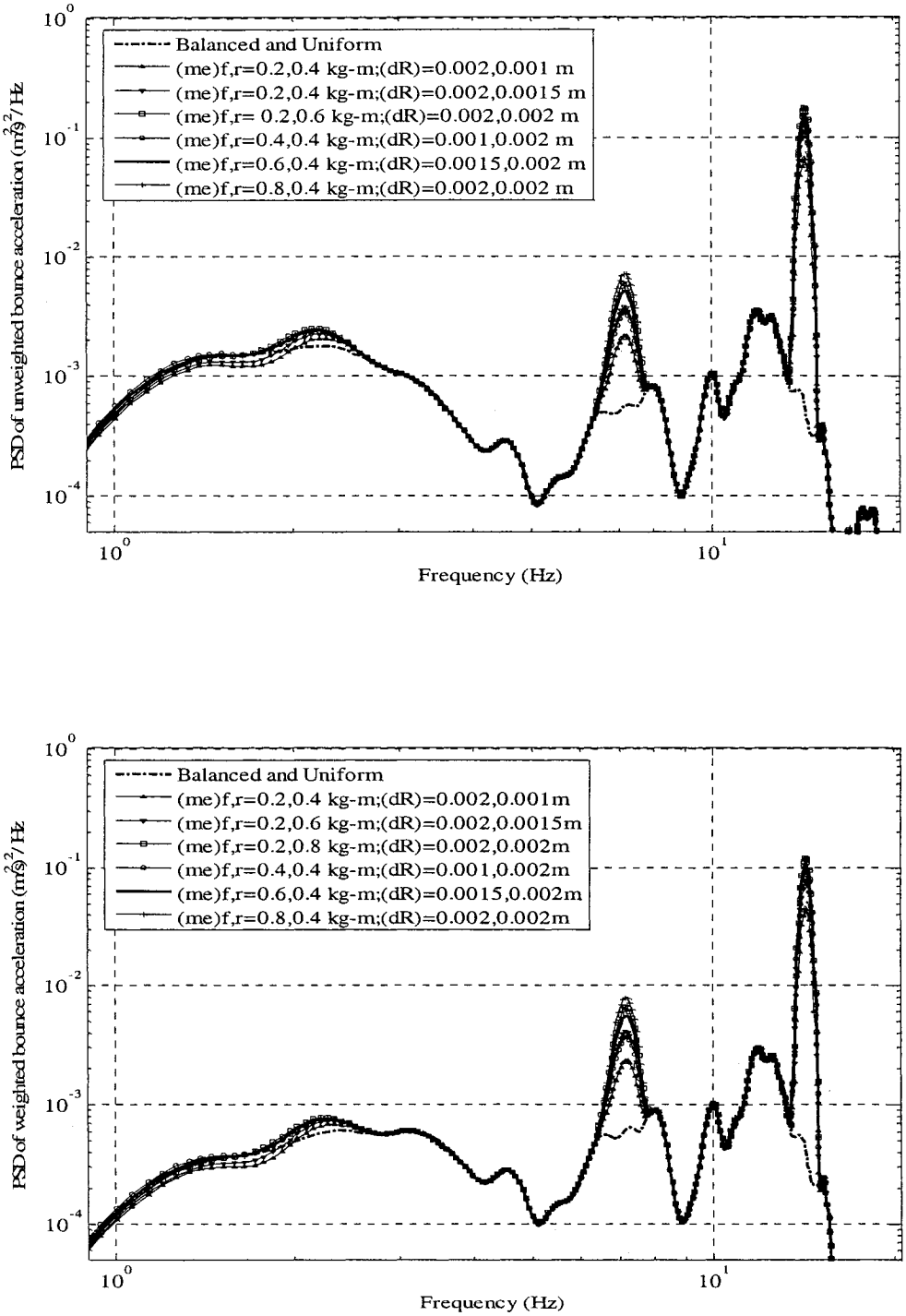

Figure 4.61: Effect of wheel unbalance and non-uniformity on PSD of the unweighted and weighted bounce acceleration at 80 km/h (Smooth road)

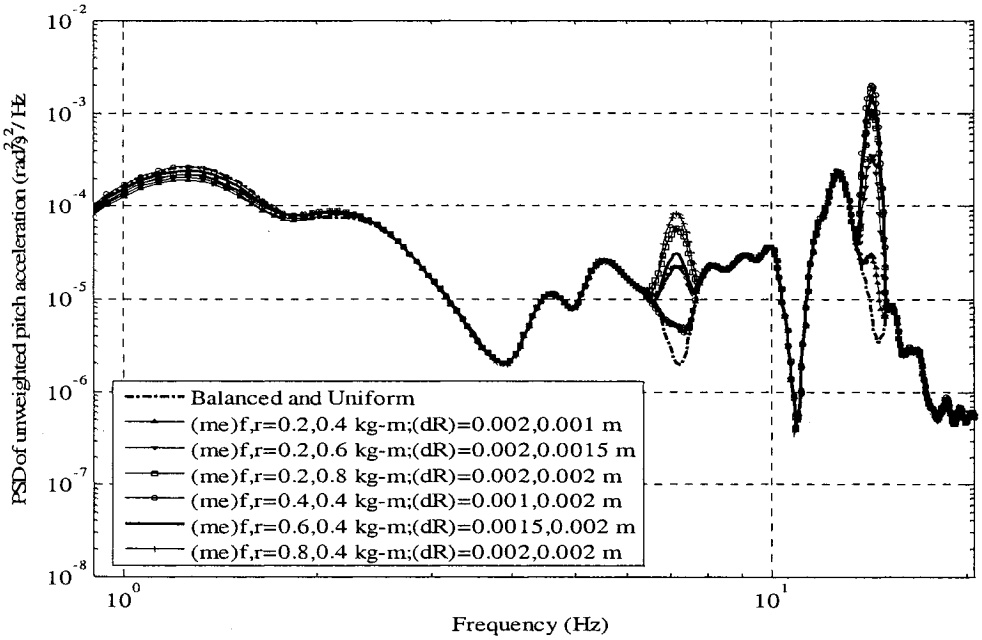

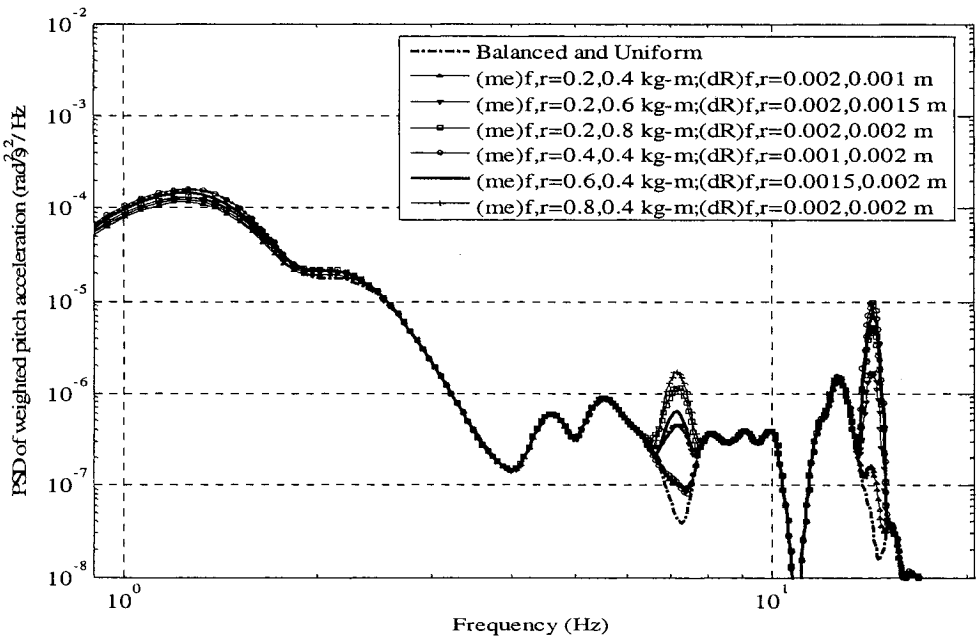

Figure 4.62: Effect of wheel unbalance and non-uniformity on PSD of unweighted and weighted pitch at 80 km/h (Smooth road)

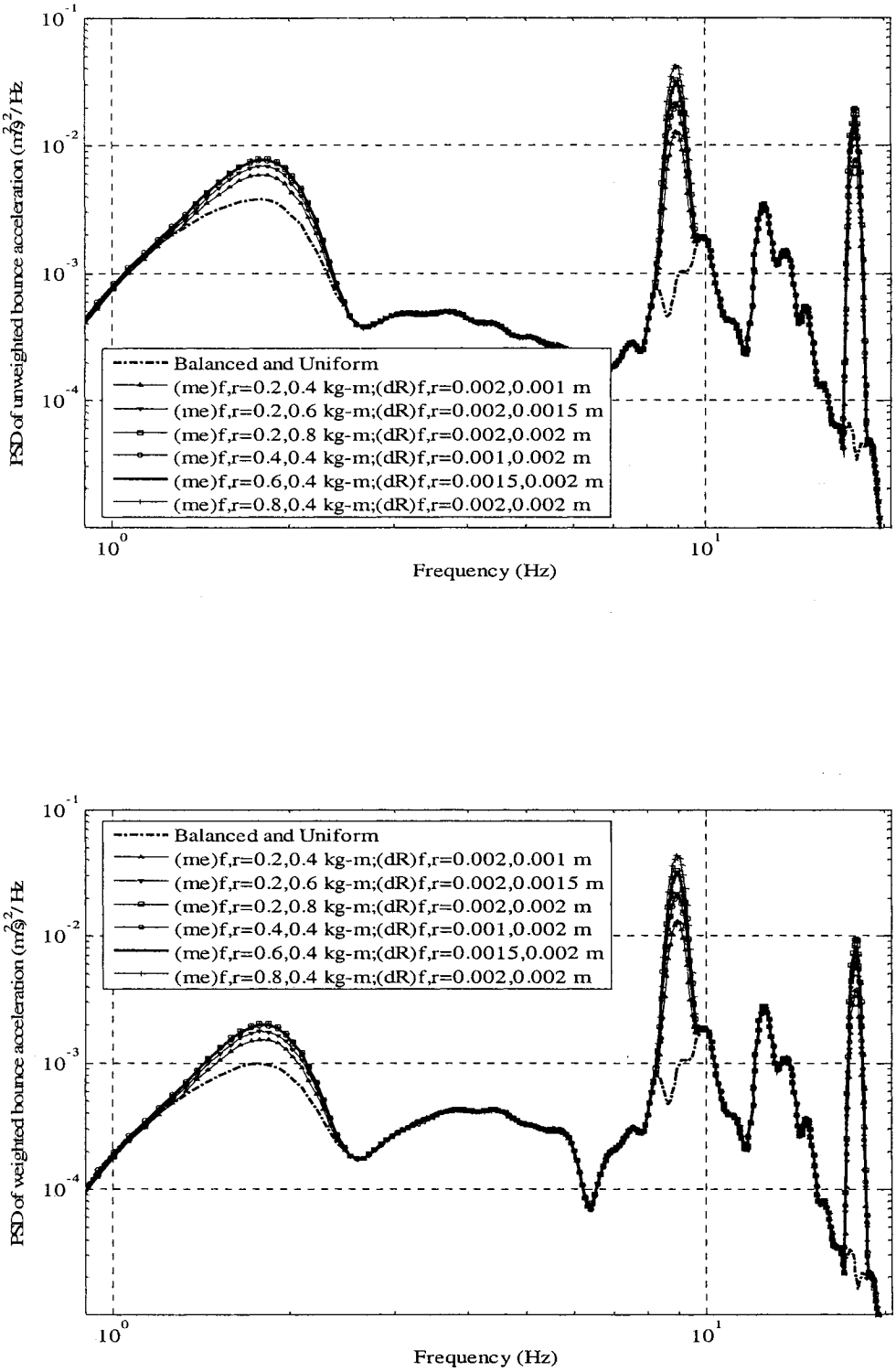

Figure 4.63: Effect of wheel unbalance and non-uniformity on PSD of unweighted and weighted bounce acceleration at 100 km/h (Smooth road)

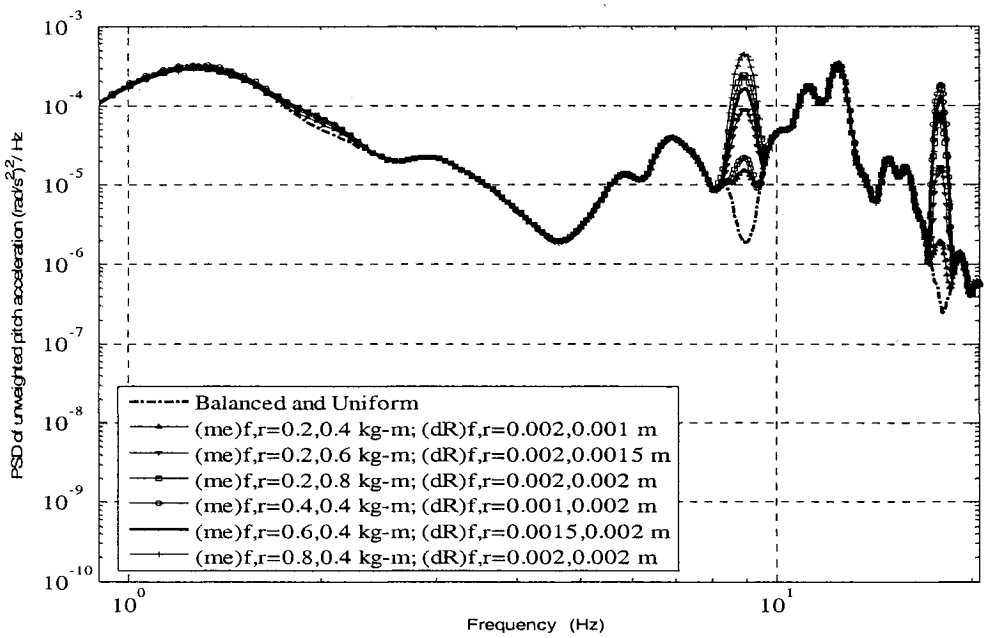

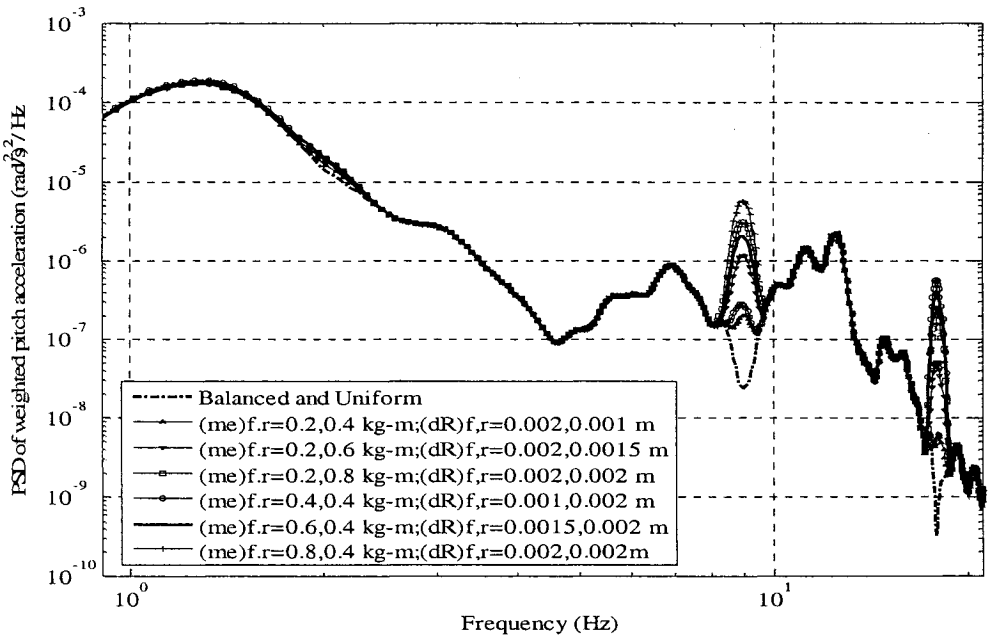

Figure 4.64: Effect of wheel unbalance and non-uniformity on PSD of unweighted and weighted pitch acceleration at 100 km/h (Smooth road)

The peak magnitudes corresponding to wheel unbalance frequency in the vertical and pitch acceleration responses shift towards higher values with increasing forward speed. The wheel unbalance and non-uniformity do not significantly affect the vibration responses in the frequency range of sprung mass resonance except for the vertical acceleration response at 100 km/h. The presence of wheel unbalance causes peaks near 7.1 Hz and 8.8 Hz, while non-uniformity causes peaks near 14.2 Hz and 17.8 Hz, respectively, at speeds of 80 and 100 km/h. The magnitudes of peaks at these predominant frequencies in the vertical and pitch acceleration spectra, however, increase with increasing non-uniformity. The results further show that the peak magnitudes of frequency weighted vertical acceleration PSD are almost unaffected at all speeds. This phenomenon can be attributed to the characteristics of the W_k-weighting filter, while the application of W_e-filter considerably attenuates the peaks in the weighted pitch acceleration response. The weighted pitch acceleration responses thus do not show significant effects of the wheel unbalance and non-uniformity (Figure 4.58).

Figure 4.65 illustrates the PSD of the front and rear tire forces as a function of the magnitudes of wheel unbalance and nonuniformities, while the speed is 60 km/h. The PSD for the front tire force shows the peak magnitude corresponding to $(me)_{f,r} = 0.8$, 0.4 kg-m and $(\Delta r)_{f,r} = 0.002$, 0.002 m combination, while for the rear axle, the response peaks for $(me)_{f,r} = 0.2$, 0.8 kg-m and $(\Delta r)_{f,r} = 0.002$, 0.002 m combination. The force responses also show peaks of considerable magnitude in the vicinity of 5.3 Hz and 10.6 Hz, which are not present when the wheels are balanced and uniform. The peak magnitude tends to increase significantly with increasing unbalance and non-uniformity, which contributes to relatively higher DLC as evident in Figure 4.56. The strong influence of operating speed

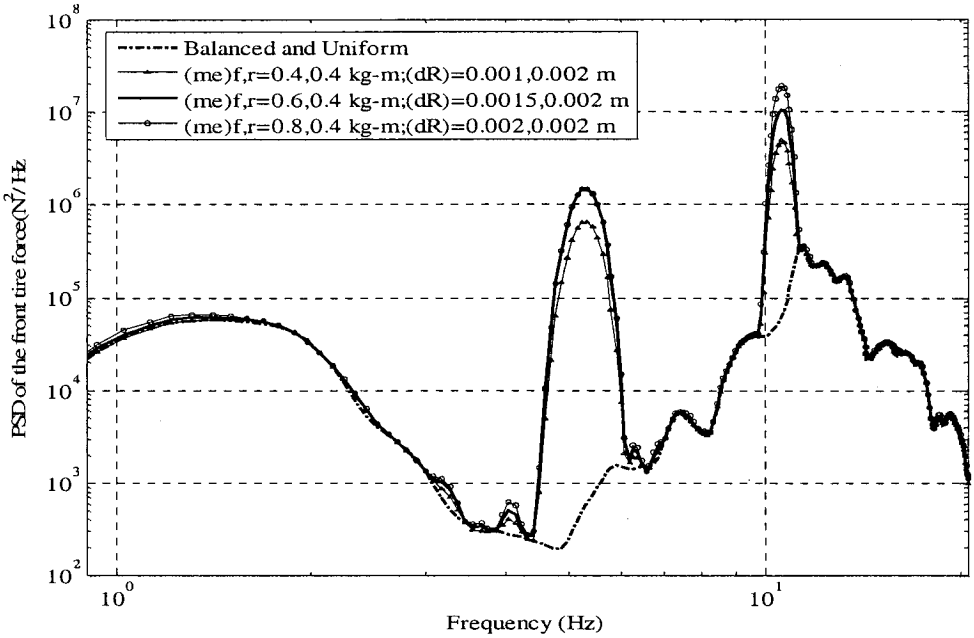

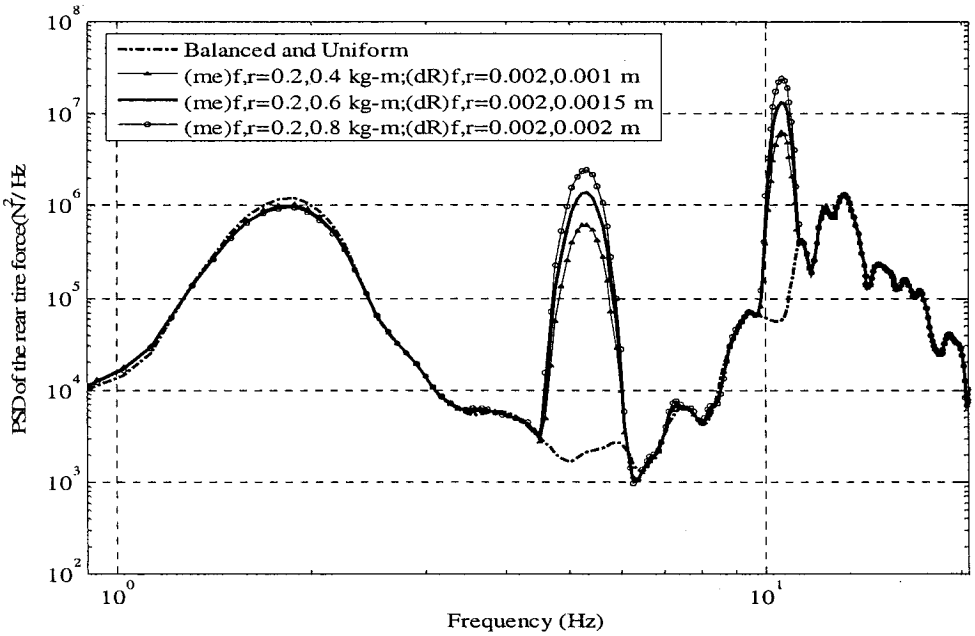

Figure 4.65: Effect of wheel unbalance and non-uniformity on PSD of the rear tire forces at 60 km/h (Smooth road)

on the corresponding predominant frequencies is evident in the tire force responses presented in Figures 4.66 and 4.67, respectively, for forward speeds of 80 and 100 km/h. The magnitudes of the peaks corresponding to wheel non-uniformity show little variation with increasing speed while the peaks corresponding to unbalance clearly shift towards higher values with increasing speed. The results further show the dominance of wheel non-uniformity peaks as compared to wheel unbalance peaks in the tire forces at speeds of 60 and 80 km/h, while opposite trend is observed for the speed of 100 km/h (Figure 4.56).

4.4.2 INFLUENCE OF ROAD ROUGHNESS

The significance of the coupled effects of wheel unbalance and non-uniformity on both the ride and tire load responses is evident from the results presented in the preceding section, when the vehicle operates on a smooth road. The relative significance of tire forces and accelerations responses may be small when the vehicle interacts with a rough road surface. The relative contributions of the coupled wheel unbalance and non-uniformity are thus investigated under excitations arising from the medium-rough and rough roads, as described in Chapter 3. The analyses are limited to a single forward speed of 80 km/h, while the results are presented in terms of dynamic tire loads and vertical and pitch accelerations (weighted and unweighted). Moreover, the magnitudes of unbalance and non-uniformity combinations considered are identical to those considered in the preceding section.

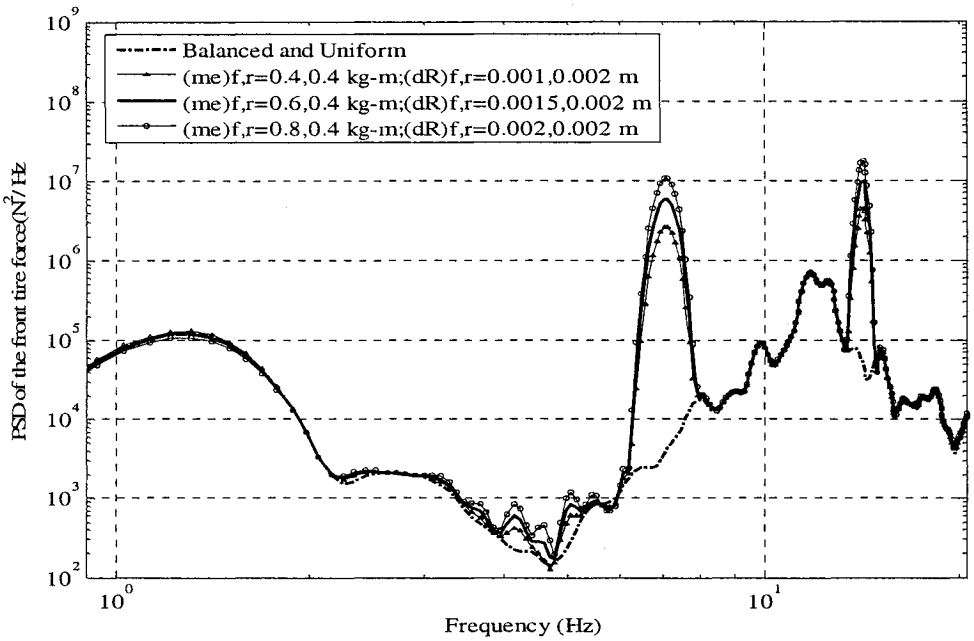

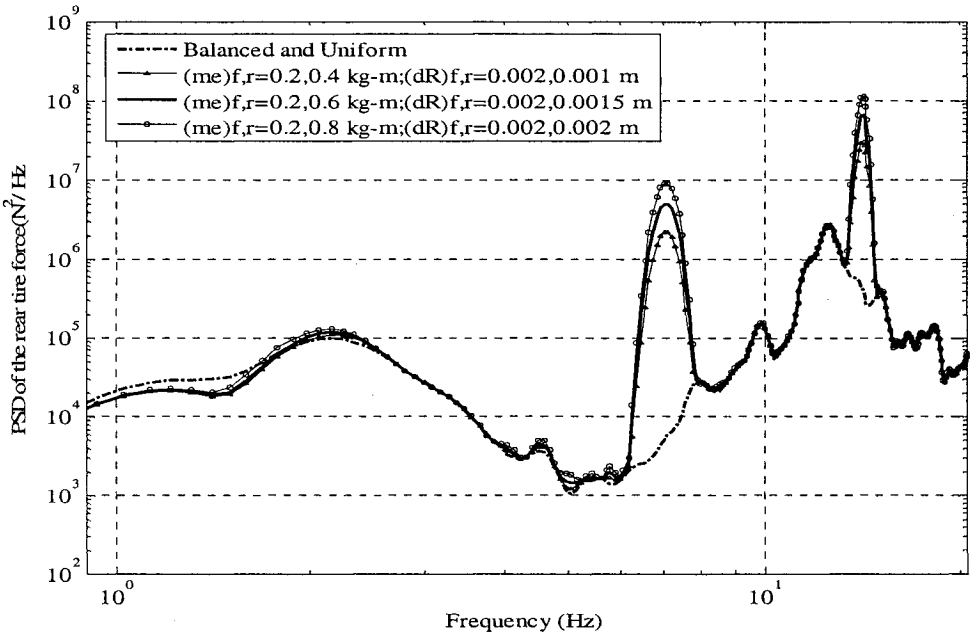

Figure 4.66: Effect of wheel unbalance and non-uniformity on PSD of the front and rear tire forces at 80 km/h (Smooth road)

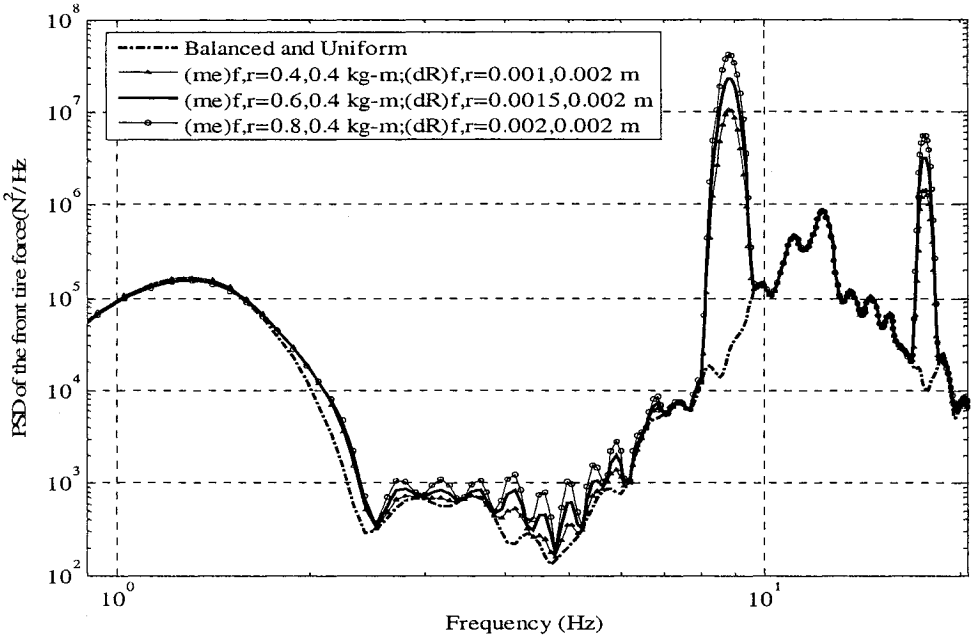

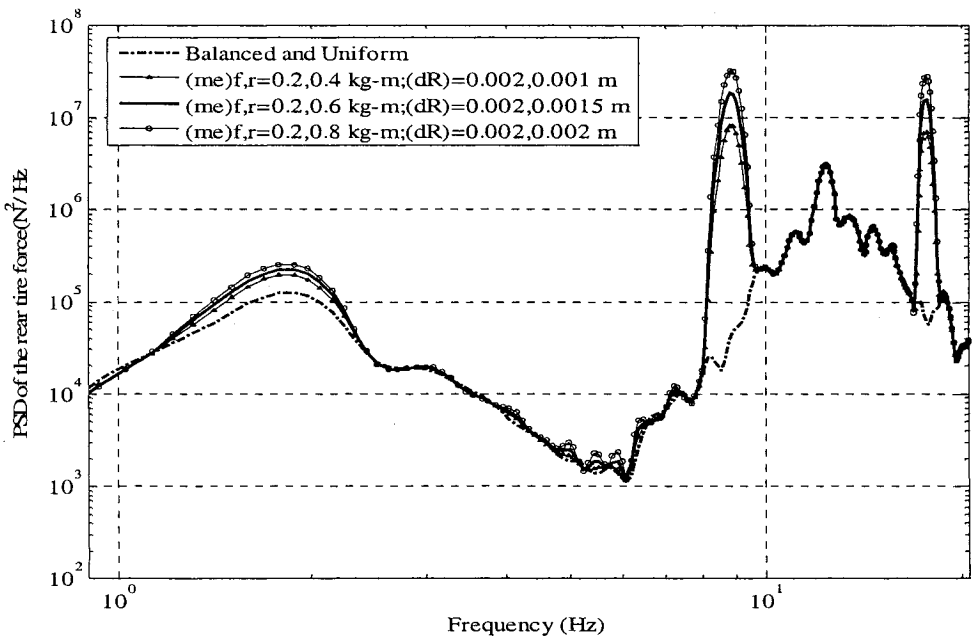

Figure 4.67: Effect of wheel unbalance and non-uniformity on PSD of the front and rear tire forces at 100 km/h (Smooth road)

Figures 4.68 to 4.70 illustrate the influence of three different road roughness types on the performance measures in terms of DLC due to front and rear axle tire forces, and unweighted and frequency-weighted overall vertical and pitch rms accelerations, respectively. It is observed that an increase in the magnitudes of the unbalance and non-uniformity of the front or the rear wheels yields considerably larger increase in the DLC of both axle tires, when the vehicle is operating on a smooth road. The relative change in the DLC due to increasing unbalance and non-uniformity, however, diminishes under medium-rough and rough road operations, as evident in Figure 4.68. The results, therefore, suggest that the combined effects of wheel unbalance and non-uniformity are more pronounced, when the contribution due to tire-road interactions are relatively small. Similar trends are also evident in the weighted and unweighted overall rms vertical and pitch acceleration responses (Figures 4.69 and 4.70). It can also be noted that the weighted pitch acceleration values are considerably lower than the unweighted values, especially for the medium-rough and rough road operations, while the weighted bounce acceleration values are either close to or slightly lower than their respective unweighted values. This can be attributed to the predominant effect of wheel unbalance and non-uniformity on the vertical vibration in the 5-19 Hz frequency range, where the amplitude ratio of the W_k-weighting filter is appreciable. The pitch vibration responses in this frequency range are mostly attenuated by the W_e-filter.

From the results presented above, it is apparent that there is considerable increase in all performance measures with increase in non-uniformity for the smooth road. The percentage increment for all performance measures reduces with increase in road

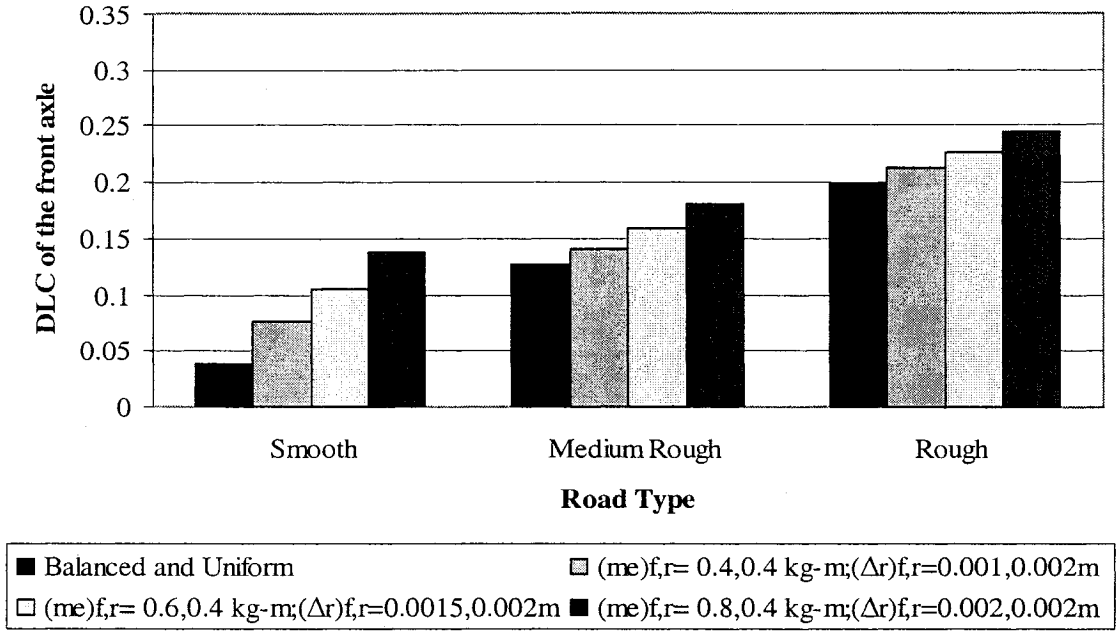

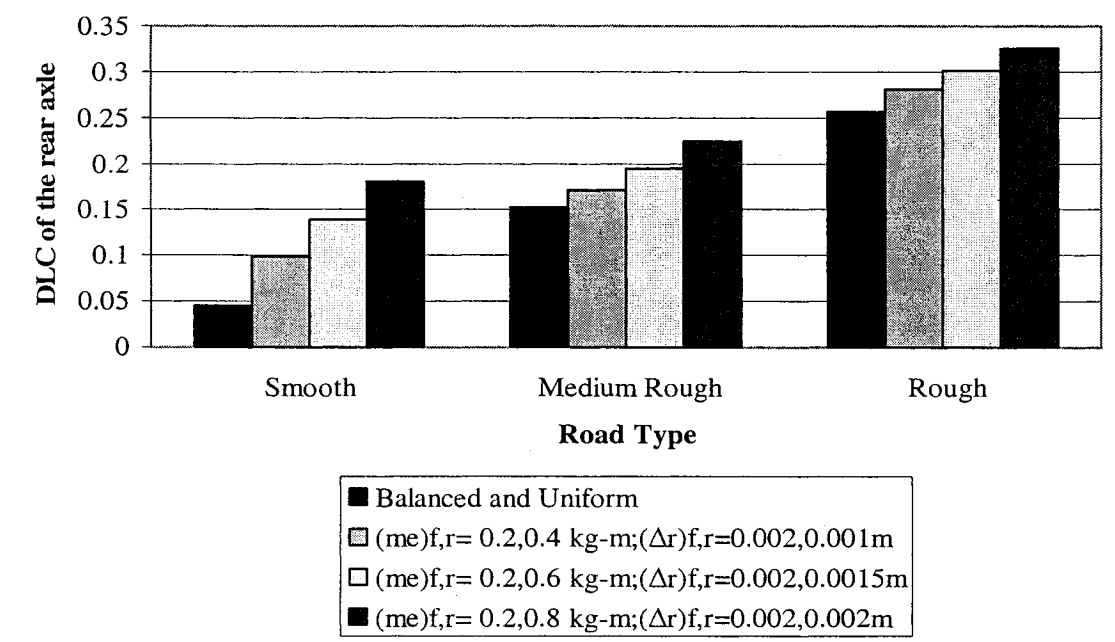

Figure 4.68: Influence of road roughness on DLC values for the front and rear axle at 80 km/h with wheel unbalance and non-uniformity

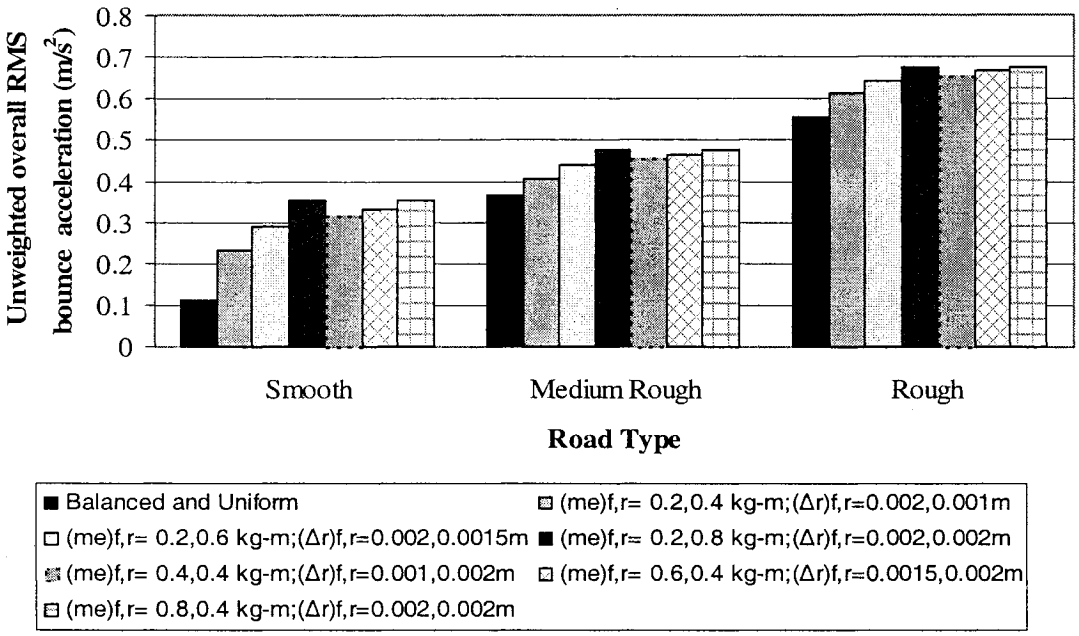

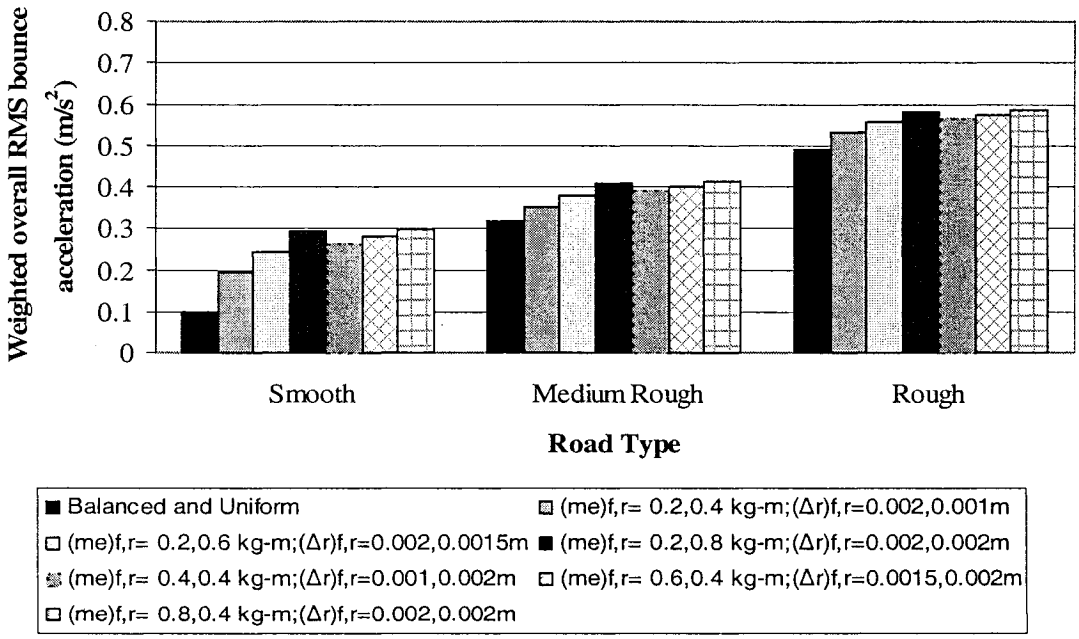

Figure 4.69: Influence of road roughness on overall unweighted and weighted rms bounce acceleration values at 80 km/h with wheel unbalance and non-uniformity

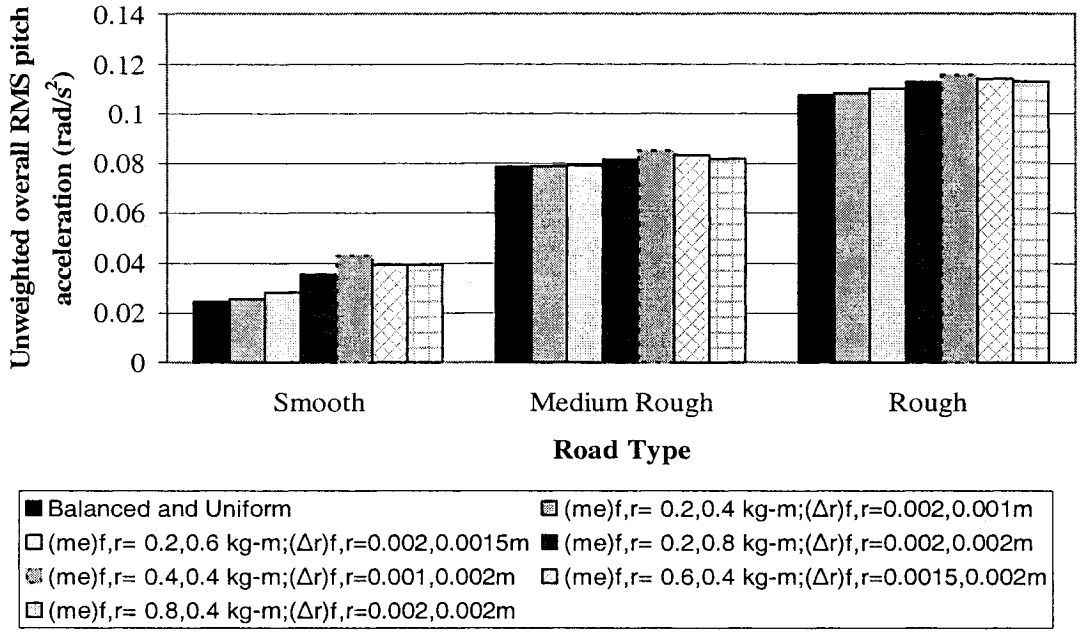

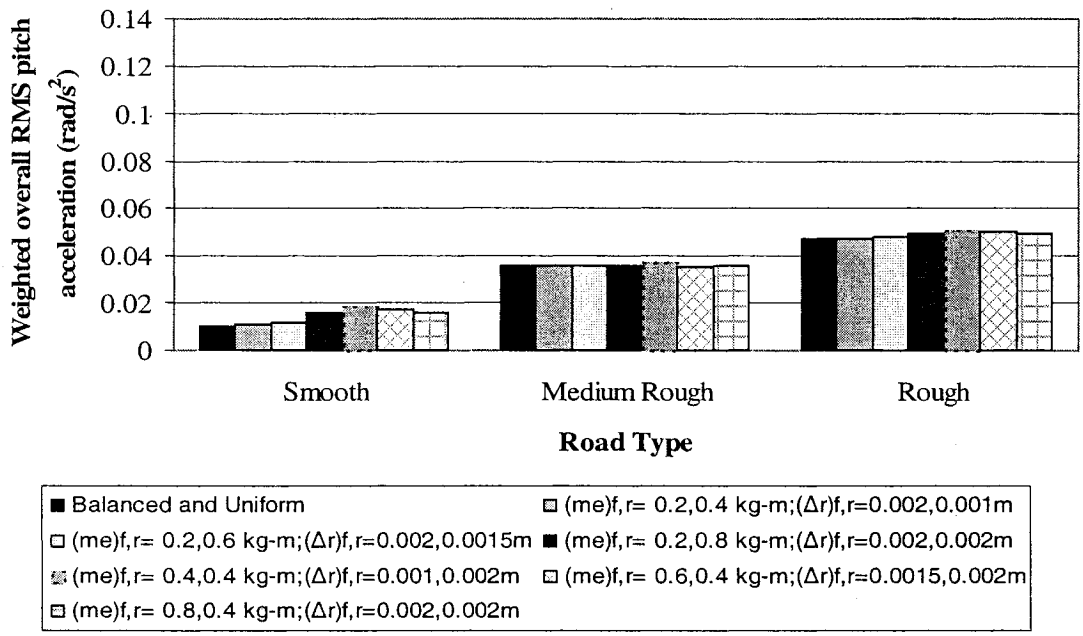

Figure 4.70: Influence of road roughness on overall unweighted and weighted rms pitch acceleration values at 80 km/h with wheel unbalance and non-uniformity

roughness. This can be attributed to the increasing contribution from the road with increase in roughness. The non-uniformity and unbalance combination of $(me)_{f,r}$ = 0.2, 0.8 kg-m and $(\Delta r)_{f,r}$ = 0.002, 0.002 m yields the maximum values of performance measures for vertical acceleration and DLC of the rear axle, while $(me)_{f,r}$ = 0.8, 0.4 kg-m and $(\Delta r)_{f,r}$ = 0.003, 0.002 m combination yields the maximum values for the DLC of the front axle tire, for all road types. The maximum values of performance measure related to pitch acceleration are observed for $(me)_{f,r}$ = 0.4, 0.4 kg-m and $(\Delta r)_{f,r}$ = 0.001, 0.002 m combination. With varying magnitudes of unbalance and non-uniformity, the changes in weighted bounce and unweighted pitch acceleration values are very small, especially for medium-rough and rough road conditions.

Figures 4.71 to 4.76 clearly exhibit the higher diminishing effects of the wheel non-uniformity than wheel unbalance with increasing road roughness in the bounce and pitch accelerations, and tire force spectra. The PSD of front and rear tire forces under vehicle's interactions with the medium-rough and rough roads, are presented in Figures 4.71 and 4.72, respectively. The results show that the wheel nonuniformities yield significant peak responses near 14.2 Hz, while unbalance near 7.1 Hz, irrespective of the road roughness. The magnitudes of the peaks relative to the responses of the baseline vehicle, however, are considerably smaller than those observed for the smooth road in Figure 4.66. The peak magnitudes of the rear tire forces in the vicinity of the sprung mass resonance under rough road operation vary slightly with varying magnitudes of unbalance and non-uniformity. The ratios of the peak response with and without unbalance and non-uniformity, observed near predominant frequencies are slightly higher as compared to those observed while considering the separate effects of unbalance and

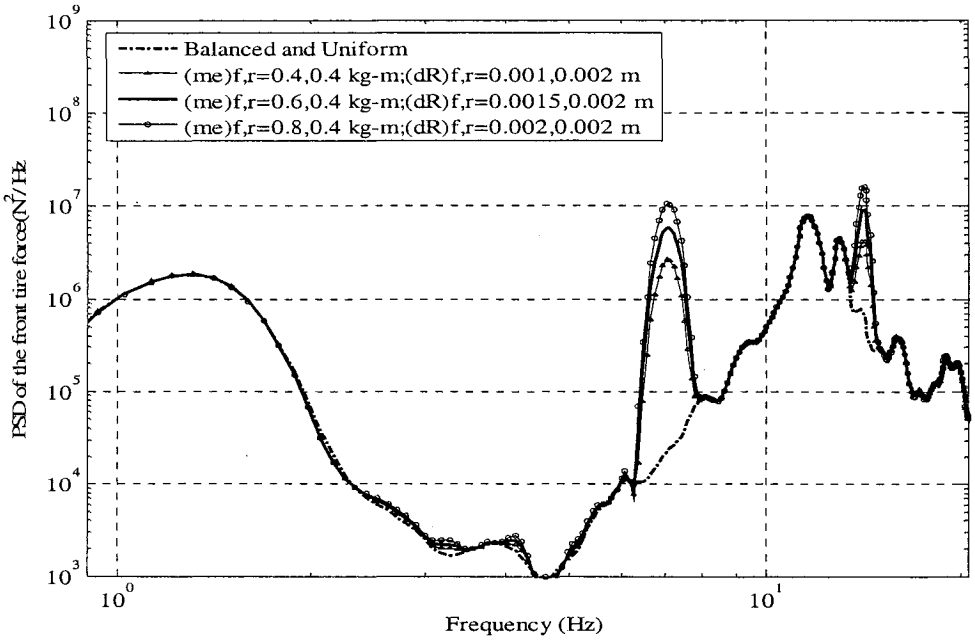

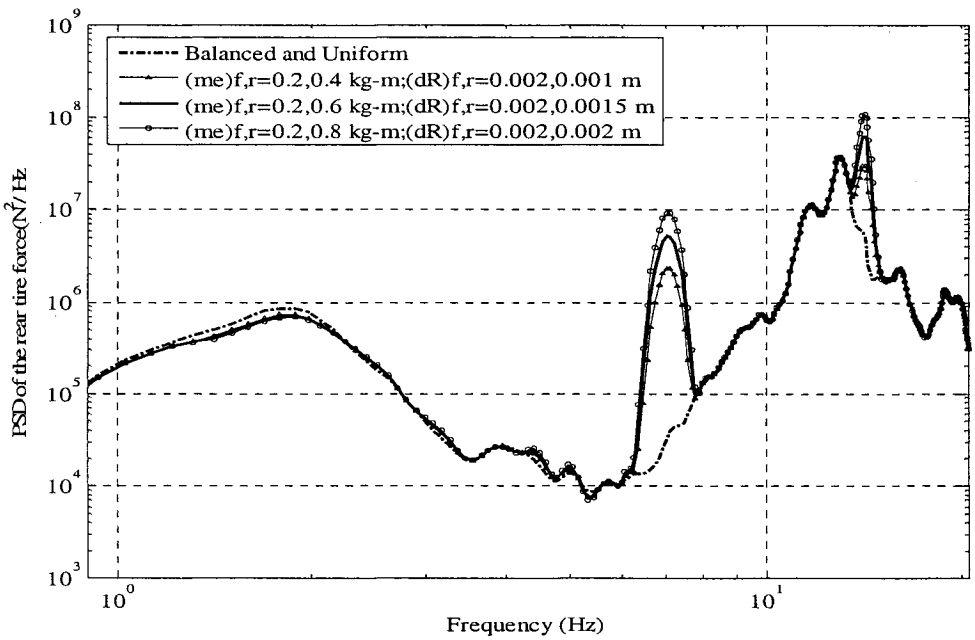

Figure 4.71: Effect of wheel unbalance and non-uniformity on PSD of the front and rear tire forces at 80 km/h (Medium-rough road)

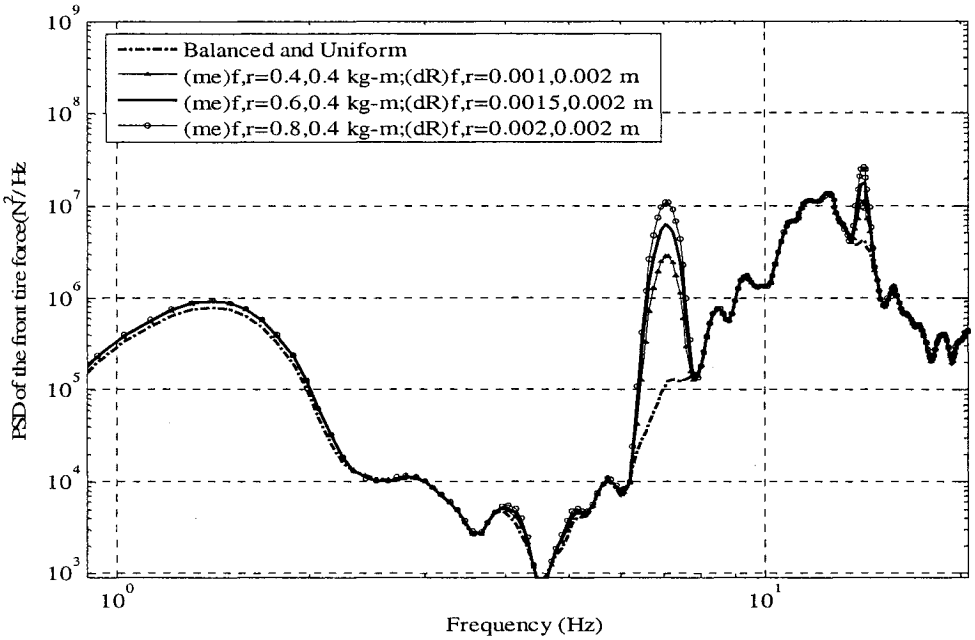

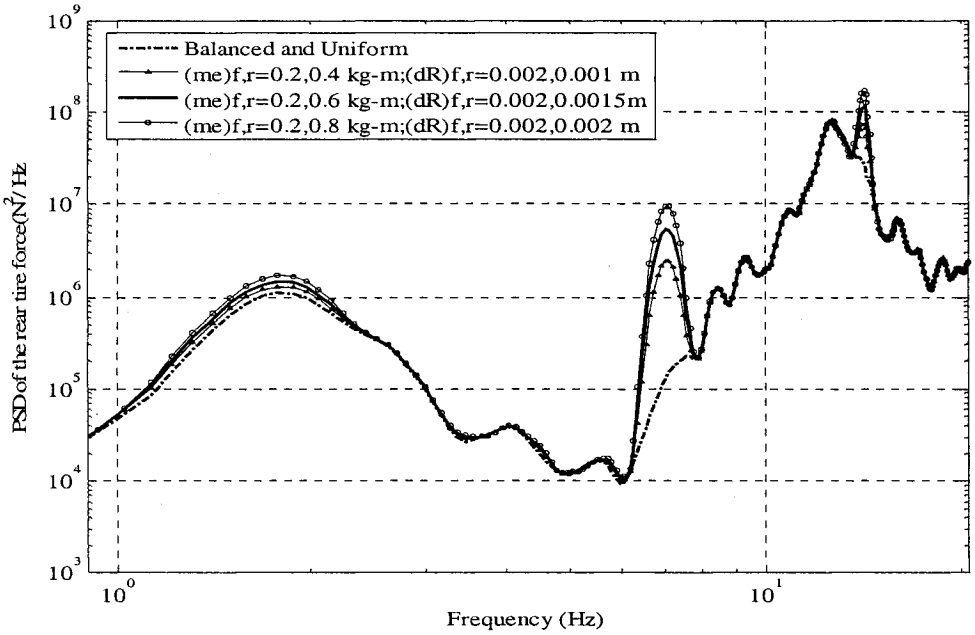

Figure 4.72: Effect of wheel unbalance and non-uniformity on PSD of the front and rear tire forces at 80 km/h (Rough road)

non-uniformity. These results clearly show that the wheel unbalance and non-uniformity yield most notable effects on the tire forces, when vehicle operations on smooth road are considered.

The vertical and pitch acceleration responses of the vehicle sprung mass tend to increase with increasing road roughness in majority of the frequency range considered, as evident in Figures 4.73 to 4.76. While both wheel unbalance and non-uniformity induce larger responses near 7.1 and 14.2 Hz, respectively, the relative increase in the acceleration PSD diminishes with increasing road roughness. The insignificant effect of combination of wheel unbalance and non-uniformity on the vertical acceleration response is clearly evident under rough road excitation (Figure 4.74). Moreover, the application of frequency-weighting tends to further reduce the effect of wheel unbalance and non-uniformity on the pitch acceleration PSD response of the vehicle under rough road excitations, as evident in Figure 4.76. The peak magnitudes of the bounce acceleration (unweighted and weighted) exhibit a significant variation with increasing unbalance and non-uniformity in the vicinity of sprung mass resonance, under rough road condition, resulting in higher overall bounce rms acceleration values, as evident from Figure 4.69.

4.4.3 INFLUENCE OF PHASE

The influence of phase differences in the front and rear wheel unbalance and runouts on the performance measures are further investigated for a forward speed of 80 km/h and smooth road excitations. The analyses are performed for $0°, 45°$ and $90°$ phase angle in both the self exciting sources and two magnitudes of non-uniformity and unbalance combinations: $(me)_{f,r} = 0.2, 0.4$ kg-m and $(\Delta r)_{f,r} = 0.002, 0.001m$; and $(me)_{f,r} = 0.8,$

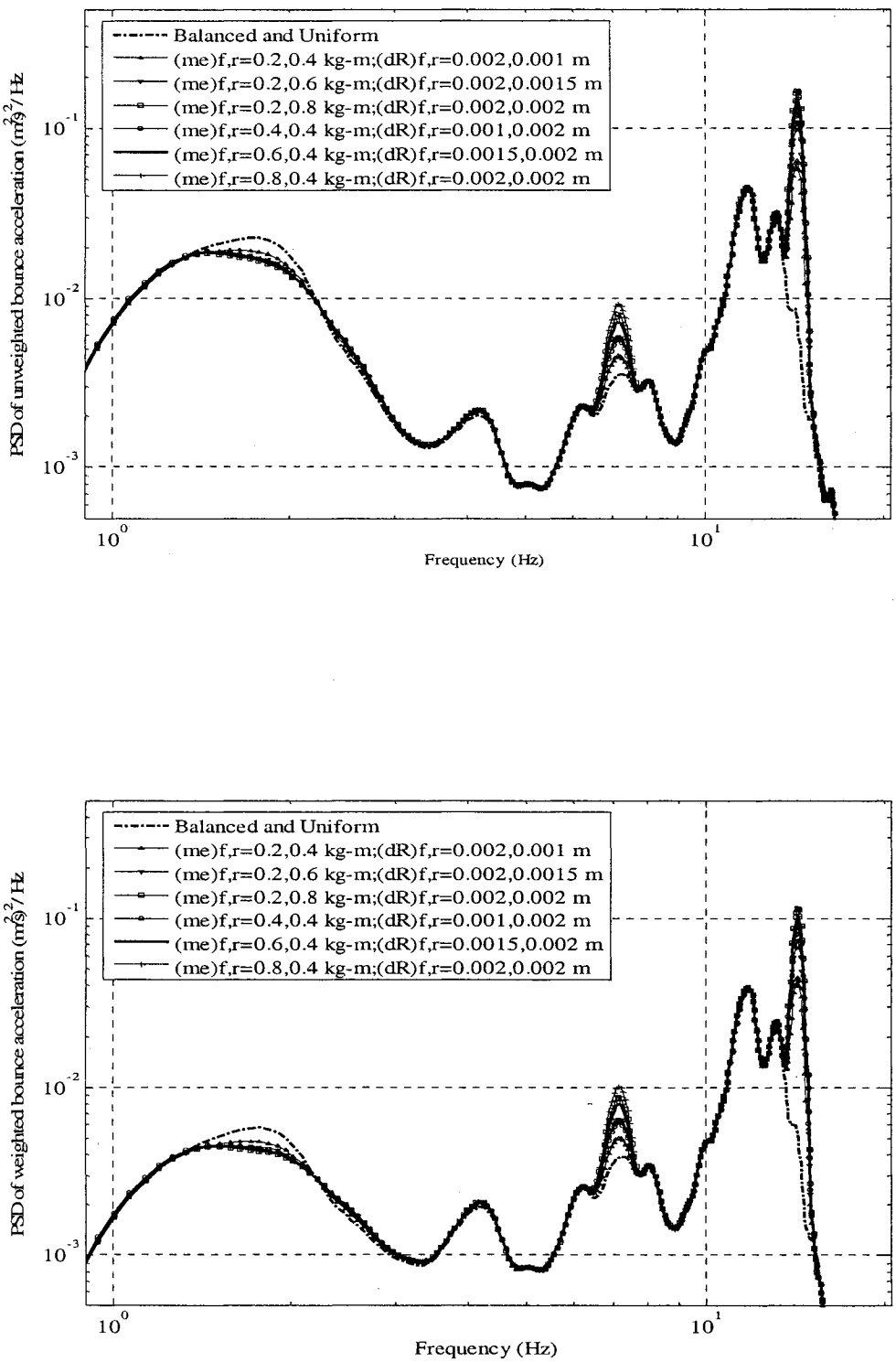

Figure 4.73: Effect of wheel unbalance and non-uniformity on PSD of unweighted and weighted bounce acceleration at 80 km/h (Medium-rough road)

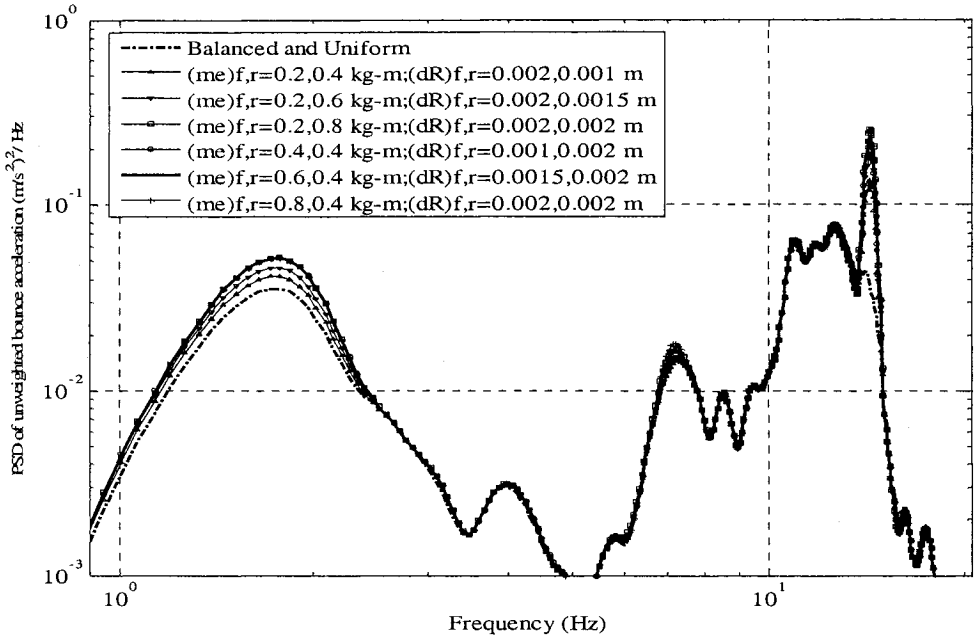

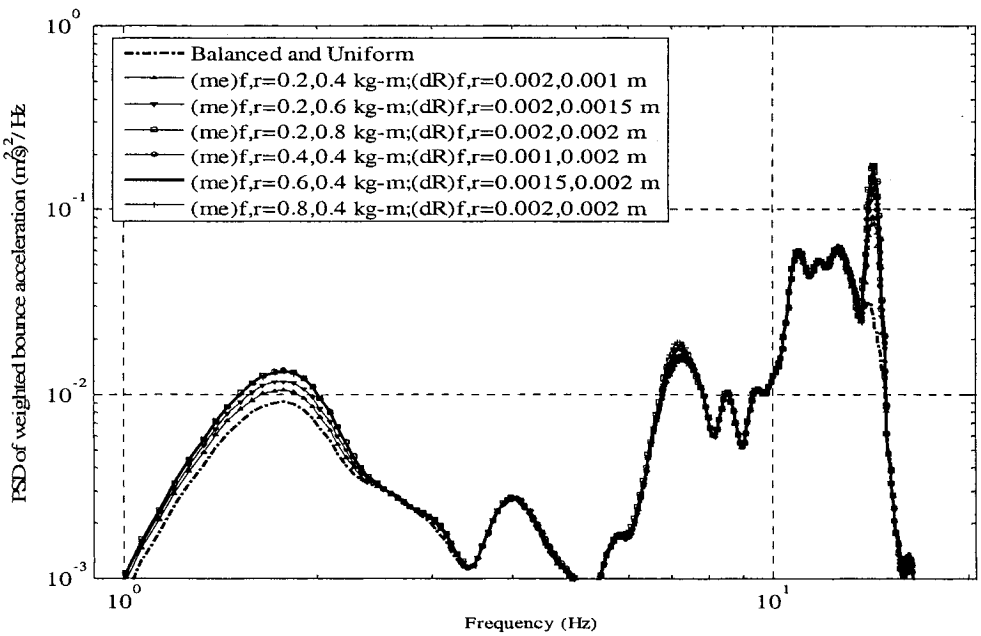

Figure 4.74: Effect of wheel unbalance and non-uniformity on PSD of unweighted and weighted bounce acceleration at 80 km/h (Rough road)

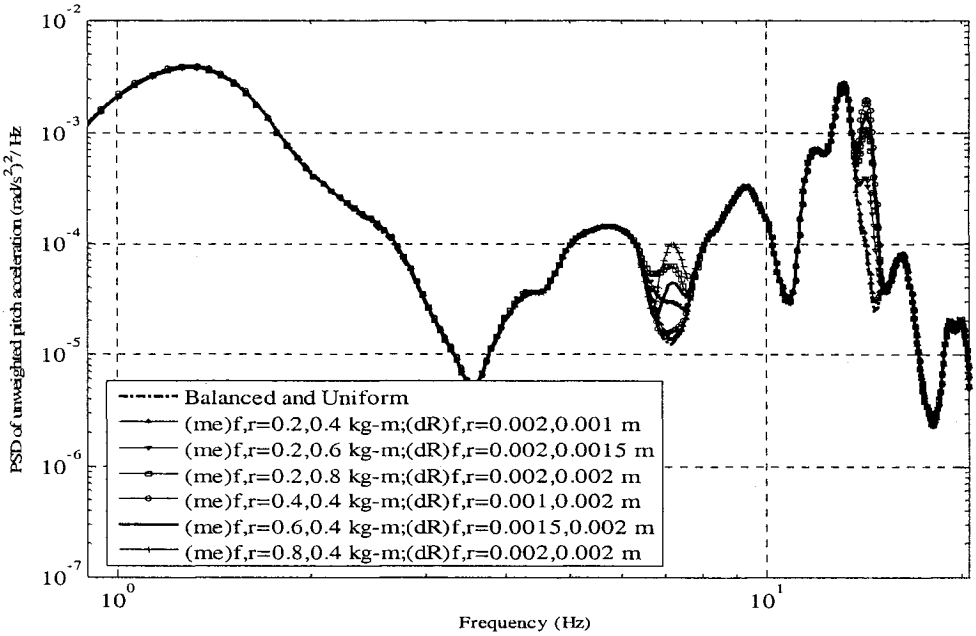

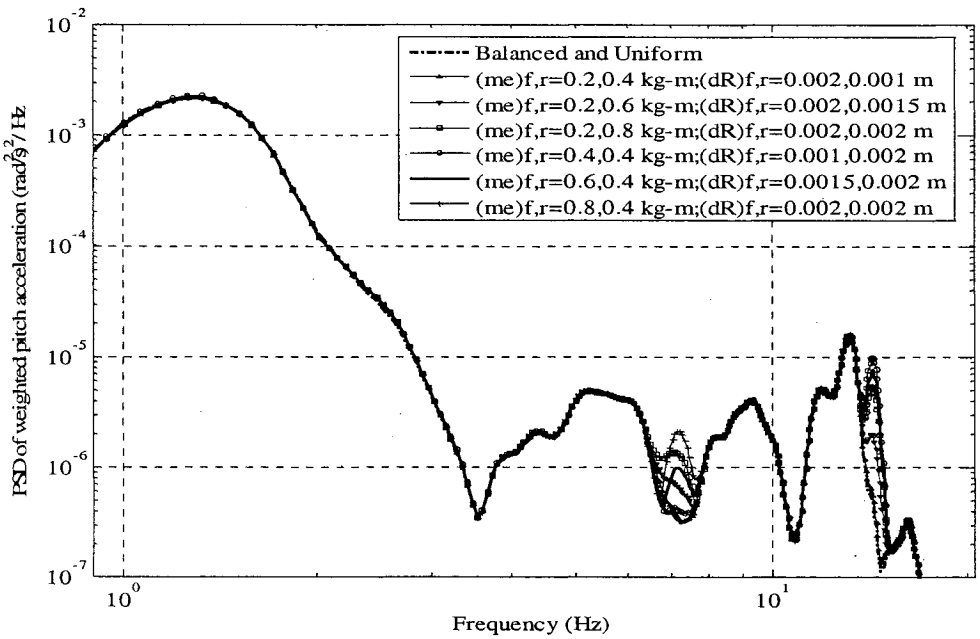

Figure 4.75: Effect of wheel unbalance and non-uniformity on PSD of unweighted and weighted pitch acceleration at 80 km/h (Medium-rough road)

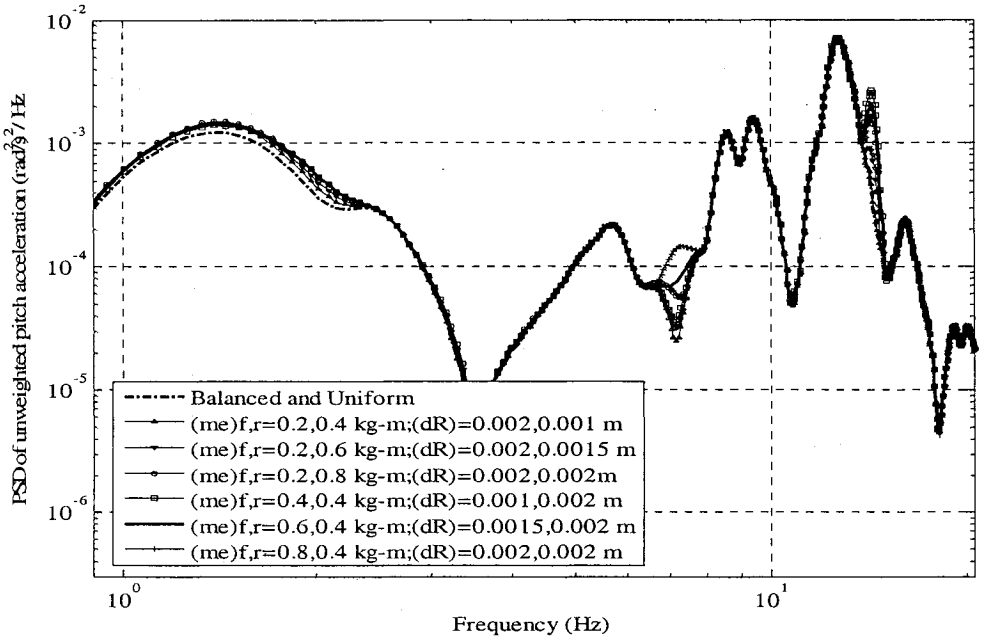

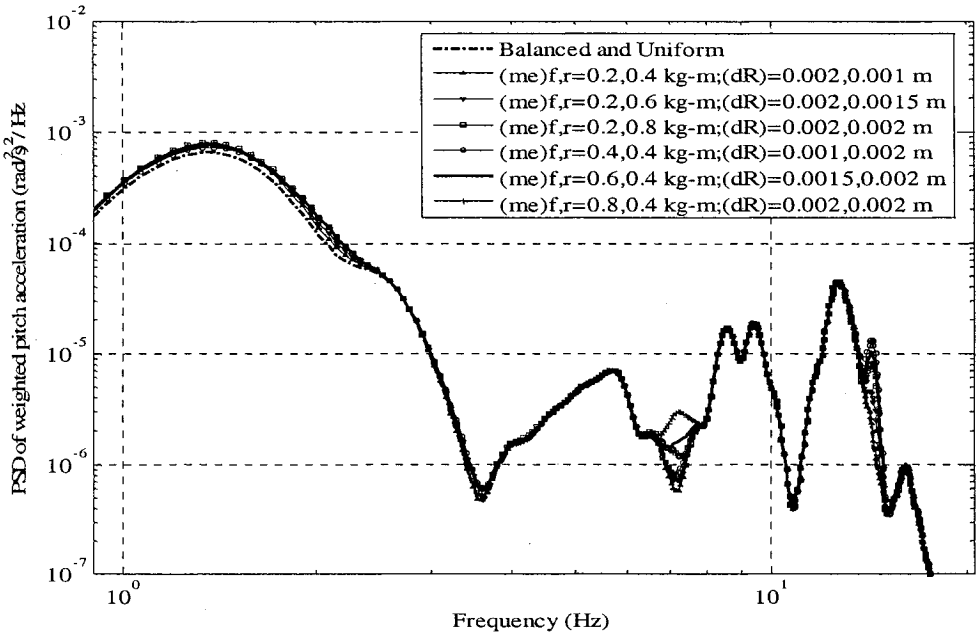

Figure 4.76: Effect of wheel unbalance and non-uniformity on PSD of unweighted and weighted pitch acceleration at 80 km/h (Rough road)

0.4 kg-m and $(\Delta r)_{f,r} = 0.002, 0.002\,m$. Figures 4.77 and 4.78 show the influence of phase differences on the unweighted and frequency-weighted vertical and pitch accelerations, respectively, for both sets of wheel unbalance and non-uniformity considered. The results show that the unweighted and weighted bounce rms accelerations decrease considerably with increasing phase difference angle between the front and rear wheels unbalance and run-out, while the corresponding pitch acceleration increase, as observed under uncoupled effects. The weighted bounce rms acceleration values are observed to be close to their unweighted values which can be attributed to the magnitude ratios of the W_k-weighting filter in the predominant frequency range of 7-14 Hz. The unweighted pitch acceleration values increase significantly with increasing phase angle, while the weighted values exhibit only small change with increasing phase angle.

4.5 VARIATIONS IN TIRE-TERRAIN CONTACT PATCH

The tire-terrain interaction is modeled using an adaptive foot-print tire model, as discussed in Chapter 2. The radial contact between tire and terrain renders a contact patch, which changes its orientation with the wheel center at each time instant. The change in contact patch at a given speed is mostly influenced by the terrain roughness, inflation pressure, load and the vehicle responses if the wheel is balanced and uniform. The tire-terrain contact patch can also vary with the mass unbalance and wheel non-uniformity. The effects of mass unbalance, wheel run-out and the combinations of the two on the contact patch are investigated under excitations arising from the smooth road to ensure the minimal contribution due to road roughness, while the speed of 100 km/h is used.

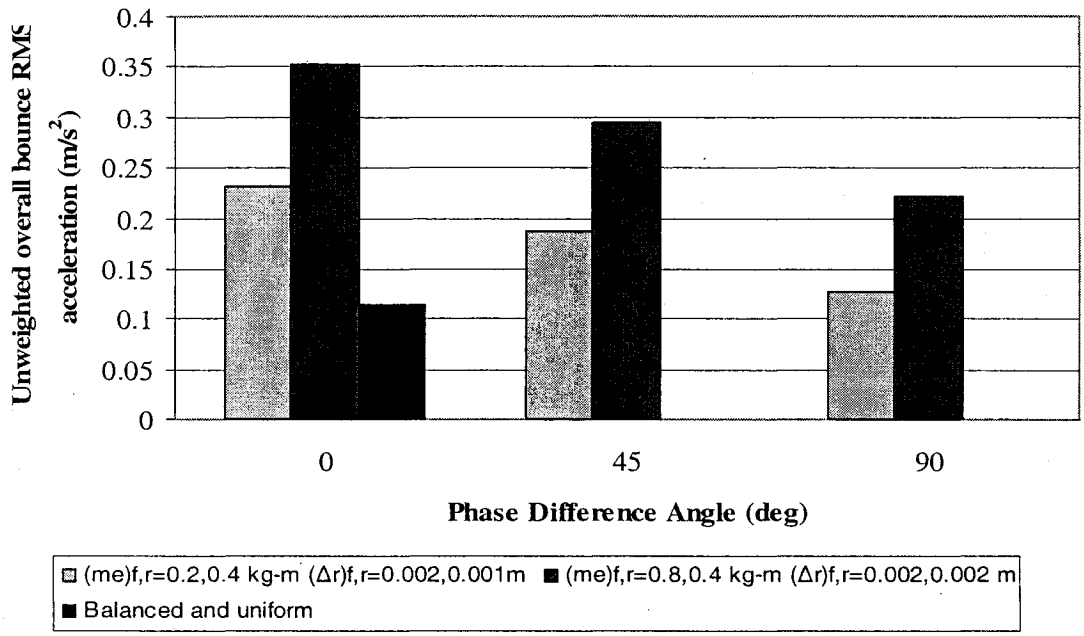

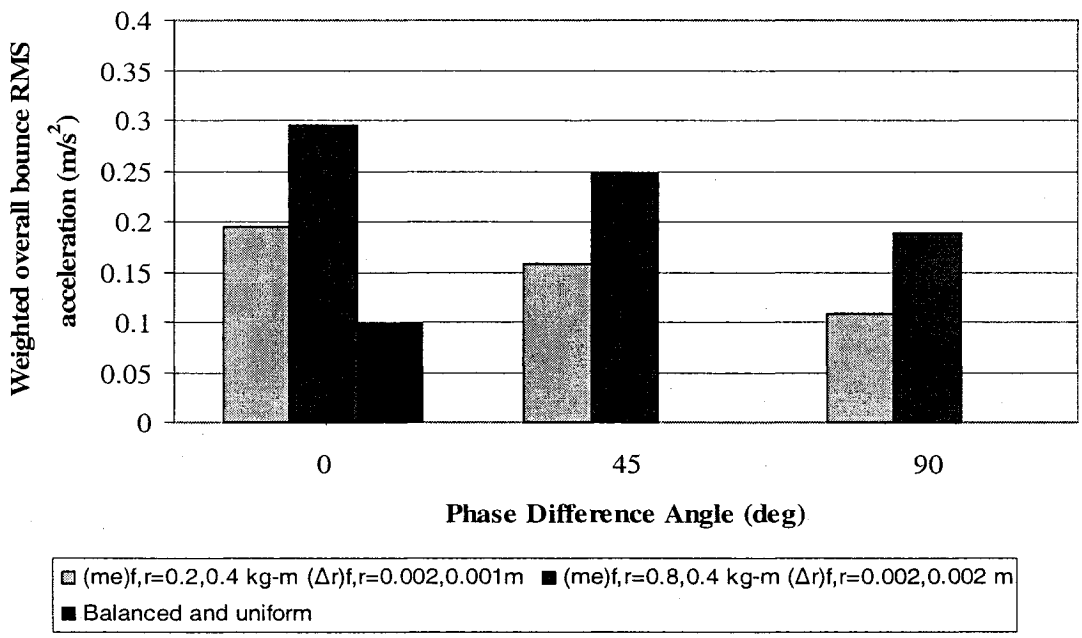

Figure 4.77: Influence of phase on overall unweighted and weighted rms bounce acceleration at 80 km/h with wheel unbalance and non-uniformity (Smooth road)

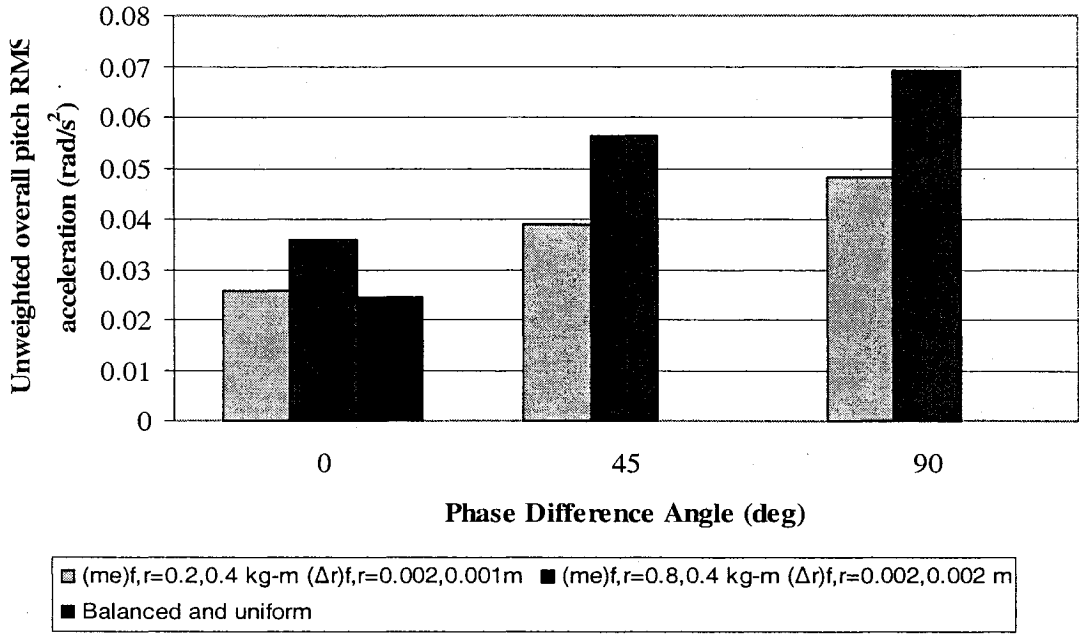

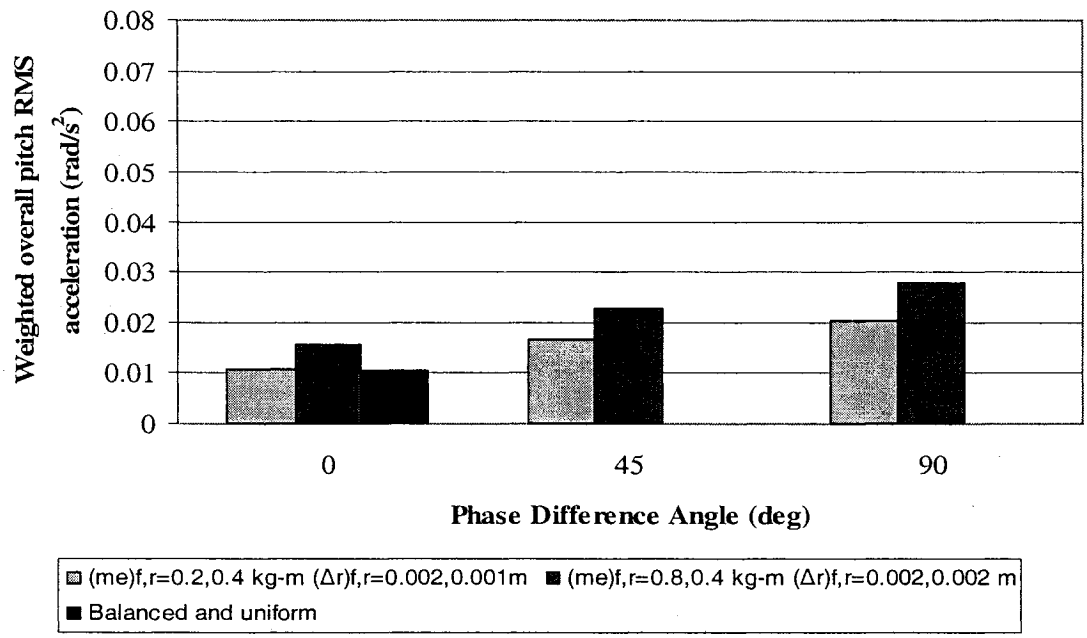

Figure 4.78: Influence of phase on overall unweighted and weighted rms pitch acceleration at 80 km/h with wheel unbalance and non-uniformity (Smooth road)

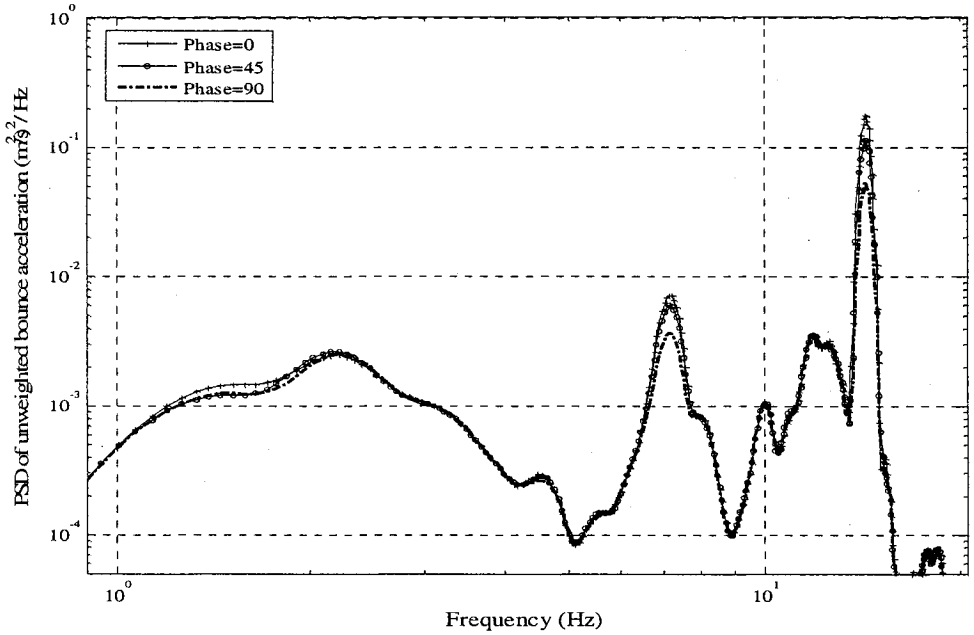

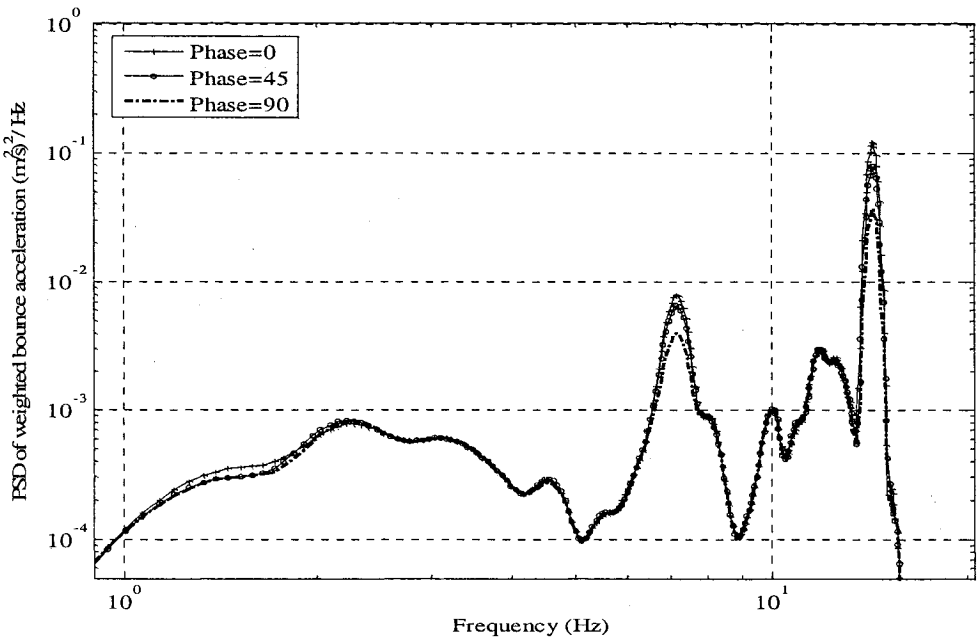

Figure 4.79: Effect of wheel unbalance and non-uniformity on PSD of the unweighted and weighted bounce acceleration with smooth road at 80 km/h (0.8, 0.4 kg-m and 0.002, 0.002 m)

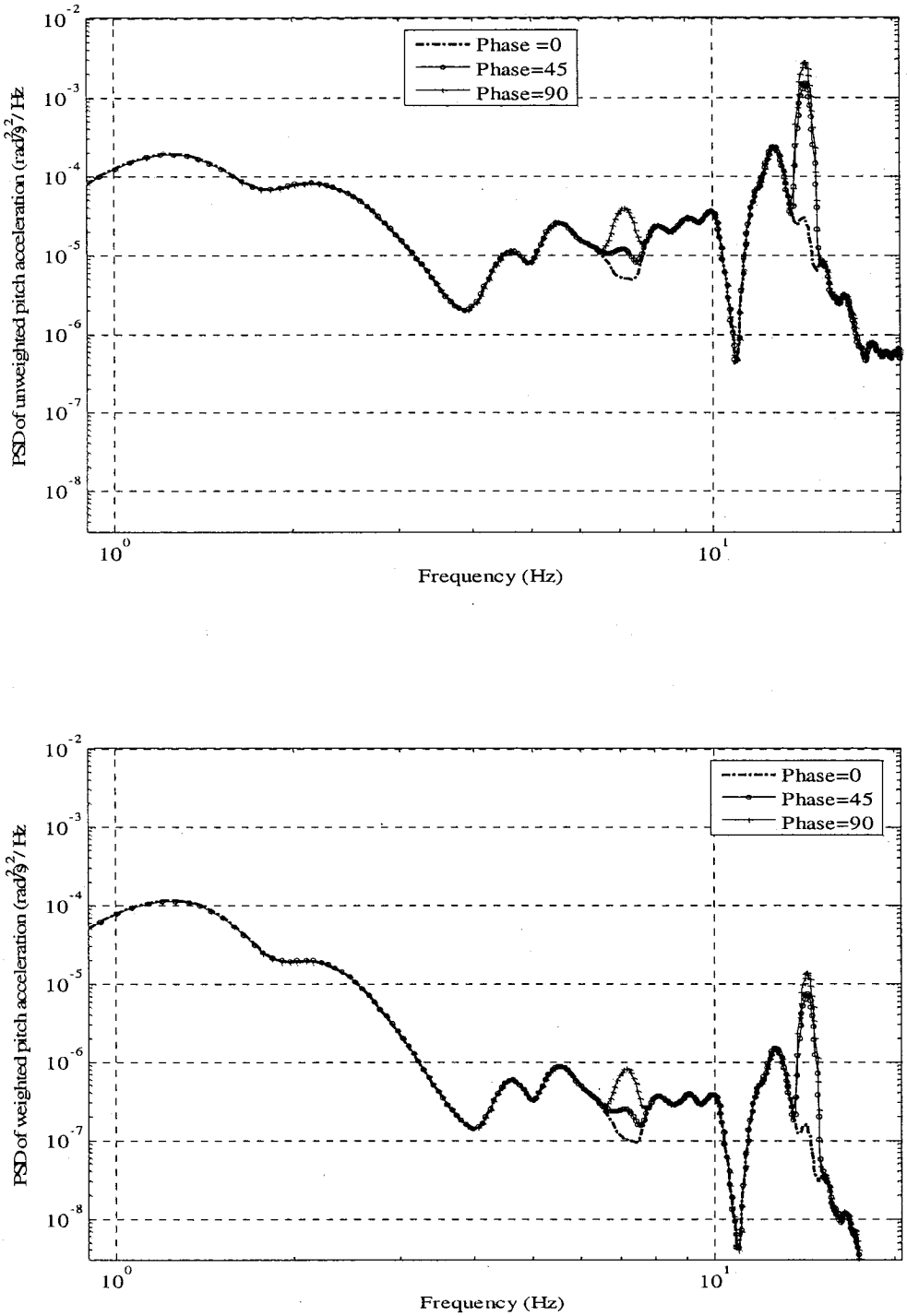

Figure 4.80: Effect of wheel unbalance and non-uniformity on PSD of the unweighted and weighted pitch acceleration with smooth road at 80 km/h (0.2, 0.4 kg-m and 0.002, 0.001 m)

4.5.1 INFLUENCE OF WHEEL UNBALANCE

The changes in the tire-terrain contact patch due to wheel unbalance alone are analyzed for wheel unbalance of $(me)_{f,r}$ = 0.2, 1.2 kg-m, while the eccentricity is considered as 0.4 m. The operation at 100 km/h would yield predominant frequency of excitation near 8.8 Hz. Figure 4.81 illustrates a comparison of variations in the tire-terrain contact patch of a balanced and uniform wheels with those of the unbalanced wheels. The results show considerably larger variations in the wheels contact patches in the presence of mass unbalance. The effect of unbalance is more pronounced in the rear wheel contact patch than the front wheel, which is attributed to the higher degree of mass unbalance of the rear wheel. The peak to peak variations in the contact patch for the front and rear wheels increase with inclusion of the wheel unbalance, which leads to larger variations in the dynamic tire forces and thus increase in DLC and overall rms ride acceleration values.

4.5.2 INFLUENCE OF WHEEL NON-UNIFORMITY

The effect of wheel non-uniformity or radial run-out on the changes in tire-terrain contact patches are also investigated for radial run-out of $(\Delta r)_{f,r}$ =0.002, 0.002 m, and vehicle speed of 100 km/h, while subjected to smooth road excitation. Figure 4.82 illustrates variations in the tire-terrain contact patch for the front and rear wheels with and without radial run-out, while the wheels are balanced in both cases. Figure clearly shows that the contact patches for the front and rear wheel are dominated by the wheel non-uniformity frequency of 17.8 Hz. The peak to peak variations in the contact patches increase significantly when the wheel non-uniformity is present, which would cause higher

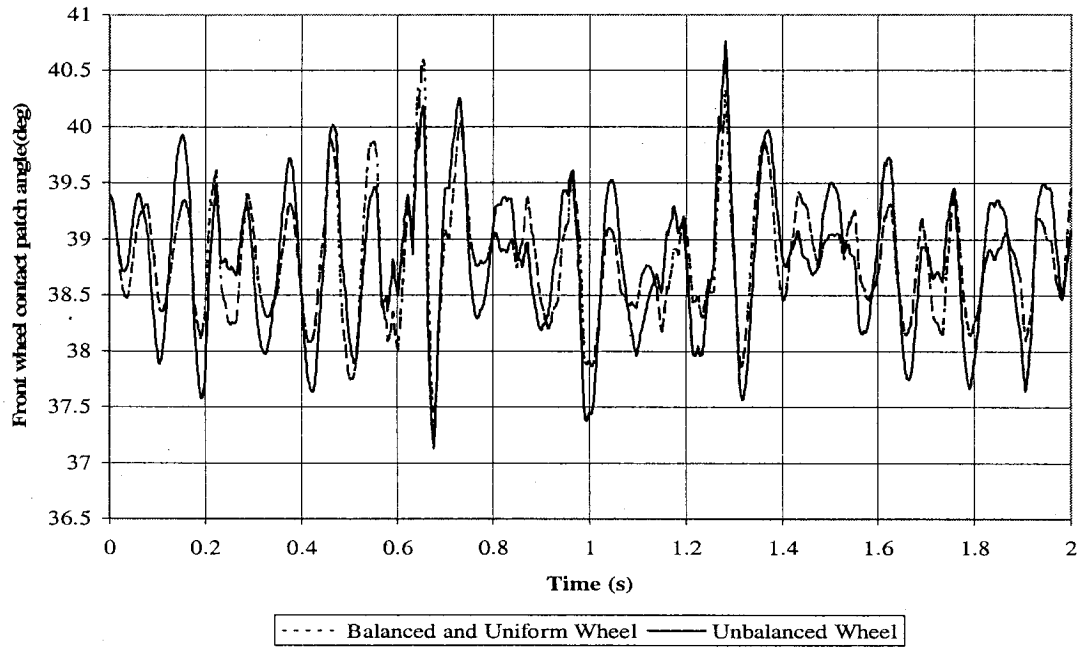

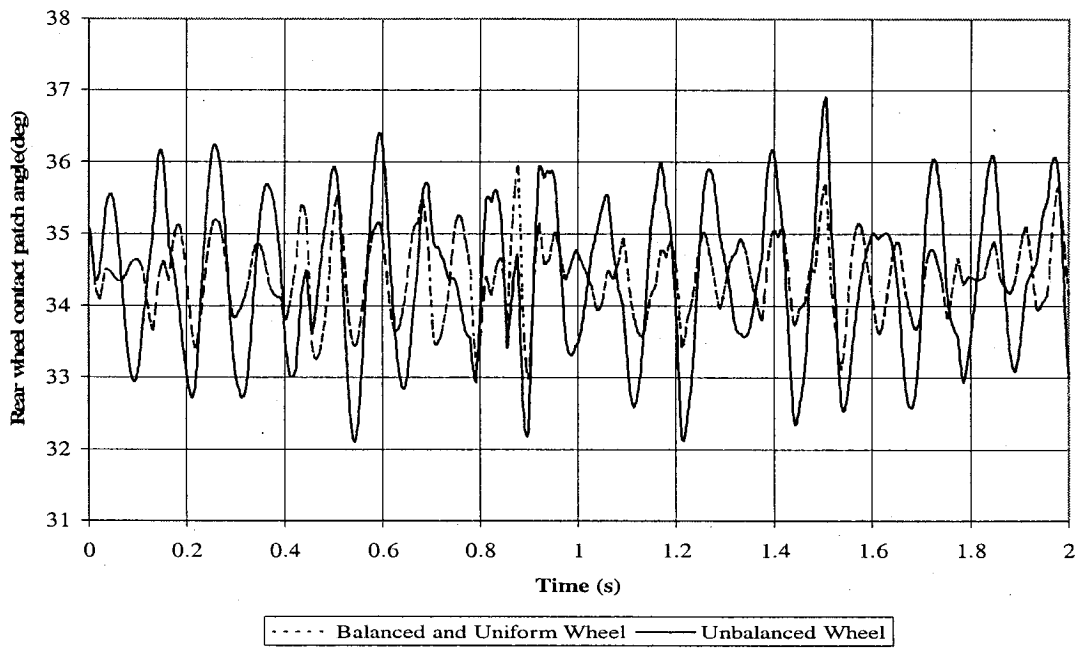

Figure 4.81: Comparison of variations in the front and rear wheel contact patch angles of the balanced and unbalanced wheels (100 km/h; Smooth road)

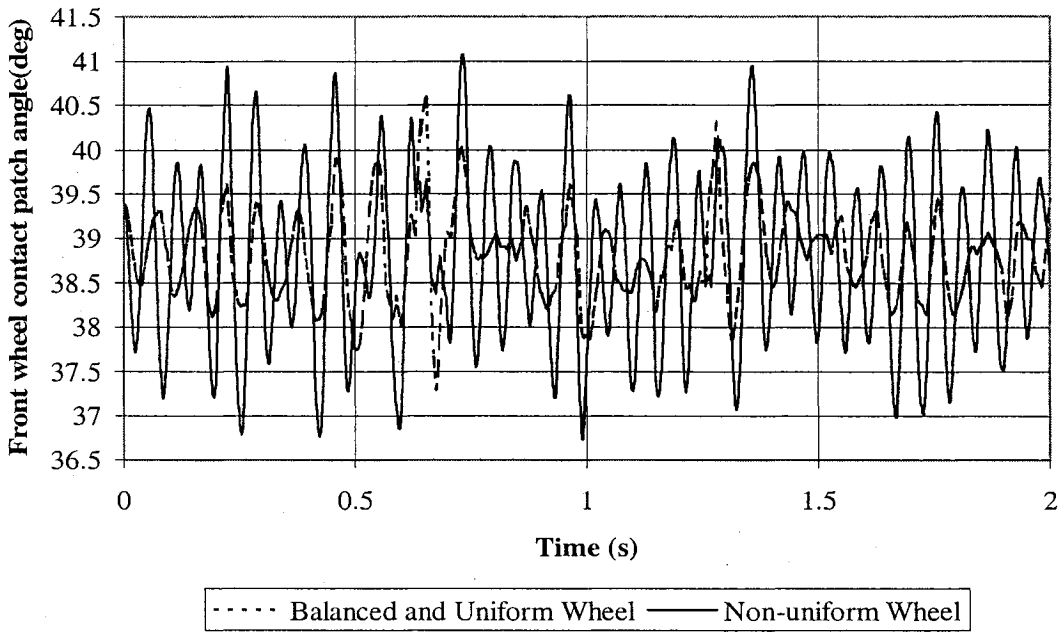

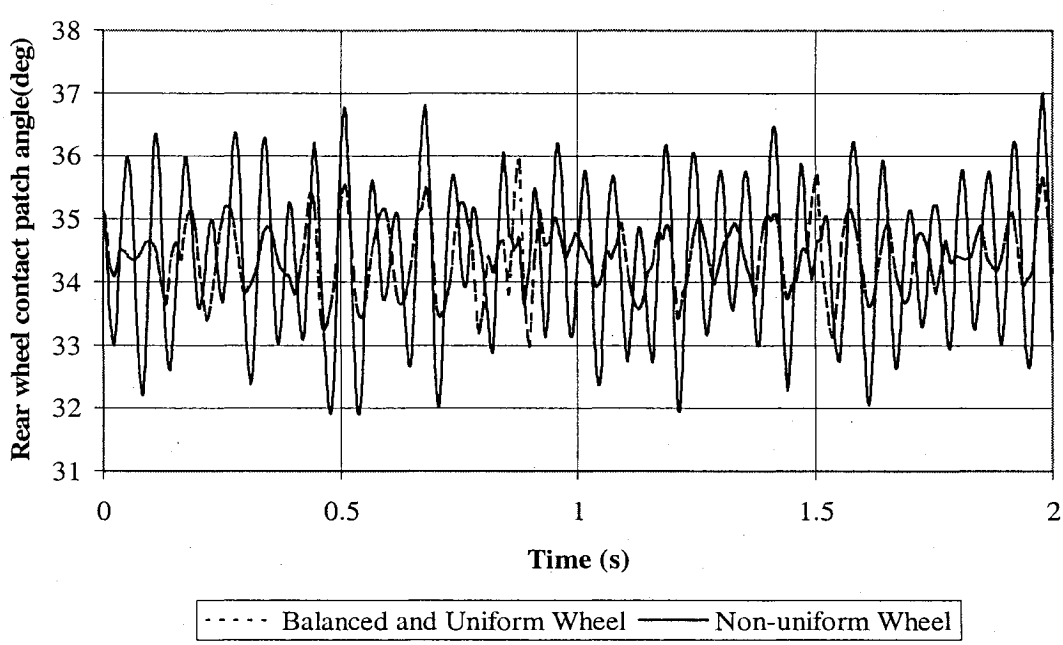

Figure 4.82: Comparison of variations in the front and rear wheel contact patch angles of the uniform and non-uniform wheels (100 km/h; Smooth road)

variations in the dynamic tire forces.

4.5.3 INFLUENCE OF COUPLED WHEEL UNBALANCE AND NON-UNIFORMITY

Figure 4.83 illustrates the variations in the front and rear wheel contact patches in the presence of both the unbalance and radial run-out, $(me)_{f,r}$ = 0.2, 1.2 kg-m and $(\Delta r)_{f,r}$ = 0.002, 0.002 m. The results are attained for forward speed of 100 km/h, while operating on a smooth road. The figure also illustrates the contact patch variations of wheels in the absence of mass unbalance and radial run-out. The variations in the contact patches of wheels with unbalance and run-out reveal predominant oscillations near the rotational speed of 8.8 Hz due to mass unbalance during compression and extension, and near 17.6 Hz due to radial run-out during rebound alone. This can be attributed to the characteristic waveform induced by the assumed wheel non-uniformity, as discussed in Chapter 2. Referring to Figures 4.81 and 4.82, it can be concluded that peak to peak variations in the wheel-terrain contact patches with unbalance and non-uniformity are far more than those obtained for non-uniformity or unbalance alone.

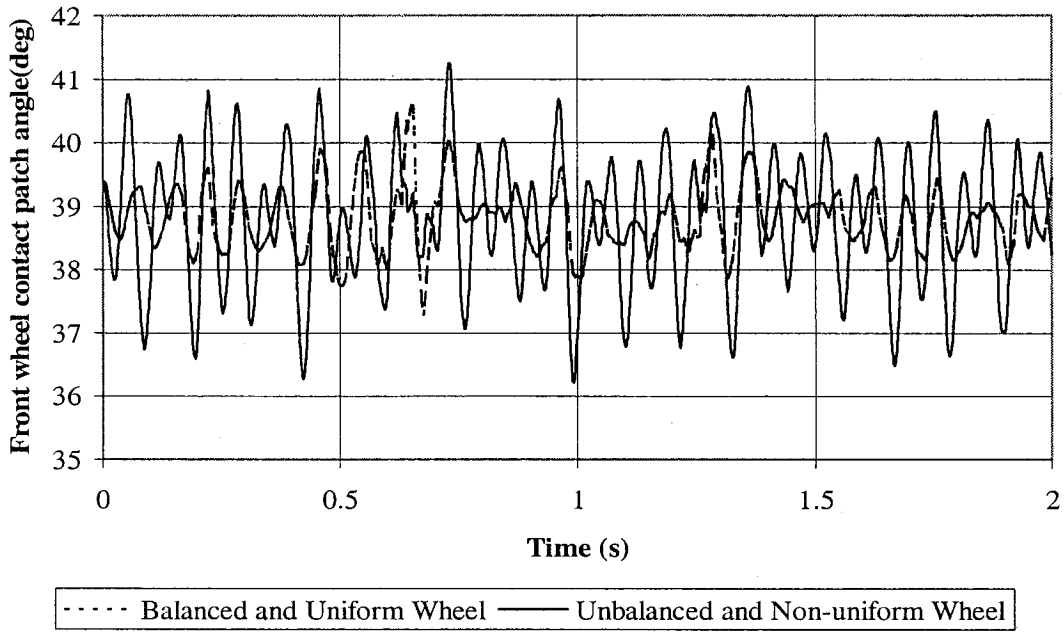

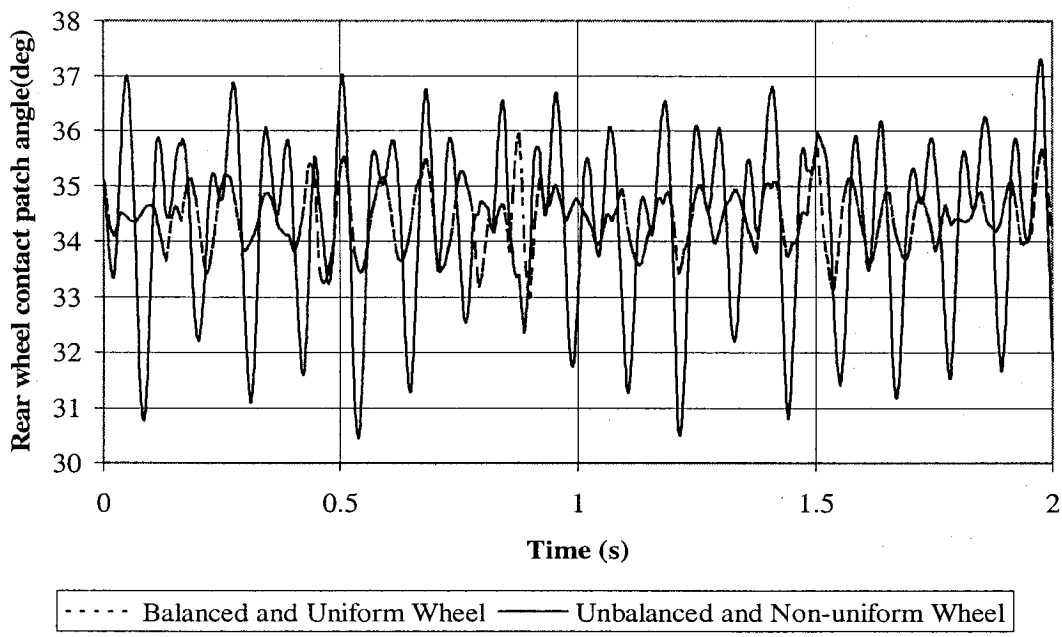

Figure 4.83: Comparison of variations in the front and rear wheel contact patch angles of the balanced and uniform wheels to the unbalanced and non-uniform wheels (100km/h; Smooth road)

4.6 SUMMARY

In this chapter, a comprehensive parametric study is carried out to study the effects of mass unbalance and radial run-out using the pitch plane vehicle model developed in Chapter 2. The effects of operating factors, vehicle speed and road roughness are analyzed in conjunction with the wheel unbalance and non-uniformity, while the effect of phase is also observed. The response characteristics of the vehicle are analyzed using performance measures described in Chapter 3. The effects of magnitudes of wheel unbalance and non-uniformity on the performance measures are observed involving variations in each operating parameter to deduce their contributions individually and collectively. Each of the two sources of self-excitation, wheel unbalance and non-uniformity are observed to contribute considerably to the performance measures of overall ride and tire force variations. The wheel unbalance was observed to contribute mainly at higher speeds, while the non-uniformity at comparatively lower speeds. The last section of this chapter discusses the comparison of variations in the tire-terrain contact patch for the unbalanced and non-uniform wheels with those derived for the balanced and uniform wheels. The time domain results show that the contact patch variations occur at the predominant frequencies associated with each source of vibration, while the increase in peak to peak magnitudes increase with increase in mass unbalance and radial run-out.

CHAPTER 5

CONCLUSIONS AND RECOMMENDATIONS FOR FUTURE WORK

5.1 GENERAL

As set out in Chapter 1, the overall objective of this thesis research was to study the effects of wheel unbalance and wheel non-uniformity on the vehicle ride and dynamic tire force responses. The specific objectives included development of a comprehensive mathematical model of a commercial vehicle using a non-linear adaptive foot-print tire model, characterization of wheel unbalance and wheel non-uniformity to incorporate them in the mathematical model of a vehicle, and analysis of effects of wheel unbalance and wheel non-uniformity on the performance measures relevant to ride and dynamic tire forces through comprehensive parametric study. In the present chapter, highlights of the research work are summarized together with major conclusions and some recommendations for future work.

5.2 HIGHLIGHTS OF THE PRESENT WORK

From the review of literature, it was concluded that the ride dynamic environment and dynamic wheel loads of heavy commercial vehicles could be influenced by the self-excitation sources of vibration, such as wheel unbalance and tire non-uniformity. Furthermore, the characterization and effects of such sources have been explored in a very few studies. Major highlights and contributions of this study are summarized below.

- **Development of representative vehicle model**

An in-plane model of a two axle truck is formulated to study its interactions with the road in terms of vertical tire loads transmitted to the road, vertical and angular acceleration responses of the sprung and unsprung masses, assuming negligible contribution due to roll dynamics of the vehicle. Two closely spaced rear axles are grouped together and represented by a single composite axle. The vehicle body, chassis and cargo are characterized by a rigid sprung mass with two degrees of freedom: vertical and pitch motions. The front and composite rear wheel and axle assemblies are represented by rigid masses with only vertical degree of freedom (DOF). Each unsprung mass is coupled to the sprung mass through the respective suspension components, modeled as parallel combinations of linear energy restoring and dissipative elements. The tire-terrain interactions are represented by adaptive foot-print tire model having radial contact with undeformable road. Free vibration analysis of the analytical model is carried out to identify the important natural frequencies and modes of vibration. The analytical model is then validated by comparing the PSD of tire forces and ride accelerations with the previously reported results. The vehicle model is analyzed for stochastic excitations arising from different road conditions in conjunction with sources of self excitation: wheel unbalance and wheel non-uniformity, which forms the notable contribution of this dissertation research.

- **Characterization of tire-terrain interaction using adaptive foot-print tire model**

Due to several limitations of the most commonly used point contact tire model, such as: overestimation of tire forces, more frequent wheel hop and inability to incorporate

wheel non-uniformity, an adaptive foot-print tire model is used in this study. The road wheel-terrain interaction is modeled based on the concept of continuous radial spring representation and is expanded to include damping effects. The road wheel interaction is represented by a radially distributed continuous spring and a damping element taking into account an equivalent stiffness. An equivalent damper is incorporated to account for the dissipative characteristics of the wheel. At each time instant, the contact patch is formed in between the tire and the road, which varies according to the road roughness and self-excitations in the wheel assembly. The wheel non-uniformity and wheel unbalance could be easily incorporated within this tire model.

- **Characterizations of wheel unbalance and wheel non-uniformity**

The unbalance can exist in any plane of the wheel, while this work is limited to in-plane wheel unbalance only. In order to characterize the wheel non-uniformity (radial run-out), the wheel is assumed to have an elliptical shape with very small magnitude of radial run-out. The locus traced by this new wheel with radial run-out can be obtained by expressing the equation of ellipse and circle in terms of their polar co-ordinates and then deriving the expression for the variations in the radial difference as a function of the angular displacement or time. The derived expression is then included in the equation for calculating the height of wheel center at each time instant.

- **Analysis of wheel unbalance and wheel non-uniformity**

As the tire force variation and ride accelerations of the vehicle are strongly related to the operating parameters, a comprehensive parametric study is carried out to observe the

influences of road roughness, vehicle speed, and phase angle in conjunction with wheel unbalance and wheel non-uniformity. The vehicle speeds used are 60 km/h, 80 km/h, and 100 km/h. The random road profiles are characterized into three types according to their roughness indices; smooth, medium-rough and rough. The performance measures used are dynamic load coefficient (DLC) for variation of dynamic tire forces and overall rms bounce and pitch accelerations (unweighted and weighted). The frequency weighting filters proposed in ISO-2631-1 (1997) are applied to determine the overall weighted ride accelerations.

A detailed parametric study is conducted to study the influences of road roughness, vehicle speed and phase angle between the unbalance/non-uniformity parameters of the front and rear wheels is carried out in three stages: (i) excitations due to wheel unbalance alone; (ii) excitations due to wheel non-uniformity alone; and (iii) excitations due to combined wheel unbalance and non-uniformity. For the study of wheel unbalance, five sets of unbalance masses are used in the range of 0.2 kg-m to 0.8 kg-m for the front wheel and 0.2 kg-m to 1.2 kg-m for the rear wheels, while the magnitudes of wheel non-uniformity varied from 0.001m to 0.003 m. The phase angles between the unbalanced masses/wheel non-uniformities of the front and rear wheels are also varied in the 0° to 90° range.

5.3 CONCLUSIONS

The major conclusions drawn from the present research work are summarized below:

- At a particular vehicle speed, the DLC due to the front and rear wheel forces, increase with increase in magnitudes of unbalance and the increment follows nearly square function of the vehicle speed. The DLC due to tire forces of the unbalanced wheels are observed to be 3 to 4 times higher than those of the vehicle with balanced wheels, when the vehicle operates on a smooth road at lower speeds. For a given vehicle speed and a given magnitude of unbalance mass, the DLC values increase with increase in road roughness. The contribution of mass unbalance is far more pronounced under smooth road conditions.
- The variations in the overall unweighted bounce rms acceleration values with increasing unbalance nearly follow a square function curve with more significant increment under smooth road conditions and higher speeds. The frequency-weighted acceleration values exhibit the same trend but with comparatively small increments. The overall unweighted pitch rms acceleration values show similar trends except that the frequency-weighted values remain almost unaffected due to characteristics of W_e-weighting filter.
- With increasing phase difference between the front and rear wheel unbalance masses, the overall unweighted bounce rms acceleration values decrease and the overall pitch rms acceleration values increase, while their corresponding weighted values show the same trend with relatively small change.
- The predominant frequency due to wheel non-uniformity is observed to be nearly twice the wheel angular frequency, while that due to mass unbalance is equal to the wheel angular frequency. Considering the frequency-response characteristics

of the W_k-weighting filter, the vertical vibration caused by the mass unbalance could have significant effect on the ride quality of the vehicle.

- At a particular vehicle speed, the DLC values increase nearly linearly with increasing magnitudes of wheel non-uniformity or radial run-out. The vehicle speed corresponding to the predominant frequency, falling in the vicinity of unsprung mass resonance, shows the maximum increment for the DLC due to that particular axle tires. The maximum increment in DLC due to front axle is observed at a speed of 60 km/h, while DLC due to rear wheels at 80 km/h. The effect of non-uniformity diminishes at higher speeds. At lower speeds, the DLC values are almost 5 to 6 times higher than the DLC due to uniform wheels. It is thus concluded that the wheel run-out contributes significantly to the potential road damage, particularly on smooth road surfaces.
- The overall unweighted bounce rms acceleration values increase nearly linearly with increasing magnitude of non-uniformity, while showing the maximum increment at the lowest speed considered, 60 km/h. The weighted rms bounce acceleration values at this speed are almost 5 times higher than the weighted values for the uniform wheel, which further suggest that radial run-out could deteriorate the vertical ride quality of the vehicle in a considerable manner.
- The overall unweighted rms pitch acceleration values do not show considerable increase with increasing magnitude of non-uniformity at all speeds except at 80 km/h. The maximum weighted pitch acceleration value at 80 km/h is observed to be almost 2 times higher than the weighted value for the uniform wheel and thus giving significant impact on the ride quality.

- The change in the performance measures of ride and potential road damage with respect to varying magnitudes of wheel non-uniformity is most significant under smooth road operation with higher magnitude of non-uniformity in the rear wheel showing more significant effects.
- For a given speed and road type, the overall unweighted and weighted pitch rms acceleration values increase significantly with increase in phase difference between the front and rear wheel non-uniformities, while the overall bounce rms acceleration values (unweighted and weighted) show an opposite trend.
- The vehicle operation under the combined effects of wheel unbalance and non-uniformity shows greater influences on all the performance measures as compared to those observed under the individual effects of wheel unbalance and non-uniformity. The spectra of ride accelerations and tire forces exhibit two predominant frequencies, corresponding to those due to wheel unbalance and non-uniformity excitations, respectively.
- The DLC values increase nearly linearly with increasing magnitudes of non-uniformity and unbalance, yielding maximum increment corresponding to a speed of 100 km/h for the front axle, while for the rear axle it is at 80 km/h. The latter is due to the presence of predominant frequency of wheel non-uniformity in the vicinity of rear wheel resonance. The maximum DLC values at these speeds are observed to be nearly 4 to 5 times higher than the DLC values due to uniform and balanced wheels.
- For a given road condition, the overall unweighted bounce and pitch rms accelerations increase considerably with increasing magnitudes of wheel non-

uniformity and unbalance. The increment is more pronounced at lower speeds of 60 and 80 km/h considered in this study. The weighted values exhibit the same trend but with small increments. The maximum weighted bounce and pitch acceleration values are almost twice higher as compared to the corresponding weighted values for balanced and uniform wheel, at a speed of 60 km/h under smooth road conditions. The combined contribution of unbalance and non-uniformity on ride comfort is thus evident even at lower speed.

- For a given speed and road type, the overall unweighted bounce rms acceleration values decrease considerably, while the overall unweighted pitch acceleration values increase with increase in the phase angle between the non-uniformities and unbalance masses located in front and rear wheels. The weighted values for bounce and pitch rms accelerations exhibit the same trend with only minimal change.

5.4 RECOMMENDATIONS FOR FUTURE WORK

The present research work yields significant insight into the effects of wheel unbalance and non-uniformity on ride accelerations and dynamic tire loads for a commercial vehicle but it represents only a preliminary effort in understanding the effects of wheel unbalance and non-uniformity on the ride response. Although the study clearly demonstrates useful results with a simplified analytical model, the potential usefulness and accuracy can be further enhanced upon consideration of the following:

- The ride acceleration values calculated at the center of gravity of the vehicle body can be transformed into accelerations at the seat so as to investigate the results according to comfort and safety guidelines defined in ISO 2631-1 [69].
- Although the in-plane vehicle model developed in this study provides reasonable results on the fundamental behavior of the vehicle in the presence of wheel unbalance and radial run-out, it is unable to predict the effects on vehicle ride along the lateral and roll axes. The ride quality along these axes is important, since the vehicle frequently negotiates right and left track elevation differences. The involvement of lateral and roll axes in the vehicle model demands modeling of wheel unbalance and wheel non-uniformity in three dimensions, which can lead to more accurate analysis in compliance with the practical cases. The estimation of optimal values of wheel unbalance and non-uniformity for ride comfort and potential road damage can be made from such a model.
- The analytical vehicle model with inclusion of wheel unbalance and non-uniformity should be validated with field test data.
- Further efforts are needed to model the wheel unbalance in two-planes.
- The characterization of the wheel non-uniformity in the present research work can be extended to analyze the effect of non-uniform wheels for the tracked vehicles.

REFERENCES

1. Cebon, D., "Interaction Between Heavy Vehicles and Roads" The Thirty-Ninth L. Ray Buckendale Lecture, SAE Sp-951, 1993.

2. Captain, K. M., Boghani, A. B. and Wormley, D. N., "Analytical Tire Models for Dynamic Vehicle Simulation", Vehicle System Dynamics, No. 8, pp. 1-32, 1979.

3. Ahmed, A. K. W., "Ground Transportation Systems", Encyclopedia of Vibration, Vol. 2, pp. 603-620, 2002.

4. Ni, E. J., "A Mathematical Model for Tire/ Wheel Assembly Balance", Tire Science and Technology, TSTCA, Vol. 21, No. 4, October-December, pp 220-231, 1993.

5. Van Deusen, B. D., "A Statistical Technique for the Dynamic Analysis of Vehicles Traversing Rough Yielding and Non-Yielding Surfaces", CR-659, NASA, Washington, D.C., 1969.

6. Chiesa, A. and Rinoapoli, L., "Vehicle Stability Studied with Nonlinear Seven Degree Model", SAE Paper No. 670476. Presented at Mid-Year Meeting, NY, 1967.

7. Schuring, D., "Analysis and Simulation of Dynamical Vehicle-Terrain Interaction", Cornell Aeronautical Laboratory Inc. Cornell University, Buffalo, NY, Technical Memorandum CAL No. VJ-2330-G-56, AD 690 841, 1969.

8. Van Deusen, B. D., "A Study of the Vehicle Ride Dynamics Aspect Ground Mobility, Vol. III, Theoretical Dynamics Aspects of Vehicle Systems", Chrysler Corp., Detroit, Michigan, AD 467 026.

9. Lins, W. F., "Comparison of Time Domain and Frequency Domain Analysis of Off-Road Vehicles", SAE Paper No. 690353, 1969.

10. Grant, J.W., "Research in Suspension Dynamics for Off-Road Mobility", Mobility Systems Laboratory, USATACOM, Warren, Michigan, 1970.

11. Jurkat, M.P., "Mathematical Formulations of Wheeled Vehicle Dynamics for Hybrid Computer Simulations", Report No. SIT-DL-70-1452, Stevens Institute of Technology, Hooken, NJ, AD 742 744, 1970.

12. Kozin, F. and Bugdanoff, J.L., "On the Statistical Analysis of the Motion of Some Simple Two-Dimensional Linear Vehicles Moving on a Random Track", Int. J. Mechan., Sci. 2:168-178, 1960.

13. Bugdanoff, J.L. and Kozin, F., "Additional Results on the Statistical Analysis of a Linear Vehicle Using Measured Ground Power Spectral Density", Report No. 8390LL96, Land Locomotion Laboratory, USATACOM, Warren, Michigan, AD 438 406, 1963.

14. Lessem, A.S., "Dynamics of Wheeled Vehicles; Report 1, A Mathematical Model for the Traversal of Rigid Obstacles by a Pneumatic Tire", U.S. Army Engineer Waterways Experimental Station, CE, Vicksburg, Mississippi, AD 834 324, 1968.

15. The AMC' 71 Vehicle Mobility Model", Draft Report, Surface Mobility Division, USATACOM, Warren, Michigan, 1971.

16. Davis, D.C., "A Radial-Spring Terrain-Enveloping Tire Model", Vehicle System Dynamics, No. 1:55-60, 1975.

17. Clark, S. K., "The Rolling Tire under Load", SAE Paper No. 650493. Presented at the Mid-Year Meeting, Chicago, Illinois, 1965.

18. Dodge, R. N., "The Dynamic Stiffness of a Pneumatic Tire Model", SAE Paper 650491. Presented at the Mid-Year Meeting, Chicago, Illinois, 1965.

19. Tielking, J.T., "Plane Vibration Characteristics of a Pneumatic Tire Model", SAE Paper No. 650492. Presented at the Mid-Year Meeting, Chicago, Illinois, 1965.

20. Dhir, A. and Sankar, S., "Analytical Wheel Models for Ride Dynamic Simulation of Off-road Tracked Vehicles", Vehicle System Dynamics, No. 27, pp. 37-63, 1997.

21. Creighton, D. C., "Revised Vehicle Dynamic Module: User's Guide for Computer Program VEHDYN II", WES Technical Report No. SL-86-9, U.S. Army Engineer Waterways Experiment Station, Vicksburg, Mississippi, 1986.

22. Murphy, N. R. and Ahlvin, R. B., "AMC-74 Vehicle Dynamics Module", Technical Report No. M-76-1, U.S. Army Engineer Waterways Experiment Station, Vicksburg, Mississippi, 1986.

23. Wang, K., Dynamic Analysis of a Tracked Snowplowing Vehicle and Assessment of Ride Quality", M.A.Sc. Thesis, Concordia University, Quebec, Montreal, 1998.

24. Demic, M., "The Definition of the Tires Limit of Admissible Nonuniformity by Using the Vehicle Vibratory Model", Vehicle System Dynamics, No. 31, pp. 183-211, 1999.

25. Long, W. C., "Factors Affecting Performance of Hubs, Drums, Wheels, and Rims on Truck Tractors and Trailers", Society of Automotive Engineers, 650187.

26. Demic, M., "Laboratory Investigations of the Tire Nonuniformity from the Aspect of Vibratory Comfort and Handling (in Serbian), MVM 52/83, 1983.

27. Demic, M., "A Supplement to Standardization of Nonuniformity of Passenger Car Tires with Respect to Oscillatory Comfort and Handling, ISATA, Milan, 1984.

28. Demic, M. "Nonuniformity of Tires and Vehicle Oscillatory Comfort, Mobility and Vehicle Mechanics No. 19 (3), pp.33-42, 1994.

29. Kenny, T., "Quantifying Tire, Rim and Vehicle Effects on Ride Quality", SAE 890369, SAE Warrendale, PA, 3/89.

30. W d. K.-Leitline, Wirtschaftverband der Deutschen Kautschukindustrie, E. V. Frankfurt.

31. Zastava Normes9.01398, "The Tires for Passenger Cars", 1992.

32. Lloyd Nedley A., "Effect of Wheel Nonuniformities on Tire-Wheel Assembly and the Vehicle." SAE, 680005.

33. Rakheja, S., Politis, H., Juras, D. and Boileau, P., "Evaluation del'exposition aux vibration globales du corps des operateurs du Metro de Montrealet etude du comportement dynamique et de leur systeme de suspension", Technical report submitted to IRSST, Montreal, 2004.

34. Stutts, D.S., Krousgrill, C. M. and Sodel, W., "Parametric Excitation of Tire-Wheel Assemblies by a Stiffness Non-Uniformity.", Journal of Sound and Vibration No. 179(3), pp. 499-512, 1995.

35. Bohler, H., "Simulation of the Dynamic Loads of a Tractor with the Help of a Multi-Body-System Program", ISTVS, 13th Int. Conf., Munich, Germany, 1999.

36. Mitschke, M., "Dynamic der Kraftfahrzeuge", Springer, 1973.

37. Simic, D., "Vehicle Dynamics" (in Serbian) Naucna Knjiga, Belgrade, 1980.

38. ISO Standard 1925, "Mechanical Vibration Balancing Vocabulary"

39. Lyons, J., "Dynamic Balancing; Causes, Corrections and Consequences" IRD Balancing Division, EntekIRD International, 1998.

40. Srinivasan, P., "The Effect of Wheel Unbalance on Vehicle Dynamics", Degree of Mechanical Engineer Thesis, California Institute of Technology, Pasadena, California, 1956.

41. Smith, A. R., "Frame Bending, Fifth Wheel Locations –Special Body Moving and Loading Problem", SAE special report SR 260, 1965.

42. Ribartis, Aurell, J. and Andersers, E., "Ride comfort Aspects of Heavy Truck Design", SAE Tran., 781064, pp. 4046-4069, 1975.

43. Michelberger, P. and Szole, D., "Speed Dependent Vertical Vibrations of Elastic Vehicle Bogies", Int. J. Vehicle Design, 8(1), pp. 8-95, 1985.

44. Rakheja, S. and Woodrooffe, J.H.F., "Role of Suspension Damping in Enhancement of Road Friendliness of Heavy Vehicles", Heavy Vehicle Systems, Int. J. of Vehicle Design, Vol. 3, 1996.

45. Cebon, D., "Vehicle Generated Road Damage, A Review", Vehicle System Dynamics, Vol.18, pp., 107-150, 1989.

46. Woodrooffe, J.H.F., "Heavy Truck Suspension Dynamics, Methods for Evaluating Suspension Road Friendliness and Ride Quality", SAE 962152, 1996.

47. Missio, G. K. and Carson, R.M., "Corrugation of Unmetalled Roads, Part I: Vehicle Dynamics", Proceedings of IMECHE Vol. 203, pp. 205-214.

48. Hedrick, J. K. and Yi, K., "The Effect of Alternative Heavy Truck Suspension on Flexible Pavement Response ", Presented at the second International symposium heavy vehicle weights and dimensions, Vol.1,Kelowana British Columbia, Canada, June 8-22,1989

49. Cole, D. J. and Cebon, D., "Simulation and Measurement of Dynamic Tire Forces", Presented at the second International Symposium of Heavy Vehicle Weights and Dimensions, Vol.2, Kelore, 1989.

50. Sweatman, P. F., "A Study of Dynamic Wheel Forces in Axle Group Suspensions of Heavy Vehicles", ARRB Special Report No. 127, 1983.

51. Cebon, D., "Vehicle Generated Road Damage, A Review", Vehicle System Dynamics, Vol.18, pp. 107-150, 1989.

52. Smith, A. R., "Frame Bending, Fifth Wheel Locations-Special Body Moving and Loading Problem", SAE Special Report SR 260, 1965.

53. Ribartis, Aurell, J. and Andersers, E., "Ride Comfort Aspects of Heavy Truck Design" , SAE Tran., 781064, pp.,4046-4069, 1975.

54. Stiharu, I. and Rakheja, S., "CONCAVE 03-95, "Laboratory Testing and Characterization of an Air Ride Spring." prepared for Forestry Engineering Research Institute of Canada, 1995.

55. Siddiqui Owais, M., "Dynamic Analysis of a Modern Urban Bus for Assessment of Ride Quality and Dynamic Wheel Load", M.A.Sc. Thesis, Concordia University, Quebec, Montreal, 2000.

56. Stikeleather, L.F., "Review of Ride Vibration Standards and Tolerance Criteria", SAE Transactions paper No. 760413, pp.1460-1467, 1976.

57. Van Deusen, B. D., "Human Response to Vehicle Vibration", SAE Transactions, Paper No. 680090, pp.328-345, 1968.

58. Dieckmann, D., "Einfluss Vertikaler Mechanischer Schwingungen auf den Menschen", Internationale Zeitschrift Angewandte- Pshysiologie, Vol.16, pp. 519-564, 1957.

59. Goldman, D. E., "A review of Subjective Responses to Vibratory Motion of the Human Body in the Frequency Range 1 to 70 cps", Report No. 4 , Naval Medical Research Institute, 1948.

60. Janeway, R. N., "Passenger Vibration Limits", SAE Journal, Vol.56, pp.48-49, 1948.

61. Von Eldik Thieme, H.C.A., "Passenger Riding Comfort Criteria and Methods of Analyzing Ride and Vibration Data", SAE Paper No. 295 A, 1961.

62. Butkunas, A. A., "Power Spectral Density and Ride Evaluation", SAE Transactions Paper No. 660138, pp.681-687, 1966.

63. VDI- 2057, "Assessing the Effects of Vibration on Human Beings", Verein Deutscher Ingenieure, Translated and Published by Peter Peregrinus Ltd., 1963.

64. Lee, R., and Pradko, F., "Analytical Analysis of Human Vibration", SAE Transactions paper No. 680091, pp.346-370, 1968.

65. Pradko, L., Lee, R., and Kaluza, V., "Theory of Human Vibration Response", ASME Paper No. 66 WA/BHF -15, 1966.

66. International Organization for Standardization, "Guide for Evaluation of Human Exposure to Whole Body Vibrations", ISO-2631, 1974.

67. Smith, C. C., "On Using the ISO Standard to Evaluate the Ride Quality of Broad-Band Vibration Spectra in Transportation Vehicles", Transactions ASME, Journal of Dynamic Systems, Measurements, and Control, pp.440-443, 1976.

68. International Organization for Standardization, "Guide for Evaluation of Human Exposure to Whole Body Vibrations", ISO-2631, 1978.

69. International Organization for Standardization, "Mechanical Vibration and Shock-Evaluation of Human Exposure to Whole Body Vibration", ISO-2631-1, 1997.

70. Anon, "The AASHO Road Test, Report 6, Special Studies", Highway Research Board, Washington D.C., Special Report 61F, 1962.

71. Anon, "The AASHO Road Test, Report 5, Pavement Research", Highway Research Board, Special Report 61E, 1962.

72. Peattie, K.R., "Flexible Pavement Design Ch.1" Developments in Highway pavement Engineering, 1 Pell PS ed. Applied Science Publishers Ltd, London, 1978.

73. Scrivner , F.H. and Duzan, H.C., "Application of AASHO Road Test Equations to Mixed Traffic", Proc. of a Conf. on the AASHO Road Test, St. Louis, MO., National Academy of Sciences-National Research Council, Special Report 73, 1962.

74. Anon, "The AASHTO Guide for Design of pavement Structures", American Association of State Highway and Transport Officials, Volume 1, 1986.

75. Addis, R.R. and Whitmarsh, R.A., "Relative Damaging Power of Wheel Loads in Mixed Traffic", Transport and Road Research Laboratory Report, LR 979, 1981.

76. Kinder, D.F., and Lay, M.G., "Review of the Fourth Power Law", ARRB, Internal Report AIR000-248, 1988.

77. Thrower, E.N., "A Parametric Study of a Fatigue Prediction Model for Bituminous Road Pavements.", TRRL, Laboratory Report LR892, 1979.

78. Anon, "Impacts of Heavy Freight Vehicles", OECD, Paris, 1982.

79. Christison, J.T., "Pavements Response to Heavy Vehicle Test Program: Part2-Load Equivalency Factors", Canroad Transportation Research Corporation, Vol.9, 1986.

80. Anon, "Heavy Trucks, Climate and Pavement Damage", OECD Road Transport Research, Paris, 175 p, 1988.

81. Gillespie, T.D., *et al.*, "Effects of Heavy Vehicle Characteristics on Pavement Response and Performance", Transportation Research Board, NCHRP Report 1-25 (1), 1992.

82. Baker, R. and Alpab, "The Speed Effect in Pavement Deflection", Acta Technics, 85 (1-2), pp. 11-28, 1977.

83. Mitchell, C.G.B. and Gyness, L., "Dynamic Pavement Loads Measured for a Variety of Truck Suspension", 2nd International Conference on Heavy Vehicle Weights and Dimensions, Kelowna, British Columbia, 1989.

84. Dickerson, R.S. and Mace, D.G.W., "Dynamic Pavement Force Measurements, with a Two Axle Heavy Goods Vehicle", SR 688, 1981.

85. Hazh, W.D., "Measurements of Road Loading by HGV Suspensions Survey of the German Research Program", IMechE Conference on Road Wear, The Interaction between Vehicle Suspension and the Road, London, 1991.

86. OECD, "Dynamic Loading of Pavements", OECD Report, 1992.

87. Rakheja, S. *et al.*, "Ride Vibration of Articulated Vehicles and Significance of Secondary Suspension", SAE Noise and Vibration Conference, pp 139-147, 1989.

88. Rakheja, S. and Woodrooffe, J.H.F., "Role of Suspension Damping in Enhancement of Road Friendliness of Heavy Vehicles", Int. J. of Vehicle System Design, Vol. 3, 1996.

89. Cebon, D., "Examination of Road Damage Caused by Three Articulated Vehicles", Proc. ARRB/ FORS Symposium of Heavy Vehicle Suspension Characteristics, Camerra, pp. 143-162, 1987.

90. Cebon, D., "An Investigation of the Dynamic Interaction between Wheeled Vehicles and Road Surfaces", Ph. D Thesis, University of Cambridge, 1985.

91. Tec, P., "Road Damaging Potential of Measured Dynamic Tire Forces in Fixed Traffic", Department of Mechanical Engineering, University of Cambridge, 1994.

92. Ferrari, P., "Calculation of the Deformations Caused by Vehicles to Flexible Pavements", 3rd International Conference Structural Design of Asphalt Pavements, University of Michigan, Ann Arbor, 1972.

93. Hardy, M.S. and Cebon, D., "The Responses of Flexible Pavements to Moving Dynamic Loads", Proc. Inst Acoustics, 10(2), pp. 485-492, 1988.

94. Cole, D.J. and Cebon, D., "Assessing the Road Damaging Potential of Heavy Vehicles", Proc. IMechE, Part D.205, pp. 223-233, 1991.

95. Gillespie, T.D., "Heavy Truck Ride", SAE SP 607, 1985.

96. Heath, A. and Good, M.C., "Heavy Vehicle Design Parameters and Dynamic Pavement Loading", Australian Road Research, 15(4), pp. 249-263, 1985.

97. Sayers, M. and Gillespie, T.D., "Dynamic Pavement /Wheel Loading for Trucks with Tandem Suspensions", Proc. 8th IAVSD Symposium on the Dynamics of Vehicles on Roads and on Railway Tracks, Cambridge, MA, Swets and Zeitlinger, 1983.

98. Chan, G.P. *et al.*, "Laboratory Measured Tire Pavement Contact Pressures", FHWA, Load Equivalencies Workshop, Washington D.C., 1988.

99. Haas, R.C.G. and Papaginnaks, A.T., "Understanding Pavement Rutting", Special Workshop on Rutting in Asphalt Pavements, Toronto, Roads and Transport Association Canada, 1986.

100. Huhatla, M., "Field Test to Compare Tires", FHWA Load Equivalence Workshop, Washington D.C., 1988.

101. Bonaquist, R., "An assessment of the Increased Damage Potentials of Wide Based Single Tires", 7th Int. Conf. on Asphalt Pavements, Ed. Brown S.F. and Hicks R.G., Nottingham, UK, International Society for Asphalt Pavements, 1992.

102. Eisenmann, J., Birman, D., and Hilmes, A., "Effects of Commercial VehicleDesign on Road Stress Research Relating to the Roads", Stressund Autobahn, (Translated by TRRI as WP/V and ED/97/29), 37 (6), pp.238-244, 1987.

103. Haas, R.C.G. and Papaginnaks, A.T., "Understanding Pavement Rutting", Special Workshop on Rutting in Asphalt Pavements, Toronto, Roads and Transport Association Canada, 1996.

104. Mitchell, C.G.B. and Gyeness, L., "Dynamic Pavement Loads Measured for a Variety of Truck Suspension 2nd International Conference on Heavy Vehicle Weights and Dimensions, Kelowna, British Columbia, 1989

105. Monismith, C.L., Sousa, J. and Lysmer, J., "Modern Pavement Design Technology including Dynamic Load Conditions", SAE Conf. on Vehicle Pavement Interactions, SP 765, Indianapolis, SAE Tran. 881845, 1989.

106. Hahn, W.D., "Effects of Commercial Vehicle Designs on Road Stress Vehicle Research Results", Institut fur Kruftfahrwesen Universitat, 1985.

107. Sweatman, P.F., "Effect of Heavy Vehicles Suspension on Dynamic Road Loading", Australian Road Research Report, ARR116, 1980.

108. Papagiannakis, A.T. and Woodrooffe, J.H.F., "Suitability of Alternative Pavement Roughness Statistics to Describe Dynamic Axle Loads of Heavy Vehicles", Proc. of the 2nd Int. Symposium of Heavy Vehicle Weights and Dimensions, June 18-22, Kelowna, B.C., 1989.

109. Orr, L.W., "Truck Pavement Factors-The Truck Manufacturers View Point", SAE Special Publication, SP 765, Paper No.881842, Nov, 1988.

110. Woodrooffe, J.H.F., Leblanc, P.A., and Papgiannakis, A.T., "Suspension Dynamics Experimental Findings and Regulatory Implications", SAE Paper No. 881847, 1988.

111. Throwes, E.N., "A parametric Study of Fatigue Prediction Model for Bituminous Road Pavements", TRRRL Report LR 892, 1979.

112. Ulliditz, P. and Bush, C., "Mathematical Models for Predicting Pavement Performance", Transport Research Rec.949, TRB, pp. 32-44, 1983.

113. Dhir, A., "Ride Dynamics of high Mobility Wheeled/Tracked Off-road Vehicles: Computer Simulation with Field Validation", Ph.D. Thesis, Concordia University, Quebec, Montreal, 1993.

114. ISO "Measurement and evaluation of human exposure to whole body mechanical vibration and repeated shocks", International Standards ISO-2631-1987.

115. Baurn, J. M., Bannett and Came, T. G., "Truck Ride Improvement Using Analytical and Optimization Methods", SAE paper 770609, 1977.

116. International Standard ISO-2631-1 Part-1: General requirement, "Mechanical Vibration and shock, Evaluation of human exposure to whole-body vibration", 1997.

117. Muluka, V., "Optimal Suspension Damping and Axle Vibration Absorber for Reduction of Dynamic Tire Loads", M.A.Sc. Thesis, Concordia University, Quebec, Montreal, 1998.

118. Damien, T.M. *et al.* "Pavement profiling various pavements: Ottawa/Smith Falls", John Emery Geotechnical Engineering Report, 1982.

119. Stutts, D. S., Soedel, W., Jha, S. K., "Fore-Aft Forces in Tire-Wheel Assemblies Generated by Unbalanced and the Influence of Balancing", Tire Science and Technology, TSTCA, Vol. 19, No.3, July-September, pp. 142-162, 1991.

120. Leatherwood, J. D., Barker, Linda, M., "A user oriented and computerized model for estimating vehicle ride quality" NASA TP-2299, 1984.

121. Pacejka, H. B. and Bekker, E., "The Magic Formula Tire Model" Vehicle System Dynamics 21, pp. 1-18, 1993.